Design, Synthesis and Biological Evaluation of Novel Small Molecule Inhibitors for Early Diagnosis and Therapy of Diseased States

Ph.D. Thesis

by

SAGNIK SENGUPTA

DISCIPLINE OF CHEMISTRY
INDIAN INSTITUTE OF TECHNOLOGY INDORE
APRIL 2019

Design, Synthesis and Biological Evaluation of Novel Small Molecule Inhibitors for Early Diagnosis and Therapy of Diseased States

A THESIS

Submitted in partial fulfillment of the requirements for the award of the degree of

DOCTOR OF PHILOSOPHY

by

SAGNIK SENGUPTA

DISCIPLINE OF CHEMISTRY
INDIAN INSTITUTE OF TECHNOLOGY INDORE
APRIL 2019

Indian Institute of Technology Indore
Academic Office
Thesis submitted on 2 April 2019
Administrative Officer

INDIAN INSTITUTE OF TECHNOLOGY INDORE

CANDIDATE'S DECLARATION

I hereby certify that the work which is being presented in the thesis entitled **Design, Synthesis and Biological Evaluation of Novel Small Molecule Inhibitors for Early Diagnosis and Therapy of Diseased States** in partial fulfillment of the requirements for the award of the degree of **DOCTOR OF PHILOSOPHY** and submitted in the **DISCIPLINE OF CHEMISTRY, INDIAN INSTITUTE OF TECHNOLOGY INDORE**, is an authentic record of my own work carried out during the time period from JANUARY 2013 to MARCH 2019 under the supervision of **Dr. VENKATESH CHELVAM**, Associate Professor, Discipline of Chemistry, IIT Indore.

The matter presented in this thesis has not been submitted by me for the award of any other degree of this or any other institute.

Sagnik Sengupta
Signature of the student with date
(SAGNIK SENGUPTA)

This is to certify that the above statement made by the candidate is correct to the best of my knowledge.

Venkatesh 02/04/19.
Signature of Thesis Supervisor with date
(Dr. VENKATESH CHELVAM)

SAGNIK SENGUPTA has successfully given his Ph.D. Oral Examination held on 30.10.19

Signature of Chairperson (OEB)
Date: 30/10/19

Signature of External Examiner
Date: 30/10/2019

Signature(s) of Thesis Supervisor(s)
Date: 30.10.19

Signature of PSPC Member #1
Date: 30-10-19

P.V. Kodgire
Signature of PSPC Member #2
Date: 30/10/2019

Tushar kanti Chatterjee.
Signature of Convener, DPGC
Date: 30/10/19

Tushar kanti Chatterjee.
Signature of Head of Discipline
Date: 30/10/19

Acknowledgements

It is my great pleasure to acknowledge all the individuals who have helped and supported me over the last six years for the completion of this thesis. I would like to express my deep sense of gratitude and thanks to my supervisor, Dr. Venkatesh Chelvam for giving me the opportunity to work on such an exciting research area. His excellent supervision, advice, and guidance from the very early stage made the completion of this study possible.

I also like to extend my gratitude to my PSPC members, Dr. Biswarup Pathak, and Dr. Prashant Kodgire for their guidance and valuable suggestions during my whole research work.

With great pleasure, I express my respect to Prof. Pradeep Mathur (Director, Indian Institute of Technology Indore) for his encouragement and providing all the facilities at the Indian Institute of Technology Indore.

I would like to acknowledge IIT Indore for providing laboratory, and financial support during my work.

I would also like to thank Dr. Rajneesh Misra, Dr. Apurba K. Das, Dr. Tushar Kanti Mukherjee, Dr. Sampak Samanta, Dr. Shaikh M. Mobin, Dr. Amrendra Kumar Singh, Dr. Satya S. Bulusu, Dr. Anjan Chakraborty, and Dr. Tridib Kumar Sarma for their guidance.

I extend my deep appreciations to my present group members. Mr. Ramesh Reddy B. for helping me during critical organic transformations. I am thankful to Mr. Premansh Dudhe for his assistance during manuscript preparation. I appreciate the efforts of Mr. Amit Pandit for performing the *in silico* studies. I am grateful to Ms. Mena Asha Krishnan for helping me in biological studies and last but not the least Mr. A.V.R. Krishna Rao for his cooperation during my research work. I extend my thanks to Mr. Bishnubasu Giri, Ms. Jyotsana Tyagi for their generous help and co-operation to make my work successful.

I would like to thank the Ministry of Human Resource and Development (MHRD), New Delhi for a research fellowship.

I am thankful to Mr. Kinney Pandey, Mr. Ghanshyam Bhavsar and Mr. Manish Kushwaha, Ms. Sarita Batra, and Mr. Rameshwar Dauhare for their technical help and support. I would also like to acknowledge Ms. Anjali Bandiwadekar, Mr. Rajesh Kumar, other library staffs, and non-technical staff of IIT Indore for their constant help, during my Ph.D. programme.

I would personally like to extend my admiration to all my friends during various times of my Ph.D. period, Dr. Dnyanesh Rasale, Dr. Debashish Majee, Dr. Soumen Biswas, Dr. Shivendra Singh, Dr. Thaksen Yadav, Dr. Biju Majumdar, Dr. Kuber Singh Rawat, Mr. Sagar Biswas, Dr. Rohit Rai, Mr. Soumya Kanti Dey, Mr. Sayan Maity, Ms. Mitali Chhabra, Dr. Vikas Sharma, Dr. Ankur Saxena, Dr. Mayur Sawant, Dr. Aniket Kulkarni, Dr. Piyush Joshi who were always there to support and never let me down during these PhD days.

I feel extremely grateful to Dr. Pranab Ghosh who inspired me to opt for synthetic organic chemistry as a domain for higher studies. I could never achieve anything without his guidance, blessings, and support.

Most importantly, none of this would have been possible without the support of my family, and I deeply express my love and gratitude to my lovable grandparents (late Mr. Sudhir Ranjan Sengupta and late Mrs. Renuka Sengupta), my parents (Mr. Saran Sengupta and Mrs. Krishna Sengupta), my aunts (Ms. Supriti Sengupta and late Mrs. Arati Gupta), my elder sister (Mrs. Susmita Goswami) my elder brother and sister-in-law (Mr. Satyaki Sengupta, Mrs. Tapanwita Sengupta) for their support throughout my Ph.D. and in my life.

SAGNIK SENGUPTA

DEDICATED TO MY FAMILY, FRIENDS AND TEACHERS

Abstract

Cancer is the second leading cause of death globally after cardiovascular disease. In 2019, according to the National Centre for Health Statistics report, 606,880 cancer deaths are projected to occur in the United States of America. Over the years, the burden of cancer incidence has shifted to low and middle-income countries especially to India because of relatively low cancer awareness, inadequacy in the availability of early diagnostic tools and lack of affordable curative services compared to patients in high income-countries. Among all the cancers, prostate cancer (PCa) is the second most diagnosed cancer in men in Western countries. A recent report reveals that approximately 174,650 new PCa cases were registered and 31,620 estimated deaths took place in the year 2019 in the Western countries. The epidemiology of PCa in India as per Population Based Cancer Registries (PBCRs) reveal that the incidence of PCa is high in metropolitan cities like Delhi, Kolkata, Pune, etc. The cumulative cost to treat PCa is very high and advanced stages of PCa drastically affect the quality of life due to bone disintegration, pain, obstruction of urination, and erectile dysfunction along with other health issues. The treatment of advanced stages of PCa is difficult because of metastasis to distant organs. Therefore, early detection of the disease plays a pivotal role to constitute an effective treatment strategy for lowering mortality. Recently, the development of targeted diagnostic and therapeutic tools for a lethal disease like cancer has gained significant attention in the field of medicinal chemistry research.

Prostate-specific membrane antigen (PSMA), also known as glutamate carboxypeptidase II (GCPII), or N-acetyl-aspartyl-glutamate peptidase I (NAAG peptidase), is a useful biomarker for imaging and therapy of PCa. PSMA is an integral binuclear zinc peptidase transmembrane protein predominantly expressed in the epithelial cells of the malignant prostate gland. The biomarker belongs to a family of cell surface transmembrane proteins over-expressed during prostate carcinoma and exploited to deliver chemical tools for the early diagnosis of prostate

malignancy. PSMA also found to be expressed in the neovasculature of solid tumors in brain, bladder, and breast, etc., PSMA undergoes internalization or endocytosis, after binding with inhibitors or ligands and targeted bioconjugates, through clathrin-coated pits and quickly recycles to the cell surface to repeat the rounds of internalization. Collectively, these unique qualities make PSMA an interesting as well as an excellent candidate for applications in bioimaging and tumor-targeted drug delivery. Various efforts have been made to design and synthesize low molecular weight inhibitors or ligands for targeting PSMA.

The main objective of the thesis work is to design and synthesize new small molecular weight ligands and subsequently transform them to potential diagnostic and therapeutic bioconstructs for early diagnosis and treatment of $PSMA^+$ cancers. The thesis work comprises of following chapters:

1. Aminoacetamides: A new class of small molecule inhibitors or ligands for prostate specific membrane antigen expressing ($PSMA^+$) cancers
2. Synthesis of fluorescent and radiopharmaceutical bioconjugates using aminoacetamide as targeting ligand for detection of prostate specific membrane antigen expressing ($PSMA^+$) cancers
3. Design, synthesis and biological evaluation of novel thiourea derivatives as small molecule inhibitors for prostate specific membrane antigen
4. Tyrosine-based asymmetric urea ligand for prostate carcinoma: Tuning biological efficacy through *in silico* studies
5. Novel solid-phase strategy for the synthesis of ligand-targeted fluorescent-labeled chelating peptide conjugates as a theranostic tool for cancer

1. **Aminoacetamides: A new class of small molecule inhibitors or ligands for prostate specific membrane antigen expressing ($PSMA^+$) cancers**

In this chapter, mimicking the structural features of N-acetyl-aspartyl-glutamic acid (NAAG), a natural substrate of PSMA, we have designed and synthesized a new class of homing ligands, aminoacetamides, to evaluate their potency as inhibitors of PSMA. Glutamate carboxypeptidase II (GCPII) receptor complexed with a urea-based inhibitor, JB7, (PDB-4NGM) was retrieved from the protein data bank, and docking studies were performed by Surflex Dock method using Sybyl X2.1.1 software to analyze the binding interactions of this new class of inhibitor at the active site of PSMA. The study reveals that the inclusion of a methylene carbon unit after the amide functionality in NAAG generates new hydrogen bonding interactions with the glutamic acid side chain in the binding pocket of PSMA. Observing this phenomenon, we have designed a small library of inhibitors containing the aminoacetamide structural moiety. A methodical *in silico* docking study has been performed for each derivative to understand the structural requirements necessary for optimum interactions in the PSMA binding pockets. Moreover, a novel and simple chemical methodology has been designed to synthesize aminoacetamide analogs and was characterized thoroughly by various spectroscopic techniques.

Finally, the most promising aminoacetamide derivatives based on docking scores have been further evaluated through fluorescence-based PSMA enzyme inhibition assay, and half-inhibitory concentrations (IC_{50}) were determined.

2. **Synthesis of fluorescent and radiopharmaceutical bioconjugates using aminoacetamide as targeting ligand for detection of prostate specific membrane antigen expressing ($PSMA^+$) cancers**

In this chapter, we have synthesized PSMA targeted bioconstructs as diagnostic tools for the detection of $PSMA^+$ cancers using the most potent glutamic acid based aminoacetamide derivative as the targeting

moiety. The PSMA targeted rhodamine B conjugate was evaluated *in vitro* on malignant cell lines over-expressing PSMA biomarker (LNCaP; $PSMA^{+}$) and on negative cell lines lacking PSMA (PC-3; $PSMA^{-}$) protein to prove high specificity of the bioconjugate in drug-delivery applications.

The PSMA targeted radionuclear chelating conjugate will be utilized to deliver radionuclides such as ^{99m}Tc for the detection of prostate cancer using scintigraphy technique.

3. Design, synthesis and biological evaluation of novel thiourea derivatives as small molecule inhibitors for prostate specific membrane antigen

In this chapter, we have performed *in silico* docking studies and observed the scope of modifications in designing new small molecule inhibitors or targeting ligands for PSMA. Envisaging PSMA's bimetallic zinc protein structure, we have designed glutamate-thiourea-heterodimers which may improve the affinity of small molecule ligands at the PSMA cavity due to sulphur's superior electron donating ability in comparison to oxygen. We have also predicted that the introduction of branched chain amino acids and aryl groups can increase the hydrophobic interactions at the binding site of PSMA significantly. Several carboxylic acid protected thiourea derivatives have been synthesized by a novel one-pot synthetic methodology using bis(benzotriazolyl)methanethione as an efficient thiocarbonyl transfer agent. Among the designed thiourea inhibitors, according to molecular docking studies, glutamate acid-based thiourea derivative has shown the highest binding affinity for PSMA protein. In order to experimentally evaluate the binding affinity of the glutamic acid-based thiourea ligands, the most potent thiourea derivative was radiolabelled with ^{99m}Tc-radioisotope by attaching a chelating moiety via a peptidic spacer.

In vitro binding affinity analysis have been performed on cell lines over-expressing PSMA biomarkers (LNCaP and 22RV1). Competition experiments, by blocking the PSMA receptors with a known high-

affinity ligand such as 2-phosphonomethyl pentanedioic acid (2-PMPA), have been carried out to prove the selectivity of the newly synthesized PSMA targeted radiotracer conjugate.

4. Tyrosine-based asymmetric urea ligand for prostate carcinoma: Tuning biological efficacy through *in silico* studies

In this chapter, a new low molecular weight ligand, (*S*)-2-(3-((*S*)-1-carboxy-2-(4-(carboxymethoxy)phenyl)ethyl)ureido)pentanedioic acid (CYUE) has been designed by performing extensive *in silico* docking studies of GCPII protein complexed with a known urea-based inhibitor, JB7, (PDB-4NGM). Guided by structure-activity relationships studies, we have modified phenolic –OH group of tyrosine-glutamic acid-based urea moiety to obtain a more potent ligand or inhibitor with high predicted activity and affinity. The targeting ligand has been fluorescently labeled with rhodamine B via a peptidic spacer using solid phase peptide synthesis chemistry and selectively targeted to $PSMA^{+}$ cancer cells.

The binding affinity of the PSMA targeted CYUE rhodamine B conjugate was determined to be 88 nM using Fluorescence Activated Cell Sorting (FACS) technique in LNCaP cells. The cancer cell uptake was further examined by performing *in vitro* studies using laser scanning confocal microscopy on $PSMA^{+}$ (LNCaP) and $PSMA^{-}$ (PC-3) cell lines.

5. Novel solid-phase strategy for the synthesis of ligand-targeted fluorescent-labeled chelating peptide conjugates as a theranostic tool for cancer

In this chapter, we have developed a novel synthetic strategy for building new bioconstructs, with several components, in a continuous process without the isolation of any of the intermediates. The various components that are assembled include the cell surface protein recognition ligand, a peptide spacer for enhanced solubility and binding affinity, a fluorescent tag for tissue staining and a chelating core to tether diagnostic or therapeutic cargos. This goal is smoothly

achieved, in high chemical yield and purity, by strategically introducing differentially protected dibasic amino acids such as lysine whose α- and ε-amino groups are protected as base labile Fmoc and trifluoroacetyl (Tfa) protecting groups, respectively, during the peptide conjugate synthesis. The whole concept is successfully demonstrated using commercially available and less-expensive cysteine-labeled 2-chlorotrityl resin. The methodology is found to be general and can be significantly useful for acid-sensitive resins that contain acid-labile orthogonal amino acids with 4-methoxytrityl (Mmt) and 4-methyltrityl (Mtt) protecting groups.

The newly synthesized bioconjugates, that can selectively target $PSMA^+$ and FR^+ cancers, were further evaluated by performing *in vitro* studies using laser scanning confocal microscopy on $PSMA^+$ LNCaP cells, FR^+ epithelial CHO-β cells and $PSMA^-$, FR^- PC-3 cells. *In vitro* specificity of bioconjugates was further examined by prior incubation of LNCaP cells and CHO-β cells with a 100-fold excess of 2-PMPA and folic acid to block PSMA and folate receptors, respectively. Blocked LNCaP and CHO-β cells display minimal uptake of bioconjugates, confirming the specificity of the delivered bioconjugates.

List of Patent and Publications

1. Chelvam V., **Sengupta S.**, Krishnan M.A., Pandit A. (2018), New small molecule inhibitors/ligands for early diagnosis and therapy of prostate specific membrane antigen ($PSMA^{+}$) cancers and neurodegenerative diseases, Application No. 201821044594, Indian Patent.

2. **Sengupta S.**, Krishnan M.A., Dudhe P., Reddy R.B., Giri B., Chattopadhyay S., Chelvam V. (2018), Novel solid-phase strategy for the synthesis of ligand-targeted fluorescent-labelled chelating peptide conjugates as a theranostic tool for cancer, Beilstein J. Org. Chem., 14, 2665–2679 (DOI: 10.3762/bjoc.14.244). (Impact Factor: 2.762)

3. **Sengupta S.**, Krishnan M.A., Chattopadhyay S., Chelvam V. (2019), Comparison of prostate specific membrane antigen ligands in clinical translation research for diagnosis of prostate cancer, Cancer Reports, 2, 1–22 (DOI: 10.1002/cnr2.1169).

4. **Sengupta S.**, Krishnan M.A., Pandit A., Dudhe P., Sharma R., Chelvam V. (2019), Tyrosine-based asymmetric urea ligand for prostate carcinoma: Tuning biological efficacy through *in silico* studies, Bioorg. Chem., 91, 1–13 (DOI: 10.1016/j.bioorg.2019.103154). (Impact Factor: 3.926).

5. Reddy R. B., Dudhe P., Chouhan P., **Sengupta S.**, Chelvam V. (2018), Synthesis of tubuphenylalanine and epi-tubuphenylalanine via regioselective hydroboration-oxidation of 1,1-substituted amino alkenes, Tetrahedron, 74, 6946–6953 (DOI: 10.1016/j.tet.2018.10.024). (Impact Factor: 2.645)

6. Krishnan M.A., **Sengupta S.**, Chelvam V. (2018), Preparation of ligand targeted drug conjugates for cancer therapy and their evaluation in vitro, Curr. Protoc. Chem. Biol., 25, 1–25 (DOI: 10.1002/cpch.50). (Impact Factor: 7.0)

7. Pandit A., **Sengupta S.**, Krishnan M.A., Reddy R. B., Sharma R., Chelvam V. (2018), First report on 3D-QSAR and molecular dynamics based docking studies of GCPII inhibitors for targeted drug delivery applications, J. Mol. Struct., 1159, 179–192 (DOI: 10.1016/j.molstruc.2018.01.059). (Impact Factor: 2.011)

8. Krishna Rao A. V. R., Reddy R. B., **Sengupta S.**, Chelvam V. (2018), Efficient turn-on nanosensor by dual emission-quenching mechanism of functionalized Se doped ZnO nanorods for mercury (II) detection, Appl. Nanosci., 00, 1-15 (DOI: 10.1007/s13204-018-0875-9). (Impact Factor: 2.951)

9. **Sengupta S.**, Krishnan M.A., Pandit A., Chelvam V. (2019), A new class of thiourea derivatives for diagnosis of prostate cancer (Manuscript under preparation).

10. **Sengupta S.**, Krishnan M.A., Pandit A., Chelvam V. (2019), Aminoacetamides, a new class of inhibitors for early diagnosis of neurodegenerative diseases (Manuscript under preparation).

TABLE OF CONTENTS

List of Figures

Chapter 1 Introduction

Chapter 2 Aminoacetamides: A New Class of Small Molecule Inhibitors/Ligands for Prostate Specific Membrane Antigen Expressing ($PSMA^{+}$) Cancers

Chapter 3 Synthesis of Fluorescent and Radiopharmaceutical Bioconjugates using Aminoacetamide as Targeting Ligand for Detection of Prostate Specific Membrane Antigen Expressing ($PSMA^+$) Cancers

Chapter 5 Tyrosine-based Asymmetric Urea Ligand for Prostate Carcinoma: Tuning Biological Efficacy through *in silico* Studies

List of Tables

Chapter 1 Introduction

Chapter 2 Aminoacetamides: A New Class of Small Molecule Inhibitors/Ligands for Prostate Specific Membrane Antigen Expressing ($PSMA^+$) Cancers

Chapter 4 Design, Synthesis and Biological Evaluation of Novel Thiourea Derivatives as Small Molecule Inhibitors for Prostate Specific Membrane Antigen

Chapter 5 Tyrosine-based Asymmetric Urea Ligand for Prostate Carcinoma: Tuning Biological Efficacy through *in silico* Studies

LIST OF SCHEMES

Chapter 5 Tyrosine-based Asymmetric Urea Ligand for Prostate Carcinoma: Tuning Biological Efficacy through *in silico* Studies

Chapter 6 Novel Solid Phase Strategy for Synthesis of Ligand Targeted Fluorescent Labelled Chelating Peptide Conjugates as a Theranostic Tool for Cancer

ACRONYMS

Abbreviations used for amino acids, peptides, derivatives, substituents, reagents, etc. are largely in accordance with the recommendations of the IUPAC-IUB commission on Biochemical Nomenclature, 1974, Pure and Applied Chemistry, 40, 315-331. All amino acids are in *L*-configuration. Standard three letter code is used for all amino acids. Additional abbreviations used in this thesis are listed below.

ACN	Acetonitrile
Ala	Alanine
Boc	*tert*-butyloxycarbonyl
Cys	Cysteine
$CDCl_3$	Chloroform-d
DCM	Dichloromethane
DCC	Dicyclohexylcarbodiimide
DCU	Dicyclohexylurea
DMF	Dimethyl Formamide
DIPEA	Diisopropylethyl amine
EDT	Ethanedithiol
EtOAc	Ethyl Acetate
ESI-MS	Electrospray Ionization Mass Spectrometry
FTIR	Fourier Transform Infrared
Fmoc	Fluorenylmethyloxycarbonyl
Gly	Glycine
HPLC	High-Performance Liquid Chromatography
HCl	Hydrochloric Acid

Leu	Leucine
Lys	Lysine
MeOH	Methanol
Me	Methyl
M	Molar
N	Normal
NaCl	Sodium Chloride
$NaHCO_3$	Sodium Hydrogen Carbonate
Na_2SO_4	Sodium Sulphate
NMR	Nuclear Magnetic Resonance
Ph	Phenyl
pH	The negative logarithm of hydronium-ion concentration ($-\log_{10}[H_3O^+]$)
Phe	Phenylalanine
PyBOP	Benzotriazol-1yl-oxytripyrrolidinophosphonium hexafluorophosphate
THF	Tetrahydrofuran
TFA	Trifluoroacetic Acid
TLC	Thin Layer Chromatography
TMS	Tetramethylsilane
TIPS	Triisopropylsilane

NOMENCLATURE

λ	Wavelength
ε	Extinction coefficient
α	Alfa
β	Beta
γ	Gamma
π	Pi
Å	Angstrom
nm	Nanometre
µm	Micrometre
cm	Centimetre
°	Degree
°C	Degree Centigrade
mmol	Millimole
mL	Millilitre
µL	Microlitre
a. u.	Arbitrary Unit

Chapter 1

Introduction

1.1 Cancer and statistics

The high-quality health care service evolving in the 21st century is not merely emphasizing on the development of a cure for a disease. Instead, it's a complete health care system, effectively coordinated with technology, ensuring a patient or the consumer of the system to benefit significantly by enjoying optimal health. The health care professionals are gathering systematic information about the progression of communicable and non-communicable diseases to establish practical guidelines for early diagnosis to prevent the onset of lethal diseases.

Cancer is a disease in which a group of abnormal cells proliferates in an uncontrolled manner. The initiation and progression of cancer depend on two factors:

a) External or environmental factors, e.g., tobacco, chemicals, and radiations.
b) Internal factors, e.g., inherited mutations, hormones, and immune conditions.

These factors may act together or solely responsible for abnormal cell behavior and excessive proliferation. Further, these cells grow in masses and finally spread to other distant organs in the body which is known as cancer metastasis.

Cancer is the second leading cause of death in western countries after cardiovascular disease.[1] GLOBOCAN 2018 report estimated that there were approximately 18.1 million new cancer cases and 9.6 million cancer deaths in a single calendar year of 2018, worldwide.[2] Lung cancer is the most commonly diagnosed cancer and the leading cause of death associated with this disease followed by breast, prostate, colorectal cancer, etc. Over the years the burden of cancer incidence has shifted to low-income and middle-income countries, including India due to limited

cancer awareness and poor prognosis. The inadequate early diagnosis facilities and lack of affordable curative services have been primarily translated into a rapid increase in cancer mortality rate. Moreover, the epidemiological transition increased life expectancy, and unhealthy lifestyles have brought significant changes in cancer statistics.

Table 1.1 GLOBOCAN 2018: Incidence, mortality, and prevalence by cancer site in India[3]

Cancer site	No. of new cases registered (% of all sites)	No. of deaths (% of all sites)
Breast	162,468 (15.62%)	87,090 (12.19%)
Oral cavity	119,992 (11.54%)	72,616 (10.16%)
Cervix uteri	96,922 (9.32%)	60,078 (8.41%)
Lung	67,795 (6.52%)	63,475 (8.88%)
Prostate	25,696 (2.47%)	17,184 (2.40%)

India is a developing country, and with the limited resources available, the management of cancer has become challenging. 80% of the registered cancer cases in India have already been advanced to critical stages. Therefore, early diagnosis may play a decisive role to keep a check on cancer-related morbidity. During the last three decades, the cancer burden has just doubled in India, and unfortunately, the healthcare facilities have merely improved. The most frequent cancer sites (according to the total number of cases) in India are breast, cervical, oral cavity, lung, and colorectal. These top five account for around fifty percent of all cancers. According to the GLOBOCAN, over 1.1 million new cancer patients were registered and, 0.78 million people died of cancer in 2018 in India.[3]

1.2 Conventional cancer therapy

The above statistical data implies that the lack of early diagnostic facilities and accurate curative measures are the biggest hurdles in our fight against cancer. It is evident that conventional approaches to deal with this deadly disease meet neither the contemporary requirements nor the patients'

expectations. Till date, in India cancer therapy relies mostly on the conventional approach of surgery followed chemo or radiation therapy.

1.2.1 Surgery

It is a widespread belief that surgery is the best method to treat cancer, and mainly the root of this belief is since the beginning of 19th century when the standard treatment for breast cancer was its radical resection or mastectomy. Only in the last few decades, with new scientific data in hand, health professionals started accepting that the tumour is not an isolated organ disease, rather it is a symptom of the chronic disease, and logically, removal of a symptom does not lead to curing the disease at all. In the early stages of the disease with no metastases to the distant organs, optimal results can be expected from surgical treatment. Unfortunately, most of the cancers are diagnosed only in the advanced stages; therefore, complete cure of the disease is far from reality by performing surgery alone. Single tumour cells or micro-metastases at the early stage of the disease are not identifiable through conventional diagnostic methods, and during surgery, these small lesions escape attention and can trigger the recurrence of the disease post-treatment. Radical surgeries are associated with several risk factors such as mixing of cancer cells in the blood stream, anaesthetic complications, infections and suppression of the immune system.[4,5]

Furthermore, cancerous tissues predominantly grow in an irregular shape; hence their volume is difficult to estimate from a linear measurement resulting in poor reproducibility of tumour measurements. Differential growth of tumour components and the structure of surrounding healthy tissues frequently cause them to grow anisotropically, which further confounds uni-dimensional measures of growth and response. Thus, molecular or bio-imaging agents which can differentiate between cancerous and healthy tissues would be immensely helpful during blind radical surgeries.

1.2.2 Radiotherapy

Radiotherapy or treatment with ionizing radiation is another primary method in conventional cancer therapy which treats 30% to 40% of the patients with cancer.[6] The radiation damages the genetic material of the tumour cell thereby preventing its growth and proliferation. Unfortunately, surrounding healthy tissues are also severely affected by radiation; therefore, the use of radiotherapy has limited applications.[7]

The recent success with targeted radiation therapy has opened an entirely new avenue of cancer treatment in which higher dose of radiations are explicitly delivered to the malignant tissues expressing certain biomarkers, and healthy tissues are not affected less. More sophisticated targeted bio-constructs are under development for a variety of cancer sites including prostate, brain, and lung. The clinical success of these therapeutic warheads will decide the future of radiotherapy.

1.2.3 Chemotherapy

In chemotherapy, cytotoxic drug molecules are used to kill cancer cells. These drugs stop or slow down the growth of rapidly dividing cells. Contrary to surgery and radiotherapy, the effect of chemotherapy is not localized, and it works throughout the body. Hence, it is effective for metastasized cancer cells as well. There are two chemotherapeutic modules available:

- In neoadjuvant chemotherapy, tumour lesions are shrunk down before surgery and radiation therapy.
- In adjuvant chemotherapy, residual cancer cells are destroyed after surgery and radiation therapy.

Regrettably, the conventional chemotherapeutic agents cannot distinguish between healthy dividing cells and malignant cells, which is the root cause of severe side effects including nausea, anaemia, peripheral neuropathy, fatigue, and myelosuppression.[8–13]

1.3 Targeted delivery of cargos (cytotoxic drugs, diagnostic agents, radioisotopes and nanoparticles)

The unsatisfactory results associated with conventional treatment, off-target toxicities, and poor prognosis has led to the development of a newly refined approach called targeted delivery. In this approach, therapeutic or diagnostic modalities are delivered by exploiting targeting or homing ligands that bind selectively to the biomarkers over-expressed in the diseased cells. Receptor-mediated delivery of cargos, using specific ligand with a high degree of affinity for its target,[14] can deliver cargos selectively to cancer site, while avoiding collateral damage to healthy cells; thus, it minimizes off-site activity (Figure 1.1).

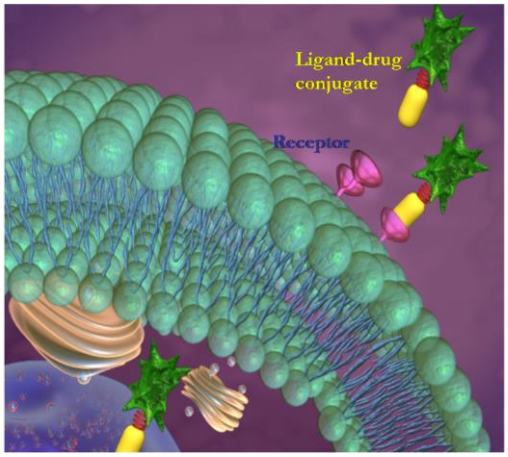

Figure 1.1 A schematic representation of molecular-targeted and ligand-targeted therapeutic modalities.[14]

The targeted delivery is executed mainly by using either monoclonal antibodies targeted at specific antigens localized on the cell surface[15–17] or small molecule ligands targeted at transmembrane proteins to deliver attached cargo selectively to diseased cells.[18]

1.4 Biomarkers and diagnosis of cancer

Unification of molecular biology and *in vivo* imaging resulted in the advent of a new discipline popularly known as ‘molecular imaging’ in the field of medical diagnosis. It allows the visualization of the cellular

functions and dynamic molecular processes in living cells non-invasively. The unique ability of this new technique allows it a multifarious entry into the field of disease diagnosis, especially in cancer, inflammatory, neurological and cardiovascular diseases. Conventional imaging techniques such as X-ray, ultrasound, computed tomography (CT), and magnetic resonance imaging (MRI) can detect only morphological and anatomical changes in organs and tissues and often fail to distinguish abnormalities arising due to inflammation and pathological diseased states.[19] Development of targeted imaging tools currently receiving significant attention in medicinal chemistry.[20–23] Most of the abnormal cells express or over-express special cell surface proteins known as "biochemical markers" that have a high affinity for their natural inhibitors or ligands. Therefore, the binding of radio-labelled or fluorescent inhibitors or ligands to the over-expressed biomarkers identifies diseased cells and distinguishes them from normal and healthy tissues. Based on this principle several new methods were discovered for molecular imaging applications. Among those methods, most commonly described modalities include magnetic resonance spectroscopic imaging (MRSI),[24] positron emission tomography (PET),[25] single photon emission computed tomography (SPECT),[26] optical and radio-nuclear imaging.[27–28] Separately or in combination with conventional tools, these techniques are employed to understand the cellular processes responsible for the onset and progression of the diseases and for the evaluation of new cancer imaging agents and drug candidates.

1.5 Molecular imaging probes

In the past few decades, technological advances in imaging dramatically improved the diagnosis of disease states.[29] The molecular imaging technique is recognized as the interface between biology, chemistry, computer imaging, and medicine.[30] It also enhances the ability of the 'clinicians' to screen the disease state as well as help them to monitor the

result of treatment. Molecular imaging techniques require special instrumentation, used alone or in combination with targeting imaging probe to visualize tissue characteristics and biochemical markers. Molecular imaging probe consists of a targeting moiety, a signal agent and a linker which connect both the targeting moiety and signal agent (Figure 1.2).[31]

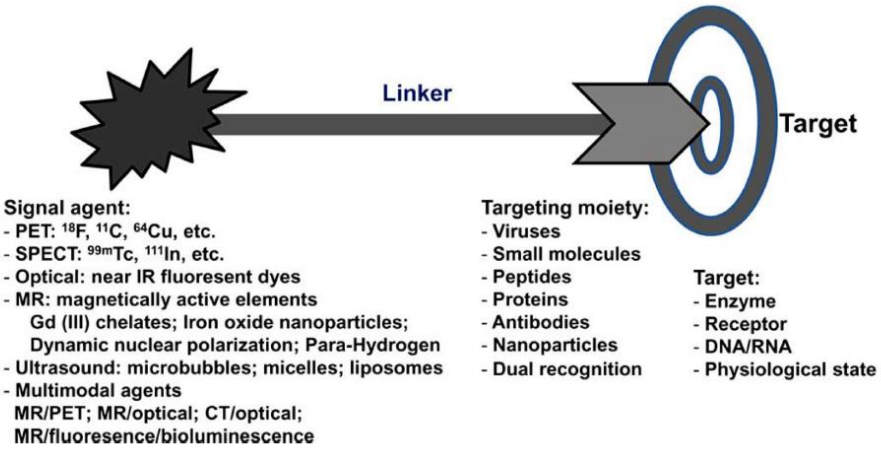

Figure 1.2 Schematic representation of molecular imaging probes

1.5.1 Characteristics of molecular imaging probes

A desirable molecular imaging probe with clinical translation potential is expected to have the following unique characteristics:

- High binding affinity to the target. Sufficient accumulation of the molecular imaging agent to the target tissue within a limited circulation time frame is a primary prerequisite for an ideal imaging tool. The association rate of the probe to the target should be higher than the dissociation rate.

- High specificity to target. The molecular imaging probe should be specific towards its target (enzyme, biomarker, transporter, etc.) that in turn simplify the quantification analysis of imaging outcome.

- High sensitivity. The molecular imaging probe must be highly sensitive so that the minimal amount of probe is required to obtain a good quality image.

- High contrast ratio. The inference derived from a low contrast image is not conclusive and sometimes misleading. Therefore, high contrast images with high signal to noise ratio are relevant to ensure appropriate interpretation of the pathological disease state.

- High stability *in vivo*. The maintenance of the architecture of the imaging probe inside a living body is the most challenging task. Presence of various enzymes or proteases in the blood serum may degrade the imaging probe. So, the quality of the image, as well as quantitative interpretation of the diseased states, predominantly depends on the stability of the imaging probe *in vivo*.

- Low immunogenicity and toxicity. Generally, molecular imaging probes are administered in low dose so that there are no profound pharmacological effects in the body. However, the biological effect of the probe after administration must be monitored closely to avoid any human immunoreactions.

- Production and economic feasibility. Low cost and easy availability of the molecular imaging probe is required for their wide distribution and routine chemical use.

1.5.2 Types of molecular imaging probes

There are several imaging modalities available for molecular imaging, including X-ray computed tomography imaging (CT), optical imaging (OI), radionuclide imaging (involving PET and SPECT), ultrasound (US) imaging and magnetic resonance imaging (MRI). Among these, targeted radionuclide imaging and optical imaging techniques have grabbed much attention for early disease diagnosis.

1.5.2.1 Radionuclide imaging probes

Radionuclide imaging techniques like PET and SPECT are the earliest modality available for cancer imaging. High sensitivity and quantifiability are the main advantages of radionuclear imaging. This is one of the main reasons for these modalities to be extensively used in clinical and preclinical research.[32] Over the past decades, with the development of radiochemistry, various radiotracers with high specificity and affinity have been discovered, and several preclinical and clinical examinations confirmed their utility as molecular imaging probes.

PET is based on the detection of high energy photon pairs generated during the collision of a positron and an electron, from which a three-dimensional image was constructed through computer-aided analysis.[33] PET imaging agents contain positron emitting radio-nuclides[34] like ^{18}F, ^{64}Cu, and ^{68}Ga. Clinically, ^{18}F labelled imaging probes, for example, ^{18}F-FDG are useful for cancer diagnosis but non-targeted and lack selectivity.[35] The main advantages of PET imaging probe are unlimited depth penetration and excellent sensitivity. However, high cost, limited availability of PET tracers as well as low spatial resolution are the main drawbacks of this modality. The low spatial resolution can be compensated through multimodal tools like OFI/PET imaging, PET/CT or PET/MRI.

SPECT utilize radionuclides that emit a single γ-ray photon for each nuclear de-excitation event for the construction of three-dimensional images. The common SPECT radioisotopes[36] include ^{99m} Tc, ^{123}I, and ^{111}In. These SPECT tracers have long decay half-lives than those of commonly employed PET tracers. Therefore, they are more convenient to transport for medical use. The resolution of PET and SPECT techniques depends both on the affinity of the homing moiety (antibody or small molecule ligand) to the receptor as well as on the energy and mode of

generation of the decay photons from the respective radioisotopes by a nuclear event. In the case of SPECT, a γ-ray is emitted from the decaying radioisotope accumulated within the targeted tissues whereas, in the case of PET, two annihilation photons are generated when a positron emitted by the decaying PET radioisotope collides with an atomic electron in the annihilation event. PET has a superior spatial resolution because of the emission of two collinear photons during each annihilation event whereas, in SPECT, only single γ-ray photon is generated for each nuclear de-excitation event. Therefore, SPECT is inherently less sensitive than PET, but cost-effectiveness, as well as clinical availability, are the main advantages of this modality.

1.5.2.2 Optical or fluorescent imaging probes

Over the last decade, we have witnessed significant improvements in the optical imaging modalities. Optical imaging modality is non-invasive, allows the clinician to visualize and monitor the patient's response to therapy in real time.[37–41] Generally, a fluorescent probe consists of a recognition moiety or ligand conjugated with a fluorophore through a peptidic spacer that targets a biomarker over-expressed during diseased state. The bioconjugate generates a signal from the targeted site. In oncology, the identification of tumour boundaries is indispensable for surgical resection and accurate removal of cancerous tissue. Precise resection of malignant tissue will reduce the chance of local recurrence. However, during surgery, it is difficult for surgeons to distinguish between malignant and normal tissues by visual inspection. MRI, PET, CT can be used to overcome this problem partially but using these modalities during surgery is difficult due to instrumentation complexity (e.g., MRI) and potential hazards (e.g., radioactivity of PET tracers).[42,43] Another major drawback is that these modalities are unable to identify microscopic tumour nodules which may cause a recurrence of malignancy later.

Intraoperative fluorescence-guided surgery is a relatively new approach in medical science.

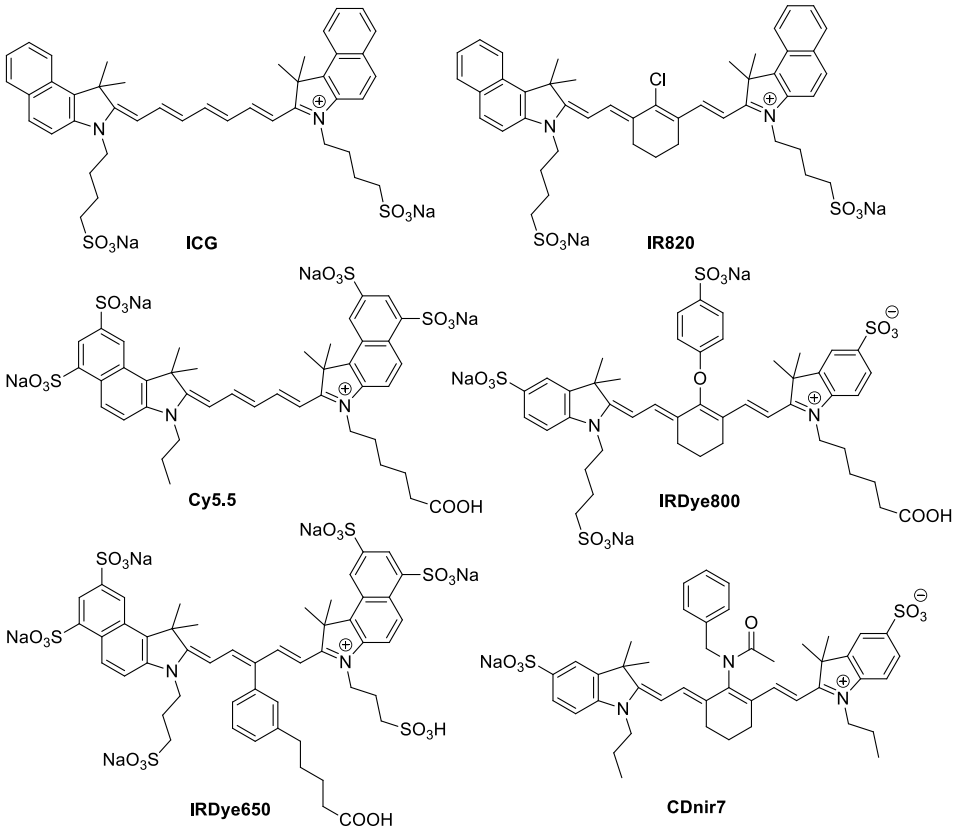

Figure 1.3 Representative NIRF dyes used in dual-modality optical fluorescence imaging

Optical imaging relies on fluorescent contrast agents, offering clear advantages such as non-invasiveness, real-time imaging, high resolution in the absence of ionizing radiation and affordable cost.[44] Furthermore, optical imaging probes have other advantages like detection of proximal metastases and assessment of therapeutic responses to treatment.[45] A fluorescent dye with emission in the range of 400–650 nm usually have limited utility for *in vivo* imaging applications due to scattering of light and interferences caused by the auto-fluorescence of endogenous substances (e.g., cytochromes, haemoglobin and water molecules). On the other hand, a fluorescent molecule with an emission range of 650–900 nm

has greater *in vivo* applications due to low background tissue absorption and deeper tissue penetration.[46–49] Some representative NIR dyes used in optical imaging are shown in figure 1.3.

Among them, isocyanine green (ICG) is the only NIR dye which was approved by Food and Drug Administration (FDA) in the United States for clinical use,[50,51] and IRdye800CW has entered clinical trials.[52] Image-guided surgery has been performed with a folate-fluorescein probe on patients with ovarian cancer.[53] Thus, optical imaging systems are potential candidates for clinical translation.

1.6 The prostate cancer

Prostate cancer (PCa) is the second most diagnosed cancer in Western countries. Recent literature report on PCa reveals approximately 174,650 new cases and 31,620 estimated cancer deaths in the Western countries[54] in 2019 making it as a lethal disease with significant health burden on the society. The estimated healthcare cost for treating and maintaining newly diagnosed PCa patients is quite expensive and amounts to 8–10 billion dollars per annum in the USA.[55] Earlier, it was considered that the incidence of PCa in India is far lower as compared to the Western countries. However, due to the increased migration of rural population to the urban areas, changing lifestyles, increased awareness, and easy access to medical facilities, more cases of prostate cancer are being detected. According to demographic analysis, the rate of PCa incidence in India is not far behind from that of the Western world. Population Based Cancer Registries (PBCRs) of India suggest that the incidence of PCa is highest in metropolitan cities like Delhi, Kolkata, Pune etc.[56]

Advanced stages of PCa significantly impact the quality of life due to bone disintegration, pain, obstruction of urination, and erectile dysfunction among other disorders.[57] PCa in its advanced stages tends to metastasize to distant organs and bones which results in cognitive decline, muscle wasting and osteoporosis. Metastatic PCa is difficult to treat. Therefore,

early detection of this disease is necessary for minimizing disease-related morbidity and mortality. The well-known diagnostic methods are based on the triad of digital rectal examination (DRE), blood prostate specific antigen (PSA) measurement, and ultrasound-guided prostate biopsy.[58] However, by DRE, only the most advanced stages of prostate cancer can be detected.[59] The prostate biopsy is expensive and painful.[60] The use of PSA as a diagnostic serum marker still has some drawbacks. It is known that the concentration of this protein in the bloodstream increases during the development of cancer but also secreted as a result of benign prostatic hypertrophy (BPH), prostatitis, or other traumas to prostate cells.[61–62] Although diagnostic techniques like trans-rectal ultrasound together with magnetic resonance imaging (MRI) and computerized tomography (CT) can identify the growth asymmetry and enlargement of prostate gland, these modalities are too expensive and difficult to use on a routine basis. Moreover, it is difficult to distinguish between malignant disease with BPH with the help of CT or MRI scan.[63] As a result, there is an unmet need to develop more specific and effective diagnostic tools for the early detection of PCa. Surgery,[64–65] radiation therapy,[66] hormone administration, and chemotherapy are commonly used to treat this lethal disease. Unfortunately, none of these therapeutic techniques is effective against the metastatic disease, and each technique has several disadvantages that patients often decline their use and side effects associated with those therapeutic strategies often outweigh their benefits.[67,68] Therefore, safer and more potent methods are necessary to detect and treat PCa.

1.7 Importance of prostate specific membrane antigen (PSMA)

Untiring efforts by various researchers across the world have led to the discovery of a unique cancer biomarker called prostate specific membrane antigen (PSMA) that is highly expressed on PCa cells.[69] Unlike PSA, prostate-specific membrane antigen (PSMA), a plasma membrane-

associated protein,[70] is a useful target biomarker for imaging and radiotherapy of PCa. PSMA, which is also known as folate hydrolase 1 (FOLH 1), glutamate carboxypeptidase II (GCPII), or N-acetyl-aspartyl-glutamate peptidase I, NAAG peptidase, is an integral binuclear zinc peptidase membrane protein predominantly localized in the epithelial cells of the prostate gland.[71] The extracellular portion of GCPII folds into three distinct domains: the protease domain (domain I, residues 57–116 and 352–590), the apical domain (domain II, residues 117–351), and the C-terminal domain (residues 591–750) (Figure 1.4). Amino-acid residues from all three domains are involved in substrate recognition. Although the asymmetric unit of the crystal contains a monomer of GCPII, a homodimer is formed through crystallographic two-fold symmetry. It exhibits carboxypeptidase activity by hydrolyzing NAAG into N-acetyl-L-aspartate (NAA) and L-glutamate[72–75] and also acts as folate hydrolase in the membrane brush border of the small intestine.[76–77] Figure 1.4 shows a subunit (in grey) of GCPII, while the other is colored according to organization into three domains.[78] The dark green spheres represent two Zn^{2+} ions, the red sphere represent Ca^{2+} ion near the monomer–monomer interface, whereas the yellow sphere represents chloride ion.

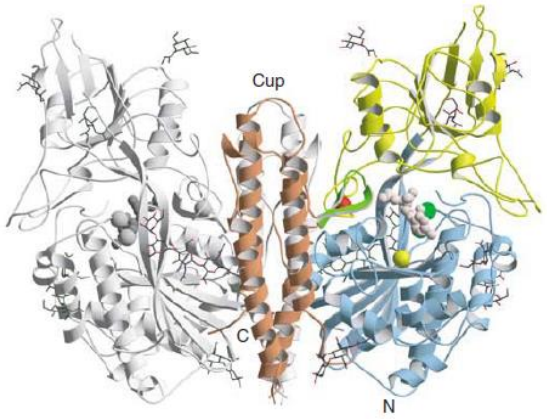

Figure 1.4 Structure of glutamate carboxypeptidase II. Three-dimensional structure of the dimer. One subunit is shown in grey, while the other is

colored according to organization into domains. Domain I, light blue; domain II, yellow; domain III, brown. The dinuclear zinc cluster at the active site is indicated by dark green spheres, the Ca^{+2} ion near the monomer–monomer interface by a red sphere, and the Cl^{-} ion by a yellow sphere.[78]

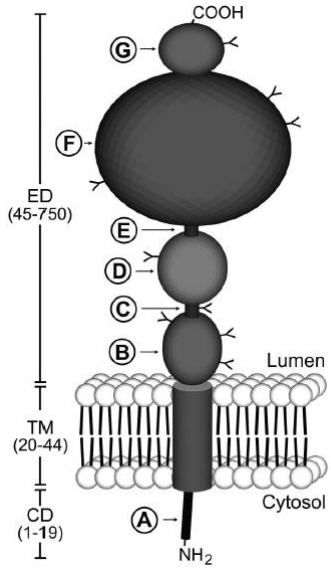

Figure 1.5 Schematic illustration of prostate specific membrane antigen

The schematic illustration shows that PSMA consist of a short NH_2-terminal cytoplasmic domain (CD), a hydrophobic transmembrane region (TM), and a large extracellular domain (ED). The extracellular domain of PSMA is highly glycosylated[79] at nine predicted sites indicated by an alphabet Y (Figure 1.5).

The low expression of PSMA in the normal prostate epithelial cells increases to several folds during high-grade, metastatic and androgen-insensitive prostate carcinoma.[80] The PSMA concentration increases from 0.25 nM to approximately 3.5 nM in PCa patients' biological fluids, including urine. PSMA, a 750 amino acids residue, 90-kDa glycoprotein, is over-expressed on the surface of tumour cells as a non-covalent homodimer in primary (>94.3%) and metastatic (>57.7%) PCa.[81] Elevated PSMA levels is associated with the aggressiveness of tumour growth.

Moreover, PSA is a secretory protein; thus, metastases of PCa cannot be detected by the PSA test.[81,82] On the other hand, metastases can be diagnosed by PSMA imaging as PSMA is a membrane-anchored protein. PSMA can be used for drug targeting applications because it undergoes internalization through clathrin-coated pits and rapidly recycles on the cell surface for additional rounds of internalization.[83] PSMA is also expressed in the neovasculature of many solid tumours but not in the vasculature of healthy tissues.[84–86] Due to the above-given facts, various efforts have been directed to synthesize a variety of low molecular weight inhibitors that can selectively target PSMA.

1.7.1 Biological function of PSMA

In the small intestine, PSMA is known as folate hydrolase 1 (FOLH 1), and it hydrolyzes folyl-poly-γ-glutamate to generate glutamic acid and folate. Folic acid is essential for several functions of our body, it is vital for red blood cells as well as for the synthesis and repair of DNA and RNA. NAAG (N-acetylaspartyl glutamate) is one of the three predominant neurotransmitters found in the central nervous system, and after catalytic hydrolysis, it produces a neurotransmitter called glutamate (Figure 1.6).[87]

Glutamate is a common and abundant excitatory neurotransmitter in the central nervous system; however, excess glutamate can kill or damage neurons resulting in several neurological disorders. Therefore, the balance, which NAAG peptidase contributes to, is quite important. Increased level of PSMA or GCPII has been shown to increase the concentration of glutamate in the extracellular space. GCPII cleaves NAAG into N-acetylaspartate and glutamate (Figure 1.7).

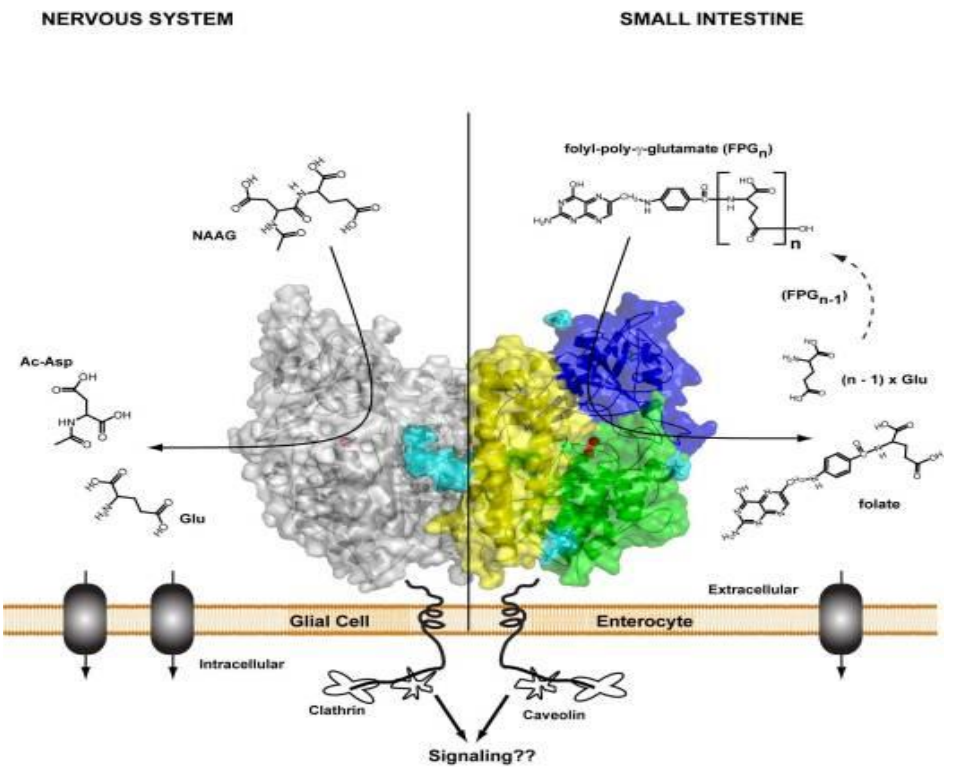

Figure 1.6 Biological function of PSMA.[87]

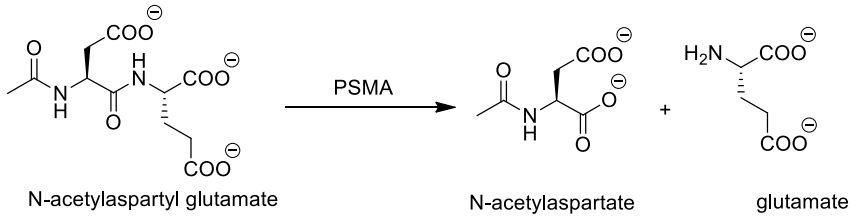

Figure 1.7 Hydrolysis of N-acetylaspartyl glutamate (NAAG).

In the catalytic mechanism discussed here for GCPII, Glu424 acts as a base. An approximate 20 Å deep funnel leads from the surface of GCPII to the active site that contains two zinc ions. The binding of NAAG in the cavity of PSMA is shown in Figure 1.8. The aspartyl residue of the substrate does not interact with S1 pocket (left) whereas glutamate residue interacts with S1' pocket significantly. Lys699 and Tyr700 are called 'glutamate sensor' amino acid residues and are shown in the box.

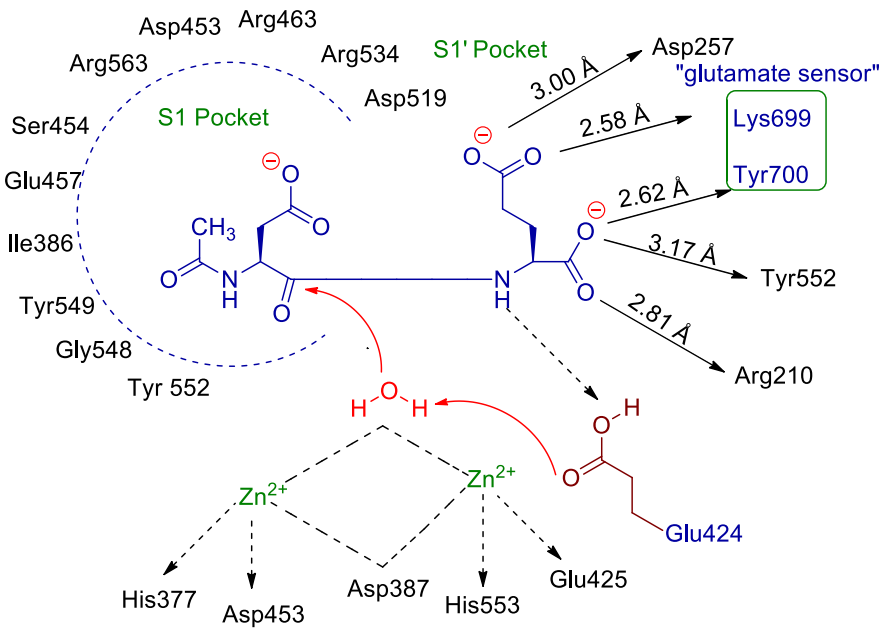

Figure 1.8 Binding site of PSMA.

Glu424 participates in the hydrolysis of NAAG substrate. In the glutamate complex, that is, in the free state of the catalytic centre, one of its carboxylate oxygens is hydrogen-bonded (2.56 Å) to the water molecule bridging the two zinc ions, whereas the other interacts with the free amino group of the bound glutamate, the product of the cleavage reaction. The first step of the catalytic reaction is the activation of the central nucleophile, HO–H, with the help of a base, Glu424. There is a formation of hydroxyl ion which acts as a nucleophile to attack the peptide bond of the substrate at the carbonyl group of the aspartyl residue of NAAG. Proton gets transported by Glu424 to the amino group of leaving product, glutamate. Mimicking the structure of NAAG few inhibitors have been designed for PSMA.

1.8 Reported inhibitors for PSMA

Currently, ^{111}In-labeled capromab pendetide (ProstaScint, Cytogen) is the only U.S. Food and Drug Administration approved radiopharmaceutical for imaging prostate cancer.[88] However, this antibody-based agent has had

limited clinical use due to its slow distribution and clearance.[89] Recent studies revealed that low molecular weight ligands could also be used for delivering imaging as well as therapeutic cargos selectively to malignant tissues. Literature reports suggested that many different scaffolds are available for inhibition of PSMA.[90,91] Some of these PSMA scaffolds have been radio-labelled and adapted for imaging of prostate cancer in preclinical trials.[92–99] These scaffolds can be categorized into three major class: (i) glutamate-urea heterodimers,[92–96,99] (ii) glutamate containing phosphoramidates[97] (iii) 2-(phosphophenylmethyl)pentanedioic acid.[98]

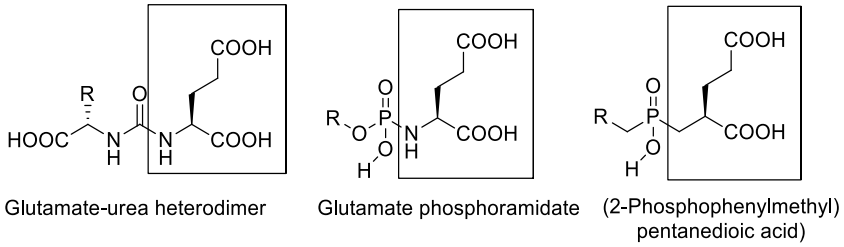

Figure 1.9 Structural scaffolds for PSMA inhibitors.

Among these small molecule inhibitors glutamate-urea heterodimer scaffolds grab the major attention after the first promising results obtained with *N*-[*N*-[(*S*)-1,3-dicarboxypropyl]carbamoyl]-*S*-[^{11}C]methyl-*L*-cysteine ([^{11}C]DCMC) and *N*-[*N*-[(*S*)-1,3-dicarboxypropyl]carbamoyl]-*S*-3-[^{125}I]iodo-L-tyrosine ([^{125}I]-DCIT) imaging agents.[100] Presently, glutamic acid-based urea inhibitors[101,14] and glutamic-urea-lysine hetero dimmers[92–96] are in spot-light due to their sub-nanomolar binding affinity and impressive preclinical results.

1.9 Organization of the thesis

The present thesis has been summarized into seven chapters to gain deep insight into the complete research work carried out.

Chapter 1 describes the introduction of the subject, an extensive review of the existing technologies and the scope of the thesis.

Chapter 2 depicts the discovery of a novel class of PSMA ligands, amino-acetamides, and their biological evaluation for *in vitro* efficacy.

Chapter 3 describes the successful development of novel diagnostic tools for detection of $PSMA^+$ cancers using aminoacetamides as a homing ligand.

Chapter 4 deals with design, synthesis and biological evaluation of novel thiourea derivatives as small molecule inhibitors for prostate specific membrane antigen.

Chapter 5 describes the design, synthesis and biological evaluation of a tyrosine-based asymmetric urea ligand for enhanced binding affinity in the S1 pocket of PSMA protein.

Chapter 6 deals with the introduction of a novel solid phase peptide synthesis strategy for the synthesis of ligand-targeted fluorescent-labelled chelating peptide conjugates.

1.10 References

1. Nagai H., Kim Y. H. (2017). Cancer prevention from the perspective of global cancer burden patterns, J. Thorac. Dis., 9, 448–451 (DOI: 10.21037/jtd.2017.02.75).

2. Bray F., Ferlay J., Soerjomataram I., Siegel R. L., Torre L. A., Jemal A. (2018), Global cancer statistics 2018: Globocan estimates of incidence and mortality worldwide for 36 cancers in 185 countries, CA Cancer J. Clin., 68, 394–424 (DOI: 10.3322/caac.21492).

3. Globocan India. (2018) The Global Cancer Observatory. https://www.gco.iarc.fr/today/data/factsheets/populations/356-india-fact-sheets.pdf. Accessed 23 March 2019.

4. Baum M., Demicheli R., Hrushesky W., Retsky M. (2005), Does surgery unfavourably perturb the "natural history" of early breast

cancer by accelerating the appearance of distant metastases?, Eur. J. Cancer, 41, 508–515 (DOI: 10.1016/j.ejca.2004.09.031).

5. Demicheli R., Retsky M. W., Hrushesky W.J., Baum M., Gukas I. D. (2008), The effects of surgery on tumor growth: A century of investigations, Ann. Oncol., 19, 1821–1828 (DOI: 10.1093/annonc/mdn386).

6. Baskar R., Lee K. A., Yeo R., Yeoh, K. (2012), Cancer and radiation therapy: Current advances and future directions, Int. J. Med. Sci., 9, 193–199 (DOI: 10.7150/ijms.3635).

7. Zackrisson B., Mercke C., Strander H., Wennerberg J., Cavallin-Stahl E. (2003), A systematic overview of radiation therapy effects in head and neck cancer, Acta Oncol., 42, 443–461 (DOI: 10.1080/02841860310014886).

8. van der Hul R. L., Seynaeve C., van Gell B. N., Verweij J. (2003), Low dose of methotrexate and vinblastine, given weekly to patients with desmoid tumors, is associated with major toxicity. Sarcoma, 7, 153–157 (DOI: 10.1080/13577140310001644779).

9. Onyenadum A., Gogas H., Markopoulos C., Bafaloukos D., Aravantinos G., Mantzourani M., Koutras A., Tzorakoelefterakis E., Xiros N., Makatsoris T., Fountzilas G., Kalofonos H. P. (2007), Mitoxantrone plus vinorelbine in pretreated patients with metastatic breast cancer, J. Chemother., 19, 582–589 (DOI: 10.1179/joc.2007.19.5.582).

10. Rahmani R., Zhou X. J. (1993), Pharmacokinetics and metabolism of vinca alkaloids, Cancer Surv., 17, 269–281 (PMID: 8137344).

11. Rowinsky E. K., Chaudhry V., Cornblath D. R., Donehower R. C. (1993), Neurotoxicity of taxol, J. Natl. Cancer Inst. Monogr., 15, 107–115 (PMID: 7912516).

12. Rowinsky E. K., Eisenhauer E. A., Chaudhry V., Arbuck S. G., Donehower R. C. (1993), Clinical toxicities encountered with paclitaxel (Taxol), Semin. Oncol., 20, 1–15 (PMID: 8102012).

13. Ivachtchenko A. V., Kiselyov A. S., Tkachenko S. E., Ivanenkov Y. A., Balakin K. V. (2007), Novel mitotic targets and their small-molecule inhibitors, Curr. Cancer Drug Targets, 7, 766–784 (DOI: 10.2174/156800907783220499).

14. Kularatne S. A., Chelvam V., Santhapuram H. K. R., Wang K., Vaitilingam B., Henne W. A., Low P. S. (2010) Synthesis and biological analysis of prostate-specific membrane antigen-targeted anticancer prodrugs. J. Med. Chem., 53, 7767–7777 (DOI: 10.1021/jm100729b).

15. Gisselbrecht C. (2008), Use of rituximab in diffuse large B-cell lymphoma in the salvage setting, Br. J. Haematol., 143, 607–621 (DOI: 10.1111/j.1365-2141.2008.07383.x).

16. Hall P. C., Cameron D. A. (2009), Current perspective-trastuzumab, Eur. J. Cancer, 45, 12–18 (DOI: 10.2147/BCTT.S6070)

17. Jean G. W., Shah S. R. (2008), Epiderm growth factor receptor monoclonal antibodies for the treatment of metastatic colorectal cancer, Pharmacotherapy, 28, 742–754 (DOI:10.1592/phco.28.6.742).

18. Srinivasarao M., Low P.S. (2017), Ligand-targeted drug delivery, Chem. Rev., 117, 12133–12164 (DOI: 10.1021/acs.chemrev.7b00013).

19. Hricak H., Choyke P. L., Eberhardt S. C., Leibel S. A., Scardino P. T. (2007), Imaging prostate cancer: A multidisciplinary perspective, Radiology, 243, 28–53 (DOI: 10.1148/radiol.2431030580).

20. Ojima I. (2008), Guided molecular missiles for tumor-targeting chemotherapy-case studies using the second-generation taxoids as warheads, Acc. Chem. Res., 41, 108–119 (DOI: 10.1021/ar700093f).

21. Balhorn R., Hok S., Burke P. A., Lightstone F. C., Cosman M., Zemla A., Mirick G., Perkins J., Natarajan A., Corzett M., DeNardo S. J., Albrecht H., Gregg J. P., DeNardo G. L. (2007), Selective high-affinity ligand antibody mimics for cancer diagnosis and therapy: Initial application to lymphoma/leukemia, Clin. Cancer Res., 15, 5621s–5628s (DOI: 10.1158/1078-0432.CCR-07-1128).

22. Allen T. M. (2002), Ligand-targeted therapeutics in anticancer therapy, Nat. Rev. Cancer., 2, 750–763 (DOI: 10.1038/nrc903).

23. Low P. S., Kularatne S. A. (2009), Folate-targeted therapeutic and imaging agents for cancer, Curr. Opin. Chem. Biol., 13, 256–262 (DOI: 10.1016/j.cbpa.2009.03.022).

24. He Q., Xu R. Z., Shkarin P., Pizzorno G., Lee-French C. H., Rothman D. L., Shungu D. C., Shim H. (2004), Magnetic resonance spectroscopic imaging of tumor metabolic markers for cancer diagnosis, metabolic phenotyping, and characterization of

tumor microenvironment, Dis. Markers, 19, 69–94 (DOI: 10.1155/2004/424395).

25. Fischer B. M., Siegel B. A., Weber W. A., von Bremen K., Beyer T., Kalemis A. (2016), PET/CT is a cost-effective tool against cancer: synergy supersedes singularity, Eur. J. Nucl. Med. Mol. Imaging, 43, 1749–1752 (DOI: 10.1007/s00259-016-3414-5).

26. Bhargava P., He G., Samarghandi A., Delpassand E. S. (2012), Pictorial review of SPECT/CT imaging applications in clinical nuclear medicine, Am. J. Nucl. Med. Mol. Imaging, 2, 221–231.

27. Solomon M., Liu Y., Berezin M. Y., Achilefu S. (2011), Optical imaging in cancer research: Basic principles, tumor detection, and therapeutic monitoring, Med. Princ. Pract., 20, 397–415 (DOI: 10.1159/000327655).

28. Wester H. J. (2007), Nuclear imaging probes: From bench to bedside, Clin. Cancer Res., 13, 3470–3481 (DOI: 10.1158/1078-0432.CCR-07-0264).

29. Alberti C. (2012), From molecular imaging in preclinical/clinical oncology to theranostic applications in targeted tumor therapy, Eur Rev. Med., Pharmacol. Sci., 16, 1925–1933 (PMID: 23242718).

30. Pan D., Lanza G. M., Wickline S. A., Caruthers S. D. (2009), Nanomedicine: Perspective and promises with ligand-directed molecular imaging, Eur. J. Radiol., 70, 274–285 (DOI: 10.1016/j.ejrad.2009).

31. Chen K., Chen X. (2010), Design and development of molecular imaging probes, Curr. Top. Med. Chem., 10, 1227–1236 (DOI: 10.2174/156802610791384225).

32. Cornelissen B. (2014), Imaging the inside of a tumour: A review of radionuclide imaging and theranostics targeting intracellular epitopes, J. Labelled Comp. Radiopharm., 57, 310–316 (DOI: 10.1002/jlcr.3152).

33. Ametamey S. M., Honer M., Schubiger P. A. (2008), Molecular imaging with PET. Chem. Rev., 108, 1501–1516 (DOI: 10.1021/cr0782426).

34. Zhu A., Lee D., Shim H. (2011), Metabolic PET imaging in cancer detection and therapy response, Semin. Oncol., 38, 55–69 (DOI: 10.1053/j.seminoncol.2010.11.012).

35. Kelloff G. J., Hoffman J. M., Johnson B., Scher H. I., Siegel B. A., Cheng E. Y., Cheson B. D., O'shaughnessy J., Guyton K. Z., Mankoff D. A., Shankar L., Larson S.M., Sigman C. C., Schilsky R. L., Sullivan D. C. (2005), Progress and promise of FDG-PET imaging for cancer patient management and oncologic drug development, Clin. Cancer Res., 11, 2785–2808 (DOI: 10.1158/1078-0432.CCR-04-2626).

36. Mariani G., Bruselli L., Kuwert T., Kim E. E., Flotats A., Israel O., Watanabe N. (2010), A review on the clinical uses of SPECT/CT, Eur. J. Nucl. Med. Mol. Imaging, 37, 1959–1985. (DOI:10.1007/s00259-010-1390-8).

37. Laura M. A., Pier Carlo M., Antonio R. (2012), Optical and multimodal peptide-based probes for in vivo molecular imaging, Anticancer Agents Med. Chem., 12, 476–499 (DOI: 10.2174/187152012800617858).

38. Kuil J., Velders A. H., van Leeuwen F. W. B. (2010), Multimodal tumor-targeting peptides functionalized with both a radio- and a

fluorescent label, Bioconjugate Chem., 21, 1709–1719 (DOI: 10.1021/bc100276j).

39. Moss J. A., Vavere A. L., Azhdarinia A. (2012), Design of peptide imaging agents for whole-body and intraoperative molecular imaging, Curr. Med. Chem., 19, 3255–3265 (DOI: 10.2174/092986712801215856).

40. Lee S., Xie J., Chen X. (2010), Peptide-based probes for targeted molecular imaging, Biochemistry, 49, 1364–1376 (DOI: 10.1021/bi901135x).

41. Ferro-Flores G., Ramirez F. D. M., Melendez-Alafort L., Santos-Cuevas C. L. (2010), Peptides for in vivo target-specific cancer imaging, Mini Rev. Med. Chem., 10, 87–97 (DOI: 10.2174/138955710791112596).

42. Weissleder R., Pittet M. J. (2008), Imaging in the era of molecular oncology, Nature, 452, 580–589 (DOI: 10.1038/nature06917).

43. Kubben P. L., ter Meulen K. J., Schijns O. E. M. G., ter Laak-Poort M. P., van Overbeeke J. J., Santbrink H. V. (2011), Intraoperative MRI-guided resection of glioblastoma multiforme: A systematic review, Lancet Oncol., 12, 1062–1070 (DOI: 10.1016/S1470-2045(11)70130-9).

44. Mondal S. B., Gao S., Zhu N., Liang R., Gruev V., Achilefu S. (2014), Real-time fluorescence image-guided oncologic surgery, Adv. Cancer Res., 124, 171–211 (DOI: 10.1016/B978-0-12-411638-2.00005-7).

45. Kawakubo K., Ohnishi S., Hatanaka Y., Hatanaka K. C., Hosono H., Kubota Y., Sakamoto N. (2015), Feasibility of using an enzymatically activatable fluorescence probe for the rapid

evaluation of pancreatic tissue obtained using endoscopic ultrasound-guided fine needle aspiration: a pilot study, Mol. Imaging Biol., 18, 463–471 (DOI:10.1007/s11307-015-0898-5.

46. Ntziachristos V., Bremer C., Weissleder R. (2003), Fluorescence imaging with near-infrared light: New technological advances that enable in vivo molecular imaging, Eur. Radiol., 13, 195–208 (DOI: 10.1007/s00330-002-1524-x).

47. Koo V., Hamilton P. W., Williamson K. (2006), Non-invasive in vivo imaging in small animal research, Cell Oncol., 28, 127–139 (PMID: 16988468).

48. Fayed T. A. (2011), Reviews in fluorescence 2009. In: Geddes C. E. (ed) Extension of fluorescence response to the near-IR region, Springer, New York, NY, pp. 75–111 (ISBN 978-1-4419-9672-5) (DOI: 10.1007/978-1-4419-9672-5_4).

49. Tong H., Lou K., Wang W. (2015), Near-infrared fluorescent probes for imaging of amyloid plaques in Alzheimer's disease, Acta Pharm. Sin B., 5, 25–33 (DOI: 10.1016/j.apsb.2014.12.006).

50. Schaafsma B. E., Mieog J. S., Hutteman M., vander Vorst J. R., Kuppen P. J., Löwik C. W., Frangioni J. V., van de Velde C. J., Vahrmeijer A. L. (2011), The clinical use of indocyanine green as a near-infrared fluorescent contrast agent for image-guided oncologic surgery, J. Surg. Oncol., 104, 323–332 (DOI: 10.1002/jso.21943).

51. Namikawa T., Sato T., Hanazaki K. (2015), Recent advances in near-infrared fluorescence-guided imaging surgery using indocyanine green, Surg. Today, 45, 1467–1474 (DOI: 10.1007/s00595-015-1158-7).

52. Adams A., Mourik J.E., vander Voort M., Pearlman P. C., Nielsen T., Mali W. P., et al. (2012), Estimation of detection limits of a clinical fluorescence optical mammography system for the near-infrared fluorophore IRDye800CW: Phantom experiments, J. Biomed. Opt., 17, 076022-1–076022-6 (DOI: 10.1117/1.jbo.17.7.076022).

53. van Dam G.M., Themelis G., Crane L. M., Harlaar N. J., Pleijhuis R. G., Kelder W., Sarantopoulos A., de Jong J. S., Arts H. J., van der Zee A. G., Bart J., Low P. S., Ntziachristos V. (2011), Intraoperative tumor-specific fluorescence imaging in ovarian cancer by folate receptor-α targeting: First-in-human results, Nat. Med., 17, 1315–1319 (DOI: 10.1038/nm.2472).

54. Siegel R. L., Miller K. D., Jemal A. (2019), Cancer Statistics, 2019, CA Cancer J. Clin., 69, 7–34 (DOI: 10.3322/caac.21551).

55. Wilson L. S., Tesoro R., Elkin E. P. (2007), Cumulative cost pattern comparison of prostate cancer treatments, Cancer, 109, 518–527 (DOI: 10.1002/cncr.22433).

56. Jain S., Saxena S., Kumar A. (2014), Epidemiology of prostate cancer in India, Meta Gene, 2, 596–605 (DOI: 10.1016/j.mgene.2014.07.007).

57. Katz A. (2007), Quality of life for men with prostate cancer, Cancer Nurs., 30, 302–308 (DOI: 10.1097/01.NCC.0000281726.87490.f2).

58. Zeller J. L. (2007), Grading of prostate cancer, JAMA, 298 (13), 1596 (DOI: 10.1001/jama.298.13.1596).

59. Chodak, M. D.; Keller, P.; Schoenberg, H. W. (1989), Assessment of screening for prostate cancer using the digital rectal

examination, J. Urol., 141, 1136–1138 (DOI: 10.1016/s0022-5347(17)41192-x).

60. Essink-Bot M., de Koning H. J., Nijs H. G. J., Kirkels W. J., van der Mass P. J., Schroder F. H. (1998), Short term effects of population-based screening for prostate cancer on health-related quality of life, J. Natl. Cancer Inst., 90, 925–931 (PMID: 9637143).

61. Linn M. M., Ball R. A., Maradiegue A. (2007), Prostate-specific antigen screening: friend or foe?, Urol. Nurs., 27, 481–489 (PMID: 18217530).

62. D'Amico A. V., Roehrborn C. G. (2007), Effect of 1 mg/day finasteride on concentration of serum prostate specific antigen in men with androgenic alopecia: A randomized controlled trial, Lancet Oncol., 8, 21–25 (DOI: 10.1016/S1470-2045(06)70981-0).

63. Holves A. M., Heesakkers R. A. M., Adang E. M. (2008), The diagnostic accuracy of CT and MRI in the pelvis of lymph nodes in patients with prostate cancer: A meta-analysis, Clin. Radiol., 63, 387–395 (DOI: 10.1016/j.crad.2007.05.022).

64. Bill-Axelson A., Holmberg L., Ruutu M., Häggman M., Andersson S-O., Bratell S. Spångberg A., Busch C., Nordling S., Garmo H., Palmgren J., Adami H-O., Norlén B. J., Johansson J-E. (2005), Radical prostatectomy versus watchful waiting in early prostate cancer, N. Engl. J. Med., 352, 1977–1984 (DOI: 10.1056/nejmoa043739)

65. Weber B. A., Robert B. L., Chumbler N. R., Mills T. L., Algood C. B. (2007), Urinary, sexual and bowel dysfunction and bother after

radical prostatectomy, Urol. Nurs., 27, 527–533 (PMID: 18217536).

66. Brenner D. J., Curtis R. E., Ron E. (2000), Second malignancies in prostate carcinoma patients after radiotherapy compared with surgery, Cancer, 88, 398-406 (DOI: 10.1002/(sici)1097-0142(20000115)88:2).

67. Kumar R. J., Bargawi A., Crawford E. D. (2005), Adverse events associated with hormonal therapy for prostate cancer, Rev. Urol., 7, 37–43 (PMID: 16985883).

68. Hsiao C., Li T-K., Chan Y-L. (2008), WRC-213, an L-methionine conjugated mitoxantrone derivative, displays anticancer activity with reduced cardiotoxicity and drug resistance: Identification of topoisomerase II inhibition and apoptotic machinery, Biochem. Pharmacol., 75, 847–856 (DOI: 10.1016/j.bcp.2007.10.012).

69. Ghosh A., Heston W. D. (2004), Tumor target prostate specific membrane antigen (PSMA) and its regulation in prostate cancer, J. Cell Biochem., 91, 528–539 (DOI: 10.1002/jcb.10661).

70. Gang M. C., Chang S. S., Sadelain M., Bander N. H., Heston W. D. (1999), Prostate specific membrane antigen (PSMA)-specific monoclonal antibodies in the treatment of prostate and other cancers, Cancer Metastasis Rev., 18, 483–490 (PMID: 10855791).

71. Davis M. I., Bennett M. J., Thomas L. M., Bjorkman P. J. (2005), Crystal structure of prostate-specific membrane antigen, a tumor marker and peptidase, Proc. Natl. Acad. Sci. U S A., 102, 5981–5986 (DOI: 10.1073/pnas.0502101102).

72. Robinson M. B., Blakely R. D., Couto R., Coyle J. T. (1987), Hydrolysis of the brain dipeptide N-acetyl-L-aspartyl-L-glutamate:

Identification and characterization of a novel N-acetylated alpha-linked acidic dipeptidase activity from rat brain, J. Biol. Chem. 262, 14498–14506 (PMID: 3667587).

73. Slusher B. S., Robinson M. B., Tsai G., Simmons M. L., Richards S. S., Coyle J. T. (1990), Rat brain N-acetylated alpha-linked acidic dipeptidase activity: Purification and immunologic characterization, J. Biol. Chem. 265, 21297–21301 (PMID: 2250024).

74. Berger U. V., Carter R. E., Coyle J. T. (1995), The immunocytochemical localization of N-acetylaspartyl glutamate, its hydrolysing enzyme NAALADase, and the NMDAR-1 receptor at a vertebrate neuromuscular junction, Neuroscience, 64, 847–850 (DOI: 10.1016/0306-4522(95)92578-8).

75. Carter R. E., Feldman A. R., Coyle J. T. (1996), Prostate-specific membrane antigen is a hydrolase with substrate and pharmacologic characteristics of a neuropeptidase, Proc. Natl. Acad. Sci. USA. 93, 749–753.

76. Pinto J. T., Suffoletto B. P., Berzin T. M., Qiao C. H., Lin S., Tong W. P., May F., Mukherjee B., Heston W. D. (1996), Prostate-specific membrane antigen: A novel folate hydrolase in human prostatic carcinoma cells, Clin. Cancer Res., 2, 1445–1451.

77. Heston W. D. (1997), Characterization and glutamyl preferring carboxypeptidase function of prostate specific membrane antigen: A novel folate hydrolase, Urology, 49, 104–112 (DOI: 10.1016/S0090-4295(97)00177-5).

78. Mesters J. R., Barinka C., Li W., Tsukamoto T., Majer P., Slusher B. S., Konvalinka J., Hilgenfeld R. (2006), Structure of glutamate

carboxypeptidase II, a drug target in neuronal damage and prostate cancer, EMBO J., 25, 1375–1384 (DOI: 10.1038/sj.emboj.7600969).

79. Rajasekaran A. K., Anilkumar G., Christiansen J. J. (2005), Is prostate-specific membrane antigen a multifunctional protein?, Am. J. Physiol. Cell. Physiol., 288, C975–C981 (DOI: 10.1152/ajpcell.00506.2004).

80. Jemaa A. B., Bouraoui Y., Sallami S., Banasr A., Rais N. B., Ouertani L., Nouira Y., Horchani A., Oueslati R. (2010), Co-expression and impact of prostate specific membrane antigen and prostate specific antigen in prostatic pathologies, J. Exp. Clin. Cancer Res., 29(1), 171 (DOI: 10.1186/1756-9966-29-171).

81. Mohan K., Donavan K.C., Arter J.A., Penner R.M., Weiss G.A. (2013), Sub-nanomolar detection of prostate-specific membrane antigen in synthetic urine by synergistic, dual-ligand phage, J. Am. Chem. Soc., 135, 7761–7767 (DOI: 10.1021/ja4028082).

82. Zang X., Jones C. M., Long T. Q., Monge M. E., Zhou M., Walker L. D., Mezencev R., Gray A., McDonald J. F., Fernandez F. M. (2014), Feasibility of detecting prostate cancer by ultraperformance liquid chromatography-mass spectrometry serum metabolomics, J. Proteome Res., 13, 3444–3454 (DOI: 10.1021/pr500409q).

83. Liu H., Rajasekaran A. K., Moy P. (1998), Constitutive and antibody induced internalization of prostate-specific membrane antigen, Cancer Res., 58, 4055–4060.

84. Heitkötter B., Steinestel K., Trautmann M., Grünewald I., Barth P., Gevensleben H., Bögemann M., Wardelmann E., Hartmann W.,

Rahbar K., Huss S. (2018), Neovascular PSMA expression is a common feature in malignant neoplasms of the thyroid, Oncotarget, 9, 9867–9874 (DOI: 10.18632/oncotarget.23984).

85. Wernicke A. G., Edgar M. A., Lavi E., Liu H., Salerno P., Bander N. H., Gutin P. H. (2011), Prostate-specific membrane antigen as a potential novel vascular target for treatment of glioblastoma multiforme, Arch. Pathol. Lab Med., 135, 1486–1489 (DOI: 10.5858/arpa.2010-0740-OA).

86. Fragomeni R. A. S., Amir T., Sheikhbahaei S., Harvey S. C., Javadi M. S., Solnes L. B., Kiess A. P., Allaf M. E., Pomper M. G., Gorin M. A., Rowe S. P. (2018), Imaging of non-prostate cancers using PSMA-targeted radiotracers: Rationale, current state of the field, and a call to arms, J. Nucl. Med., 59, 871–877 (DOI: 10.2967/jnumed.117.203570).

87. Barinka C., Rojas C., Slusher B., Pomper M. (2012), Glutamate carboxypeptidase II in diagnosis and treatment of neurologic disorders and prostate cancer, Curr. Med. Chem., 19, 856–870 (DOI: 10.2174/092986712799034888).

88. Han M., Partin A. W. (2001), Current clinical applications of the ^{111}In-capromab pendetide scan (ProstaScint® Scan, Cyt-356), Rev. Urol., 3, 165–171.

89. Kobayashi H., Choyke P. L., Ogawa M. (2016), Monoclonal antibody-based optical molecular imaging probes; considerations and caveats in chemistry, biology and pharmacology, Curr. Opin. Chem. Biol., 33, 32–38 (DOI: 10.1016/j.cbpa.2016.05.015).

90. Byun Y., Mease R. C., Lupold S. E., Pomper M. G. (2009), Drug design of zinc-enzyme inhibitors. In: Supuran C. T., Winum J, -Y.

(ed) Recent development of diagnostic and therapeutic agents targeting glutamate carboxypeptidase II (GCPII). John Wiley & Sons, Inc. New York, pp. 881–910 (ISBN 9780470275009) (DOI:10.1002/9780470508169.ch36).

91. Tsukamoto T., Wozniak K. M., Slusher B. S. (2007), Progress in the discovery and development of glutamate carboxypeptidase II inhibitors. Drug Discov. Today, 12, 767–776 (DOI: 10.1016/j.drudis.2007.07.010).

92. Foss C. A., Mease R. C., Fan, H., Wang Y., Ravert H. T., Dannals R. F., Olszewski R., Heston W. D., Kozikowski A. P., Pomper M. G. (2005), Radiolabeled small molecule ligands for prostate specific membrane antigen: *In vivo* imaging in experimental models of prostate cancer, Clin. Cancer Res., 2005, 11, 4022–4028 (DOI: 10.1158/1078-0432.CCR-04-2690).

93. Mease R. C., Dusich C. L., Foss C. A., Ravert H. T., Dannals R. F., Seidel J., Prideaux A., Fox J. J., Sgouros G., Kozikowski A. P., Pomper M. G. (2008), N-[N-[(S)-1,3-Dicarboxypropyl]carbamoyl]-4-[18F]-fluorobenzyl-L-cysteine, [^{18}F]DCFBC: A new imaging probe for prostate cancer, Clin. Cancer Res., 14(10), 3036–3043 (DOI: 10.1158/1078-0432.CCR-07-1517).

94. Maresca K. P., Hillier S. M., Fernia F. J., Keith D., Barone C., Joyal J. L., Zimmerman C. N., Kozikowski A. P., Barrett J. A., Eckelman W. C., Babich J. W. (2009), A series of halogenated heterodimeric inhibitors of prostate specific membrane antigen (PSMA) as radiolabeled probes for targeting prostate cancer, J. Med. Chem., 52, 347–357 (DOI: 10.1021/jm800994j).

95. Chen Y., Foss C. A., Byun Y., Nimmagadda S., Pullambhatla M., Fox J. J., Castanares M., Lupold S. E., Babich J. W., Mease R. C., Pomper M. G. (2008), Radiohalogenated prostate-specific membrane antigen (PSMA)-based ureas as imaging agents for prostate cancer, J. Med. Chem., 51, 7933–7943 (DOI: 10.1016/j.bbrc.2009.10.017).

96. Banerjee S. R., Pullambhatla M., Byun Y., Nimmagadda S., Green G., Fox J. J., Horti A., Mease R. C., Pomper M. G. (2010), ^{68}Ga-labeled inhibitors of prostate-specific membrane antigen (PSMA) for imaging prostate cancer, J. Med. Chem., 53, 5333–5341 (DOI: 10.1021/jm100623e).

97. Lapi S. E., Wahnishe H., Pham D., Wu L. Y., Nedrow-Byers J. R., Liu T., Vejdani K., VanBrocklin H. F., Berkman C. E., Jones E. F. (2009), Assessment of an ^{18}F-labeled phosphoramidate peptidomimetic as a new prostate-specific membrane antigen-targeted imaging agent for prostate cancer, J. Nucl. Med., 50, 2042–2048 (DOI: 10.2967/jnumed.109.066589).

98. Misra P., Humblet V., Pannier N., Maison W., Frangioni J. V. (2007), Production of multimeric prostate-specific membrane antigen small molecule radiotracers using a solid-phase ^{99m}Tc preloading strategy, J. Nucl. Med., 48, 1379–1389 (DOI: 10.2967/jnumed.107.040303).

99. Banerjee S. R., Foss C. A., Castanares M., Mease R. C., Byun Y., Fox J. J., Hilton J., Lupold S. E., Kozikowski A. P., Pomper M. G. (2008), Synthesis and evaluation of technetium-99m- and rhenium-labeled inhibitors of the prostate-specific membrane antigen (PSMA), J. Med. Chem., 2008, 51, 4504–4517 (DOI: 10.1021/jm800111u).

100. Kularatne S. A., Wang K., Santhapuram H. K. R., Low P. S. (2009), Prostate-specific membrane antigen targeted imaging and therapy of prostate cancer using a PSMA inhibitor as a homing ligand, Mol. Pharm., 6, 780–789 (DOI: 10.1021/mp900069d).

101. Kularatne S. A., Zhou Z., Yang J., Post C. B., Low P. S. (2009), Design, synthesis, and preclinical evaluation of prostate-specific membrane antigen targeted ^{99m}Tc-radioimaging agents, Mol. Pharm., 6, 790–800 (DOI: 10.1021/mp9000712).

Chapter 2

Aminoacetamides: A New Class of Small Molecule Inhibitors/Ligands for Prostate Specific Membrane Antigen Expressing ($PSMA^+$) Cancers

2.1 Introduction

Despite the development of new modalities for the early detection of prostate cancer (PCa), it is still the second most diagnosed cancer among men in Western countries.[1] The statistics of 2019 reveals 174,650 newly diagnosed cases and 31,620 estimated deaths due to prostate carcinoma in the Western world.[2] The identification of over-expressed membrane-bound cell surface protein, prostate specific membrane antigen (PSMA), is an important breakthrough for prostate carcinoma diagnosis and therapy. During the development of LNCaP cell lines, PSMA was discovered, and the most interesting fact is that it preserves all the known features of prostate carcinoma.[3]

PSMA has 86% sequence homology with glutamate carboxypeptidase II (GCPII) enzyme.[4–6] PSMA consist of 750 amino acids, and it is a type II glycoprotein.[7] Although the expression of PSMA is present in the epithelial of normal prostate gland it's up-regulation (10-100 fold) takes place only during primary prostate cancer and lymph node metastases.[8] Studies also revealed that the PSMA expression is also present in the endothelium of tumour associated neovasculature of non-prostatic solid tumours.[9–11] The features above makes PSMA is an attractive target for immunotherapy.[12–14] As an added advantage, this metalloprotease has two predominant but poorly understood enzymatic activities: the hydrolysis of γ-glutamyl derivatives of folic acid[15,16] to release glutamate and the liberation of *N*-acetyl aspartate and glutamate after the proteolysis of neuro peptide *N*-acetyl-α-linked-aspartylglutamate (NAAG).[17] A new

class of small molecule PSMA inhibitors can be designed by mimicking the structure of NAAG.

Enormous efforts have been carried out to develop new inhibitors for GCPII over the past decades that can strongly bind to PSMA. At the beginning of this journey, Jackson *et al* first reported the most potent inhibitor 2-(phosphonomethyl)pentanedioic acid (PMPA) in 1996.[18] After the discovery of this potent inhibitor the scenario of constructing new inhibitors for PSMA got a new direction and extensive structure-activity relationships study has been performed to design new inhibitors such as urea-based small molecules[19–27] and phenylalkylphosphoramidates[28] for PSMA. Another interesting feature of these inhibitors is that they generally exist in (*S*)-configuration and found to be more active than the (*R*)-configuration.[29] Therefore, synthesis of enantiomerically pure inhibitors are a prerequisite for further preclinical testing as well as to avoid undesired pharmacological effect by the other enantiomer.

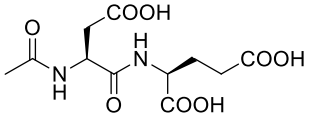

NAAG

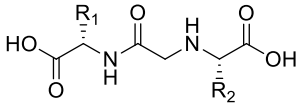

Designed inhibitor

Figure 2.1 Structure of NAAG and structural scaffold of newly designed PSMA inhibitor

Based on the previous literature, in this chapter, we have described the molecular design, synthesis and biological evaluation of enantiomerically pure aminoacetamides as potent inhibitors of PSMA. A systematic *in silico* docking study has been performed with glutamic acid based aminoacetamide compounds to examine their binding and interactions at the active site of PSMA. The study reveals that an extension of one methylene carbon unit after the amide group generates new hydrogen bond interactions with the glutamic acid side chain residue in the binding pocket

of PSMA. Observing this phenomenon, we have designed and synthesized a small library of inhibitors containing the aminoacetamide structural moiety. A methodical *in silico* docking study has been performed upon each derivative to understand the structure-activity relationships of this class of newly designed inhibitors through their hydrogen bonding interactions in the binding pocket of PSMA. After the *in silico* molecular docking studies, a novel and simple synthetic methodology have been designed to synthesize the aminoacetamide derived inhibitors. The first three most potent derivatives, as per molecular modelling score, has been further evaluated through fluorescence-based PSMA enzyme inhibition assay to determine their inhibition concentration (IC_{50}) values.

2.2 Results and Discussion

2.2.1 Docking method

In the drug discovery program, for the prediction of the binding mode of an active ligand or inhibitor over a protein, docking studies are usually performed. In the present work, glutamate carboxy peptidase II (GCPII) receptor or prostate specific membrane antigen (PSMA), complexed with a urea-based inhibitor, JB7, (PDB 4NGM) was retrieved from protein data bank and used as a reference to perform docking studies of newly designed aminoacetamide derived inhibitors by Surflex Dock method and Sybyl X2.1.1 software.

2.2.1.1 Interpretation of docking results

The initial design of the small molecule inhibitor is based on the understanding of the active catalytic site of metalloprotease enzyme, PSMA. In figure.2.2 the site of cleavage of the substrates has been shown for both NAAG and folyl-γ-glutamate by PSMA enzyme. Keeping the architecture of endogenous PSMA substrates, e.g. NAAG as well as folyl-γ-Glu constant, at S1 pocket, a methylene carbon unit has been inserted after the scission of the amide bond, in the newly designed inhibitors, to

enhance the number of new interactions in the binding pocket of PSMA. In our initial model, S1 pocket contains another L-glutamic acid residue which is strategically attached with a methylene carbon unit through an amide bond to form the aminoacetamide moiety. The carbonyl oxygen of amino-acetamide moiety coordinates with the Zn atoms present at the active site of PSMA.

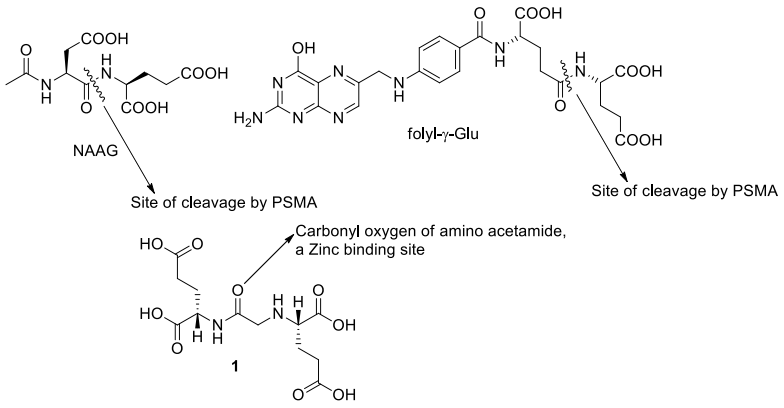

Figure 2.2 Design of lead aminoacetamide peptidomimetic **1** for PSMA enzyme inhibition

Further a small library of L-glutamic acid-based aminoacetamide inhibitors **1–10** (Figure 2.3), which closely resembles NAAG as well as folyl-γ-Glu, has been designed to examine the structural and functional requirements necessary for binding at the active site of the PSMA protein.

2.2.1.2 General method for molecular docking study

In docking study, protomol represents the protein active site which provides information about every possible interaction between the protein and ligands or inhibitors of study at the active site. To define protomol for docking studies, the first step is the protein preparation. In protein preparation, all the water molecules are excluded, the ligand was extracted, and hydrogen atoms were added to the receptor. To minimize the energy of the protein, Force field AMBER7FF99 was applied. Finally, protomol was generated at the active site of co-crystallised ligand (JB7)

and utilized for molecular docking studies of newly designed ligands. The first and most important step in docking is a validation of the docking procedure which is carried out by re-docking the co-crystallised ligand, JB7, with the active site of the protein.

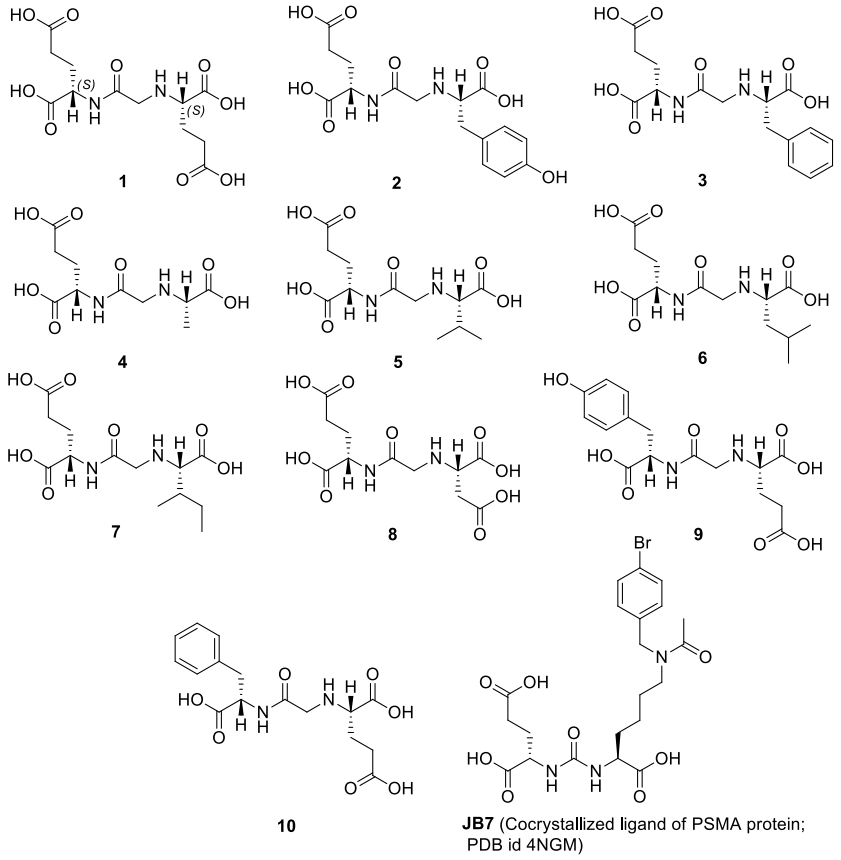

Figure 2.3 Design of a library of peptidomimetics **1–10** based on aminoacetamide scaffold

2.2.1.3 Outcome of the molecular docking study

Molecular docking study is used to examine ligand-protein interactions of the designed ligands that are responsible for the inhibitory activity of PSMA enzyme. The results of docking study are reported in the form of docking score which depends on various parameters like hydrogen bonding, lipophilic and π-π interactions. In the present study, various aminoacetamide based ligands were designed, and their protein binding

affinity was analyzed through molecular docking. After validation using standard ligand, JB7, same docking protocol was extended to the newly designed ligands **1–10** (Figure 2.3) and the generated docking scores of ligands **1–10** and JB7 are shown in table 2.1.

Table 2.1 Molecular docking scores of aminoacetamide ligands **1–10** and JB7 with GCPII protein (PDB 4NGM)

Rank	Ligand	Docking score
1	JB7	16.38
2	**1**	13.96
3	**3**	13.63
4	**2**	12.51
5	**6**	12.01
6	**9**	11.99
7	**8**	11.45
8	**4**	11.35
9	**7**	10.94
10	**10**	10.79
11	**5**	10.67

Surflex Dock module of Sybyl X 2.1.1. program was utilized to find the binding conformations of JB7 and newly designed aminoacetamide derivatives **1–10** at the active site of GCPII protein. It is well documented that the active site of the GCPII protein contains hydrophobic (S1 pocket) and hydrophilic pocket (S1' pocket) and the interactions at S1' site is believed to be more critical for better binding affinity. Literature report suggests that JB7 interact with several aminoacids residues such as Tyr 700, Arg 210, Lys 699, Asn 257, Gly 518, Tyr 552, Glu 424, Asn 519, Arg 536 and Arg 534 through hydrogen bonds that are critical for better binding of a ligand with the protein. The aforementioned aminoacid interactions should be taken into consideration while performing docking studies of the newly designed ligands **1–10** with GCPII protein.

Table 2.2 shows a correlation between amino acid residues of S1 and S1' pockets present in PSMA protein and the newly designed amino-

acetamide ligands **1–10** interacting through hydrogen bonds. During the re-docking study of JB7 with the protein, similar amino acids interactions were observed as reported for JB7 with native protein (PDB 4NGM). In addition, an extra hydrogen bonding interaction with Lys 699 and Arg 536 residues was also observed (Table 2.2).

Table 2.2 Hydrogen bonding interactions between GCPII protein and aminoacetamide ligands **1–10** along with the bond distance of interaction in Å.

Site	Amino acid residue	JB7 H-bonding interaction with GCPII in Å from PDB 4NGM	JB7 Post or re docking interactions with GCPII in Å	H-bonding interactions of ligands 1-10 with GCPII protein in Å									
				1	**3**	**2**	**6**	**9**	**8**	**4**	**7**	**10**	**5**
S1' site of GCPII (Hydrophilic pocket)	**Arg 210**	2.8	2.3	2.72 2.05	1.89 2.47	1.87	1.74 2.41	2.03	2.12	2.34	2.18	2.03	1.86 2.49
	Asn 257	2.89	2.03	1.90	1.94 2.40		1.89 2.70	1.92	2.72 1.91	2.32 2.73	2.00 2.41	1.78	1.93
	Lys 699	2.7	2.47, 2.06	1.83	1.87 2.52	2.08	1.98	2.59 1.79		2.25, 2.55		1.88	1.9
	Tyr 552	2.63	2.65	1.72	1.89	2.66 1.79	2.33 2.54	2.64	2.27	1.7	2.35	2.45	2.16
	Tyr 700	2.53	1.8	2.73		1.84	2.2		2.32 2.06	2.27		2.69	2.72
	Glu 424	3.01		2.06 2.03	2.04 1.85	2.79 1.85	2.67 2.23	2.41 2.01	2.1	1.91			
	Glu 425			2.01	2.13		2		2.55	2.55			2.13 2.74 2.44
S1 site of GCPII (Hydrophobic pocket)	**Gly 518**	3.04, 3.05	1.88	2.4	2.15				1.76	2.44 1.85	1.94	1.9	
	Asn 519	2.98	2.16	2.10	2.47 2.07		1.99	1.81	2.04	2.28	2.08		
	Arg 534	2.84	2.03	1.91 1.92	2.09		2.21	2.03	2.03	1.83 2.06	2.04	2.53	
	Arg 536	2.99, 3.0	2.32, 1.99, 1.96	2.21 2.21					2.68 2.57 1.90			2.61 2.08 2.31	
	Asp 453			2.51		2.57							
	Asp 387					2.56 2.72					2.37		
	Ser 454					2.29					1.72 2.30 1.89		

	Tyr 549					2.34		1.8			2		
	Ser 517					2.03		2.23		2.05			
	Arg 463								2.4				
Total number of hydrogen bonds at S1'/S1		**6/6**	**6/6**	**9/7**	**10/4**	**7/6**	**11/2**	**7/4**	**8/7**	**9/6**	**4/8**	**5/5**	**9/0**

Moreover, in the Surflex dock module of SYBYL, hydrogen bond distance more than 3 Å length are considered as weak and are not visible during docking study. As a result, hydrogen bonding interaction of JB7 with aminoacid residue Glu 424 of the protein was not observed which is of the order of 3.1 Å in length (Figure 2.4). After successful validation of the docking procedure of JB7 with GCPII, a similar protocol was applied for studying the docking interactions of newly designed aminoacetamide derivatives **1–10** with GCPII.

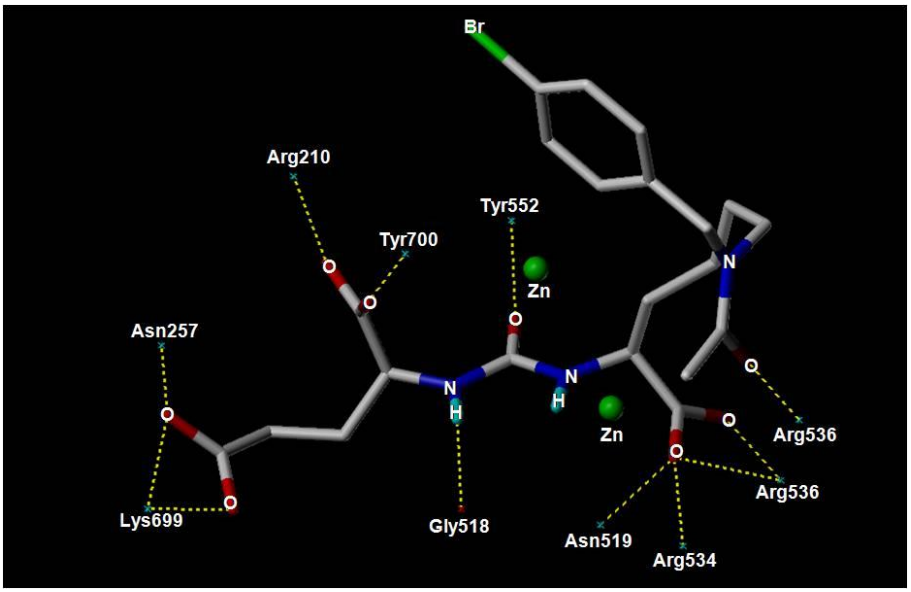

Figure 2.4 Molecular docking study of JB7 with GCPII protein (PDB 4NGM)

Among the newly designed aminoacetamide ligands, the docking score of **1** is found to be the highest followed by ligands **3** (second most active) and **2** (third most active) in the series (Table 2.1). The docking conformation

of the most active ligand, **1**, in the series show nine hydrogen bonding interactions at hydrophilic S1' pocket with Tyr 700, Arg 210, Lys 699, Asn 257, Tyr 552, Glu 424 and Glu 425 (new hydrogen bonding interactions) residues. This fact suggests that the glutamate moiety of **1** interact strongly with the protein active site compared to JB7. However, ligand **1** exhibits similar hydrogen bonding interaction as JB7 with hydrophobic S1 pocket (Figure 2.5). Insertion of an extra methylene group after the amide bond leads to an increase in the number of hydrogen bond interactions with aminoacid residues such as Arg 210, Asn 257, Glu 424, Asn 519 and Arg 534.

The carbonyl oxygen of amino acetamide ligand in **1** also interacts with the hydroxy group of Tyr 552 in S1' pocket of PSMA with a bond length of 1.72 Å which is considerably less than the bonding interaction (2.65 Å) of urea carbonyl oxygen moiety of JB7 with OH group of Tyr 552. It is important to note that Tyr 552 is positioned near Zn atoms of GCPII protein, which is important for the catalytic activity of PSMA.

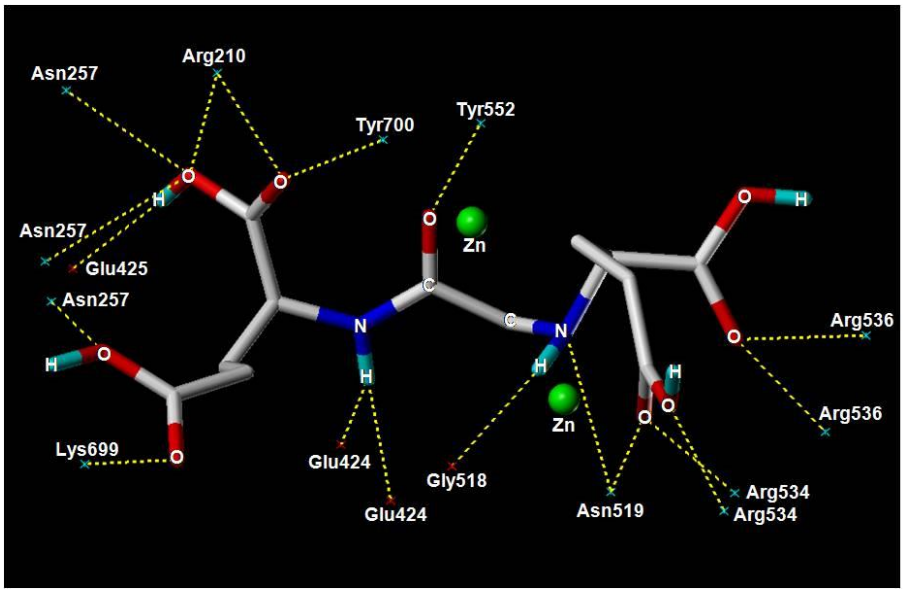

Figure 2.5 Molecular docking study of inhibitor **1** (henceforth labelled as AAPT) at GCPII active cavity (PDB 4NGM); green spheres represents Zn atom at the active site of GCPII

The strong interaction of **1** with Tyr 552 residue at the active site of the protein might help inhibit the catalytic activity of GCPII. This strong hydrogen bonding interaction of **1** with GCPII could be responsible for higher binding affinity of **1** among other ligands in the series. Though ligand **1** forms a greater number of hydrogen bonds due to the presence of polar glutamate scaffold, the overall docking score of JB7 was found to be higher as compared to **1**. This is because the efficacy of inhibitory activity of ligands not only depends on polar interactions but also on other non-polar interactions such as lipophilic and π-π stacking interactions due to the presence of benzyl group in the lysine moiety of JB7.

Further, to analyse the effect of polar and non-polar substituents on the efficiency of ligands to inhibit the activity of GCPII enzyme, several derivatives of amino acetamide ligands such as **2–10** have been designed and synthesized for evaluation. After glutamate ligand **1**, phenylalanine (**3**) and tyrosine (**2**) derivatives were observed to have better docking scores compared to the other designed analogs **4–10**.

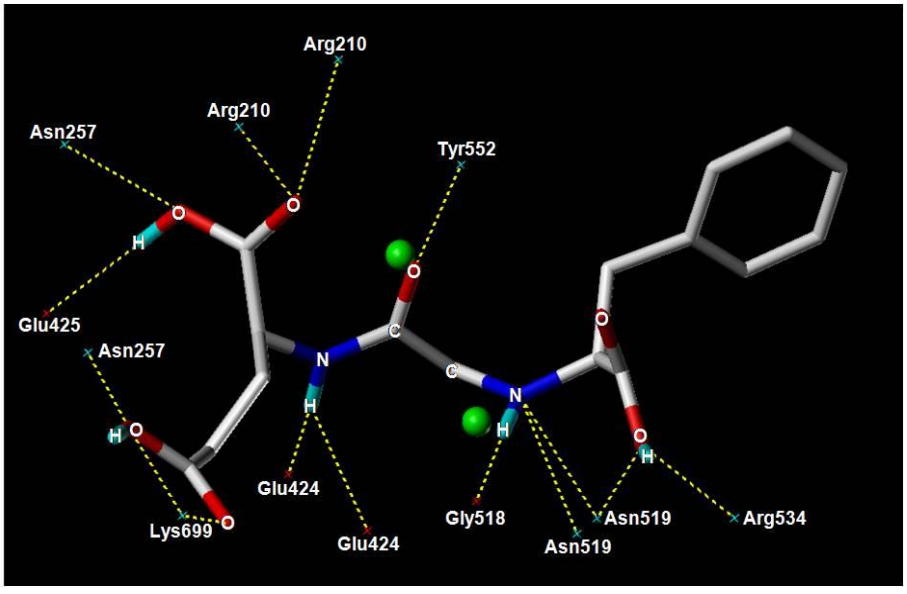

Figure 2.6 Computational docking of aminoacetamide inhibitor **3** in the active site of GCPII (PDB 4NGM); green spheres represent Zn atoms in the active site of GCPII

The docking conformation of the second most active ligand, **3**, in series show ten hydrogen bonding interactions with the active site residues such as Arg 210, Asn 257, Lys 699, Tyr 552 and Glu 424 at the hydrophilic pocket of the enzyme. Slightly less activity of **3** as compared to **1** is due to the lesser number of hydrogen bonding interactions (Table 2.2) of **3** at the hydrophobic pocket of GCPII enzyme as shown in Figure 2.6.

Because of the presence of hydroxyl group of tyrosine moiety in **2**, there is a change in the orientation of tyrosine moiety leading to change in the total number of amino acid interactions of **2** as compared to **3** with GCPII (Figure 2.7). At S1' site (hydrophilic pocket), **3** forms seven hydrogen bonding interactions with Arg 210, Asn 257, Lys 699 and Glu 425 aminoacid residues, whereas **2** forms only two hydrogen bonding interactions with Arg 210 and Lys 699 and no interaction with Asn 257 and Glu 425 residues when compared to **3**. However, **2** forms an additional H-bonding interaction with Tyr 552 along with a new interaction with Tyr 700 in the active site of GCPII in comparison to **3**. Including two interactions of both **2** and **3** with Glu 424 residue, the total number interactions of **2** and **3** at hydrophilic pocket are seven and ten respectively.

At S1 site (hydrophobic pocket), **3** forms four hydrogen bonding interactions with Gly 518, Asn 519 and Arg 534 which were absent in **2**. Due to change in the orientation of **2,** it forms six new interactions with Asp 453, Asp 387, Ser 454, Tyr 549 and Ser 517 aminoacid residues that were absent in **3**.

This study infers that at GCPII active site, **3** forms fourteen hydrogen bonding interactions while **2** forms only thirteen interactions. This may be the plausible reason for less docking score of ligand **2** when compared to **3**.

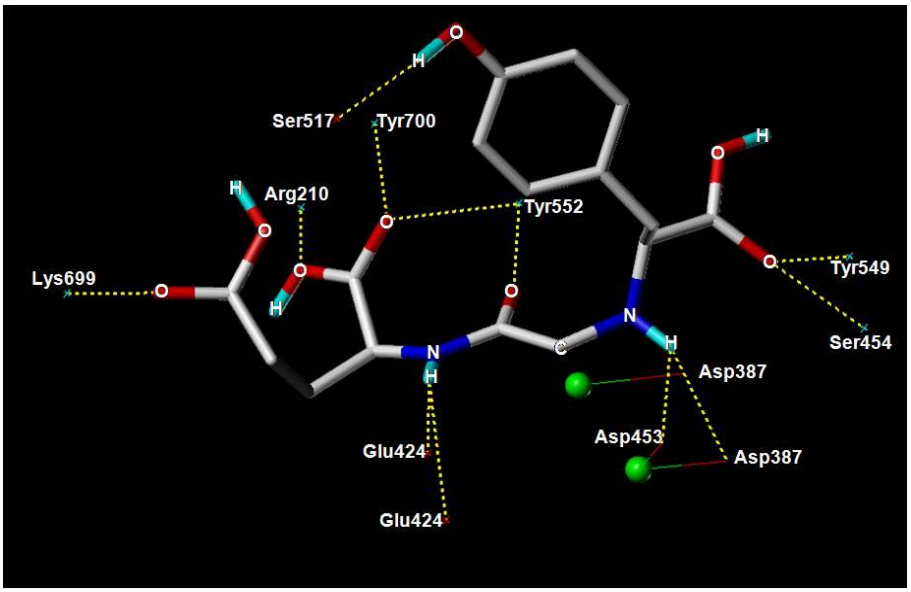

Figure 2.7 Hydrogen bonding interactions of aminoacetamide inhibitor **2** in the active site of GCPII (PDB 4NGM) in comparison to **3**; green spheres represent Zn atoms in the active site of GCPII

In summary, we have designed and developed aminoacetamide derivatives as a new class of GCPII inhibitor through extensive molecular docking studies. Ten aminoacetamide based ligands or inhibitors (**1–10**) have been rationally designed and through molecular docking study top three rank derivatives (**1–3**) were selected for detailed analysis of amino acid-ligand interactions. However, derivatives **4–10** were also studied for various interactions at the active site of GCPII without detailed interpretation of the theoretical data presented in table 2.2. Further based on this study, inhibitors **1–3** were chemically synthesized by deprotection of carboxy protecting groups (benzyloxy and *tertiary*-butyl) from their precursors **15a–c** (Schemes 2.1 and 2.2) and selected for further *in vitro* biological evaluation to inhibit GCPII activity. Carboxy protected acetamide precursors **15d–j** of acetamide based GCPII inhibitors **4–10** were also synthesized and completely characterized for future studies if required. As per molecular docking studies GCPII inhibitors **4–10** (Table 2.1) had poor docking scores when compared to inhibitors **1–3** and hence not

synthesized chemically in the lab though their precursors **15d–j** were synthesized, characterized using various spectroscopic techniques and readily available for future experimental studies (Scheme 2.1, Figure 2.8).

2.2.2 Synthesis of aminoacetamide derivatives 15a–j

Based on the docking study, ten different derivatives of protected aminoacetamide moiety has been synthesized by using a novel and simple procedure developed at our laboratory. The procedure for the synthesis of amino acetamide derivatives **15a–j** has been described in Schemes 2.1 and 2.2. Briefly, bromoacetic acid **12** was coupled with the amino group of protected amino acids **11a–c** in the presence of dicylohexylcarbodimide to afford bromoacetamide intermediates **13a–c**. In the next step, nucleophilic substitution of bromo group in **13a–c** by the amino group of *tertiary*-butylcarboxy amino esters **14a–j** in the presence of DIPEA at 80 °C for 16–20 h in THF afforded protected aminoacetamide precursors **15a–j** (Scheme 2.1).

Scheme 2.1 Synthesis of carboxylic acids protected aminoacetamide precursors **15a–j** of aminoacetamide based GCPII inhibitors, **1–10**

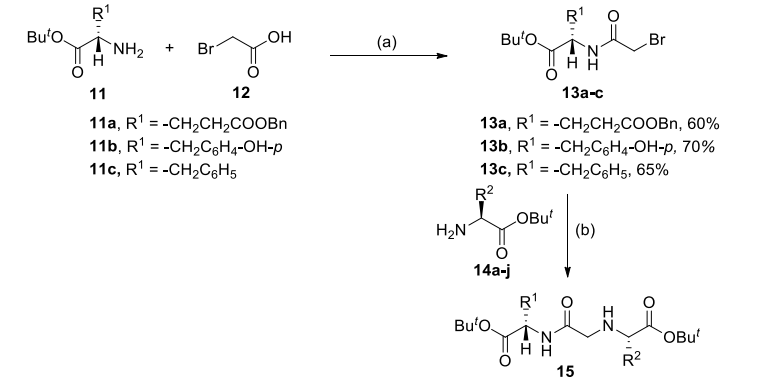

Reagents and conditions: (a) DCC, CH_2Cl_2, 0 °C to rt, 12 h; (b) THF, DIPEA, 80 °C, 18–20 h

Scheme 2.2 Synthesis of aminoacetamide based GCPII inhibitors **1–3** from precursors **15a–c**

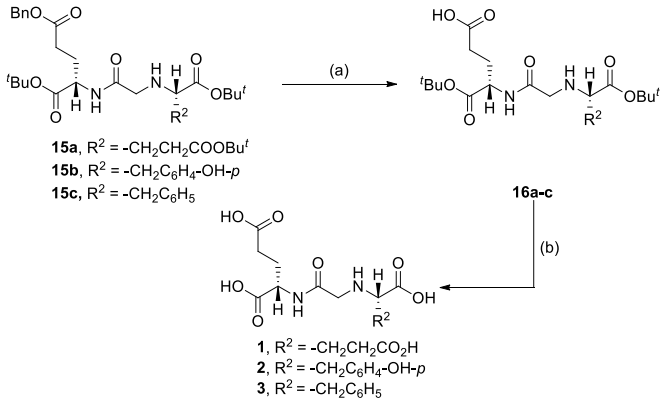

Reagents and conditions: (a) 10% Pd-C/H_2, MeOH, rt, 24 h; (b) CF_3COOH: CH_2Cl_2 (1:1), rt, 2 h

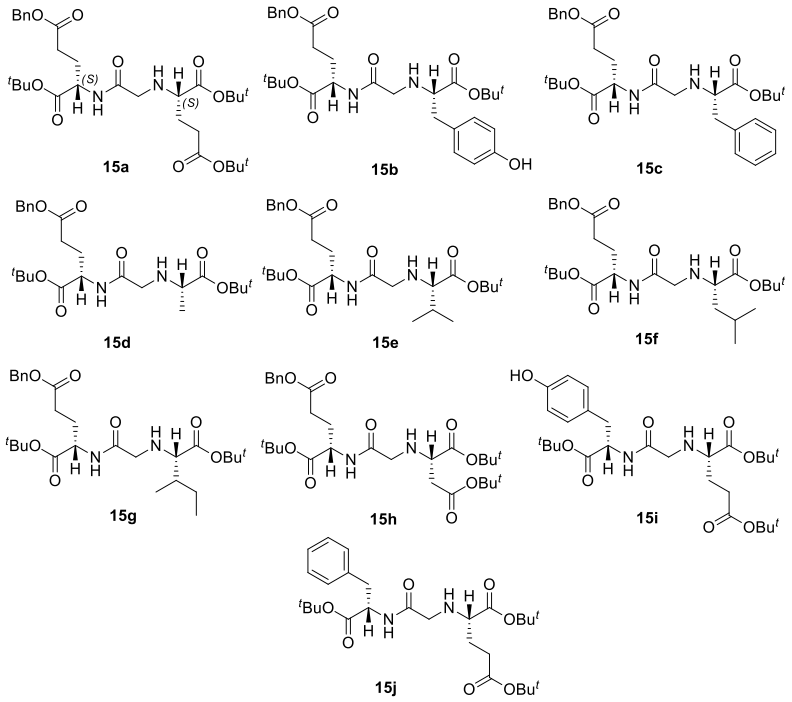

Figure 2.8 Synthesized carboxylic acids protected amino acetamide based GCPII inhibitor precursors **15a–j**

Encouraged by the best docking score, the three most high ranking aminoacetamide derivatives **1–3** were chemically synthesized. Debenzylation of **15a–c** in presence of H_2/Pd-C and MeOH at room

temperature resulted in the formation of **16a–c** (Scheme 2.2). Subsequent deprotection of *tertiary*-butylcarboxy groups in **16a–c** with trifluoroacetic acid yielded the inhibitors **1–3**. The deprotection reaction was performed in the presence of trifluoroacetic acid and CH_2Cl_2 mixture (1:1) at room temperature. The inhibitors **1–3** were further purified through Buchi Reveleris preparative high-performance liquid chromatography using reverse phase pentafluorophenyl (RP-PFP) column. The inhibitors **1–3** were then biologically evaluated using fluorescence-based enzyme inhibition assay to determine half-inhibitory concentration, IC_{50}.

2.2.3 *In vitro* GCPII inhibition assay

After the successful synthesis of GCPII inhibitors **1–3**, *in vitro* evaluation of the three most potent aminoacetamide derivatives **1–3** were performed using prostate cancer cell line, LNCaP, expressing GCPII or PSMA protein. Briefly, membrane portion of PSMA enzyme was extracted from $PSMA^+$ LNCaP cell line by following a reported protocol.[30] The isolated PSMA enzyme was incubated with various concentrations of the inhibitors **1–3** in the presence of a competitive inhibitor, *N*-acetylaspartylglutamate (NAAG).

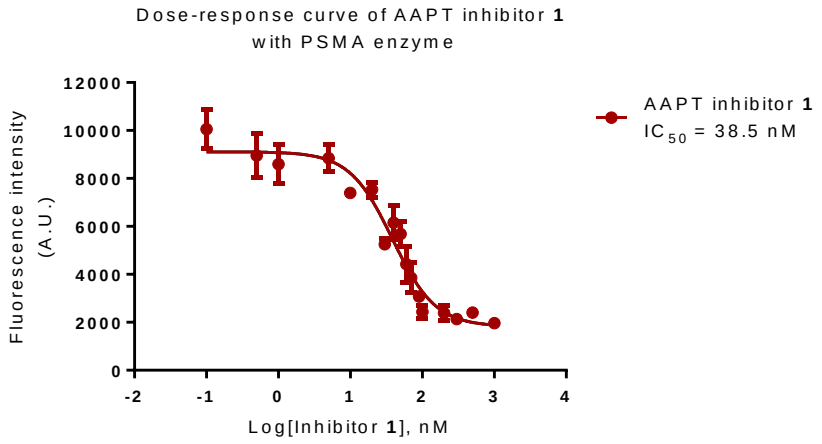

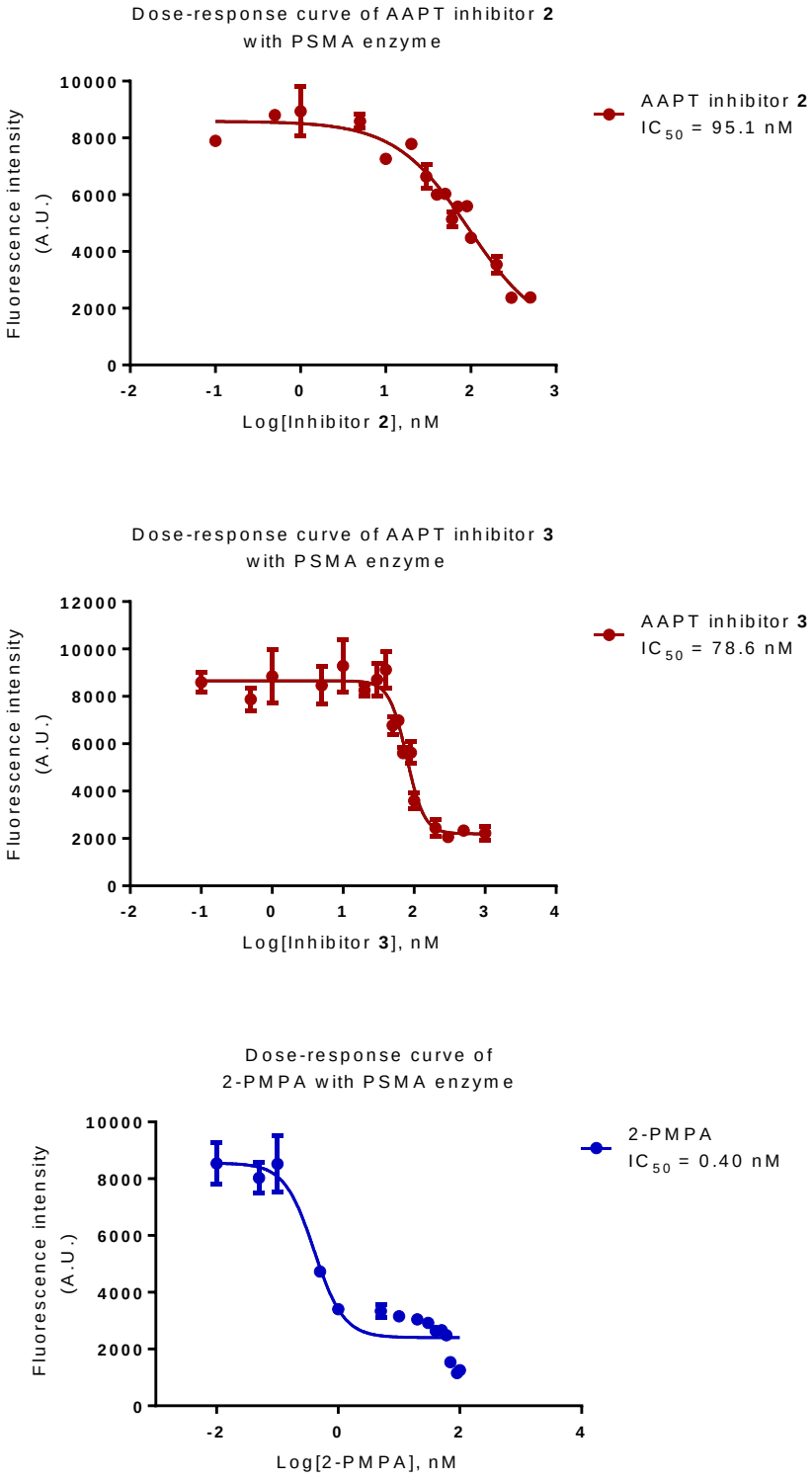

Figure 2.9 (a) Dose-response curve of aminoacetamide inhibitor **1** (IC_{50} = 38.5 nM, (b) inhibitor **2** (IC_{50} = 95.1 nM), (c) inhibitor **3** (IC_{50} = 78.6 nM)

and (d) 2-PMPA from PSMA or GCPII enzyme inhibition assay, SD (n = 3)

The amount of glutamic acid released by the hydrolysis of NAAG was measured by incubating a working solution of Amplex Red reagent for 30 min at 37 °C. The fluorescence emission intensity from the oxidation product of Amplex Red reagent, resorufin, is measured at 590 nm by excitation at 530 nm. A plot of dose v/s response curve is drawn using log [Inhibitors **1–3**] versus fluorescence emission intensity to provide experimental inhibitory concentration, IC_{50}, values for the inhibitors **1–3**.

Simultaneously, GCPII enzyme inhibition assay was also performed with a standard PSMA inhibitor, 2-(phosphonomethyl)pentanedioic acid (PMPA) who's IC_{50} is reported to be 0.28 nM and experimentally we have observed a value of IC_{50} = 0.40 nM validating our assay for inhibiting GCPII with our new inhibitors **1–3** (Figure 2.9).

2.3 Conclusion

A novel class of aminoacetamide based peptidomimetics were designed by mimicking *N*-acetylaspartylglutamate (NAAG) substrate. Basic pharmacophore requirements for inhibitors **1–3** were determined computationally based on analyzing the bonding interactions and co-crystal structure of GCPII with a ligand (PDB 4NGM). A library of ten protected aminoacetamide derivatives has been synthesized through a novel and high yielding synthetic strategy developed at our laboratory. The inhibitors, **1–3**, show excellent to good GCPII inhibitory activity in nanomolar concentrations. This work clearly demonstrates that the insertion of a methylene carbon unit after the amide functionality in the native substrate is well tolerated at the active site of GCPII. These results should facilitate the future development of other NAALADase and PSMA inhibitors. In the next chapter, we have studied the application of using

fluorescently labelled inhibitor **1** to detect $PSMA^+$ cancers by fluorescent microscopy and radionuclides.

2.4 Experimental section

2.4.1 Materials and methods

Amino acids and coupling agents, reagents and solvents used in chemical synthesis were purchased from Iris Biotech GmbH, Sigma Aldrich, Merck and Spectrochem. Dry solvents were prepared by using drying agents and following usual methods. Moisture and oxygen sensitive reactions were carried out under a nitrogen atmosphere. Thin layer chromatography (TLC) was performed on silica gel glass TLC plates (60 F_{254}) and visualized under UV light to monitor the progress of the reaction. All compounds were purified by column chromatography using 100–200 or 230–400 mesh silica-gel as the stationary phase. Distilled hexane and distilled ethyl acetate were used as eluents in column chromatography.

^1H and ^{13}C NMR spectra were recorded using Bruker AV 400 MHz NMR spectrometer with TMS as an internal standard. ^1H NMR signals were reported in ppm with reference to residual $CHCl_3$ (7.25 ppm) and multiplicity was reported as s = singlet, d = doublet, t = triplet, q = quartet, m = multiplet or unresolved, and brs = broad singlet, with coupling constants in Hz. $CDCl_3$ was used as the solvent for recording NMR spectra. Mass spectra were recorded on Bruker micro TOF-Q II instrument using positive or negative mode electrospray ionization methods. Aminoacetamide ligands **1–3** were purified through Buchi reveleris prep instrument using RP-PFP column (XSelect CSH Prep Fluorophenyl 5 µm OBD, 19 mm × 150 mm) and the purity of **1–3** were determined in Dionex HPLC-Ultimate 3000 analytical liquid chromatography using 0.1% TFA eluent in acetonitrile and water with 0.1% TFA.

2.4.2 General procedure for the synthesis of 2-bromoacetamide intermediates 13a–c

Bromoacetic acid **12** (0.208 mg, 1.5 mmol), dicylohexylcarbodiimide (0.619, 3.0 mmol) were dissolved in freshly distilled dichloromethane (8 mL), and the resulting mixture was stirred at 0 °C for 30 min. A solution of **11a–c** (1.0 mmol) in dichloromethane (5 mL) was added to the reaction mixture. The reaction mixture was stirred for 12 h at room temperature. The progress of the reaction was monitored by thin layer chromatography (TLC). After completion of the reaction, dichloromethane was evaporated under reduced pressure and ethyl acetate was added to the residue of the crude reaction mixture. Dicyclohexyl urea (DCU) was filtered off from the reaction mixture through glass funnel by using Whatman filter paper. The ethyl acetate layer was concentrated under reduced pressure and the crude products **13a–c** were purified through column chromatography using distilled 15–25% ethyl acetate in hexane.

2.4.2.1 (*S*)-5-Benzyl 1-*tert*-butyl 2-(2-bromoacetamido)pentanedioate (13a)

Yellowish gummy liquid (yield = 60%), R_f = 0.56 (EtOAc : hexane = 1:4); IR (CH_2Cl_2): 3322 (N–H), 3032, 2975 (=C–H), 2928 (C–H), 1729 (C=O), 1652 (N–H), 1537 (C=C), 1454 (C–H), 1166 (C–O), 750, 699 (=C–H) cm^{-1}. ^{1}H NMR (400 MHz, $CDCl_3$): δ 7.37–7.31 (m, 5H), 7.05 (d, J = 7.28 Hz, 1H), 5.13, 5.10 (ABquartet, J = 13.28 Hz, 2H), 4.49 (ddd, J = 7.28, 5.24, 5.14 Hz, 1H), 3.83 (s, 2H), 2.49–2.38 (m, 2H), 2.27–2.20 (m, 1H), 2.07–1.99 (m, 1H), 1.46 (s, 9H). ^{13}C NMR (100 MHz, $CDCl_3$): δ 172.5, 170.3, 165.8, 135.6, 128.6, 128.3, 128.2, 83.0, 66.6, 52.8, 30.1, 28.6, 27.9, 27.3. HRMS (ESI) m/z $[M+Na]^+$ calcd. for $C_{18}H_{24}BrNO_5$, 436.0730, found, 436.0766.

2.4.2.2 (*S*)-*tert*-Butyl-2-(2-bromoacetamido)-3-(4-hydroxyphenyl) propanoate (13b)

Colourless gummy liquid (yield = 70%), R_f = 0.4 (EtOAc : hexane = 1:4); IR (CH_2Cl_2): 3341 (O–H), 3275 (N–H), 2979 (=C–H), 2933 (C–H), 1733 (C=O), 1657 (N–H), 1518(C=C), 1456 (C–H), 1155 (C–O), 750, 698 (=C–H) cm^{-1}. ^1H NMR (400 MHz, $CDCl_3$): δ 7.03 (d, J = 8.44 Hz, 2H), 6.93 (d, J = 7.32 Hz, 1H), 6.73 (d, J = 8.44 Hz, 2H), 5.96 (brs, 1H), 4.71–4.63 (m, 1H), 3.85, 3.81 (ABquartet, J = 13.80 Hz, 2H), 3.09–2.96 (m, 2H), 1.43 (s, 9H). ^{13}C NMR (100 MHz, $CDCl_3$): δ 170.1, 165.3, 155.2, 130.6, 127.2, 115.4, 82.9, 54.3, 37.1, 28.7, 27.9. HRMS (ESI) m/z $[M+Na]^+$ calcd. for $C_{15}H_{20}BrNO_4$, 380.0468, found, 380.0479.

2.4.2.3 (*S*)-*tert*-Butyl 2-(2-bromoacetamido)-3-phenylpropanoate (13c)

Colourless gummy liquid (yield = 65%), R_f = 0.52 (EtOAc : hexane = 1:4); IR (CH_2Cl_2): 3298 (N–H), 2979 (=C–H), 2933 (C–H), 1734 (C=O), 1657 (N–H), 1528 (C=C), 1456 (C–H), 1155 (C–O), 740 (=C–H) cm^{-1}. ^1H NMR (400 MHz, $CDCl_3$): δ 7.31–7.26 (m, 3H), 7.17–7.15 (m, 2H), 6.89 (d, J = 6.52 Hz, 1H), 4.72 (ddd, J = 6.52, 6.0, 4.52 Hz, 1H), 3.87, 3.83 (ABquartet, J = 13.80 Hz, 2H), 3.12 (d, J = 6.04 Hz, 2H), 1.42 (s, 9H). ^{13}C NMR (100 MHz, $CDCl_3$): δ 169.9, 164.9, 135.7, 129.5, 128.4, 127.1, 82.8, 54.1, 37.9, 28.8, 27.9. HRMS (ESI) m/z $[M+Na]^+$ calcd. for $C_{15}H_{20}BrNO_3$, 364.0519, found, 364.0522.

2.4.3 General procedure for the synthesis of protected amino acetamide derivatives 15a–j

Compound **13a–c** (1.0 mmol) and **14a–j** (1.0 mmol) were dissolved in dry THF (5 mL) and DIPEA (0.52 mL, 3.0 mmol) was added in the reaction mixture. The reaction mixture was refluxed at 80 °C for 18–20 h. The reaction progress was monitored through TLC. After the completion of the reaction, THF was evaporated under reduced pressure and 30 mL of ethyl

acetate was added to the crude reaction mixture. The organic layer was washed with distilled water (2 × 15 mL) and the resultant organic layer was dried over anhydrous sodium sulphate. The organic layer was concentrated under reduced pressure and the crude products **15a–j** were purified through column chromatography using distilled 33% ethyl acetate and hexane mixture as eluent.

2.4.3.1 (*S*)-5-Benzyl-1-*tert*-butyl-2-(2-(((*S*)-1,5-di-*tert*-butoxy-1,5-dioxopentan-2-yl)amino)acetamido)pentanedioate (15a)

Yellowish gummy liquid (yield = 75%), R_f = 0.3 (EtOAc : hexane = 1:2), IR (CH_2Cl_2): 3349 (N–H), 2978 (=C–H), 2928 (C–H), 1729 (C=O), 1682 (N–H), 1517(C=C), 1456 (C–H), 1155 (C–O), 750, 699 (=C–H) cm^{-1}. ^1H NMR (400 MHz, $CDCl_3$): δ 7.70 (d, J = 8.4 Hz, 1H), 7.40–7.26 (m, 5H), 5.10 (s, 2H), 4.52 (ddd, J = 7.99, 5.66, 4.76, 1H), 3.39 (d, J = 17.2 Hz, 1H), 3.13–3.05 (m, 1H), 3.00 (d, J = 17.2 Hz, 1H), 2.48–2.32 (m, 4H), 2.28–2.18 (m, 1H), 2.04–1.91 (m, 3H), 1.87–1.75 (m, 1H), 1.45 (s, 9H), 1.44 (s, 9H), 1.42 (s, 9H). ^{13}C NMR (100 MHz, $CDCl_3$): δ 173.7, 172.6, 171.3, 170.7, 135.9, 128.6, 128.3, 82.2, 81.9, 80.5, 66.4, 61.9, 51.7, 51.0, 32.4, 30.5, 28.7, 28.1, 28.0, 27.6. HRMS (ESI) m/z $[M+Na]^+$ calcd. for $C_{31}H_{48}N_2O_9$, 615.3252, found, 615.3308.

2.4.3.2 (*S*)-5-Benzyl-1-*tert*-butyl-2-(2-(((*S*)-1-(*tert*-butoxy)-3-(4-hydroxyphenyl)-1-oxopropan-2-yl)amino)acetamido)pentanedioate (15b)

Gummy liquid (yield = 75%), R_f = 0.25 (EtOAc : hexane = 1:2); IR (CH_2Cl_2): 3321 (O–H), 3279 (N–H), 3067, 2979 (=C–H), 2929, 2851 (C–H), 1731 (C=O), 1650 (N–H), 1537, 1517 (C=C), 1448 (C–H), 1154 (C–O), 750, 699 (=C–H) cm^{-1}. ^1H NMR (400 MHz, $CDCl_3$): δ 7.40–7.32 (m, 5H), 7.07 (d, J = 7.52 Hz, 3H), 6.70 (d, J = 7.52 Hz, 2H), 5.15, 5.10 (ABquartet, J = 12.28 Hz, 2H), 4.31–4.26 (m, 1H), 3.36 (d, J = 17.56 Hz, 1H), 3.33–3.25 (m, 1H), 3.00 (d, J = 17.56 Hz, 1H), 2.93 (dd, J = 13.8,

4.52 Hz, 1H), 2.68 (dd, *J* = 12.80, 9.28 Hz, 1H), 2.40–2.21 (m, 2H), 2.10–1.95 (m, 1H), 1.87–1.58 (m, 2H), 1.44 (s, 9H), 1.41 (s, 9H). ^{13}C NMR (100 MHz, $CDCl_3$): δ 173.4, 172.4, 171.3, 170.6, 137.2, 135.8, 129.6, 128.6, 128.4, 128.3, 126.7, 82.1, 81.8, 66.4, 63.2, 51.5, 50.6, 39.9, 30.5, 28.0, 27.9, 27.3. HRMS (ESI) m/z $[M+H]^+$ calcd. for $C_{31}H_{42}N_2O_{8,}$ 571.3014, found, 571.3007.

2.4.3.3 (*S*)-5-Benzyl-1-*tert*-butyl-2-(2-(((*S*)-1-(*tert*-butoxy)-1-oxo-3-phenylpropan-2-yl)amino)acetamido)pentanedioate (15c)

White solid (yield = 70%), R_f = 0.35 (EtOAc : hexane = 1:2); IR (CH_2Cl_2): 3326 (N–H), 2979 (=C–H), 2929 (C–H), 1723 (C=O), 1668 (N–H), 1520 (C=C), 1455 (C–H), 1154 (C–O), 735, 698 (=C–H) cm^{-1}. ^{1}H NMR (400 MHz, $CDCl_3$): δ 7.40–7.34 (m, 5H), 7.28–7.20 (m, 5H), 5.13, 5.09 (ABquartet, *J* = 14.04 Hz, 2H), 4.45–4.35 (m, 1H), 3.41–3.34 (m, 2H), 3.07–2.84 (m, 3H), 2.43–2.24 (m, 2H), 2.18–2.06 (m, 1H), 2.04–1.85 (m, 1H), 1.82–1.70 (m, 1H), 1.46 (s, 9H), 1.37 (s, 9H), 1.25–1.21 (m, 1H). ^{13}C NMR (100 MHz, $CDCl_3$): δ 173.7, 172.9, 171.9, 170.4, 155.0, 135.7, 130.6, 128.9, 128.6, 128.4, 128.3, 115.7, 82.1, 81.8, 66.6, 63.5, 51.7, 50.5, 38.9, 30.6, 28.0, 27.9, 26.9. HRMS (ESI) m/z $[M+Na]^+$ calcd. for $C_{31}H_{42}N_2O_7$, 577.2884, found, 577.2888.

2.4.3.4 (*S*)-5-Benzyl-1-*tert*-butyl-2-(2-(((*S*)-1-(*tert*-butoxy)-1-oxopropan-2-yl)amino) acetamido)pentanedioate (15d)

White solid (yield = 72%), R_f = 0.32 (EtOAc : hexane = 1:2); IR (CH_2Cl_2): 3338 (N–H), 2974 (=C–H), 2927 (C–H), 1730 (C=O), 1666 (N–H), 1523 (C=C), 1455 (C–H), 1152, 1064 (C–O), 734, 697 (=C–H) cm^{-1}. ^{1}H NMR (400 MHz, $CDCl_3$): δ 7.77 (d, *J* = 8.52 Hz, 1H), 7.36–7.30 (m, 5H), 5.12, 5.08 (ABquartet, *J* = 13.04 Hz, 2H), 4.53 (ddd, *J* = 8.52, 5.78, 5.0 Hz, 1H), 3.37 (d, *J* = 17.32 Hz, 1H), 3.16 (q, *J* = 7.04 Hz, 1H), 3.04 (d, *J* = 17.32 Hz, 1H), 2.52–2.32 (m, 2H), 2.27–2.15 (m, 1H), 2.04–1.92 (m, 1H), 1.45 (s, 9H), 1.44 (s, 9H), 1.28 (d, *J* = 7.04 Hz, 3H), 1.24 (brs, 1H). ^{13}C

NMR (100 MHz, $CDCl_3$): δ 174.5, 172.6, 171.4, 170.8, 135.8, 128.6, 128.3, 128.2, 82.3, 81.5, 66.5, 57.5, 51.6, 50.8, 30.4, 28.0, 27.9, 27.8, 19.3. HRMS (ESI) m/z $[M+Na]^+$ calcd. for $C_{25}H_{38}N_2O_7$, 501.2571, found, 501.2572.

2.4.3.5 (*S*)-5-Benzyl-1-*tert*-butyl-2-(2-(((*S*)-1-(*tert*-butoxy)-3-methyl-1-oxobutan-2-yl)amino)acetamido)pentanedioate (15e)

Yellowish gummy liquid (yield = 75%), R_f = 0.36 (EtOAc : hexane = 1:2); IR (CH_2Cl_2): 3363 (N–H), 2975 (=C–H), 2933 (C–H), 1733 (C=O), 1681 (N–H), 1513 (C=C), 1457 (C–H), 1157 (C–O), 746, 699 (=C–H) cm^{-1}.^{1}H NMR (400 MHz, $CDCl_3$): δ 7.73 (d, J = 8.28 Hz, 1H), 7.38–7.32 (m, 5H), 5.12, 5.08 (ABquartet, J = 12.56 Hz, 2H), 4.51 (ddd, J = 8.28, 5.66, 5.24, 1H), 3.40 (d, J = 17.32 Hz, 1H), 2.98–2.93 (m, 2H), 2.51–2.33 (m, 2H), 2.25–2.15 (m, 1H), 2.05–1.93 (m, 1H), 1.44 (s, 18H), 1.30–1.13 (m, 2H), 0.97–0.86 (m, 6H). ^{13}C NMR (100 MHz, $CDCl_3$): δ 173.9, 172.6, 171.6, 170.7, 135.9, 128.6, *128.4, 82.3, 81.6, 68.0, 66.5, 51.8, 51.3, 31.6, 30.5, 28.2, 28.1, 27.9, 19.5, 18.4. HRMS (ESI) m/z $[M+Na]^+$ calcd. for $C_{27}H_{42}N_2O_7$, 529.2884, found, 529.2882.

*higher intensity carbon

2.4.3.6 (*S*)-5-Benzyl-1-*tert*-butyl-2-(2-(((*S*)-1-(*tert*-butoxy)-4-methyl-1-oxopentan-2-yl)amino)acetamido)pentanedioate (15f)

Yellowish liquid (yield = 82%), R_f = 0.4 (EtOAc : hexane = 1:2); IR (CH_2Cl_2): 3354 (N–H), 2959 (=C–H), 2934 (C–H), 1734 (C=O), 1681 (N–H), 1511 (C=C), 1456 (C–H), 1155, 1081 (C–O), 749, 699 (=C–H) cm^{-1}.^{1}H NMR (400 MHz, $CDCl_3$): δ 7.74 (d, J = 8.28 Hz, 1H), 7.40–7.30 (m, 5H), 5.11, 5.08 (ABquartet, J = 12.80 Hz, 2H), 4.51 (ddd, J = 8.28, 5.40, 5.28, 1H), 3.37 (d, J = 17.32 Hz, 1H), 3.09 (t, J = 7.0 Hz, 1H), 2.99 (d, J = 17.32 Hz, 1H), 2.51–2.32 (m, 2H), 2.26–2.15 (m, 1H), 2.04–1.92 (m, 1H), 1.83–1.71 (m, 3H), 1.44 (s, 9H), 1.43 (s, 9H) 1.29–1.22 (m, 1H), 0.92 (d, J = 6.52 Hz, 3H), 0.90 (d, J = 6.52 Hz, 3H). ^{13}C NMR (100 MHz,

$CDCl_3$): δ 174.7, 172.5, 171.4, 170.6, 135.8, 128.6, 128.3, 128.2, 82.2, 81.5, 66.4, 60.9, 51.7, 50.8, 42.9, 30.4, 28.1, 27.9, 27.8, 24.9, 22.6, 22.5. HRMS (ESI) m/z $[M+Na]^+$ calcd. for $C_{28}H_{44}N_2O_7$, 521.3221, found, 521.3222.

2.4.3.7 (2*S*)-5-Benzyl-1-*tert*-butyl-2-(2-(((2*S*)-1-(*tert*-butoxy)-3-methyl-1-oxopentan-2-yl)amino)acetamido)pentanedioate (15g)

Yellowish solid (yield = 86%), R_f = 0.34 (EtOAc : hexane = 1:2); IR (CH_2Cl_2): 3347(N–H), 2977 (=C–H), 2933 (C–H), 1727 (C=O), 1668 (N–H), 1515 (C=C), 1458 (C–H), 1153 (C–O), 734, 698 (=C–H) cm^{-1}.^{1}H NMR (400 MHz, $CDCl_3$): δ 7.72 (d, J = 8.52 Hz, 1H), 7.42–7.27 (m, 5H), 5.11, 5.08 (ABquartet, J = 12.52 Hz, 2H), 4.51 (ddd, J = 8.52, 5.38, 5.24, 1H), 3.40 (d, J = 17.32 Hz, 1H), 2.95 (d, 1H, J = 17.32 Hz), 2.86 (d, J = 5.76 Hz, 1H), 2.51–2.32 (m, 2H), 2.26–2.14 (m, 1H), 2.04–1.87 (m, 4H), 1.44 (s, 18H), 1.28–1.23 (m, 1H), 0.99 (d, J = 6.80 Hz, 3H), 0.95 (d, J = 7.04 Hz, 3H). ^{13}C NMR (100 MHz, $CDCl_3$): δ 173.6, 172.6, 171.5, 170.6, 135.8, 128.6, 128.3, 128.2, 82.2, 81.5, 66.8, 66.5, 51.7, 51.3, 38.5, 30.4, 28.2, 27.9, 27.8, 25.5, 15.7, 11.7. HRMS (ESI) m/z $[M+Na]^+$ calcd. for $C_{28}H_{44}N_2O_7$, 521.3221, found, 521.3223.

2.4.3.8 (*S*)-5-Benzyl-1-*tert*-butyl-2-(2-(((*S*)-1,4-di-*tert*-butoxy-1,4-dioxobutan-2-yl)amino)acetamido)pentanedioate (15h)

Yellowish liquid (yield = 85%), R_f = 0.32 (EtOAc : hexane = 1:2); IR (CH_2Cl_2): 3327 (N–H), 2975 (=C–H), 2926 (C–H), 1723 (C=O), 1672 (N–H), 1519 (C=C), 1456 (C–H), 1149 (C–O), 750, 698 (=C–H) cm^{-1}.^{1}H NMR (400 MHz, $CDCl_3$): δ 8.00 (d, J = 8.52 Hz, 1H), 7.40–7.27 (m, 5H), 5.11, 5.08 (ABquartet, J = 12.80 Hz, 2H), 4.50 (ddd, J = 8.52, 6.14, 4.76 Hz, 1H), 3.48–3.40 (m, 2H), 3.18–3.14 (d, J = 17.32 Hz, 1H), 2.66 (dd, J = 16.7, 4.24, Hz, 1H), 2.57–2.37 (m, 3H), 2.30–2.17 (m, 1H), 2.10–1.96 (m, 1H), 1.44 (s, 9H), 1.43 (s, 9H), 1.41(s, 9H), 1.27–1.24 (m, 1H). ^{13}C NMR (100 MHz, $CDCl_3$): δ 172.6, 172.5, 171.6, 170.7, 170.4, 135.9,

128.5, 128.3, 128.2, 82.0, 81.9, 81.5, 66.4, 58.1, 51.8, 50.9, 38.8, 30.6, 28.1, *27.9, 27.2. HRMS (ESI) m/z $[M+Na]^+$ calcd. for $C_{30}H_{46}N_2O_9$, 578.3203, found, 579.3275.

*higher intensity carbon

2.4.3.9 (*S*)-Di-*tert*-butyl-2-(2-(((*S*)-1-(*tert*-butoxy)-3-(4-hydroxyphenyl) -1-oxopropan-2-yl)amino) -2-oxoethyl)amino) pentanedioate (15i)

White solid (yield = 85%), R_f = 0.25 (EtOAc : hexane = 1:2); IR (CH_2Cl_2): 3349 (O–H), 3275 (N–H), 2979 (=C–H), 2933 (C–H), 1730 (C=O), 1660 (N–H), 1517(C=C), 1456 (C–H), 1155 (C–O), 753 (=C–H) cm^{-1}.^{1}H NMR (400 MHz, $CDCl_3$): δ 7.57 (d, J = 8.44 Hz, 1H), 7.01 (d, J = 8.08 Hz, 2H), 6.72 (d, J = 8.08 Hz, 2H), 4.75–4.65 (m, 1H), 3.35 (d, J = 16.88 Hz, 1H), 3.10–2.90 (m, 4H), 2.37–2.20 (m, 2H), 1.90–1.67 (m, 2H), 1.43 (s, 18H), 1.42 (s, 9H), 1.27–1.22 (m, 1H). ^{13}C NMR (100 MHz, $CDCl_3$): δ 173.6, 172.8, 171.2, 170.6, 155.3, 130.4, 127.7, 115.7, 82.1, 81.9, 80.8, 61.6, 53.3, 50.8, 37.2, 32.3, 28.7, 28.7, 28.09, 28.06, 28.0. HRMS (ESI) m/z $[M+Na]^+$ calcd. for $C_{28}H_{44}N_2O_8$, 559.2990, found, 559.2983.

2.4.3.10 (*S*)-Di-*tert*-butyl-2-((2-(((*S*)-1-(*tert*-butoxy)-1-oxo-3-phenylpropan-2-yl)amino)-2-oxoethyl)amino)pentanedioate (15j)

White solid (yield = 80%), R_f = 0.30 (EtOAc : hexane = 1:2); IR (CH_2Cl_2): 3350 (N–H), 2979 (=C–H), 2933 (C–H), 1732 (C=O), 1682 (N–H), 1518 (C=C), 1456 (C–H), 1155, 1080 (C–O), 741 (=C–H) cm^{-1}. ^{1}H NMR (400 MHz, $CDCl_3$): δ 7.54 (d, J = 8.44 Hz, 1H), 7.30–7.15 (m, 5H), 4.80–4.65 (m, 1H), 3.36 (d, J = 17.24 Hz, 1H), 3.15–3.07 (m, 2H), 3.07–3.01 (m, 1H), 2.98 (d, J = 17.24 Hz, 1H), 2.35–2.17 (m, 2H), 1.92–1.83 (m, 1H), 1.78–1.67 (m, 2H), 1.44 (s, 9H), 1.43 (s, 9H), 1.39 (s, 9H). ^{13}C NMR (100 MHz, $CDCl_3$): δ 173.7, 172.5, 170.8, 170.5, 136.5, 129.4, 128.4, 126.9, 82.0, 81.8, 80.4, 61.6, 53.2, 50.9, 37.9, 32.3, 28.6, 28.1, 28.0, 27.9. HRMS (ESI) m/z $[M+H]^+$ calcd. for $C_{28}H_{44}N_2O_7$, 521.3221, found, 521.3226.

2.4.4 Deprotection of carboxylic benzylester precursors 15a–c to afford *tert*-butylcarboxylic acids 16a–c

Compound **15a–c** (1.0 mmol) was dissolved in MeOH (5 mL) in a 50 mL two-neck round bottom flask, 10% Pd/C (0.106 g, 0.1 mmol) was added in the solution. The reaction mixture was hydrogenated at 1 atm for 24 h at room temperature. After the completion of the reaction, Pd/C was filtered through a celite pad (sintered glass filter was half-filled with celite powder) and washed with ethyl acetate (3 × 20 mL). The ethyl acetate layer was concentrated under reduced pressure and the crude products **16a–c** were purified through column chromatography by using distilled ethyl acetate to obtain pure **16a–c**.

2.4.4.1 (*S*)-5-(*Tert*-butoxy)-4-(2-(((*S*)-1,5-di-*tert*-butoxy-1,5-dioxo-pentan-2-yl)amino)acetamido)-5-oxopentanoic acid (16a)

Colourless gummy liquid (yield = 60%). R_f = 0.58 (EtOAc : Hexane = 1:1); IR (CH_2Cl_2): 3350 (N–H), 2979 (=C–H), 2933 (C–H), 1732 (C=O), 1682 (N–H), 1518 (C=C), 1456 (C–H), 1155, 1080 (C–O), 741 (=C–H) cm^{-1}. ^1H NMR (400 MHz, $CDCl_3$): δ 7.81 (d, J = 8.44 Hz, 1H), 4.50 (ddd, J = 7.79, 6.06, 4.76 Hz, 1H), 3.43 (d, J = 16.84 Hz, 1H), 3.15–3.07 (m, 1H), 3.04 (d, J = 16.84 Hz, 1H), 2.45–2.35 (m, 4H), 2.27–2.15 (m, 1H), 2.05–2.15 (m, 1H), 2.05–1.92 (m, 2H), 1.90–1.80 (m, 1H), 1.46 (s, 9H), 1.45 (s, 9H), 1.43 (s, 9H), 1.13–1.07 (brs, 1H). ^{13}C NMR (100 MHz, $CDCl_3$): δ 175.9, 173.7, 172.9, 171.8, 170.6, 82.3, 82.0, 80.8, 61.7, 51.9, 50.8, 32.3, 30.5, 28.6, 28.1, 27.9, 27.6. HRMS (ESI) m/z calcd for $C_{24}H_{42}N_2O_9$ $[M+H]^+$: 503.3004, found. 503.3011.

2.4.5 Procedure for the deprotection of *tert*-butylcarboxylic acids in 16a–c to afford inhibitors 1–3

Precursors **16a–c** (1.0 mmol) was dissolved in CH_2Cl_2 (2 mL) in a 50 mL round bottomed flask. A mixture of trifluoroacetic acid (2.5 mL) and

CH_2Cl_2 (2.5 mL) in the ratio 1:1 was added to the reaction mixture at room temperature and stirred for 2 h. After the completion of reaction, the mixture of trifluoroacetic acid and CH_2Cl_2 were removed under reduced pressure. The products **1–3** were precipitated by the addition of ice-cold ether (5 mL). The crude products **1–3** were washed (3 × 5 mL) with ether to remove excess trifluoroacetic acid and other non-polar impurities. The products **1–3** were purified through Buchi Reveleris preparative high-performance liquid chromatography using RP-PFP column (XSelect CSH Prep Fluorophenyl 5 μm OBD, 19 mm × 150 mm). The purity of the products **1–3** was confirmed by analytical high-performance liquid chromatography and LC-MS. The purified inhibitors **1–3** were used for NAALADase or PSMA enzyme inhibition assay to determine the IC_{50}.

2.4.6 Analytical HPLC method

The purity of ligands **1–3** were analyzed using a Dionex HPLC-Ultimate 3000 system. Typically a solution of each ligand (20 μL, 1.0 mg/1.0 mL) in a mixture of CH_3CN:H_2O (1: 1) was injected via autosampler and eluted using Dionex Acclaim® 120 C_{18}, 5 μm, 4.6 mm × 250 mm analytical column at a flow rate of 1 mL/min (mobile phase, A = 0.1% trifluoro acetic acid/H_2O and B = acetonitrile). An isocratic flow of 40% B (v/v) was used during the run for 0 to 4 min and gradually gradient of B was increased to 100% B (v/v) over a period of 40-min. The chromatogram of each ligand was recorded on the Ultimate 3000 RS variable wavelength detector at 225–280 nm.

2.4.7 Preparative HPLC method

The purification of ligands **1–3** was performed using Buchi Reveleris Preparative HPLC System. Crude ligand (20 mg) was dissolved in 1:1 ratio of CH_3CN:H_2O (1 mL) and injected into the sample injector for elution using RP-PFP (Reverse Phase PentafluoroPhenyl) preparative

column (XSelect CSH Prep Fluorophenyl 5 µm OBD, 19 mm × 150 mm). A flow rate of 10 mL/min (mobile phase, A = 0.1% trifluoro acetic acid/H_2O and B = acetonitrile) is maintained throughout the run and the mobile phase gradient was increased from 1% B (v/v) to 50% B (v/v) over a period of 40 min. The mobile phase gradient was further increased to 80% B (v/v) in the next 15 min and the chromatogram was recorded at λ = 200–254 nm as well as by ELSD detector. Pure fractions of **1**–**3** were collected using automatic fraction collector, acetonitrile was evaporated under reduced pressure, lyophilized to afford pure ligands **1–3**. The pure ligands were further used for GCPII enzyme inhibition assay.

2.4.8 PSMA or GCPII enzyme inhibition assay

Fluorescent-based enzyme inhibition assay was performed to determine the IC_{50} value of the newly synthesized GCPII inhibitors **1–3** (AAPT ligands). Amplex Glutamate kit was purchased from Invitrogen, and a working solution of Amplex Red reagent (5 mL, 100 µM) was prepared. Meanwhile, membrane portion of PSMA enzyme was extracted from $PSMA^+$ LNCaP cell line by following a reported protocol. Briefly LNCaP cells (1 million) were harvested in HEPES buffer (1 mL) and lyzed twice using probe sonicator for 30 s. The lysate was ultracentrifuged at 100,000 x g for 30 min, the supernatant was discarded, and the cell pellet was homogenized by addition of HEPES buffer (1 mL) and used for PSMA enzyme inhibition assay. The isolated enzyme (100 µL, 8.3027 ng) was incubated with different concentrations (1, 5, 10, 25, 50, 75, 90, 100, 200, 300, 500 and 1000 nM) of the inhibitor **1–3** (100 µL) in the presence of *N*-acetylaspartylglutamate (NAAG) (50 µL, 30 nM) for 60 min. The amount of glutamic acid released by the hydrolysis of NAAG was measured by incubating a working solution of Amplex Red reagent (50 µL, 100 µM) for 30 min at 37 ^oC. The fluorescence emission after the oxidation of Amplex Red reagent was measured by using Synergy H1 multimode plate reader (BioTek Instruments, Inc., Winooski, VT, USA). The excitation

wavelength was fixed at 530 nm, and the fluorescence emission is measured at 590 nm. Dose v/s response inhibition curve was obtained using semi-log plot of concentration of inhibitors **1–3** versus fluorescence intensity emission to provide experimental IC_{50} values and compared with a known standard GCPII inhibitor, PMPA by following a similar procedure. The data analysis was performed using GraphPad Prism, version 6.00 for Windows (GraphPad Software, San Diego, CA).

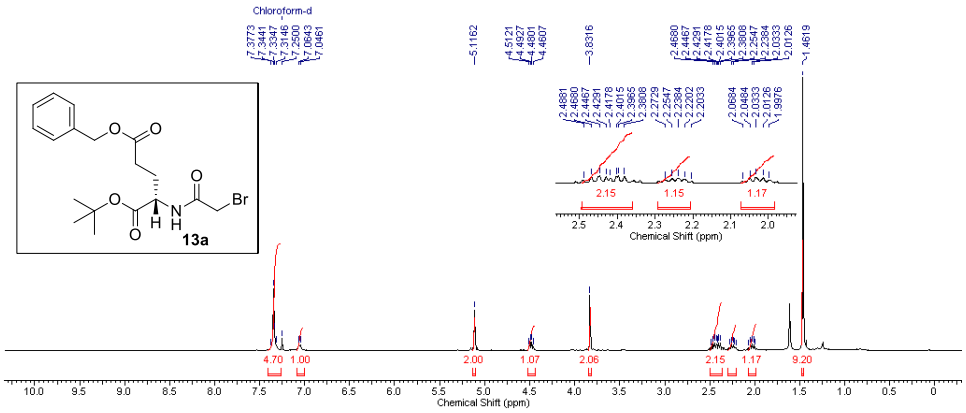

Figure 2.10 ^{1}H NMR spectrum (400 MHz, $CDCl_3$) of **13a**

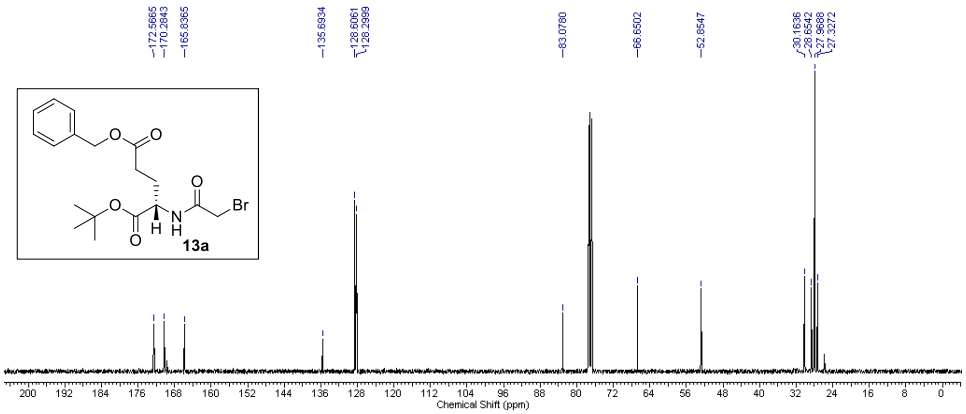

Figure 2.11 ^{13}C NMR spectrum (100 MHz, $CDCl_3$) of **13a**

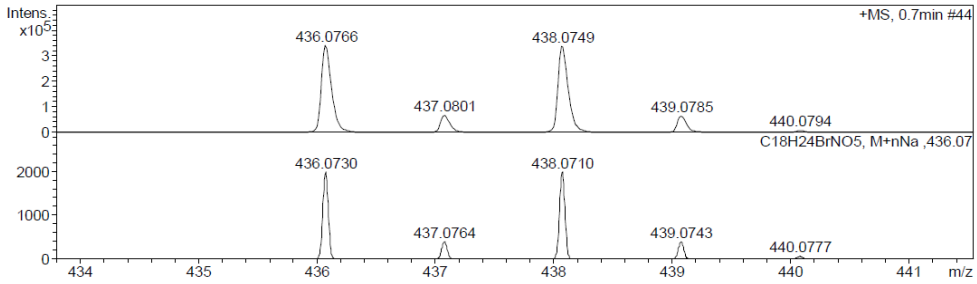

Figure 2.12 HRMS of **13a**

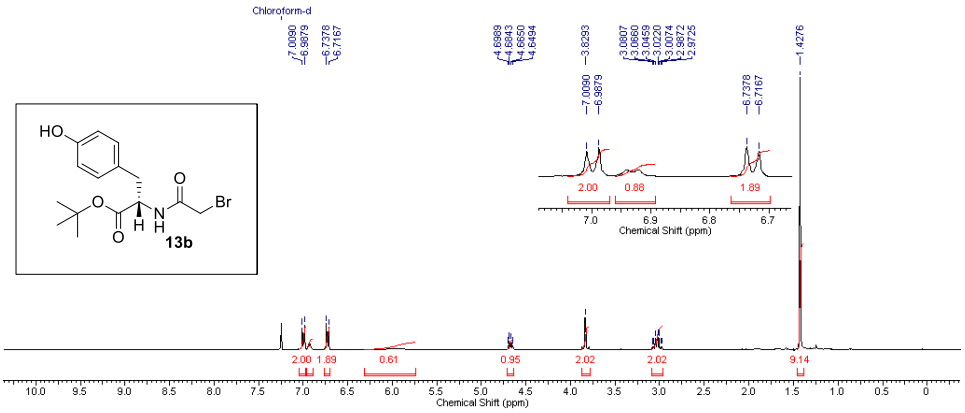

Figure 2.13 ^{1}H NMR spectrum (400 MHz, $CDCl_3$) of **13b**

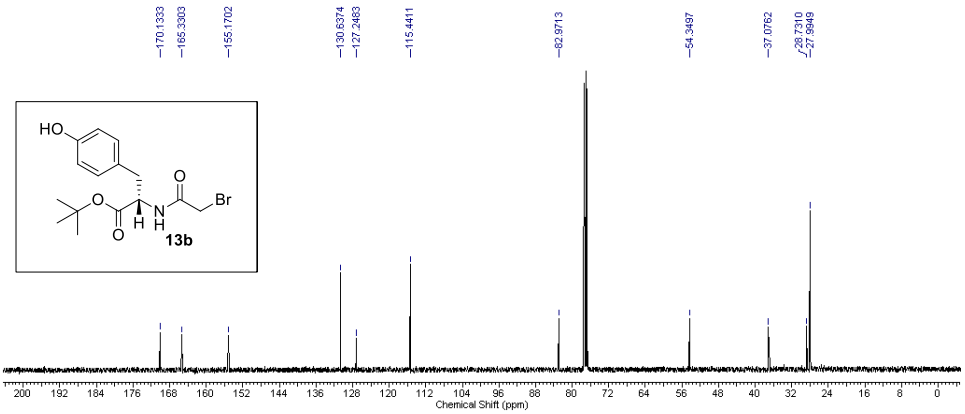

Figure 2.14 ^{13}C NMR spectrum (100 MHz, $CDCl_3$) of **13b**

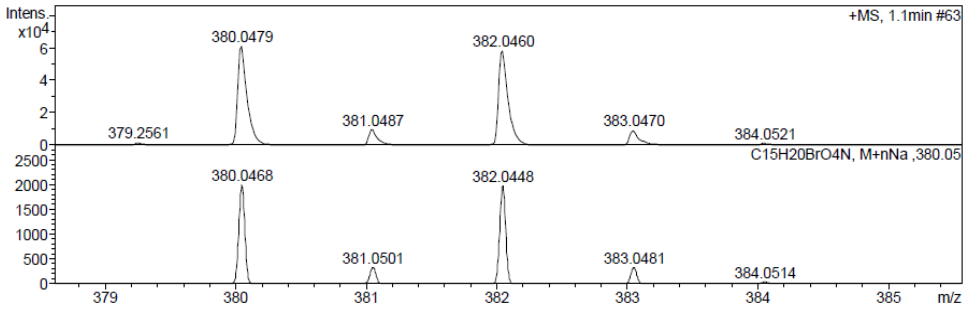

Figure 2.15 HRMS of **13b**

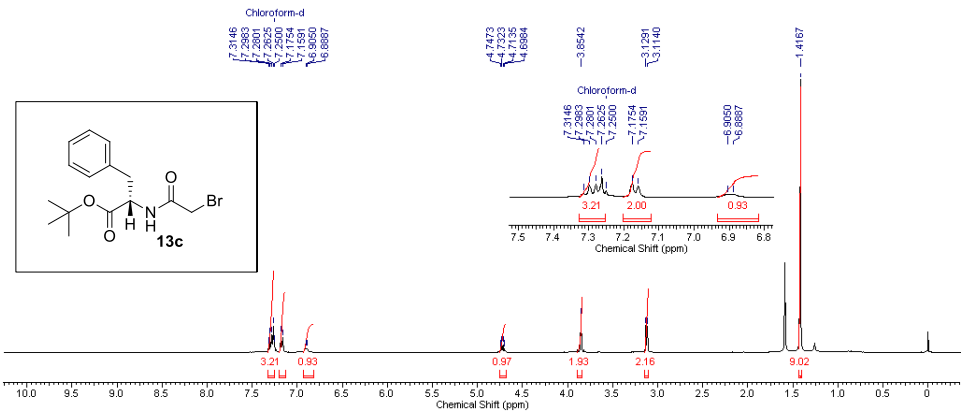

Figure 2.16 ^{1}H NMR spectrum (400 MHz, $CDCl_3$) of **13c**

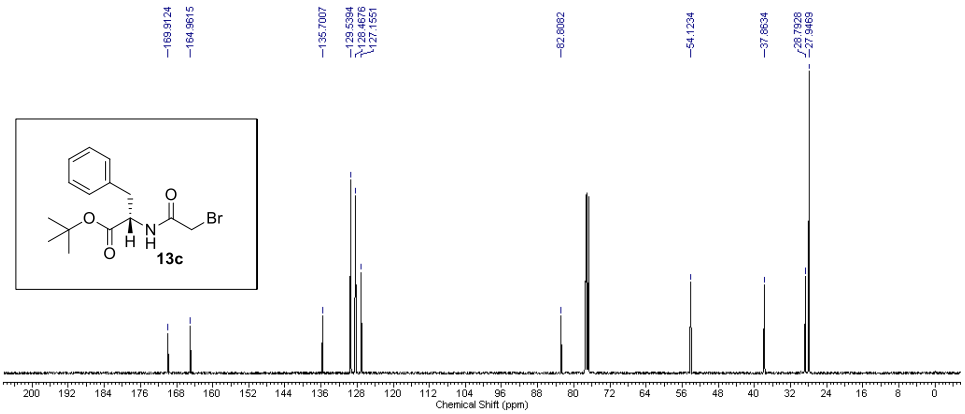

Figure 2.17 ^{13}C NMR spectrum (100 MHz, $CDCl_3$) of **13c**

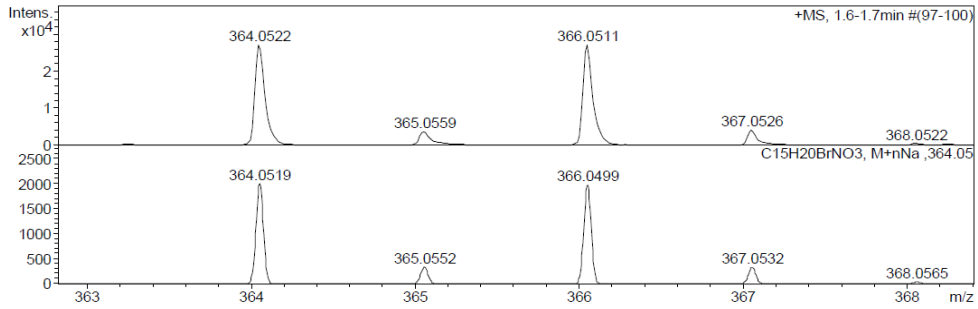

Figure 2.18 HRMS of **13c**

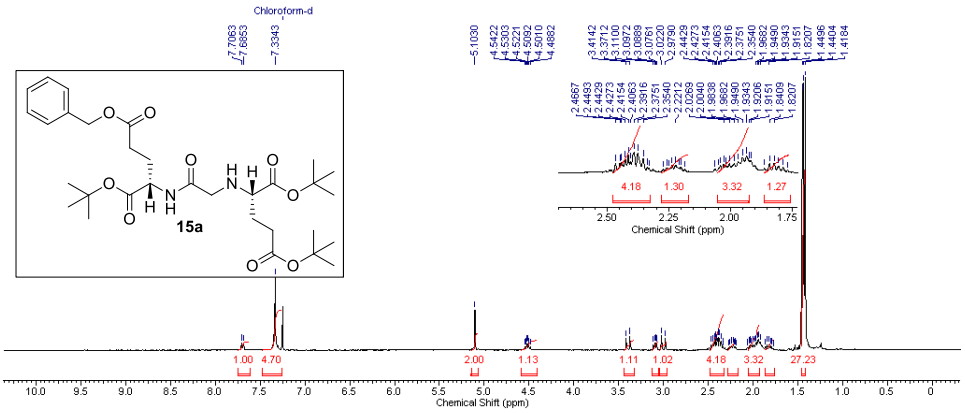

Figure 2.19 ^{1}H NMR spectrum (400 MHz, $CDCl_3$) of **15a**

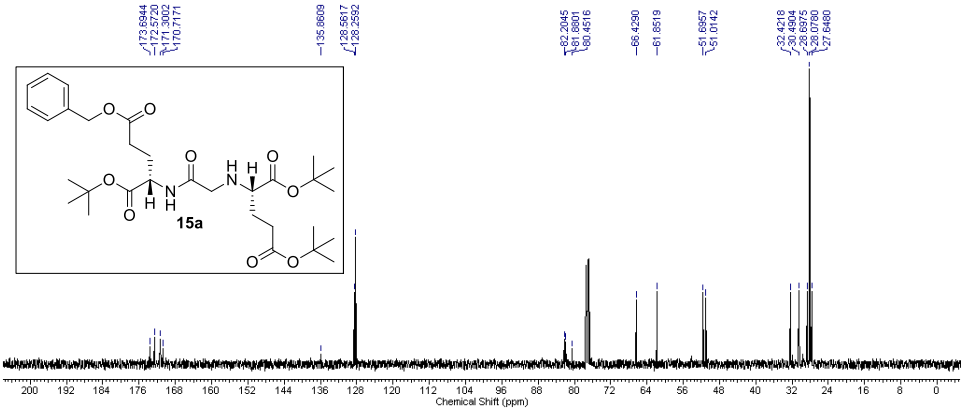

Figure 2.20 ^{13}C NMR spectrum (100 MHz, $CDCl_3$) of **15a**

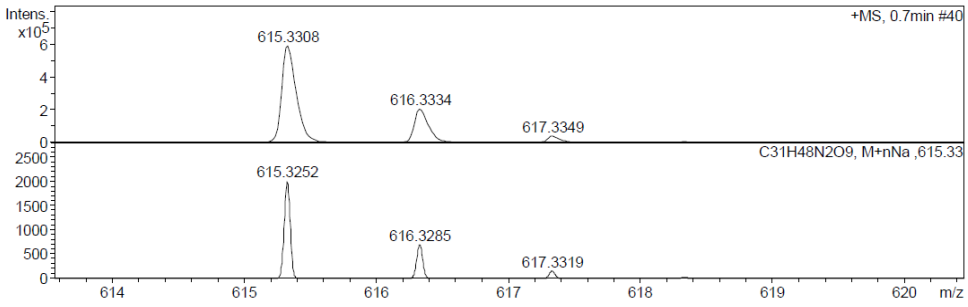

Figure 2.21 HRMS of **15a**

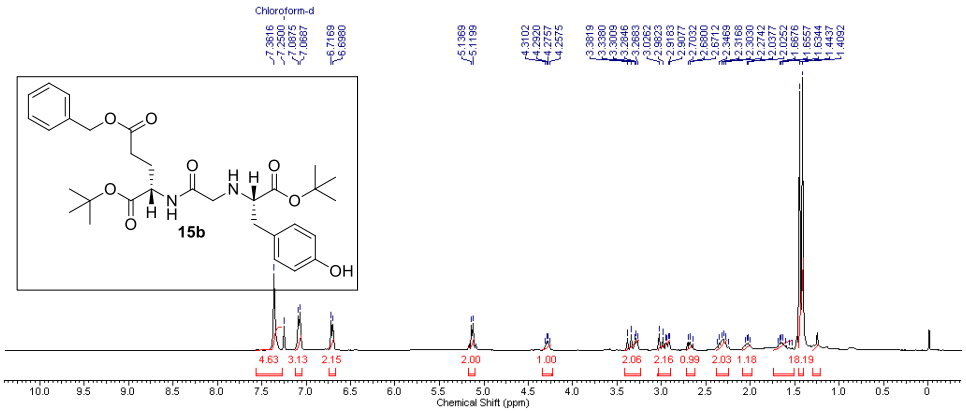

Figure 2.22 ^{1}H NMR spectrum (400 MHz, $CDCl_3$) of **15b**

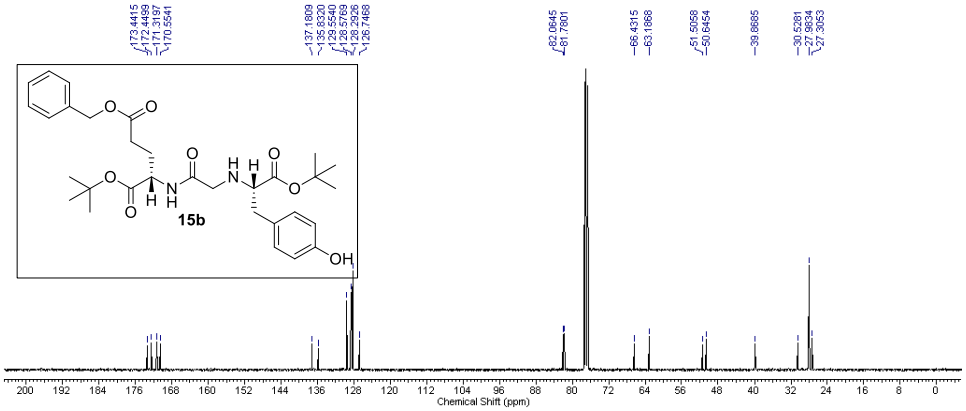

Figure 2.23 ^{13}C NMR spectrum (100 MHz, $CDCl_3$) of **15b**

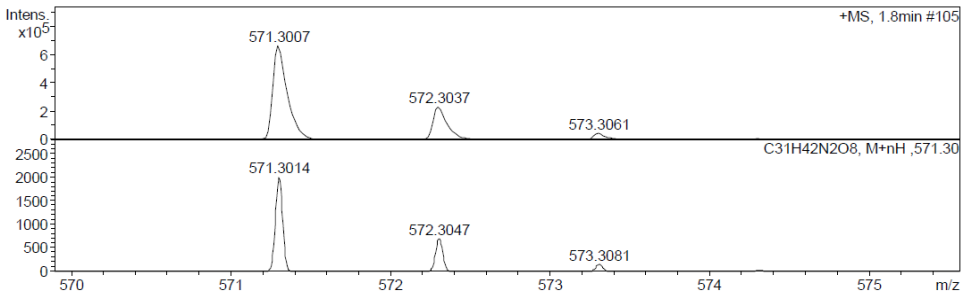

Figure 2.24 HRMS of **15b**

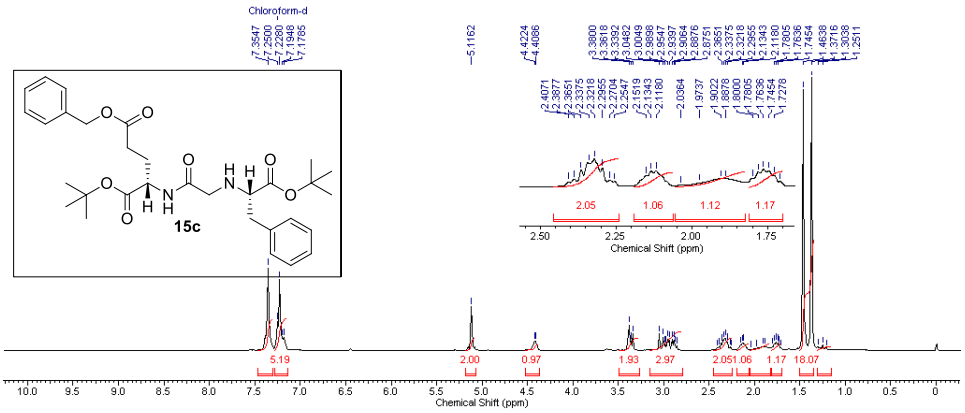

Figure 2.25 ^{1}H NMR spectrum (400 MHz, $CDCl_3$) of **15c**

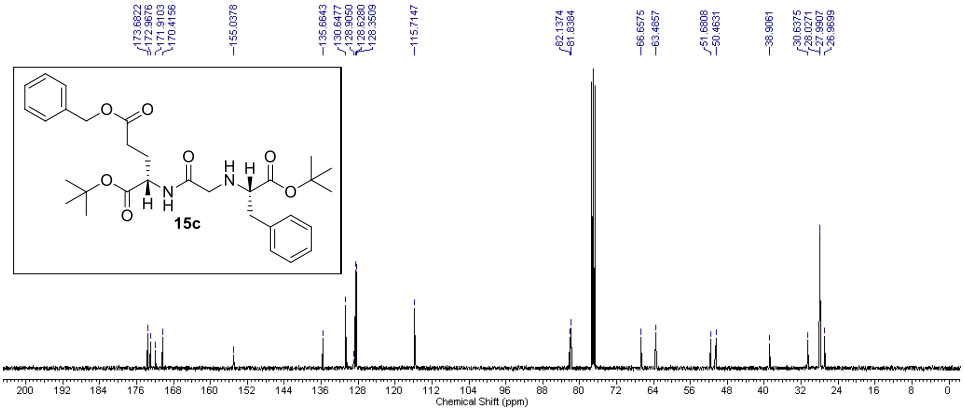

Figure 2.26 ^{13}C NMR spectrum (100 MHz, $CDCl_3$) of **15c**

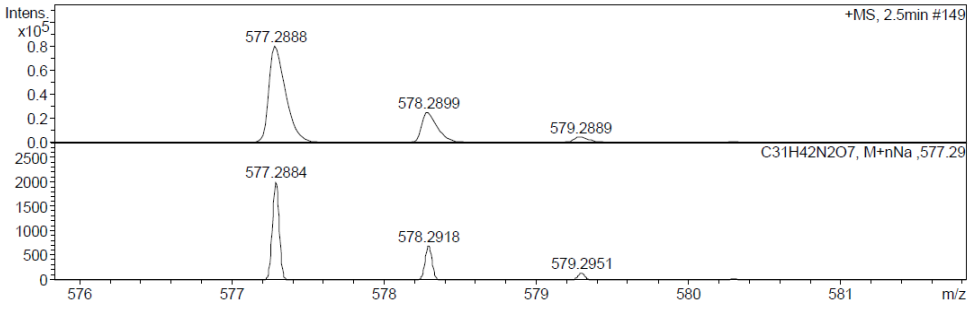

Figure 2.27 HRMS of **15c**

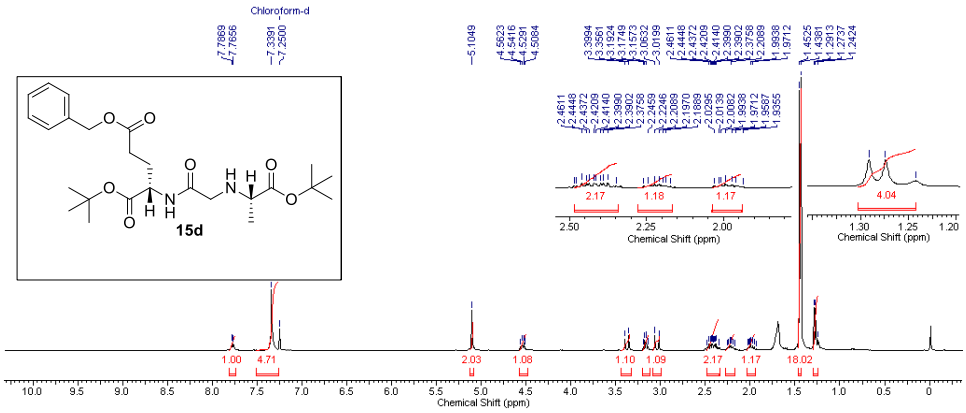

Figure 2.28 ^{1}H NMR spectrum (400 MHz, $CDCl_3$) of **15d**

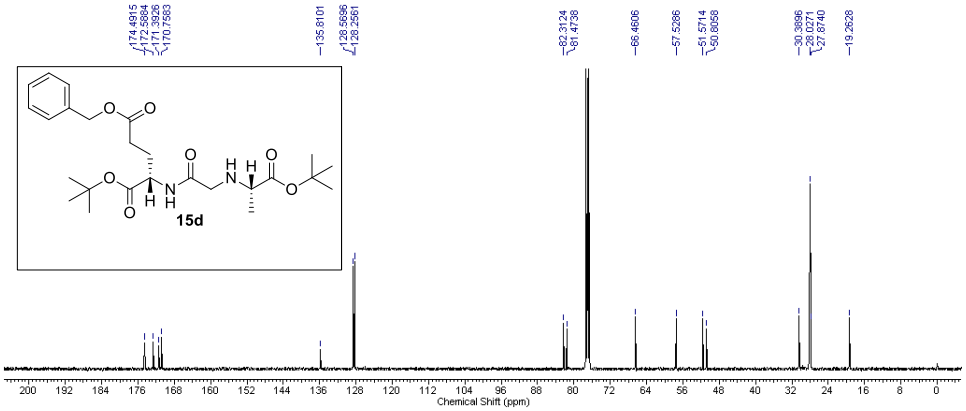

Figure 2.29 ^{13}C NMR spectrum (100 MHz, $CDCl_3$) of **15d**

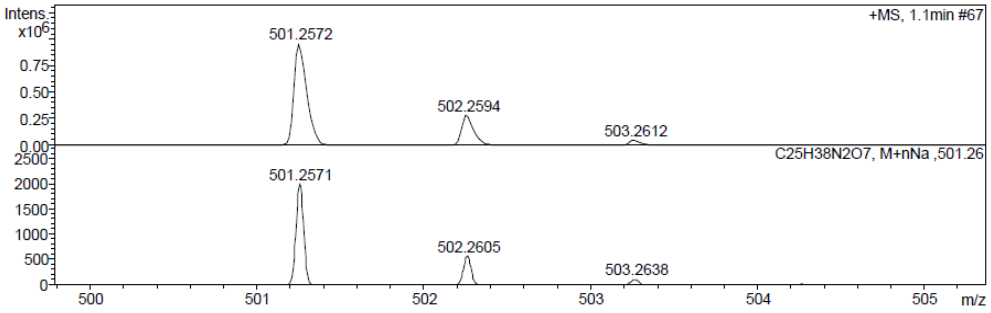

Figure 2.30 HRMS of **15d**

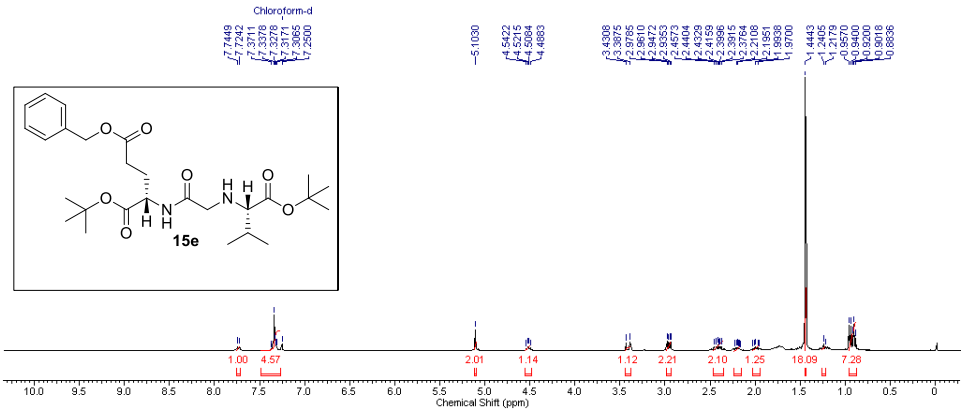

Figure 2.31 ^{1}H NMR spectrum (400 MHz, $CDCl_3$) of **15e**

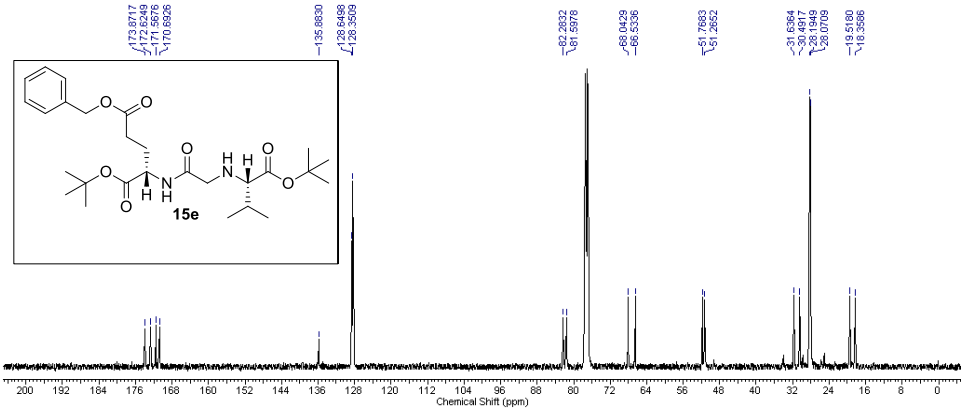

Figure 2.32 ^{13}C NMR spectrum (100 MHz, $CDCl_3$) of **15e**

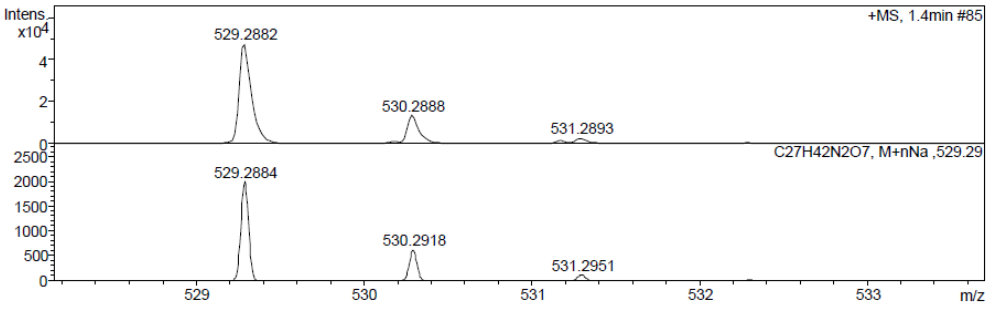

Figure 2.33 HRMS of **15e**

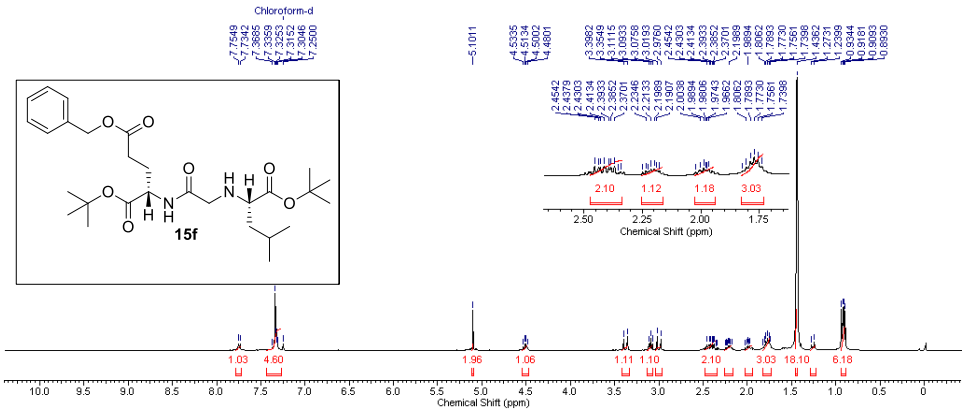

Figure 2.34 ^{1}H NMR spectrum (400 MHz, $CDCl_3$) of **15f**

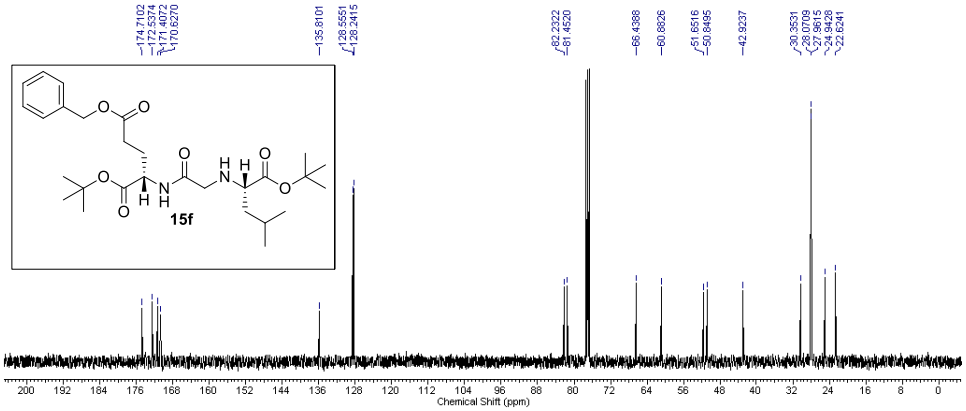

Figure 2.35 ^{13}C NMR spectrum (100 MHz, $CDCl_3$) of **15f**

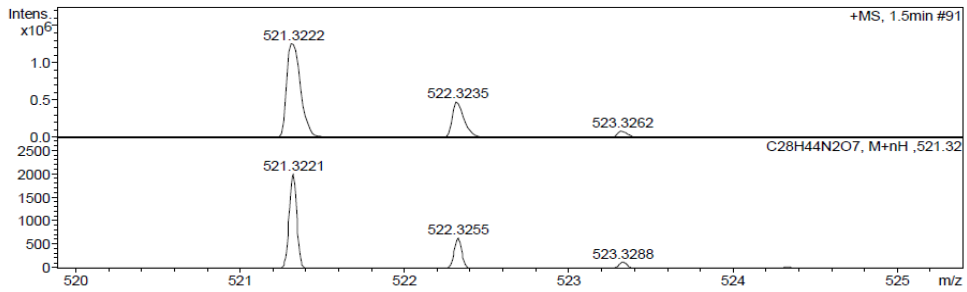

Figure 2.36 HRMS of **15f**

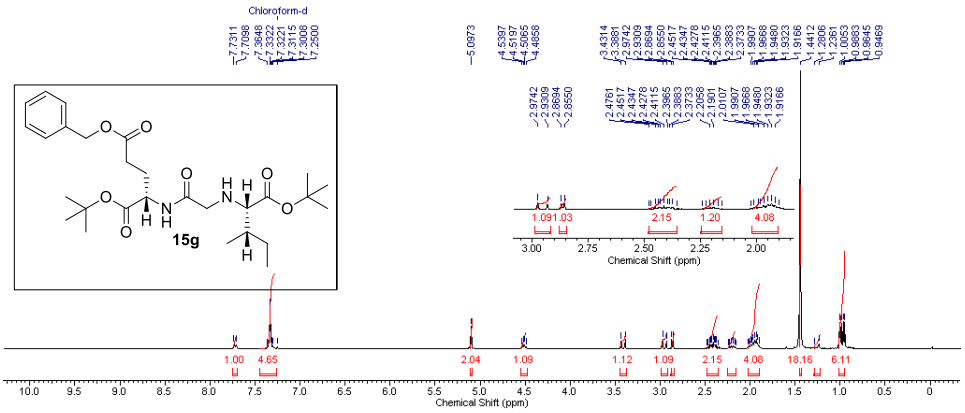

Figure 2.37 ^{1}H NMR spectrum (400 MHz, $CDCl_3$) of **15g**

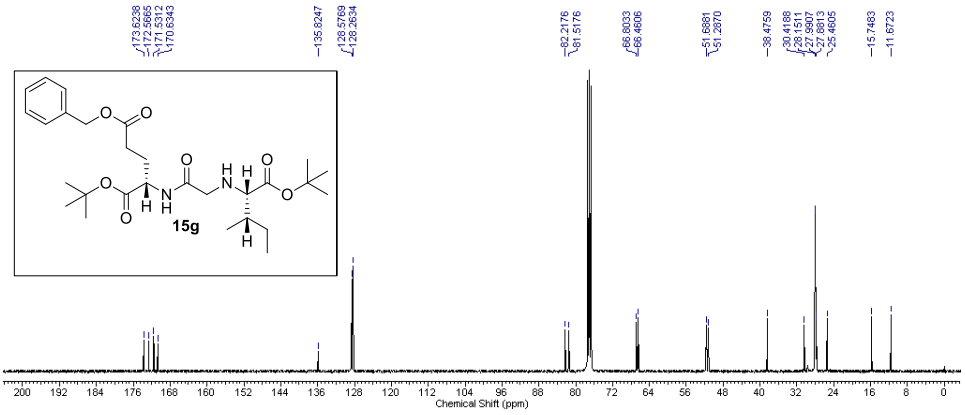

Figure 2.38 ^{13}C NMR spectrum (100 MHz, $CDCl_3$) of **15g**

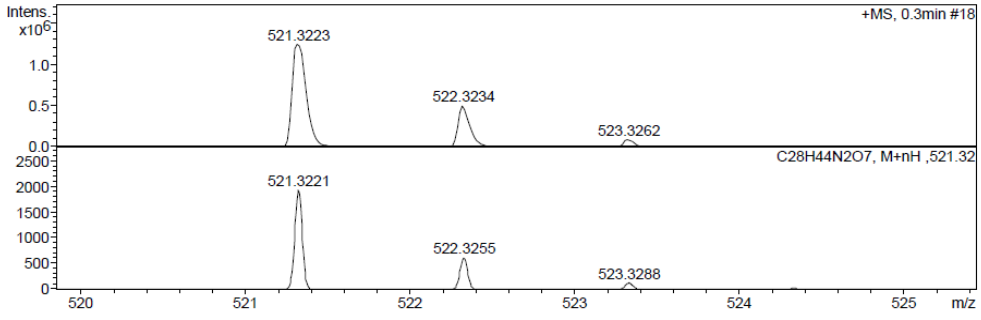

Figure 2.39 HRMS of **15g**

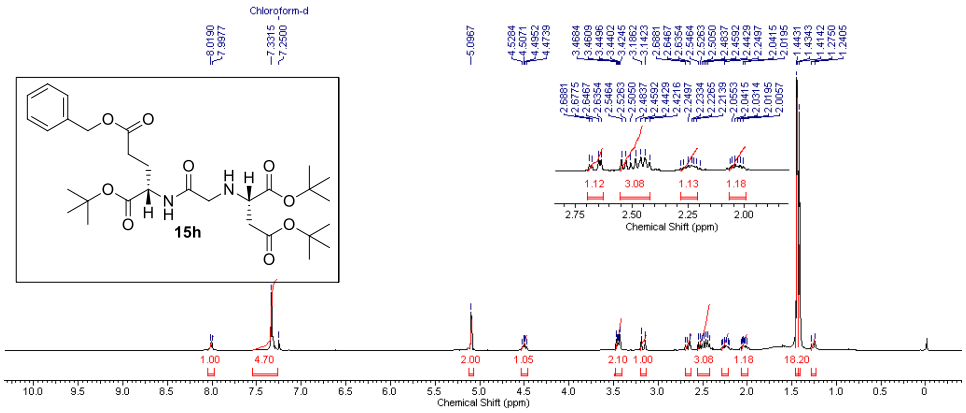

Figure 2.40 ^{1}H NMR spectrum (400 MHz, $CDCl_3$) of **15h**

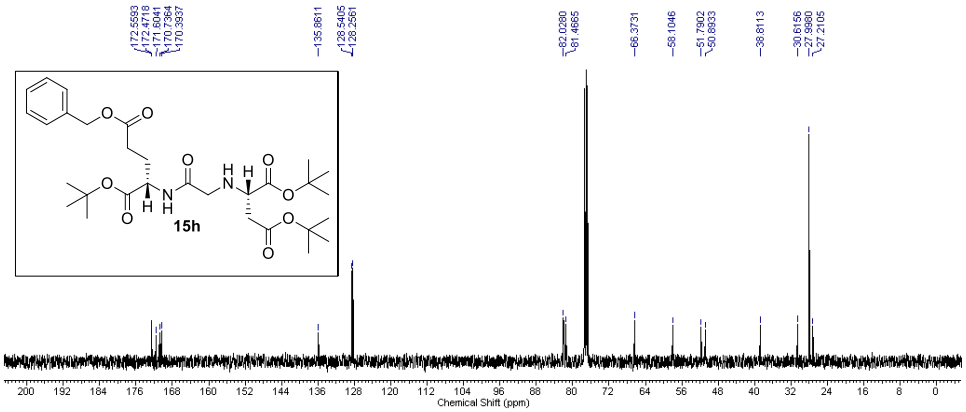

Figure 2.41 ^{13}C NMR spectrum (100 MHz, $CDCl_3$) of **15h**

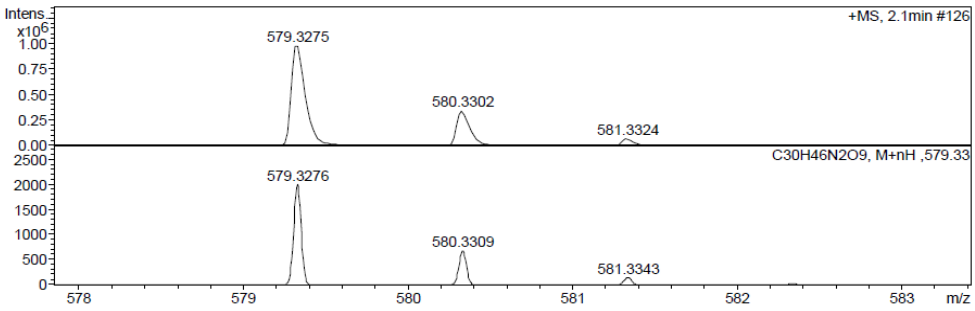

Figure 2.42 HRMS of **15h**

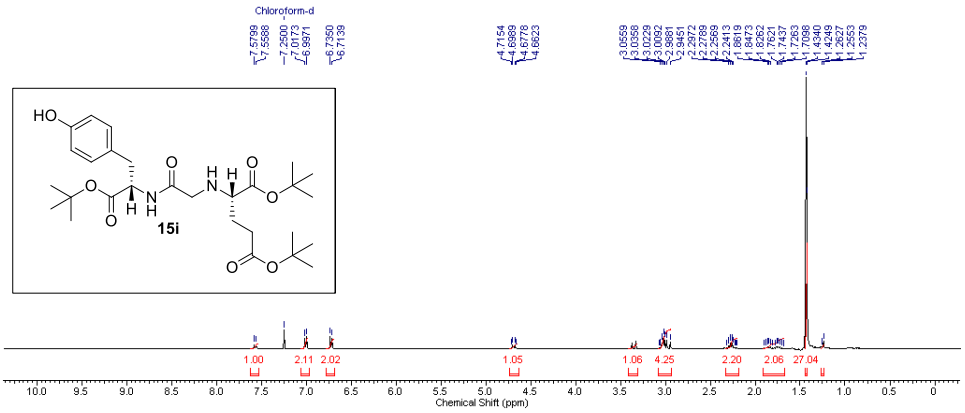

Figure 2.43 ^{1}H NMR spectrum (400 MHz, $CDCl_3$) of **15i**

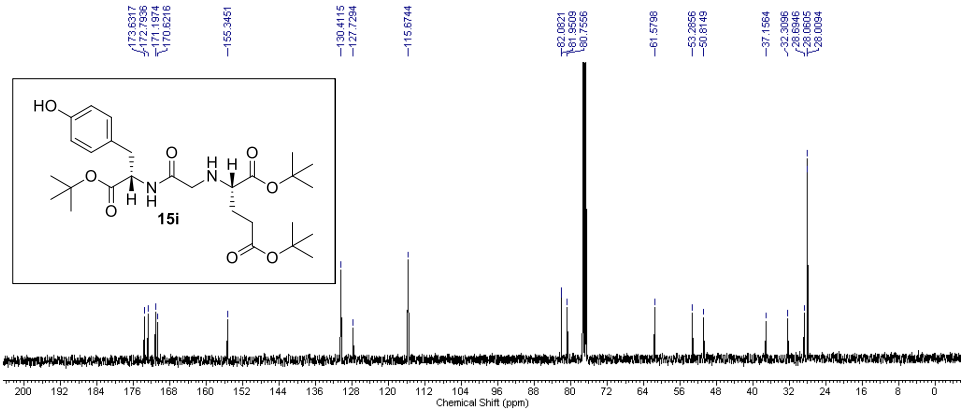

Figure 2.44 ^{13}C NMR spectrum (100 MHz, $CDCl_3$) of **15i**

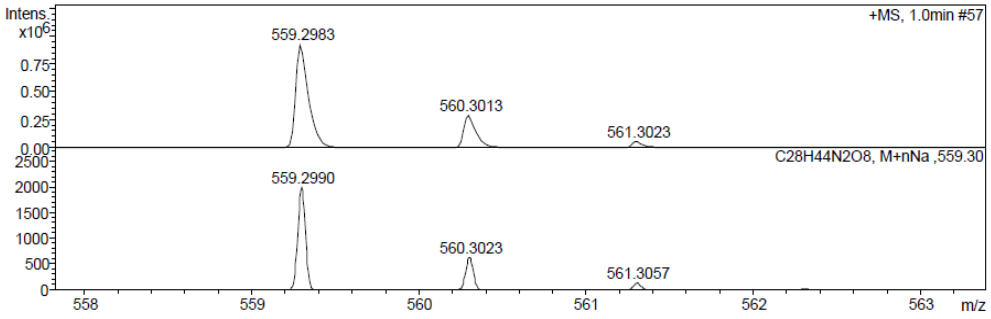

Figure 2.45 HRMS of **15i**

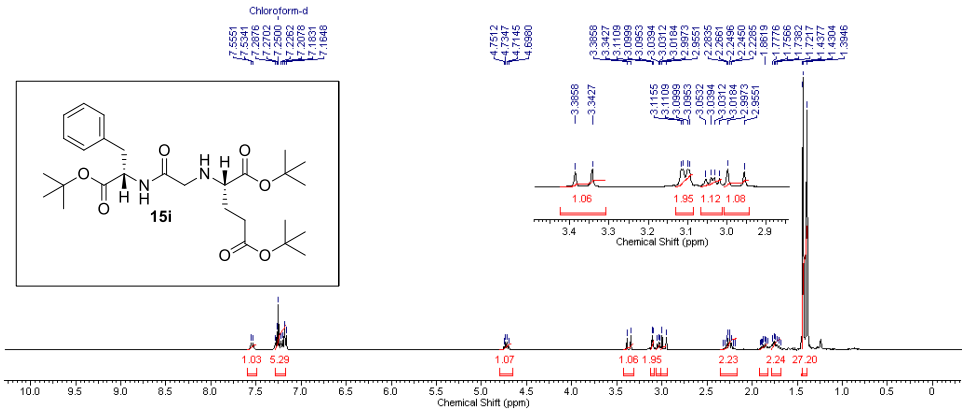

Figure 2.46 ^{1}H NMR spectrum (400 MHz, $CDCl_3$) of **15j**

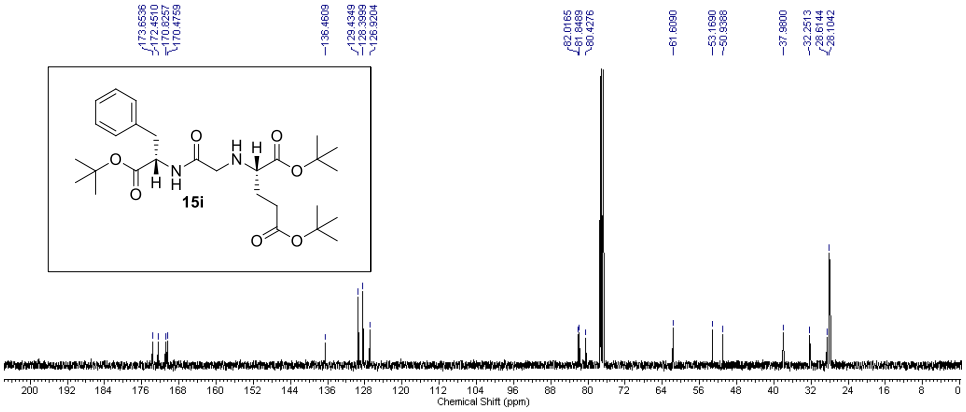

Figure 2.47 ^{13}C NMR spectrum (100 MHz, $CDCl_3$) of **15j**

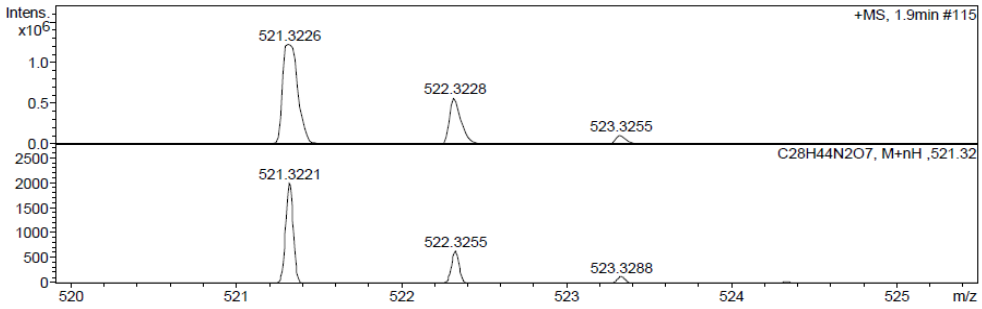

Figure 2.48 HRMS of **15j**

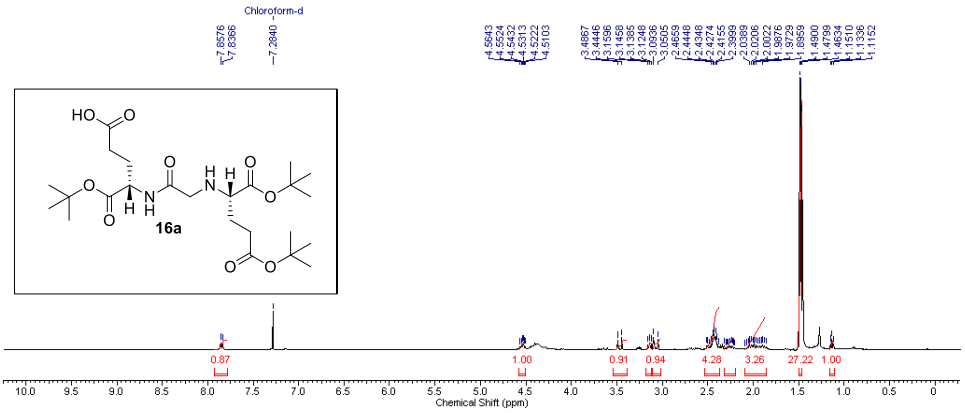

Figure 2.49 ^{1}H NMR spectrum (400 MHz, $CDCl_3$) of **16a**

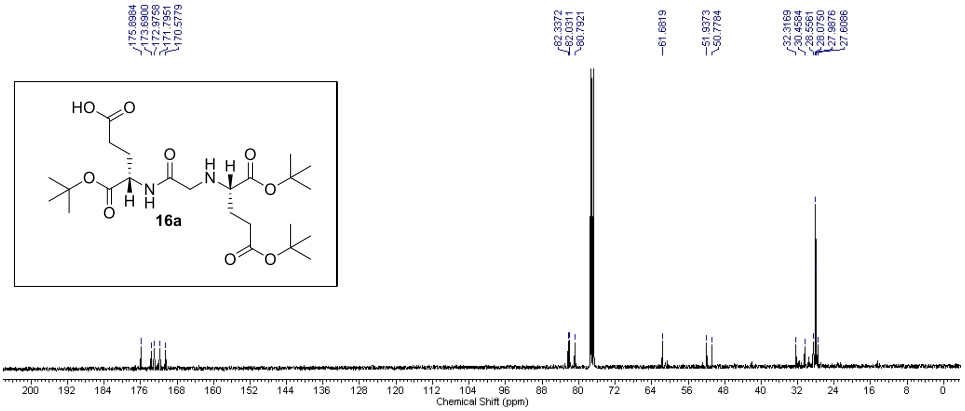

Figure 2.50 ^{13}C NMR spectrum (100 MHz, $CDCl_3$) of **16a**

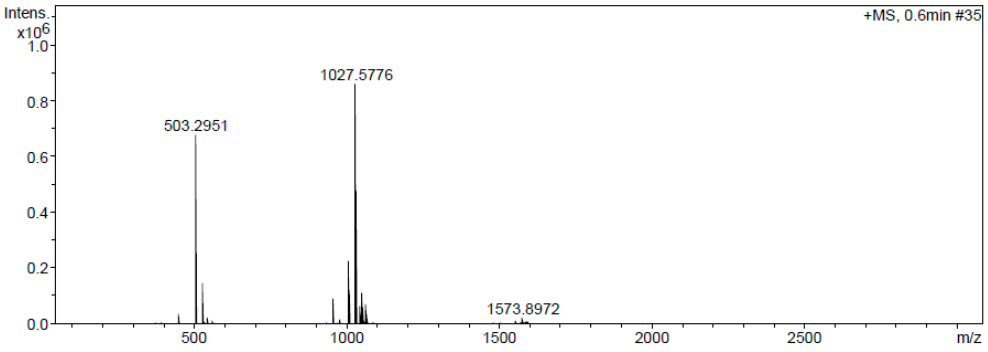

Figure 2.51 ESI-MS of **16a**

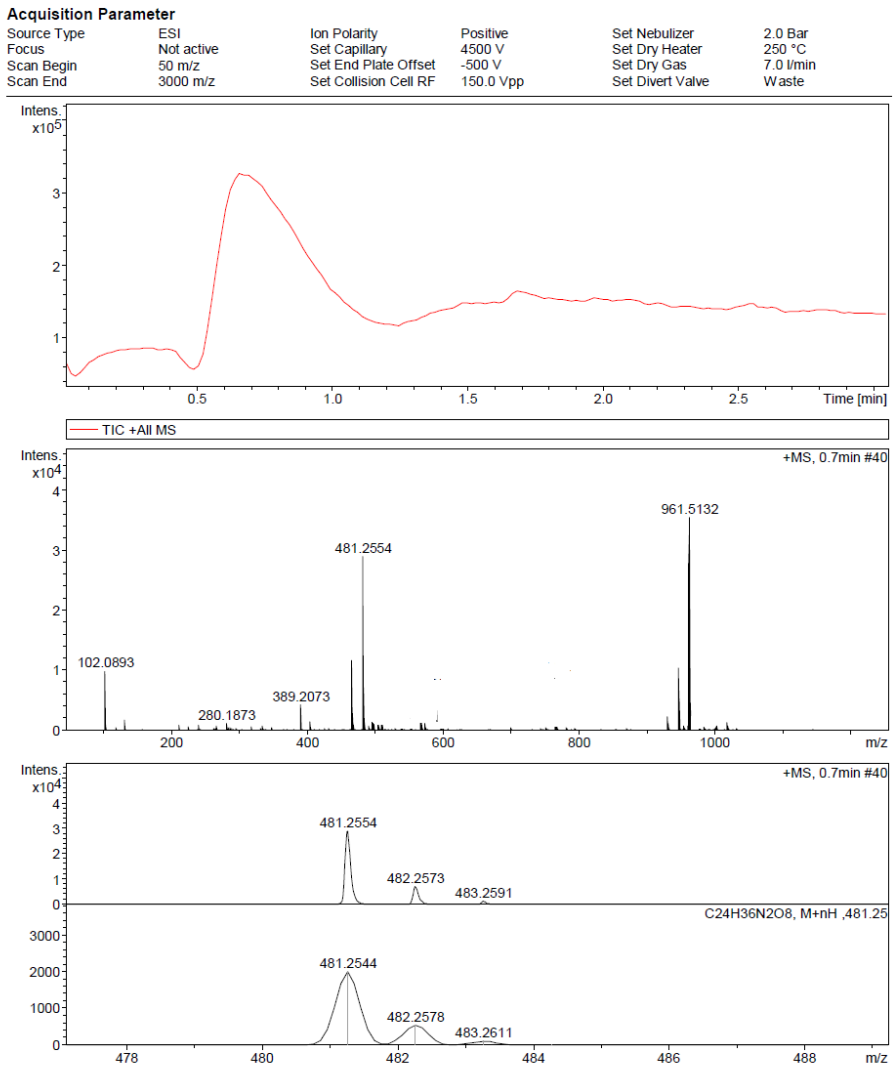

Figure 2.52 HRMS of **16b**

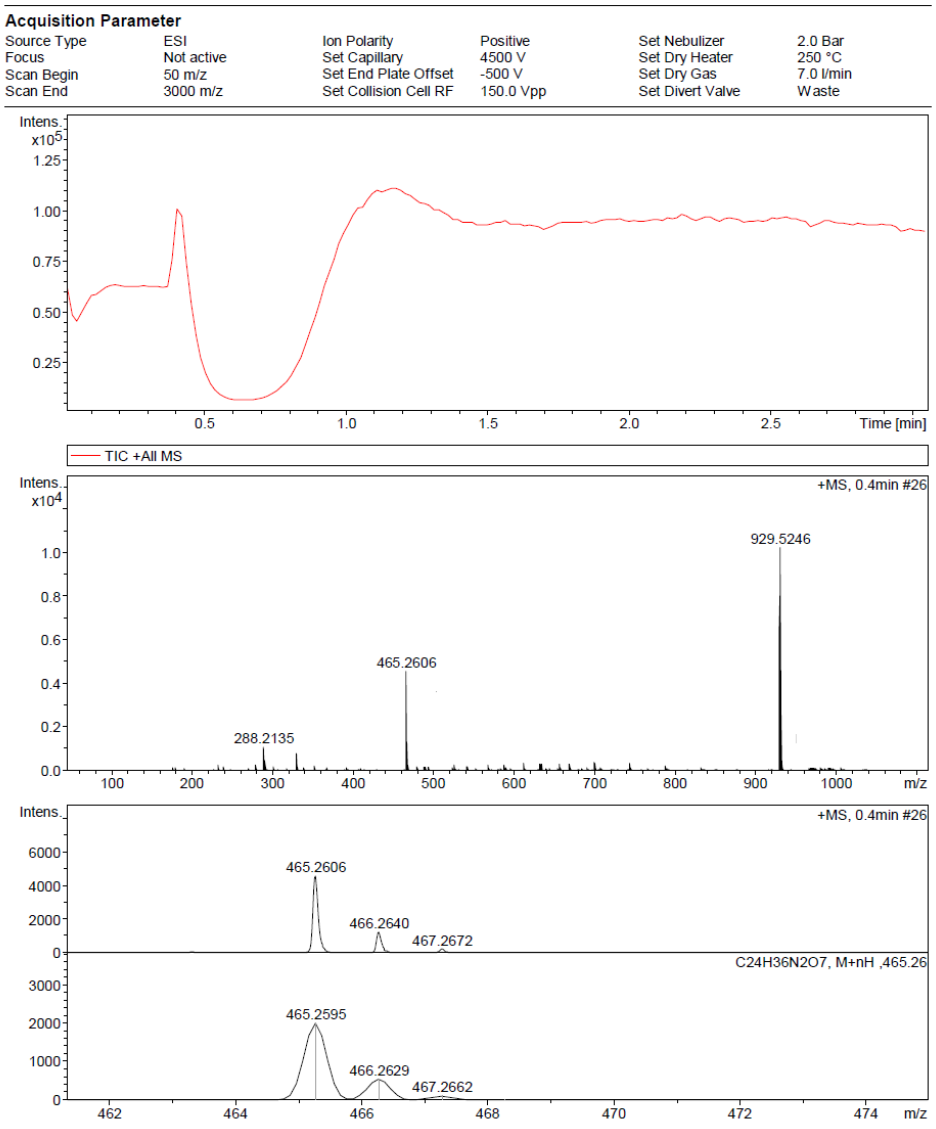

Figure 2.53 HRMS of **16c**

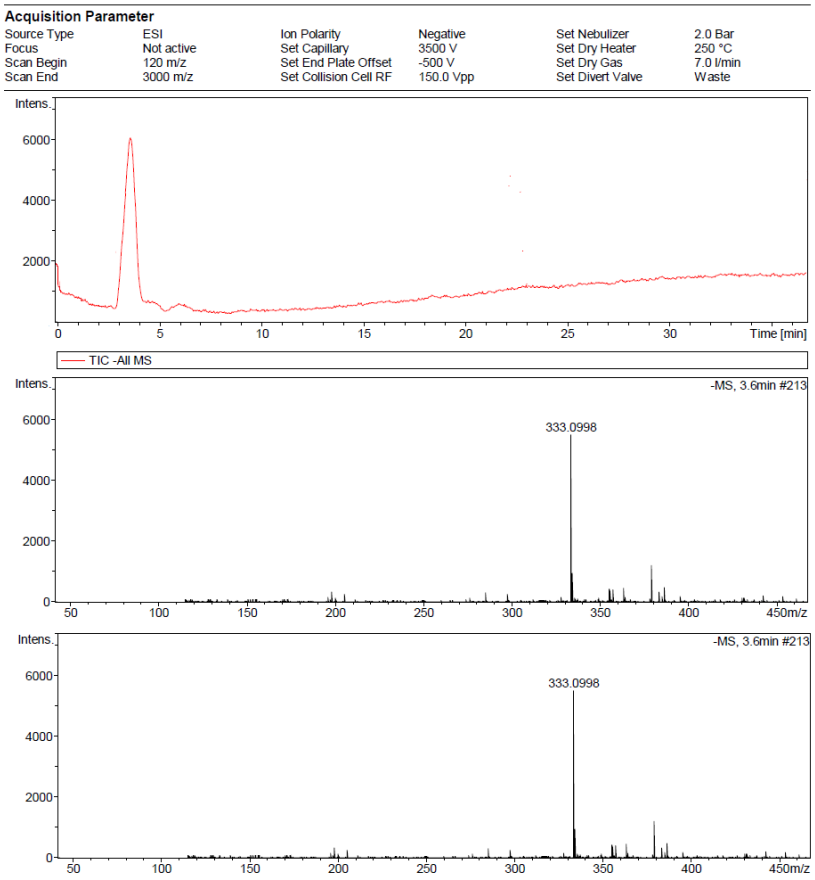

Figure 2.54 LC-MS of **1**

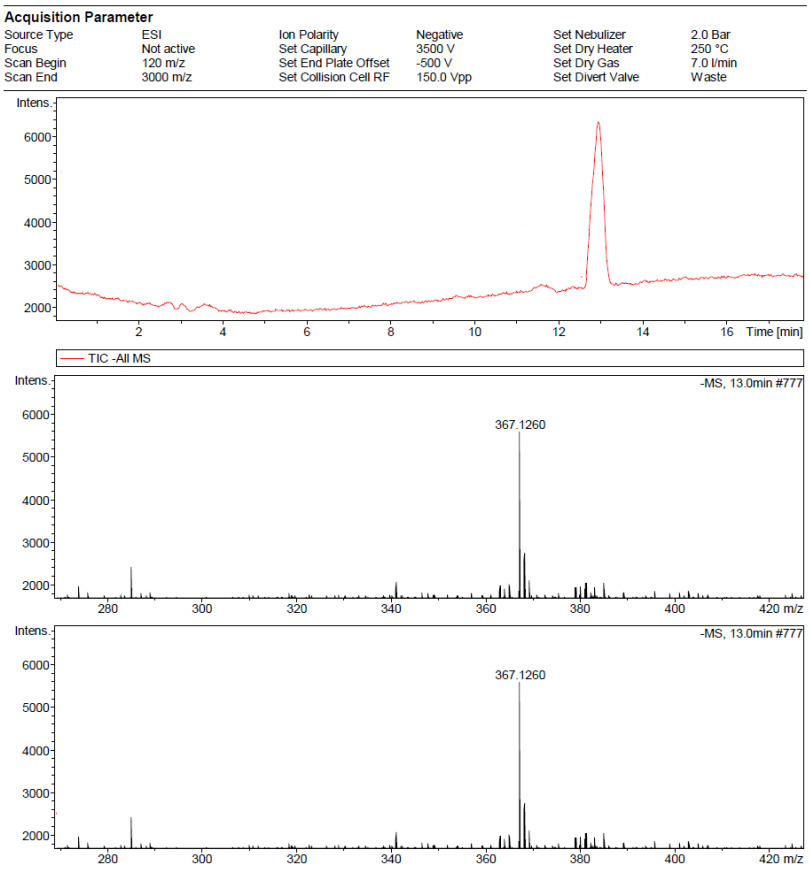

Figure 2.55 LC-MS of **2**

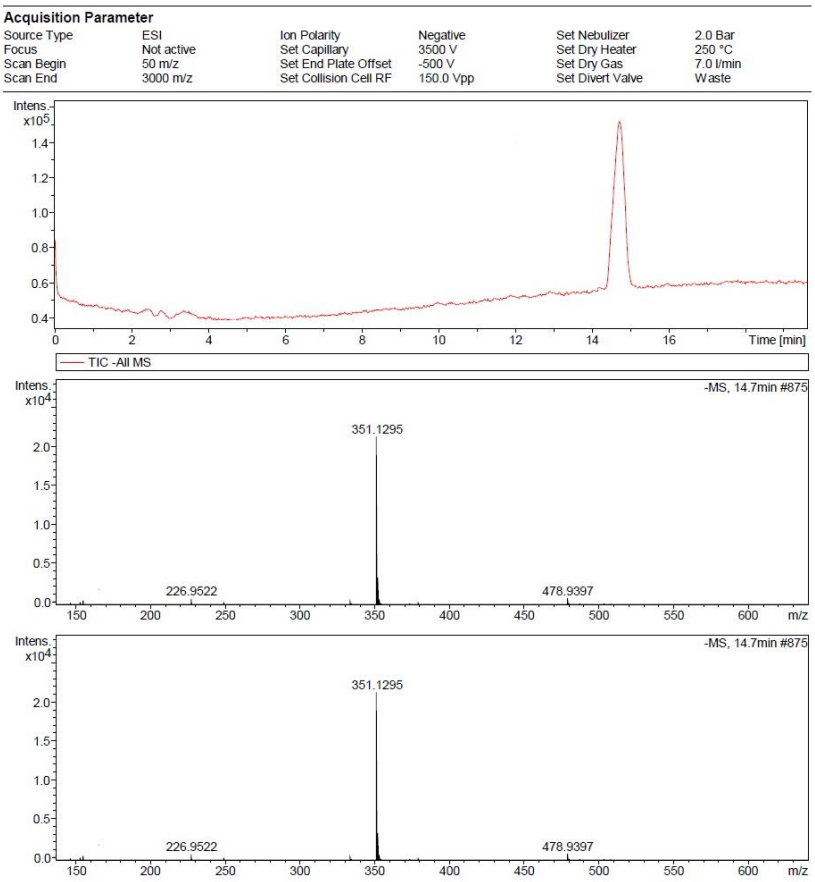

Figure 2.56 LC-MS of **3**

2.5 References

1. Wong M. C. S., Goggins W. B., Wang H. H. X., Fung F. D. H., Leung C., Wong S. Y. S., Ng C. F., Sung J. J. Y. (2016), Global incidence and mortality for prostate Cancer: Analysis of temporal patterns and trends in 36 countries, Eur. Urol., 70, 862–874 (DOI: 10.1016/j.eururo.2016.05.043).
2. Siegel R. L., Miller K. D., Jemal A. (2019), Cancer Statistics, 2019, CA Cancer J. Clin., 69, 7–34 (DOI: 10.3322/caac.21551).
3. Horoszewicz J. S., Leong S. S., Kawinski E., Karr J. P., Rosenthal H., Chu T. M., Mirand E. A., Murphy G. P. (1983), LNCaP model of human prostatic carcinoma, Cancer Res., 43, 1809–1818.
4. Barinka C., Rojas C., Slusher B., Pomper M. (2012), Glutamate carboxypeptidase II in diagnosis and treatment of neurologic disorders and prostate cancer, Curr. Med. Chem., 19, 856–870 (DOI: 10.2174/092986712799034888).
5. Carter R., Feldman A., Coyle J. (1996), Prostate-specific membrane antigen is a hydrolase with substrate and pharmacologic characteristics of a neuropeptidase, Proc. Natl. Acad. Sci. U. S. A., 93, 749−753 (DOI: 10.1073/pnas.93.2.749).
6. Tiffany C., Lapidus R., Merion A., Calvin, D., Slusher B. (1999), Characterization of the enzymatic activity of PSM: Comparison with brain NAALADase, Prostate, 39, 28−35 (DOI: 10.1002/(sici)1097-0045(19990401)39:1).
7. Rajasekaran A. K., Anilkumar G., Christiansen J. J. (2005), Is prostate-specific membrane antigen a multifunctional protein?, Am. J. Physiol. Cell. Physiol., 288, C975–C981 (DOI: 10.1152/ajpcell.00506.2004).

8. Ghosh A., Heston W. D. (2004), Tumor target prostate specific membrane antigen (PSMA) and its regulation in prostate cancer, J. Cell Biochem., 91, 528–539 (DOI: 10.1002/jcb.10661).

9. Heitkötter B., Steinestel K., Trautmann M., Grünewald I., Barth P., Gevensleben H., Bögemann M., Wardelmann E., Hartmann W., Rahbar K., Huss S. (2018), Neovascular PSMA expression is a common feature in malignant neoplasms of the thyroid, Oncotarget, 9, 9867–9874 (DOI: 10.18632/oncotarget.23984).

10. Wernicke A. G., Edgar M. A., Lavi E., Liu H., Salerno P., Bander N. H., Gutin P. H. (2011), Prostate-specific membrane antigen as a potential novel vascular target for treatment of glioblastoma multiforme, Arch. Pathol. Lab Med., 135, 1486–1489 (DOI: 10.5858/arpa.2010-0740-OA).

11. Fragomeni R. A. S., Amir T., Sheikhbahaei S., Harvey S. C., Javadi M. S., Solnes L. B., Kiess A. P., Allaf M. E., Pomper M. G., Gorin M. A., Rowe S. P. (2018), Imaging of non-prostate cancers using psma-targeted radiotracers: Rationale, current state of the field, and a call to arms, J. Nucl. Med., 59, 871–877 (DOI: 10.2967/jnumed.117.203570).

12. Tasch J., Gong M., Sadelain M., Heston W. D. (2001), A unique folate hydrolase, prostate-specific membrane antigen (PSMA): A target for immunotherapy?, Crit. Rev. Immunol., 21, 249–261 (DOI: 10.1615/CritRevImmunol.v21.i1-3.160).

13. Lu J., Celis E. (2002), Recognition of prostate tumor cells by cytotoxic lymphocytes specific for prostate-specific membrane antigen, Cancer Res., 62, 5807–5812.

14. Fracasso G., Bellisola G., Cingarlini S., Castelletti D., Prayer-Galetti T., Pagano F., Tridente G., Colombatti M. (2002), Anti-

tumor effects of toxins targeted to the prostate specific membrane antigen, Prostate, 53, 9–23 (DOI: 10.1002/pros.10117).

15. Heston W. D. (1997), Characterization and glutamyl preferring carboxypeptidase function of prostate specific membrane antigen: A novel folate hydrolase, Urology, 49, 104–112 (DOI: 10.1016/S0090-4295(97)00177-5).

16. Pinto J. T., Suffoletto B. P., Berzin T. M., Qiao C. H., Lin S., Tong W. P., May F., Mukherjee B., Heston W. D. (1996), Prostate-specific membrane antigen: A novel folate hydrolase in human prostatic carcinoma cells, Clin. Cancer Res., 2, 1445–1451.

17. Carter R. E., Feldman A. R., Coyle J. T. (1996), Prostate-specific membrane antigen is a hydrolase with substrate and pharmacologic characteristics of a neuropeptidase, Proc. Natl. Acad. Sci. USA. 93, 749–753.

18. Jackson P. F., Cole D. C., Slusher B. S., Stetz S. L., Ross L. E., Donzanti B. A., Trainor D. A. (1996), Design, Synthesis, and Biological Activity of a Potent Inhibitor of the Neuropeptidase N-Acetylated α-Linked Acidic Dipeptidase, J. Med. Chem., 39, 619–622 (DOI: 10.1021/jm950801q).

19. Foss C. A., Mease R. C., Fan, H., Wang Y., Ravert H. T., Dannals R. F., Olszewski R., Heston W. D., Kozikowski A. P., Pomper M. G. (2005), Radiolabeled small molecule ligands for prostatespecific membrane antigen: In vivo imaging in experimental models of prostate cancer, Clin. Cancer Res., 2005, 11, 4022–4028 (DOI: 10.1158/1078-0432.CCR-04-2690).

20. Mease R. C., Dusich C. L., Foss C. A., Ravert H. T., Dannals R. F., Seidel J., Prideaux A., Fox J. J., Sgouros G., Kozikowski A. P.,

Pomper M. G. (2008), N-[N-[(S)-1,3-Dicarboxypropyl]carbamoyl]-4-[18F]-fluorobenzyl-L-cysteine, [^{18}F]DCFBC: A new imaging probe for prostate cancer, Clin. Cancer Res., 14, 3036–3043 (DOI: 10.1158/1078-0432.CCR-07-1517).

21. Maresca K. P., Hillier S. M., Fernia F. J., Keith D., Barone C., Joyal J. L., Zimmerman C. N., Kozikowski A. P., Barrett J. A., Eckelman W. C., Babich J. W. (2009), A series of halogenated heterodimeric inhibitors of prostate specific membrane antigen (PSMA) as radiolabeled probes for targeting prostate cancer, J. Med. Chem., 52, 347–357 (DOI: 10.1021/jm800994j).

22. Chen Y., Foss C. A., Byun Y., Nimmagadda S., Pullambhatla M., Fox J. J., Castanares M., Lupold S. E., Babich J. W., Mease R. C., Pomper M. G. (2008), Radiohalogenated prostate-specific membrane antigen (PSMA)-based ureas as imaging agents for prostate cancer, J. Med. Chem., 51, 7933–7943 (DOI: 10.1016/j.bbrc.2009.10.017).

23. Banerjee S. R., Pullambhatla M., Byun Y., Nimmagadda S., Green G., Fox J. J., Horti A., Mease R. C., Pomper M. G. (2010), ^{68}Ga-labeled inhibitors of prostate-specific membrane antigen (PSMA) for imaging prostate cancer, J. Med. Chem., 53, 5333–5341 (DOI: 10.1021/jm100623e).

24. Banerjee S. R., Foss C. A., Castanares M., Mease R. C., Byun Y., Fox J. J., Hilton J., Lupold S. E., Kozikowski A. P., Pomper M. G. (2008), Synthesis and evaluation of technetium-99m- and rhenium-labeled inhibitors of the prostate-specific membrane antigen (PSMA), J. Med. Chem., 2008, 51, 4504–4517 (DOI: 10.1021/jm800111u).

25. Kularatne S. A., Wang K., Santhapuram H. K. R., Low P. S. (2009), Prostate-specific membrane antigen targeted imaging and therapy of prostate cancer using a PSMA inhibitor as a homing ligand, Mol. Pharm., 6, 780–789 (DOI: 10.1021/mp900069d).

26. Kularatne S. A., Zhou Z., Yang J., Post C. B., Low P. S. (2009), Design, synthesis, and preclinical evaluation of prostate-specific membrane antigen targeted ^{99m}Tc-radioimaging agents, Mol. Pharm. 6, 790–800 (DOI: 10.1021/mp9000712).

27. Kularatne S. A., Chelvam V., Santhapuram H. K. R., Wang K., Vaitilingam B., Henne W. A., Low P. S. (2010) Synthesis and biological analysis of prostate-specific membrane antigen-targeted anticancer prodrugs. J. Med. Chem., 53, 7767–7777 (DOI: 10.1021/jm100729b).

28. Misra P., Humblet V., Pannier N., Maison W., Frangioni J. V. (2007), Production of multimeric prostate-specific membrane antigen small molecule radiotracers using a solid-phase ^{99m}Tc preloading strategy, J. Nucl. Med., 48, 1379–1389 (DOI: 10.2967/jnumed.107.040303).

29. Graham K., Lesche R., Gromov A. V., Böhnke N., Schäfer M., Hassfeld J., Dinkelborg L., Kettschau G. (2012), Radiofluorinated derivatives of 2-(phosphonomethyl) pentanedioic acid as inhibitors of prostate specific membrane antigen (PSMA) for the imaging of prostate cancer, J. Med. Chem., 55, 9510−9520 (DOI: 10.1021/jm300710j).

30. Kozikowski A.P., Zhang J., Nan F., Petukhov P. A., Grajkowska E., Wroblewski J.T., Yamamoto T., Bzdega T., Wroblewska B., Neale J.H. (2004), Synthesis of urea-based inhibitors as active site probes

of glutamate carboxypeptidase II: efficacy as analgesic agents, J. Med. Chem., 47, 1729–1738(DOI: 10.1021/jm0306226).

Chapter 3

Synthesis of Fluorescent and Radiopharmaceutical Bioconjugates using Aminoacetamide as Targeting Ligand for Detection of Prostate Specific Membrane Antigen Expressing ($PSMA^+$) Cancers

3.1 Introduction

The high mortality rate and financial burden associated[1] with prostate cancer are due to the lack of sensitive diagnostic modalities. Prostate cancer is commonly screened using digital rectal examination (DRE), prostate specific antigen (PSA) test in the blood, and prostate biopsy.[2,3] These methods are not effective to detect prostate malignancy in its early stage.[4,5] Moreover, the accuracy of the PSA test is controversial due to its frequent false positive results.[3] An elevated level of PSA is observed in the blood serum during benign prostatic hypertrophy (BPH) and prostatitis. On the contrary, the men who undergo treatment for BPH may show a lower level of PSA thus leaving malignant state undiagnosed. Generally, anatomic techniques like transrectal ultrasounds, magnetic resonance imaging (MRI), and computed tomography (CT)[6] can only be used to analyze the extent of prostate enlargement and growth asymmetry. Molecular imaging techniques like Magnetic resonance imaging (MRI), single photon emission computed tomography (SPECT), and positron emission tomography (PET) are helpful to understand the physiology of the malignant tissues but not comprehensive for therapeutic monitoring. Thus, there is an unmet need to develop precise diagnostic tools for prostate cancer detection at its very early stage.

Guided by *in silico* docking studies using the cocrystal structure of GCPII with a ligand (PDB 4NGM), we have designed and synthesized a series of aminoacetamide derivatives (Chapter 2). Among those glutamic acid-based aminoacetamide derivatives (Chart 3.1) inhibitor **1**, was found to bind PSMA protein with low nanomolar affinity (IC_{50} = 38.5 nM).

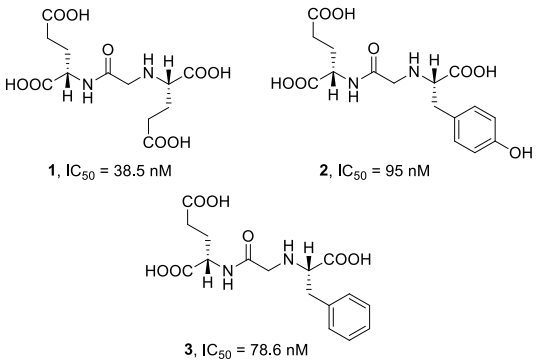

Figure 3.1 New class of PSMA inhibitors, aminoacetamides, **1**–**3**, with PSMA enzyme inhibitory concentrations (IC_{50})

In chapter 3, we have synthesized small molecule ligand-targeted bioconstructs as diagnostic tools for detection of $PSMA^+$ cancers using the most potent glutamic acid-based aminoacetamide derivative, **1**, as the targeting moiety. After synthesizing two rhodamine B bioconjugates having different peptidic spacers, *in vitro* studies were successfully carried out on malignant cell lines over-expressing PSMA biomarker (LNCaP; $PSMA^+$) and on negative cell lines (PC-3; $PSMA^-$) to prove high specificity of the bioconjugates towards cells over-expressing PSMA biomarker. The binding affinity of both the optical imaging probes has been determined in LNCaP cells using flow cytometry. Moreover, two radionuclear chelating bioconjugates were also synthesized and are ready to deliver radionuclide such as ^{99m}Tc for the detection of prostate cancer using scintigraphy techniques as a future application.

3.2 Results and Discussion

3.2.1 Synthesis of targeted fluorescent (9, 12) and radionuclear bioconstructs (18, 21)

An elaborate solid phase peptide synthesis (SPPS) was performed for the construction of required PSMA fluorescent conjugates **9** and **12** as well as radionuclide conjugates **18** and **21**, as described in Schemes 3.1, 3.2, 3.3

and 3.4. Analysis of the crystal structure[7] of PSMA reveals that small molecule ligands would reach the PSMA active site through a gradually narrowing tunnel of amino acids of 20 Å length.[8] Moreover, the inner surface of the PSMA tunnel possesses hydrophobic pockets, and hence the presence of hydrophobic amino acids in the peptidic spacer would be helpful for suitable hydrophobic interactions. Therefore, it is important to design a PSMA targeted conjugate that can pass through the tunnel effectively and reach the active site by perfect fit in the hydrophobic pockets. The α and α′-carboxylic acids of glutamic acid-based aminoacetamide derivative **1** interacts with Arg210 and Arg534 amino acid residues, and the carbonyl oxygen coordinates with the catalytic zinc atoms of PSMA. The free γ′-carboxylic acid of **1** was further utilized as bioconjugate handle to attach the fluorescent tag or chelating core through a peptidic spacer. An eight-carbon amino acid such as 8-aminocaprylic acid has been covalently attached to γ′-carboxylic acid of **1** to ensure the adequate distance between targeting ligand and peptidic spacer so that the specific binding to the protein is not compromised. Two phenylalanine (Phe) amino acid residues were also introduced to fit in the hydrophobic pockets. In the case of bioconstructs **9**, **12**, **18** and **21**, another molecule of 8-amino acid was introduced to ensure that the molecular position of the fluorescent tag (bioconstructs **9** and **12**) and chelating core (bioconstructs **18** and **21**) would lie outside the surface of protein tunnel. Moreover, differentially protected α- and ε-amino groups of lysine (Lys) amino acid, Fmoc-Lys-(Tfa)-OH, was also introduced in the peptidic spacer to attach the fluorescent tag through ε-amine group of lysine and the α-amine group will be utilized for continuing the growing peptide chain. Acidic amino acid like aspartic acid (Asp) was attached in the spacer to increase the solubility of the bioconstructs.

Scheme 3.1 Synthesis of bioconjugate **9**

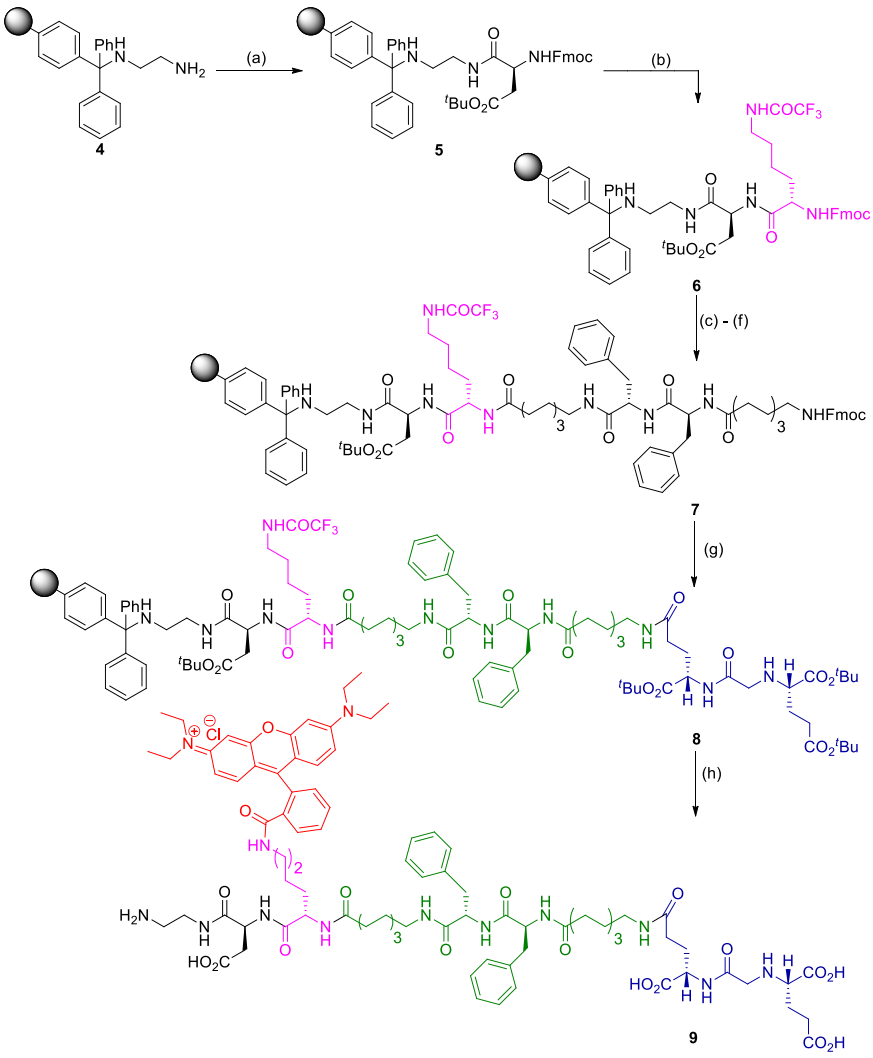

Reagents and conditions: (a) Fmoc-Asp(O^{t}Bu)-OH, PyBOP, DIPEA, DMF, 6 h; (b) (i) 20% Piperidine in DMF, rt, 30 min; (ii) Fmoc-Lys(Tfa)-OH, PyBOP, DIPEA, DMF, 6 h; (c) (i) 20% Piperidine in DMF, rt, 30 min; (ii) Fmoc-8-aminocaprylic acid, PyBOP, DIPEA, DMF, 6 h; (d) (i) 20% Piperidine in DMF, rt, 30 min; (ii) Fmoc-Phe-OH, PyBOP, DIPEA, DMF, 6 h; (e) (i) 20% Piperidine in DMF, rt, 30 min; (ii) Fmoc-Phe-OH, PyBOP, DIPEA, DMF, 6 h; (f) (i) 20% Piperidine in DMF, rt, 30 min; (ii) Fmoc-8-aminocaprylic acid, PyBOP, DIPEA, DMF, 6 h; (g) (i) 20% Piperidine in DMF, rt, 30 min; (ii) tris(*tert*-butoxy) AAPT precursor, PyBOP, DIPEA, DMF, 6 h (h) (i) 2M Piperidine in water, rt, 6–12 h; (ii)

Rhodamine B, PyBOP, DIPEA, DMF, 6 h; (iii) TFA/TIS/H_2O (95.0:2.5:2.5) (1 × 5 mL, 30 min; 2 × 5 mL, 15 min each); (iv) Evaporate TFA; (v) Precipitate in ice-cold diethylether

With these objectives in mind we begin the synthesis of bioconjugates **9** and **12** from commercially available 1,2-diaminoethyltrityl resin **4** (Schemes 3.1 and 3.2). The free amino group present in **4** was coupled with Fmoc-Asp(O^tBu)-OH using PyBOP as an amide coupling agent to provide dipeptide chain **5**. The NHFmoc amino group in the growing dipeptide chain **5** was deprotected using a solution of 20% piperidine in DMF. The Fmoc free amino group in **5** was now coupled with Fmoc-Lys(Tfa)-OH to provide tripeptide **6** with trifluoroacetyl protected ε-amino group of lysine. It is important to mention that the α-amino group of lysine was protected as NHFmoc which is labile to 20% piperidine in DMF and readily available for constructing next amide bond in the growing dipeptide chain. Whereas the ε-amino group of lysine protected as trifluoroacetyl group is stable under NHFmoc cleavage conditions and it readily undergoes deprotection in 2M aqueous piperidine. The selection of α- and ε-amine protecting groups in lysine amino acid, which are labile under different basic conditions, was crucial to strategize the synthesis of attaching the fluorescent agent to ε-amino group of lysine in the final step of the preparation of conjugates **9** and **12**. After the deprotection of NHFmoc group, the tripeptide **6** was tethered sequentially to 8-aminocaprylic acid, two phenyalanine residues, another 8-aminocaprylic acid and finally to tris(*tert*-butoxy) AAPT precursor to afford the polypeptide chain **8**. In the construction of bioconjugates **12** and **21**, 4-(Fmoc-aminomethyl)benzoic acid was introduced in the peptide spacer sequence of **11** and **20** polypeptide chains (Schemes 3.2 and 3.4). The main purpose of this exercise is to establish a new interaction of the spacer with an another remote arene-binding region present in the PSMA protein.[9]

Scheme 3.2 Synthesis of bioconjugate **12**

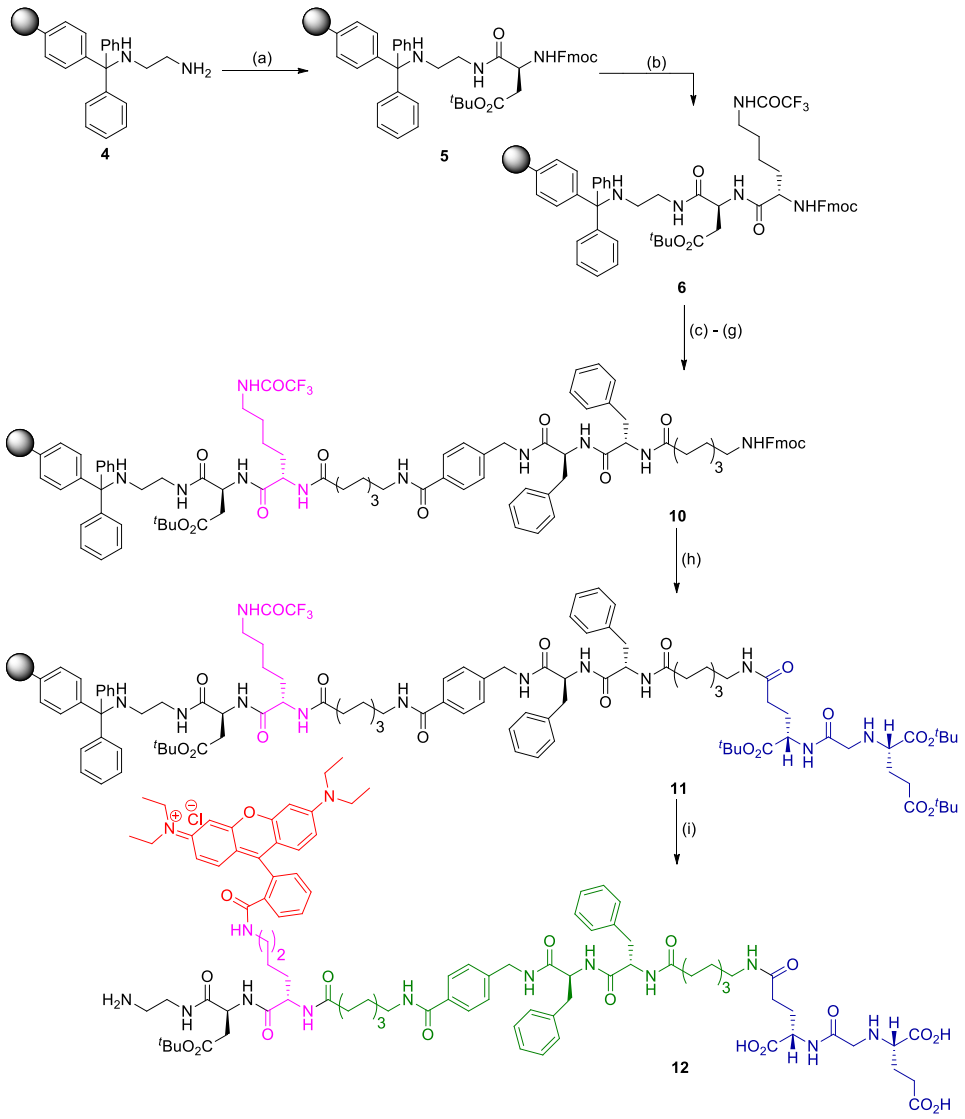

Reagents and conditions: (a) Fmoc-Asp(OtBu)-OH, PyBOP, DIPEA, DMF, 6 h; (b) (i) 20% Piperidine in DMF, rt, 30 min; (ii) Fmoc-Lys(Tfa)-OH, PyBOP, DIPEA, DMF, 6 h;(c) (i) 20% Piperidine in DMF, rt, 30 min; (ii) Fmoc-8-aminocaprylic acid, PyBOP, DIPEA, DMF, 6 h; (d) (i) 20% Piperidine in DMF, rt, 30 min; (ii) 4-(Fmoc-aminomethyl)benzoic acid, PyBOP, DIPEA, DMF, 6 h; (e) (i) 20% Piperidine in DMF, rt, 30 min; (ii) Fmoc-Phe-OH, PyBOP, DIPEA, DMF, 6 h; (f) (i) 20% Piperidine in DMF, rt, 30 min; (ii) Fmoc-Phe-OH, PyBOP, DIPEA, DMF, 6 h; (g) (i)

20% Piperidine in DMF, rt, 30 min; (ii) Fmoc-8-aminocaprylic acid, PyBOP, DIPEA, DMF, 6 h; (h) (i) 20% Piperidine in DMF, rt, 30 min; (ii) tris(*tert*-butoxy) AAPT precursor, PyBOP, DIPEA, DMF, 6 h (h) (i) 2M Piperidine in water, rt, 6–12 h; (ii) Rhodamine B, PyBOP, DIPEA, DMF, 6 h; (iii) TFA:TIS:H_2O (95.0:2.5:2.5) (1 × 5 mL, 30 min; 2 × 5 mL, 15 min each); (iv) Evaporate TFA; (v) Precipitate in ice-cold diethylether

The remote binding pocket is formed by the indole group of Trp541 and the guanidinium group of Arg511 amino acid residues in the PSMA. The bottom of the cleft, lined by Arg 463 side chain, help to position the arene ring of the spacer parallel to both the indole and guanidinium functionalities. The introduction of arene moiety in the peptidic spacer may improve the binding of the bioconjugates **12** and **21**. Having constructed the masked polypeptide chains **8** or **11**, the end game is to deprotect the trifluoroacetylamino protected lysine aminoacid under aqueous piperidine conditions as mentioned in Schemes 3.1 and 3.2, to expose free amino group from lysine that can be tagged with a fluorescent agent, rhodamine B. The trifluoroacetyl group in lysine amino acid of polypeptide chains **8** or **11** was deprotected successfully using 2M aqueous piperidine[10] and a fluorescent agent, rhodamine B was coupled to lysine amino using PyBOP as coupling agent to give *t*-butyl protected precursor of final conjugates **9** or **12**. Finally, the polypeptide chains **8** or **11** were cleaved from the resin beads with the help of cleaving cocktail TFA:TIS:H_2O (95:2.5:2.5) solution. Excess trifluoroacetic acid was evaporated under reduced pressure using rotary evaporator, and the turbid red viscous solution was precipitated by addition of ice-cold ether. The pink colored precipitate was washed thrice with ice cold ether, centrifuged and dried under an inert atmosphere to provide the final PSMA targeting rhodamine B conjugates **9** or **12**. The fluorescent conjugates were further purified by flash chromatography using RP-PFP (pentafluorophenyl) preparative column (5 µm, 10 mm × 150 mm). The purity of the **9** and **12**

was confirmed by analytical RP-HPLC, and the molecular weights were recorded using electron-spray ionization mass spectrometry (ESI-MS). The fluorescent bioconjugates **9** and **12** were further utilized for drug delivery to prostate cancer cells *in vitro*.

The synthesis of chelating linker conjugates **18** and **21** begins from commercially available 2-chlorotrityl cysteine resin **13** pre-attached to cysteine amino acid via carboxylic acid functional group (Schemes 3.3 and 3.4). The free amino group present in **13** was subsequently coupled with Fmoc-Asp(O^{t}Bu)-OH, Boc-Dap(Fmoc)-OH to form the chelating core of **18**. The chelating core can be used as a multipurpose handle for loading drug cargos, radionuclides, or nanomaterials. Other amino acids like 8-aminocaprylic acid, phenylalanine, 4-(Fmoc-aminomethyl)benzoic acid were utilized for the construction of **21** and the targeting ligand precursor tris(*tert*-butylcarboxy) AAPT was attached to the peptide sequence in a similar fashion as described earlier for the construction of bioconjugates **9** and **12**. The polypeptide chains **17** and **20** were detached from the chlorotrityl resin, and simultaneously all the carboxylic acid protecting *tert*-butyl groups of amino acids were deprotected with the help of cleavage cocktail TFA:EDT:TIPS:H_2O (92.5:2.5:2.5:2.5). After cleavage from the resin beads, excess trifluoroacetic acid was evaporated under reduced pressure using rotary evaporator, and the turbid viscous solution was precipitated by the addition of ice-cold ether. The precipitate was washed thrice with ice-cold ether, centrifuged and dried under an inert atmosphere to afford the final PSMA targeting chelating linker conjugates **18** and **21**. The bioconjugates were further purified by flash chromatography using RP-PFP (pentafluorophenyl) preparative column (5 µm, 10 mm × 150 mm). The purity of the **18** and **21** was confirmed by analytical RP-HPLC and the molecular weights were determined by HRMS.

Scheme 3.3 Synthesis of bioconjugate **18**

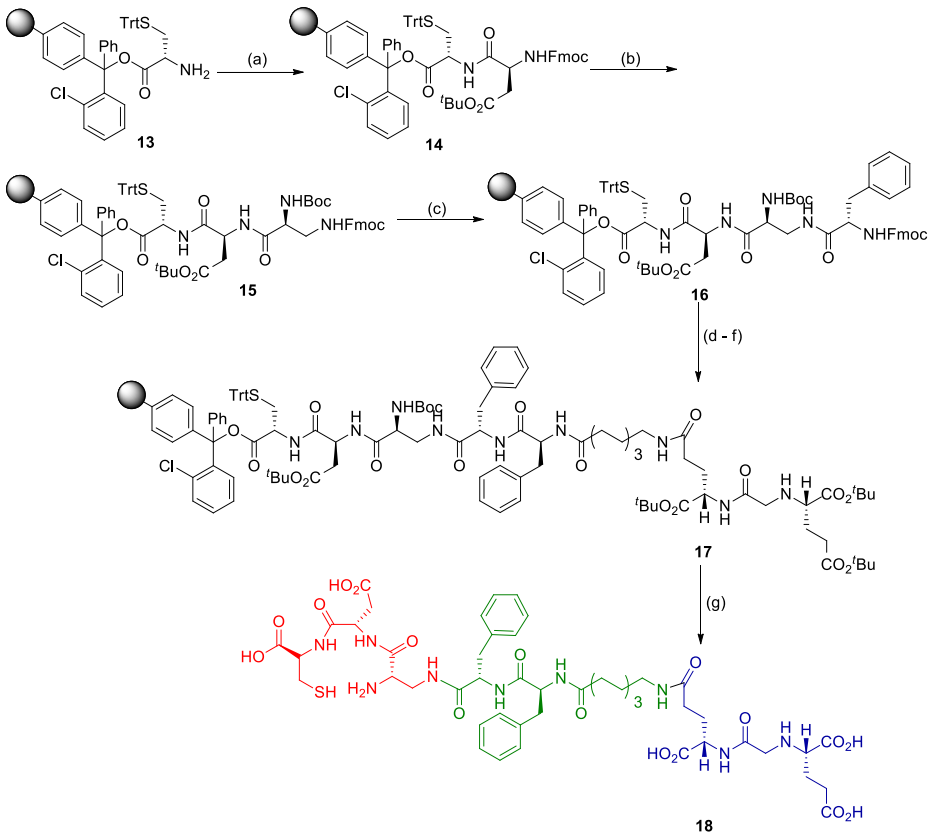

Reagents and conditions: (a) Fmoc-Asp(OtBu)-OH, PyBOP, DIPEA, DMF, 6 h; (b) (i) 20% Piperidine/DMF, rt, 30min; (ii) Fmoc-diaminopropionic (DAP) acid, PyBOP, DIPEA, DMF, 6 h; (c) (i) 20% Piperidine/DMF, rt, 30 min; (ii) Fmoc-Phe-OH, PyBOP, DIPEA, DMF, 6 h; (d) (i) 20% Piperidine/DMF, rt, 30 min; (ii) Fmoc-Phe-OH, PyBOP, DIPEA, DMF, 6 h; (e) (i) 20% Piperidine/DMF, rt, 30 min; (ii) Fmoc-8-aminooctanoic (EAO) acid, PyBOP, DIPEA, DMF, 6 h;(f) (i) 20% Piperidine/DMF, rt, 30 min; (ii) tris(*tert*-butoxy) AAPT precursor, PyBOP, DIPEA, DMF, 6 h; (g) TFA:H_2O:TIPS:EDT (92.5:2.5:2.5:2.5) (1 × 5 mL, 30 min; 2 × 5 mL, 5 min); (iv) Evaporate TFA; (v) Precipitate in ice-cold diethylether

Scheme 3.4 Synthesis of bioconjugate **21**

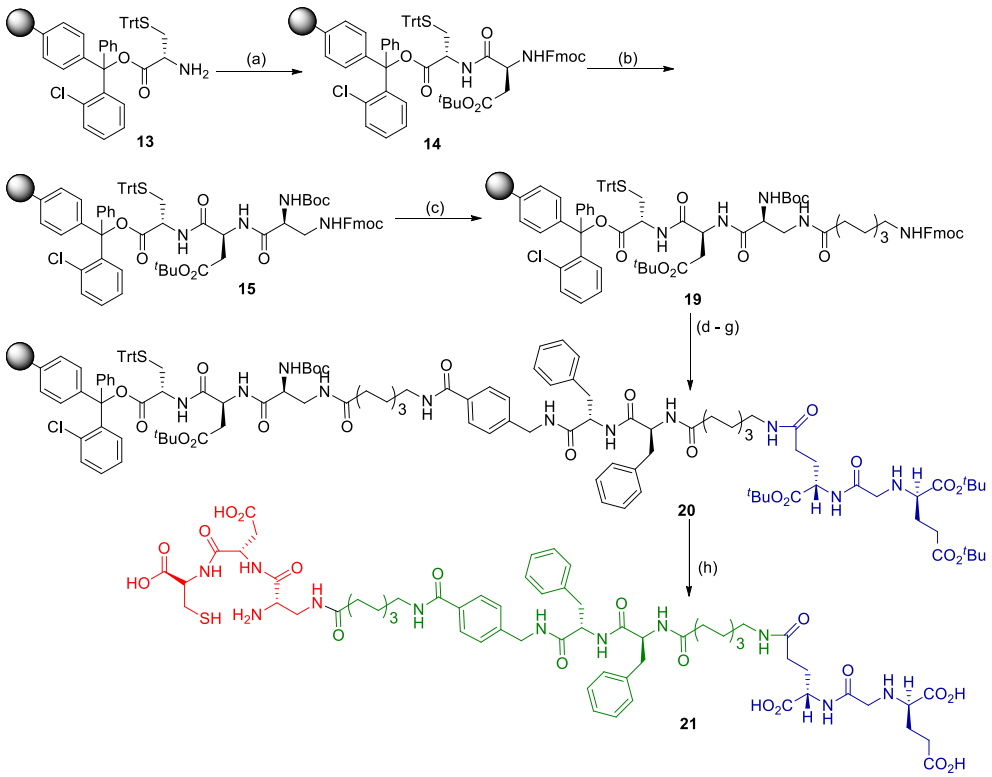

Reagents and conditions: (a) Fmoc-Asp(O^{t}Bu)-OH, PyBOP, DIPEA, DMF, 6 h; (b) (i) 20% Piperidine/DMF, rt, 30min; (ii) Fmoc-diaminopropionic (DAP) acid, PyBOP, DIPEA, DMF, 6 h; (c) (i) 20% Piperidine/DMF, rt, 30 min; (ii) Fmoc-8-aminooctanoic (EAO) acid, PyBOP, DIPEA, DMF, 6 h; (d) (i) 20% Piperidine in DMF, rt, 30 min; (ii) 4-(Fmoc-aminomethyl)benzoic acid, PyBOP, DIPEA, DMF, 6 h; (e) (i) 20% Piperidine/DMF, rt, 30 min; (ii) Fmoc-Phe-OH, PyBOP, DIPEA, DMF, 6 h; (d) (i) 20% Piperidine/DMF, rt, 30 min; (ii) Fmoc-Phe-OH, PyBOP, DIPEA, DMF, 6 h; (e) (i) 20% Piperidine/DMF, rt, 30 min; (ii) Fmoc-8-aminooctanoic (EAO) acid, PyBOP, DIPEA, DMF, 6 h;(f) (i) 20% Piperidine/DMF, rt, 30 min; (ii) tris(*tert*-butoxy) AAPT precursor, PyBOP, DIPEA, DMF, 6 h; (g) TFA:H_2O:TIPS:EDT (92.5:2.5:2.5:2.5) (1 × 5 mL, 30 min; 2 × 5 mL, 5 min); (iv) Evaporate TFA; (v) Precipitate in ice-cold diethylether

3.2.2 *In vitro* studies

The newly synthesized bioconjugates **9** and **12** that can selectively target $PSMA^+$ cancers, were further evaluated by performing *in vitro* studies using laser scanning confocal microscopy on $PSMA^+$ LNCaP cells, and $PSMA^-$ PC-3 cells. The negative cell line was used to prove the protein specificity and uptake of the ligand targeted bioconjugates **9** and **12** was via PSMA receptor mediated endocytosis.

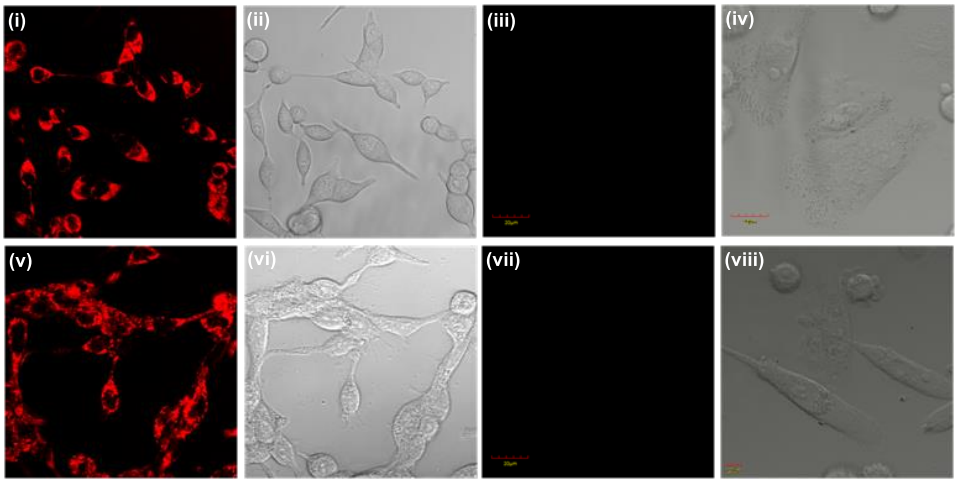

Figure 3.2 (i) Binding and internalization of PSMA targeted aminoacetamide rhodamine B conjugate **9** to LNCaP cells by confocal microscopy at 25 nM concentration; (ii) and (vi) DIC image of $PSMA^+$ (LNCaP) cells; (iii) Specificity of aminoacetamide rhodamine B **9** conjugate in $PSMA^-$ (PC-3) cell line; (iv) and (viii) DIC image of $PSMA^-$ (PC-3) cells; (v) Binding and internalization of PSMA targeted aminoacetamide arene rhodamine B conjugate **12** to LNCaP cells by confocal microscopy at 50 nM concentration; (vii) Specificity of aminoacetamide arene rhodamine B **12** conjugate in $PSMA^-$ (PC-3) cell line.

In figure 3.1 the confocal microscopic images depict the delivery of conjugates to cells via receptor-mediated endocytosis negating any possibility of non-specific uptake. The confocal microscopic images in

figure 3.1, panel (i) shows the uptake of PSMA targeted aminoacetamide rhodamine B conjugate **9** in LNCaP cells at 25 nM concentration. Panel (ii) shows the uptake of PSMA targeted aminoacetamide arene rhodamine B conjugate **12** at 50 nM concentration. The specificity of the ligand conjugates was further established by studying the uptake of bioconjugates **9** and **12** in malignant cells (PC-3) which did not express PSMA [panels (iii) and (vii)]. The absence of any rhodamine B bioconjugates **9** and **12** uptakes in the cytoplasm of the negative cell line, PC-3 cells, show that the bioconjugates are very specific which is an important criterion in targeted drug delivery systems for avoiding off-site toxicity.

The binding affinity of fluorescent conjugate **9** or **12** on $PSMA^+$ cells was estimated by analyzing uptake studies in LNCaP cells using Fluorescence Activated Cell Sorting (FACS) technique. The conjugate's ability to bind to PSMA is evaluated by measuring the mean fluorescence intensity per cell for different concentrations of the conjugate. A hyperbolic curve of different concentrations of the fluorescent inhibitor against the mean fluorescence intensity of **9** or **12** by $PSMA^+$ LNCaP cells yielded a dissociation constant K_D value of 85 nM and 130 nM (Figures 3.2 and 3.3). The curve shows a slow exponential increase in the uptake of the fluorescent conjugate **9** or **12** targeted to the PSMA receptor followed by saturation of the curve for concentrations higher than 200 nM due to full occupancy of PSMA receptors present in the LNCaP cells with the conjugates **9** or **12**. The low dissociation constant value gives undisputable evidence of the high affinity of the ligand-peptide spacer to the PSMA protein and its perfect fit inside the protein tunnel.

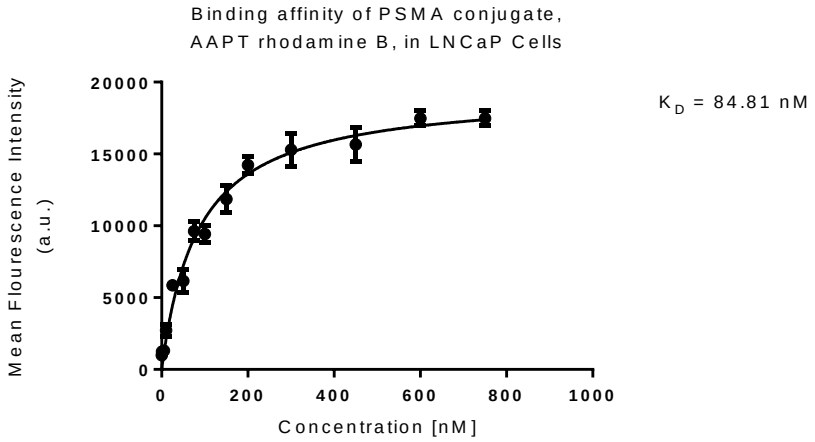

Figure 3.3 Binding of aminoacetamide-rhodamine conjugate **9** in $PSMA^+$ LNCaP cells for a range of concentrations plotted against the mean fluorescence intensity to yield a dissociation constant K_D of 85 nM

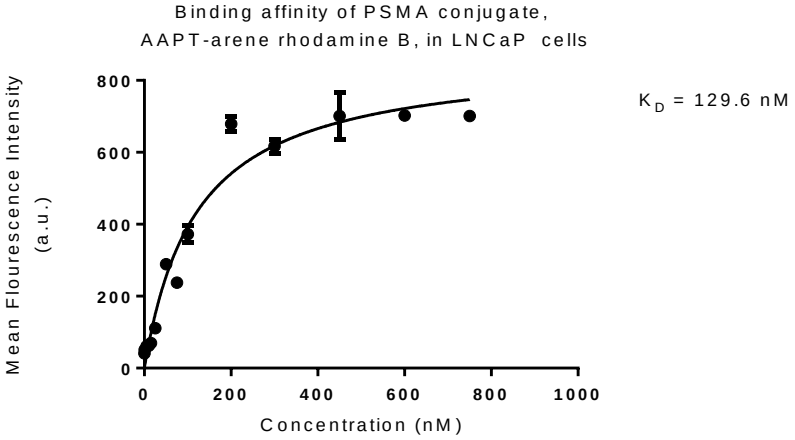

Figure 3.4 Binding of aminoacetamide-arene rhodamine conjugate **12** in $PSMA^+$ LNCaP cells for a range of concentrations plotted against the mean fluorescence intensity to yield a dissociation constant K_D of 130 nM

3.3 Conclusion

In summary, we have prepared four novel aminoacetamide-based fluorescent and radiopharmaceutical bioconjugates for imaging PCa using standard solid phase peptide synthesis strategy in high yield and purity. Successful *in vitro* application by targeted delivery and binding affinity

measurement studies have opened the path for future *in vivo* studies and clinical use of the bio-construct as an imaging agent for detection of PSMA positive cancers. In the future, the radionuclear chelating conjugates **18** and **21** will be utilized to deliver radionuclide such as ^{99m}Tc for the detection of prostate cancer using scintigraphy techniques.

3.4 Experimental section

1,2-Diaminoethanetrityl, 2-chlorotrityl cysteine resins, Fmoc-amino acids, coupling reagents and solvents used in the solid phase peptide synthesis (SPPS) as well as in the chemical synthesis were purchased from Iris Biotech GmbH, Sigma Aldrich, Merck, and Spectrochem. Peptide synthesis was performed manually by using peptide vessels (Chemglass) and standard peptide coupling procedures. The purity of peptide conjugates was analyzed using a Dionex HPLC-Ultimate 3000 Analytical HPLC instrument. The peptide conjugates were purified using RP-PFP column (XSelect CSH Prep Fluorophenyl 5 µm OBD, 19 mm × 150 mm) in Buchi Reveleris High-Performance Preparative Chromatography instrument. Mass spectra were recorded on Bruker micro TOF-Q II instrument using positive mode electrospray ionization methods.

3.4.1 Synthesis of bioconjugates 9, 12, 18 and 21

3.4.1.1 Resin swelling

All the resins used in solid phase peptide synthesis were swelled initially with CH_2Cl_2 (5 mL) for 30 minutes by bubbling nitrogen, and after draining CH_2Cl_2, the resin was swelled thrice with DMF (3 × 5 mL) for 15 minutes each.

3.4.1.2 General procedure for the Kaiser test

Few resin beads were taken in a test-tube and two drops of each of ninhydrin, phenol and 0.1% potassium cyanide solution were added to the

test-tube and heated for 2 minutes at 110 °C in a sand bath. The presence of a free amine group was confirmed by the appearance of dark blue-colored resin beads in the test tube. The Kaiser test was conducted after performing coupling of each amino acids following the procedure as described before.

3.4.1.3 General procedure for NHFmoc deprotection

The NHFmoc-amino group in the growing peptide chain was deprotected in each step using a freshly prepared solution of 20% piperidine in DMF (10 mL). Initially, 4 mL of the 20% piperidine solution in DMF was added to the resin beads and mixed for 10 minutes by bubbling nitrogen gas. The solution was drained from the resin beads, and the procedure was repeated twice with the remaining 20% piperidine solution (2 × 3 mL) for 10 minutes each to ensure complete deprotection of NHFmoc protecting group.

3.4.1.4 Solid phase peptide synthesis procedure for the preparation of AAPT rhodamine B conjugate 9

1,2-Diaminoethanetrityl resin (0.050 g, 0.06 mmol) was swelled initially with 5 mL of DCM by bubbling nitrogen gas for 30 minutes. After draining the DCM, the resin was swelled with 5 mL DMF thrice for 15 minutes each. *N*-Fmoc-Asp(O^{t}Bu)-OH (0.061 g, 0.15 mmol), PyBOP (0.078 g, 0.15 mmol) and DIPEA (0.10 mL, 0.6 mmol) in 0.5 mL DMF was added to the resin beads in the peptide vessel, and the coupling reaction was continued for 6 h. The resin was washed with DMF (3 × 3 mL) followed by isopropanol (3 × 3 mL), and the beads were dried by a stream of nitrogen gas. The completion of the reaction was confirmed by performing the Kaiser test with few dried resin beads. A solution of 20% piperidine in DMF (10 mL) was prepared, added to the resin beads in aliquots (1 × 4 mL; 2 × 3 mL), mixed for 10 minutes each, and drained to ensure complete deprotection of Fmoc protecting group of the coupled

amino acid as mentioned in the general procedure. The resin beads were washed again with DMF (3 × 3 mL) followed by isopropanol (3 × 3 mL) and dried by a stream of nitrogen gas. The formation of free amine was confirmed by performing the Kaiser test with few resin beads. Consecutively, Fmoc-Lys(Tfa)-OH (0.070 g, 0.15 mmol), Fmoc-8-aminocaprylic acid (0.057 g, 0.15 mmol), Fmoc-Phe-OH (0.058 g, 0.15 mmol) Fmoc-Phe-OH (0.058 g, 0.15 mmol) and Fmoc-8-aminocaprylic acid (0.057 g, 0.15 mmol) were attached to the growing peptide chain in the sequence as mentioned before. After the deprotection of Fmoc group from the last amino acid, Fmoc-8-aminocaprylic acid, tris(*tert*-butylcarboxy) protected AAPT precursor (0.040 g, 0.079 mmol), PyBOP (0.068 g, 0.1312 mmol) and DIPEA (0.091 mL, 0.525 mmol) in 0.5 ml DMF were added to the beads and mixed for 6 h. The completion of the reaction was confirmed by the Kaiser test. Finally, the trifluoroacetyl group of lysine was deprotected by the addition of 2M aqueous piperidine (5 mL) to the resin beads and mixed at room temperature for 6–12 h (depending on the completion of the reaction). The resin beads were washed again with DMF (3 × 3 mL) followed by isopropanol (3 × 3 mL) and dried by a stream of nitrogen gas. The complete deprotection of Tfa group was confirmed by the Kaiser test with few dried resin beads. Rhodamine B (0.038g, 0.079 mmol), PyBOP (0.068 g, 0.1312 mmol) and DIPEA (0.091 mL, 0.525 mmol) in 0.5 ml DMF was added to the resin beads in the peptide vessel and mixed for 6 h at room temperature. The resin beads were washed again with DMF (3 × 3 mL) followed by isopropanol (3 × 3 mL) and dried by a stream of nitrogen gas. The completion of the reaction was finally confirmed by performing the Kaiser test. At last, a cocktail mixture of 9.5 mL trifluoroacetic acid (TFA), 0.25 mL triisopropylsilane (TIPS), and 0.25 mL H_2O was prepared, and 5 mL of this cocktail solution was added to the resin beads, and nitrogen gas was bubbled through the beads for 30 minutes. The same procedure was repeated twice (2 × 2.5 mL) using the remaining cocktail solution for 15

minutes each. After the peptide cleavage from the resin, the mother liquor from cleavage was transferred to a 15 mL centrifuge tube fitted with a rubber septum and a needle, and concentrated under reduced pressure using rotary evaporator for 45 minutes. Ice-cold ether (5 mL) was added to the viscous solution to precipitate the bright red rhodamine bioconjugate **9**. The crude bioconjugate **9** was washed with ice-cold ether (3 × 3 mL), and the upper ether layer was discarded. The conjugate was dried using a stream of nitrogen gas and purified by flash chromatography using RP-PFP (pentafluorophenyl) preparative column (5 µm, 10 mm × 150 mm) [λ = 254 nm; mobile phase, A = 0.1% trifluoro acetic acid/H_2O and B = acetonitrile]. The purity of bioconjugate **9** was confirmed by analytical RP-HPLC, and the molecular weight was determined by HRMS (+ESI) calcd for $[M\text{-}Cl]^+$ $(C_{86}H_{118}N_{13}O_{18})^+$: 1620.8712 found 1620.8728.

3.4.1.5 Solid phase peptide synthesis procedure for the preparation of AAPT-arene rhodamine B conjugate 12

1,2-Diaminoethanetrityl resin (0.050 g, 0.06 mmol) was swelled initially with 5 mL of DCM for 30 minutes by bubbling nitrogen gas, and after draining DCM, the resin was swelled again with DMF (3 × 5 mL) thrice for 15 minutes each. *N*-Fmoc-Asp(O^tBu)-OH (0.061 g, 0.15 mmol), PyBOP (0.078 g, 0.15 mmol) and DIPEA (0.10 mL, 0.60 mmol) in 0.5 mL DMF was added to the resin beads in the peptide vessel, and the coupling reaction was continued for 6 h. The resin was washed with DMF (3 × 3 mL) followed by isopropanol (3 × 3 mL), and the beads were dried by a stream of nitrogen gas. The completion of the reaction was confirmed by performing the Kaiser test with few dried resin beads. A solution of 20% piperidine in DMF (10 mL) was prepared, added to the resin beads in aliquots (1 × 4 mL; 2 × 3 mL), mixed for 10 minutes each, and drained to ensure complete deprotection of Fmoc protecting group of the coupled amino acid as mentioned in the general procedure. The resin beads were washed again with DMF (3 × 3 mL) followed by isopropanol (3 × 3 mL)

and dried by a stream of nitrogen gas. The formation of free amine was confirmed by performing the Kaiser test with few resin beads. Consecutively, Fmoc-Lys(Tfa)-OH (0.070 g, 0.15 mmol), Fmoc-8-aminocaprylic acid (0.057 g, 0.15 mmol), 4-(Fmoc-aminomethyl)benzoic acid (0.056 g, 0.15 mmol), Fmoc-Phe-OH (0.058 g 0.15 mmol), Fmoc-Phe-OH (0.058 g 0.15 mmol), and Fmoc-8-aminocaprylic acid (0.057 g, 0.15 mmol) were attached to the growing peptide chain in sequence as mentioned before. After the deprotection of Fmoc group from the last amino acid, Fmoc-8-aminocaprylic acid, tris(*tert*-butylcarboxy) protected AAPT precursor (0.040 g, 0.079 mmol), PyBOP (0.068 g, 0.1312 mmol) and DIPEA (0.091 mL, 0.525 mmol) in 0.5 ml DMF were added to the beads and mixed for 6 h. The completion of the reaction was confirmed by the Kaiser test. Finally, the trifluoroacetyl group of lysine was deprotected by the addition of 2M aqueous piperidine (5 mL) to the resin beads and mixed at room temperature for 6–12 h (depending on the completion of the reaction). The resin beads were washed again with DMF (3 × 3 mL) followed by isopropanol (3 × 3 mL) and dried by a stream of nitrogen gas. The complete deprotection of Tfa group was confirmed by the Kaiser test with few dried resin beads. Rhodamine B (0.038g, 0.079 mmol), PyBOP (0.068 g, 0.1312 mmol) and DIPEA (0.091 mL, 0.525 mmol) in 0.5 ml DMF was added to the resin beads in the peptide vessel and mixed for 6 h at room temperature. The resin beads were washed again with DMF (3 × 3 mL) followed by isopropanol (3 × 3 mL) and dried by a stream of nitrogen gas. The completion of the reaction was finally confirmed by performing the Kaiser test.

At last, a cocktail mixture of 9.5 mL trifluoroacetic acid (TFA), 0.25 mL triisopropylsilane (TIPS), and 0.25 mL H_2O was prepared, and 5 mL of this cocktail solution was added to the resin beads, and nitrogen gas was bubbled through the beads for 30 minutes. The same procedure was repeated twice (2 × 2.5 mL) using the remaining cocktail solution for 15

minutes each. After the peptide cleavage from the resin, the mother liquor from cleavage was transferred to a 15 mL centrifuge tube fitted with a rubber septum and a needle, and concentrated under reduced pressure using rotary evaporator for 45 minutes. Ice-cold ether (5 mL) was added to the viscous solution to precipitate the bright red AAPT-arene-rhodamine B conjugate **12**. The crude bioconjugate **12** was washed with ice-cold ether (3 × 3 mL), and the upper ether layer was discarded. The conjugate was dried using a stream of nitrogen gas and purified by flash chromatography using RP-PFP (pentafluorophenyl) preparative column (5 µm, 10 mm × 150 mm) [λ = 254 nm; mobile phase, A = 0.1% trifluoro acetic acid/H_2O and B = acetonitrile]. The purity of bioconjugate **12** was confirmed by analytical RP-HPLC, and the molecular weight was determined by HRMS (+ESI) calcd for $[M\text{-}Cl]^+$ $(C_{94}H_{125}N_{14}O_{19})^+$: 1753.9240 found 1753.9271.

3.4.1.6 Solid phase peptide synthesis for the preparation of AAPT chelating linker conjugate 18

H-Cys-2-ClTrt resin (0.100 g, 0.09 mmol) was swelled in DCM (5 mL) and DMF (3 × 5 mL) as mentioned in previous solid phase peptide synthesis procedure. A solution of Fmoc-Asp(O^tBu)-OH (0.092 g, 0.225 mmol), PyBOP (0.117 mg, 0.225 mmol) and DIPEA (0.16 mL, 0.9 mmol) in 0.5 mL DMF was added to the resin beads in the peptide vessel, and the coupling reaction was continued 6 h. The resin was washed with DMF (3 × 3 mL) followed by isopropanol (3 × 3 mL), and the beads were dried by a stream of nitrogen gas. The completion of the reaction was confirmed by performing the Kaiser test with few dried resin beads. A solution of 20% piperidine in DMF (10 mL) was prepared, added to the resin beads in aliquots (1 × 4 mL; 2 × 3 mL), mixed for 10 minutes each, and drained to ensure complete deprotection of Fmoc protecting group of the coupled amino acid as mentioned in the general procedure. The resin beads were washed again with DMF (3 × 3 mL) followed by isopropanol (3 × 3 mL) and dried by a stream of nitrogen gas. The formation of free amine was

confirmed by performing the Kaiser test with few resin beads. Consecutively, Boc-Dap(Fmoc)-OH (0.096 g, 0.225 mmol), Fmoc-Phe-OH (0.087 g, 0.225 mmol), Fmoc-Phe-OH (0.087 g, 0.225 mmol), and Fmoc-8-aminocaprylic acid (0.086 g, 0.225 mmol) were attached to the growing peptide chain in sequence as mentioned before.

After the deprotection of Fmoc group from the last amino acid, Fmoc-8-aminocaprylic acid, tris(*tert*-butylcarboxy) protected AAPT precursor (0.068 g, 0.135 mmol), PyBOP (0.117 mg, 0.225 mmol) and DIPEA (0.16 mL, 0.9 mmol) in 0.5 ml DMF were added to the beads and mixed for 6 h. The completion of the reaction was confirmed by the Kaiser test. A mixture of 9.25 mL trifluoroacetic acid (TFA), 0.25 mL ethanedithiol, 0.25 mL triisopropylsilane (TIPS), and 0.25 mL H_2O was prepared, and 5 mL of this cocktail solution was added to the resin beads, and nitrogen gas was bubbled through the beads for 30 minutes. The same procedure was repeated twice (2 × 2.5 mL) using the remaining cocktail solution for 15 minutes each. After the peptide cleavage from the resin, the mother liquor from cleavage was transferred to a 15 mL centrifuge tube fitted with a rubber septum and a needle, and concentrated under reduced pressure using rotary evaporator for 45 minutes. Ice-cold ether (5 mL) was added to the viscous solution to precipitate the white chelating linker conjugate **18**. The crude AAPT chelating linker conjugate **18** was washed with ice-cold ether (3 × 3 mL), and the upper ether layer was discarded. The chelating conjugate was dried using a stream of nitrogen gas and purified by flash chromatography using RP-PFP (pentafluorophenyl) preparative column (5 µm, 10 mm × 150 mm). [λ = 225 nm; mobile phase, A = 0.1% trifluoro acetic acid/H_2O and B = acetonitrile]. Acetonitrile was removed under reduced pressure, and the pure fractions were freeze-dried to yield pure **18**. The purity of **18** was confirmed by analytical RP-HPLC, and the molecular weight was determined by ESI-HRMS (*m*/*z*): $(M + H)^+$ calcd. for $C_{48}H_{67}N_9O_{17}S$, 1073.4463; found, 1073.4480. UV/vis: λmax = 225 nm

3.4.1.7 Solid phase peptide synthesis procedure for the preparation of AAPT-arene chelating linker 21

H-Cys-2-ClTrt resin (0.100 g, 0.09 mmol) was swelled in DCM (5 mL) and DMF (3 × 5 mL) as mentioned in previous solid phase peptide synthesis procedure. A solution of Fmoc-Asp(O^{t}Bu)-OH (0.092 g, 0.225 mmol), PyBOP (0.117 mg, 0.225 mmol) and DIPEA (0.16 mL, 0.9 mmol) in 0.5 mL DMF was added to the resin beads in the peptide vessel, and the coupling reaction was continued 6 h. The resin was washed with DMF (3 × 3 mL) followed by isopropanol (3 × 3 mL), and the beads were dried by a stream of nitrogen gas. The completion of the reaction was confirmed by performing the Kaiser test with few dried resin beads. A solution of 20% piperidine in DMF (10 mL) was prepared, added to the resin beads in aliquots (1 × 4 mL; 2 × 3 mL), mixed for 10 minutes each, and drained to ensure complete deprotection of Fmoc protecting group of the coupled amino acid as mentioned in the general procedure. The resin beads were washed again with DMF (3 × 3 mL) followed by isopropanol (3 × 3 mL) and dried by a stream of nitrogen gas. The formation of free amine was confirmed by performing the Kaiser test with few resin beads. Consecutively, Boc-Dap(Fmoc)-OH (0.096 g, 0.225 mmol), Fmoc-8-aminocaprylic acid (0.086 g, 0.225 mmol), 4-(Fmoc-aminomethyl)benzoic acid (0.084 g, 0.225 mmol) , Fmoc-Phe-OH (0.087 g, 0.225 mmol), Fmoc-Phe-OH (0.087 g, 0.225 mmol), and Fmoc-8-aminocaprylic acid (0.086 g, 0.225 mmol) were attached to the growing peptide chain in sequence as mentioned before. After the deprotection of Fmoc group from the last amino acid, Fmoc-8-aminocaprylic acid, tris(*tert*-butylcarboxy) protected AAPT precursor (0.068 g, 0.135 mmol), PyBOP (0.117 mg, 0.225 mmol) and DIPEA (0.16 mL, 0.9 mmol) in 0.5 ml DMF were added to the beads and mixed for 6 h. The completion of the reaction was confirmed by the Kaiser test. A mixture of 9.25 mL trifluoroacetic acid (TFA), 0.25 mL ethanedithiol, 0.25 mL triisopropylsilane (TIPS), and 0.25

mL H_2O was prepared, and 5 mL of this cocktail solution was added to the resin beads, and nitrogen gas was bubbled through the beads for 30 minutes. The same procedure was repeated twice (2 × 2.5 mL) using the remaining cocktail solution for 15 minutes each. After the peptide cleavage from the resin, the mother liquor from cleavage was transferred to a 15 mL centrifuge tube fitted with a rubber septum and a needle, and concentrated under reduced pressure using rotary evaporator for 45 minutes. Ice-cold ether (5 mL) was added to the viscous solution to precipitate the white chelating linker conjugate **21**. The crude AAPT-arene chelating linker conjugate **21** was washed with ice-cold ether (3 × 3 mL), and the upper ether layer was discarded. The chelating conjugate was dried using a stream of nitrogen gas and purified by flash chromatography using RP-PFP (pentafluorophenyl) preparative column (5 μm, 10 mm × 150 mm) [λ = 225 nm; mobile phase, A = 0.1% trifluoro acetic acid/H_2O and B = acetonitrile]. Acetonitrile was removed under reduced pressure, and the pure fractions were freeze-dried to yield pure **21**. The purity of **21** was confirmed by analytical RP-HPLC, and the molecular weight was determined by ESI-HRMS (*m*/*z*): $(M + H)^+$ calcd. for $C_{48}H_{67}N_9O_{17}S$, 1348.6130; found, 1348.6767. UV/vis: λ_{max} = 225 nm.

3.4.1.8 Analytical RP-HPLC method

The purity of bioconjugates **9**, **12**, **18** and **21** were analyzed using a Dionex HPLC-Ultimate 3000 system. Typically a solution of bioconjugate (20 μL, 1.0 mg/1.0 mL) in a mixture of CH_3CN:H_2O (1: 1) was injected via autosampler and eluted using Dionex Acclaim ® 120 C_{18}, 5 μm, 4.6 mm × 250 mm analytical column at a flow rate of 1 mL/min (mobile phase, A = 0.1% trifluoro acetic acid/H_2O and B = acetonitrile). An isocratic flow of 40% B (v/v) was used during the run for 0 to 4 min, and gradually gradient of B was increased to 100% B (v/v) over 40 min. The chromatogram of bioconjugates was recorded on the Ultimate 3000 RS variable wavelength detector at 225–280 nm.

3.4.1.9 Preparative HPLC method for purification of bioconjugates **9**, **12**, **18** and **21**

The purification of bioconjugates **9**, **12**, **18** and **21** was performed using Buchi Reveleris Preparative HPLC System. Crude bioconjugate (20 mg) was dissolved in 1:1 ratio of CH_3CN:H_2O (1 mL) and injected into the sample injector for elution using RP-PFP (Reverse Phase PentafluoroPhenyl) preparative column (XSelect CSH Prep Fluorophenyl 5 µm OBD, 19 mm × 150 mm). A flow rate of 10 mL/min (mobile phase, A = 0.1% trifluoro acetic acid/H_2O and B = acetonitrile) is maintained throughout the run and the mobile phase gradient was increased from 1% B (v/v) to 50% B (v/v) over a period of 40 min. The mobile phase gradient was further increased to 80% B (v/v) in the next 15 min, and the chromatogram was recorded at λ = 280 or 555 nm. Pure fractions of **9**, **12**, **18** and **21** were collected using automatic fraction collector, acetonitrile was evaporated under reduced pressure, lyophilized to afford pure bioconjugates **9**, **12**, **18** and **21** and stored at 4 °C until further use.

3.4.2 *In vitro* study

3.4.2.1 Culture of cell lines

LNCaP and PC-3 cell lines were purchased from the National Centre for Cell Science (NCCS), Pune, India. The cell lines were grown as a monolayer until confluent in sterile filtered RPMI 1640 medium supplemented with 10% heat-inactivated fetal bovine serum (HIFBS), 1% Penicillin-Streptomycin antibiotic and 100 mM of sodium pyruvate in 5% CO_2:95% air humidified atmosphere, at 37 ºC.

3.4.2.2 Confocal laser scanning microscopy (CLSM) studies

LNCaP (50,000 cells/well in 0.5 mL medium) and PC-3 (25,000 cells/well in 0.5 mL medium) cells were trypsinized and seeded into Nunc Lab Tek II Chambered Coverglass System for 72 h and 48 h respectively. The

spent medium was replaced with increasing concentrations of **9** or **12** prepared in medium (0.5 mL) and incubated at 37 °C for 1 h. After rinsing with fresh medium (3 × 1.0 mL) to remove unbound conjugates, confocal images were acquired using a laser scanning confocal microscopy (FV 1000, Olympus) by excitation at 559 nm (yellow diode laser) and emission at 618 nm.

3.4.2.3 Binding affinity study of bioconjugates 9 or 12 in LNCaP cells

LNCaP cells were seeded in T-75 flasks and were grown for 72 hours. After 95% confluency, cells were trypsinized and centrifuged to form a cell pellet. Flow cytometry buffer was prepared by mixing 1X DPBS (50 mL), 25 mM HEPES buffer (1 mL) and EDTA (84 mg) and sterile filtered before use. 75,000 LNCaP cells in 100 uL of the medium were suspended in each of the Eppendorf tubes. The fluorescent conjugates **9** or **12** (400 µL medium) was added to the cell suspension (100 µL) to a final concentration of 5 to 1000 nM and incubated for 1 h at 4 °C. The treated cell suspension in each tube was centrifuged and washed with ice-cold FACS buffer (3 × 1 mL), and the LNCaP cell pellet was suspended in ice-cold FACS buffer (1 mL) for flow cytometry analysis. The mean fluorescence intensity was measured for each sample concentration (10,000 events) using flow cytometer (LSR Fortessa, BD Biosciences). A plot of mean fluorescence intensity (a.u.) versus concentration of the test article afforded the dissociation constant (K_D) value of the bioconjugates **9** or **12** in LNCaP cells. The method of non-linear regression analysis was employed assuming one-site specific binding during the calculation of K_D using GraphPad Prism 6.02 software.

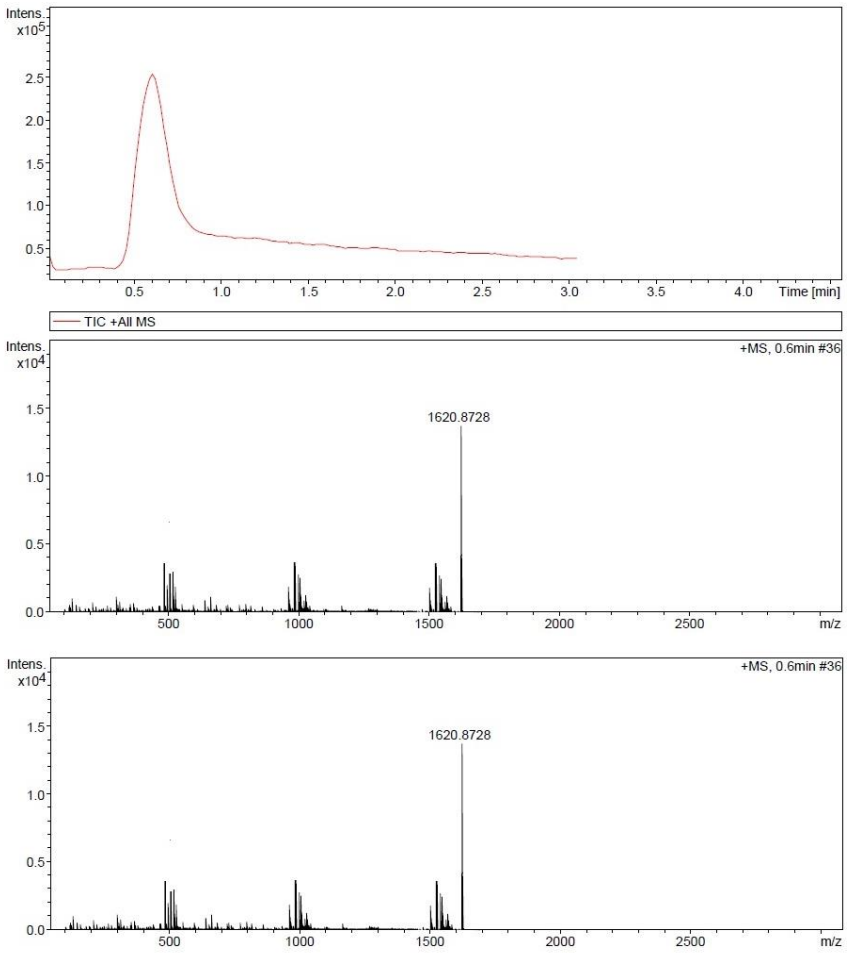

Figure 3.5 ESI-MS of AAPT rhodamine B bioconjugate **9**

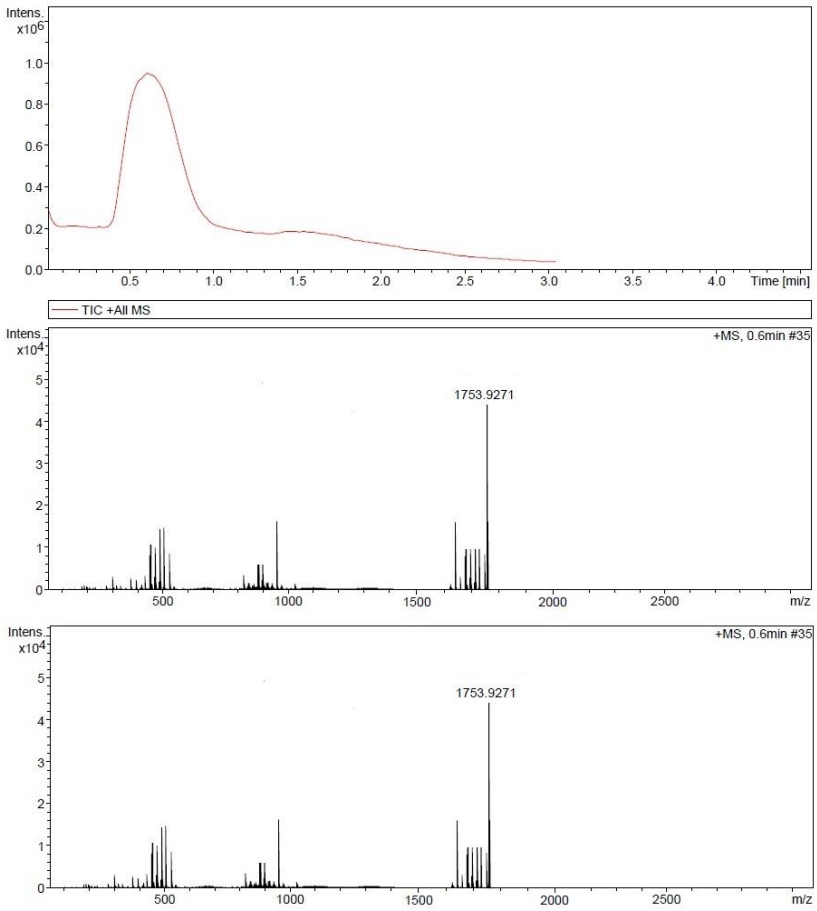

Figure 3.6 ESI-MS of AAPT-arene rhodamine B bioconjugate **12**

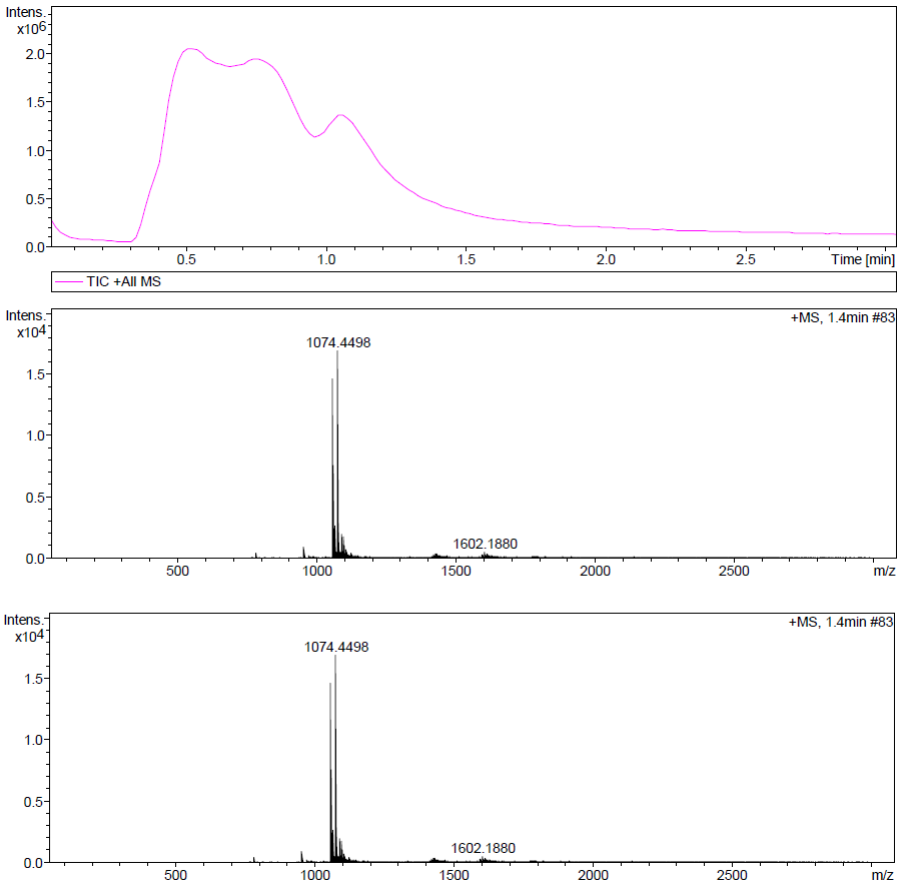

Figure 3.7 ESI-MS of AAPT chelating conjugate **18**

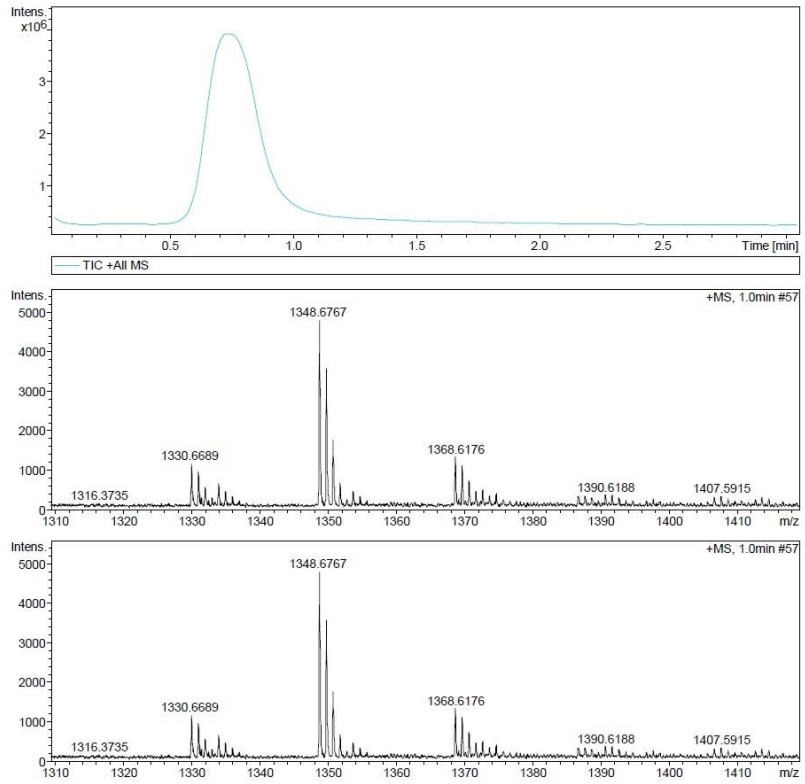

Figure 3.8 ESI-MS of AAPT-arene chelating conjugate **21**

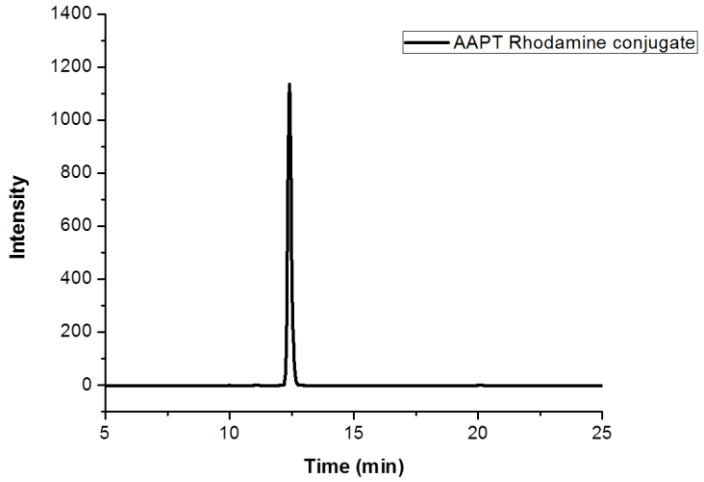

Figure 3.9 Analytical LC of pure AAPT rhodamine B bioconjugate **9** (Abs. at 225 nm)

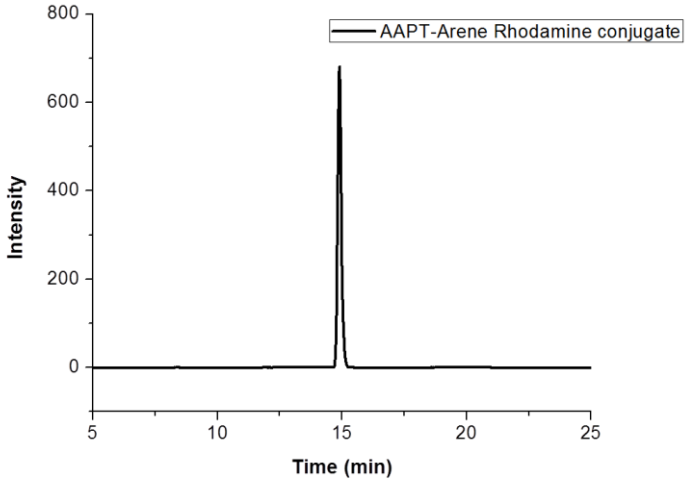

Figure 3.10 Analytical LC of pure AAPT-arene rhodamine B bioconjugate **12** (Abs. at 225 nm)

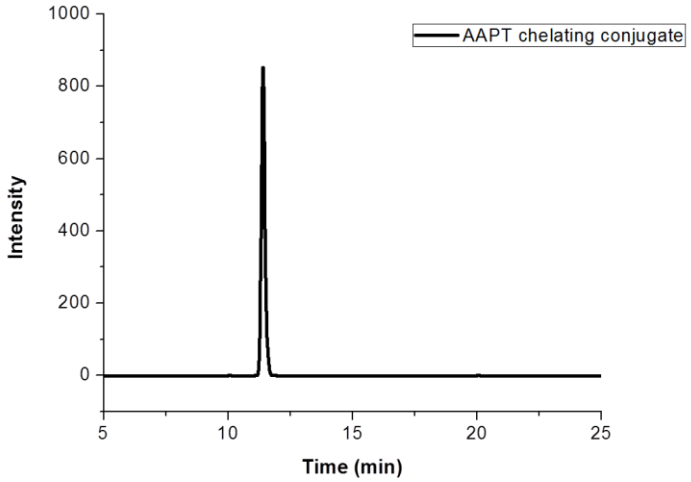

Figure 3.11 Analytical LC of pure AAPT chelating conjugate **18** (Abs. at 225 nm)

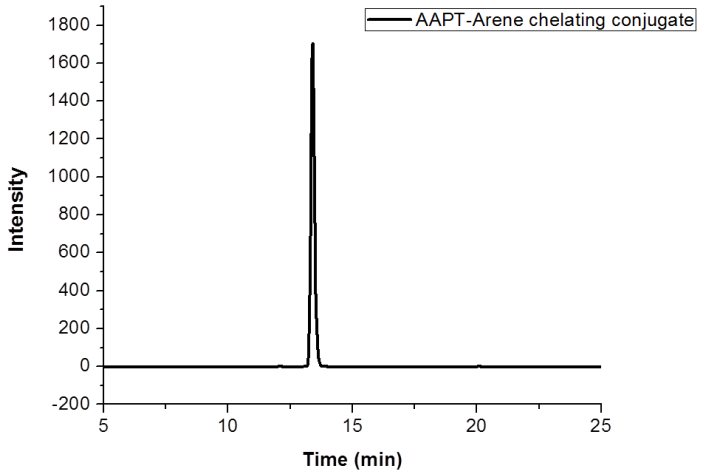

Figure 3.12 Analytical LC of pure AAPT-arene chelating conjugate **21** (Abs. at 225 nm)

3.5 References

1. Wilson L. S., Tesoro R., Elkin E. P. (2007) Cumulative cost pattern comparison of prostate cancer treatments, Cancer, 109, 518–527 (DOI:10.1002/cncr.22433).
2. Chodak M. D., Keller P., Schoenberg H. W.(1989), Assessment of screening for prostate cancer using the digital rectal examination, J. Urol., 141, 1136–1138 (DOI: doi.org/10.1016/S0022-5347(17)41192-X).
3. Linn M. M., Ball R. A., Maradiegue A. (2007), Prostate-specific antigen screening: Friend or foe? Urol. Nurs., 27, 481–489.
4. D'Amico A. V., Roehrborn C. G. (2007), Effect of 1 mg/day finasteride on concentration of serum prostate specific antigen in men with androgenic alopecia: a randomized controlled trial, Lancet Oncol., 8, 21–25 (DOI: 10.1016/S1470-2045(06)70981-0).
5. Zeller J. L. (2007), Grading of prostate cancer, JAMA., 298, 1596.
6. Holves A. M., Heesakkers R. A. M., Adang E. M. (2008), The diagnostic accuracy of CT and MRI in the pelvis of lymph nodes in patients with prostate cancer: a meta-analysis, Clin. Radiol., 63, 387–95 (DOI: 10.1016/j.crad.2007.05.022).
7. Mesters J. R., Barinka C., Li W., Tsukamoto T., Majer P., Slusher B. S., Konvalinka J., Hilgenfeld R. (2006), Structure of glutamate carboxypeptidase II, a drug target in neuronal damage and prostate cancer, EMBO J., 25, 1375–1384 (DOI: 10.1038/sj.emboj.7600969).
8. Kularatne S. A., Zhou Z., Yang J., Post C. B., Low P. S. (2009), Design, synthesis, and preclinical evaluation of prostate-specific membrane antigen targeted ^{99m}Tc-radioimaging agents, Mol. Pharm., 6, 790–800 (DOI: 10.1021/mp9000712).
9. Zhang A. X., Murelli, R. P., Barinka C., Michel J., Cocleaza A.,

Jorgensen W. L., Lubkowski J., Spiegel D. A. (2010), A remote arene-binding site on prostate specific membrane antigen revealed by antibody-recruiting small molecules, J. Am. Chem. Soc., 132, 12711–12716 (DOI: 10.1021/ja104591m)

10. Sengupta S., Krishnan M. A., Dudhe P., Reddy R. B., Giri B., Chattopadhyay S., Chelvam V. (2018), Novel solid-phase strategy for the synthesis of ligand-targeted fluorescent-labelled chelating peptide conjugates as a theranostic tool for cancer, Beilstein J. Org. Chem., 14, 2665–2679 (DOI: 10.3762/bjoc.14.244).

Chapter 4

Design, Synthesis and Biological Evaluation of Novel Thiourea Derivatives as Small Molecule Inhibitors for Prostate Specific Membrane Antigen

4.1 Introduction

Prostate cancer remains the second most common and dreaded malignancies affecting males worldwide with 174,650 newly diagnosed cases and 31,620 estimated deaths in 2019 in the Western countries.[1] Existing diagnostic methods for detection and therapeutic monitoring of primary disease like magnetic resonance imaging (MRI)[2], contrast-enhanced computed tomography (CECT)[3] and ultrasound[4] are ineffective for adequate PCa disease management.

Prostate specific membrane antigen (PSMA) protein, with significant over-expression in the malignant tissues, has emerged as a valuable clinical biomarker of PCa.[5] This differential PSMA expression in PCa has led to the exploration of PSMA as a target for molecular imaging. With recent development in radiopharmaceutical chemistry and imaging technology, molecular radioimaging of prostate cancer has increased significantly. PET radionuclides (^{18}F, ^{64}Cu, ^{68}Ga) are being used significantly in clinical imaging of cancer. However, ^{99m}Tc remains the radionuclide of choice for scintigraphic imaging due to its favourable physical properties (half-life, 6 h, E_γ = 140 keV), low dose burden to the patient, low cost, and ready availability.[6] A variety of low-molecular-weight imaging agents are currently being pursued clinically for the detection of PCa by targeting PSMA. Literature differentiates PSMA inhibitor scaffolds into three categories: (1) glutamate−urea heterodimers[7–14] (2) glutamate containing phosphoramidates[15–18] and (3) 2-(phosphinylmethyl)pentanedioic acid.[19] Among the three, glutamate-urea homodimer and glutamic-urea -heterodimer are the most preferred

classes for PSMA due to their sub nano-molar binding affinity and impressive results *in vivo* with different radioisotopes.

In order to expand the arsenal of small molecule inhibitors for PSMA, we have analyzed the scope of structural modification of urea-based ligands and its influence on PSMA inhibitory activity. Computational studies suggest the glutamate moiety to be an important pharmacophore in the inhibitor scaffold and any structural modification can result in a considerable loss of binding in the cavity of PSMA. Envisaging PSMA's bimetallic zinc protein structure, we have designed glutamate-thiourea-heterodimers which will increase binding of inhibitor in PSMA cavity due to superior electron donating ability, polarizability and larger atomic size of the sulphur atom in comparison to the oxygen atom present in glutamic acid-based urea scaffold. *In silico* studies also predict that the introduction of certain branched-chain amino acids and aryl group in the inhibitor scaffold can increase the hydrophobic interaction in the protein cavity significantly.

In this report, ten *t*-butylcarboxyl protected thiourea ligands have been synthesized by a novel one-pot synthetic methodology using bis(benzotriazolyl)methanethione as a thiocarbonyl transfer reagent. As the predicted inhibitory activity of glutamate acid-based thiourea moiety was found to be highest for PSMA protein, the conceived ligand structure was further analyzed for improved binding interactions in the PSMA cavity via computational docking study. To evaluate the binding affinity of the synthesized glutamic acid-based thiourea inhibitors experimentally, one of the high-affinity ligands was radiolabelled by attaching a ^{99m}Tc-chelating moiety via a peptidic spacer. *In vitro* binding affinity experiments have been performed on cell lines expressing PSMA (LNCaP and 22RV1) protein as well as with standard PSMA inhibitor, 2-PMPA, (competition experiment), to prove the specificity of the newly designed PSMA targeted radiotracer. This report details *in silico* design, synthesis,

development and biological evaluation of a new class of high affinity PSMA targeted radiotracers for prostate cancer detection. We have successfully established a novel class of small molecule inhibitors with high affinity to PSMA protein for sensitive and accurate radioimaging of PCa in its early stage.

4.2 Results

PSMA receptors on prostate cancer cells are known to play an important role in the central nervous system by hydrolyzing a neurotransmitter, NAAG (N-acetylaspartylglutamate) into N-acetylaspartic acid and glutamic acid. Therefore, the protein is also known as NAALADase or glutamate carboxypeptidase II (GCPII). The high sequence homology[24] of PSMA with GCPII encourages designing of new small molecule inhibitors using GCPII as a template.

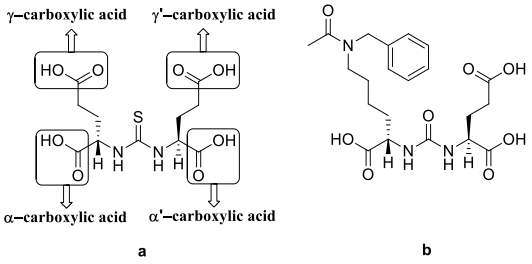

Figure 4.1 Structure of (a) glutamic acid based thiourea inhibitor, (b) co-crystallized ligand JB7 (PDB 4NGM)

The designed small molecule inhibitors could inhibit the enzymatic action of PSMA. With the proposed concept, new thiourea based PSMA inhibitors were designed by keeping the glutamic acid moiety intact to target "glutarate sensor"[25] portion of the PSMA protein (Figure 4.1). In our earlier work,[21] three-dimensional quantitative structure-activity relationships (3-D QSAR) has been developed for GCPII inhibitors using CoMFA module of SYBYL X 2.1.1.

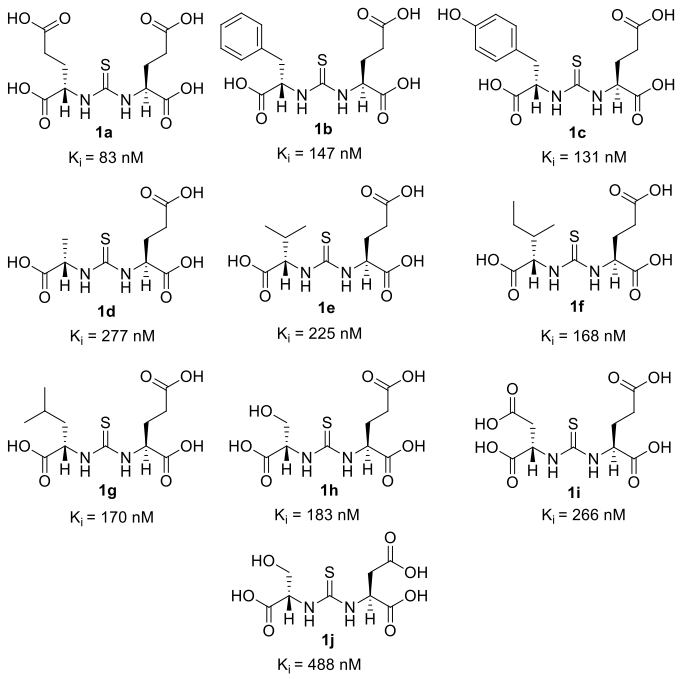

Figure 4.2 Structures of newly designed thiourea based inhibitors **1a**–**j** with predicted PSMA inhibitory activity (K_i in nM) by QSAR model

The same model was used for prediction of PSMA inhibitory activity of newly designed thiourea ligands. The structure of designed ligands **1a**–**j** along with the predicted PSMA inhibitory activity is mentioned in figure 4.2.

4.2.1 Molecular docking study of thiourea derivatives 1a–j

The interactions of newly designed inhibitors at PSMA active site were evaluated through molecular docking study. Inhibitors with best-predicted activity were selected and analyzed using the Surflex docking module of SYBYL software. For docking study, PSMA protein was retrieved from protein data bank (PDB 4NGM). Figure 4.3 represents the post-docking superimposition of structures of all the designed inhibitors at the PSMA active cavity. Docking pose of designed inhibitors depict that the thiourea moieties of all the inhibitors are oriented toward zinc atoms present at the PSMA active site which was similar to the orientation of co-crystallised

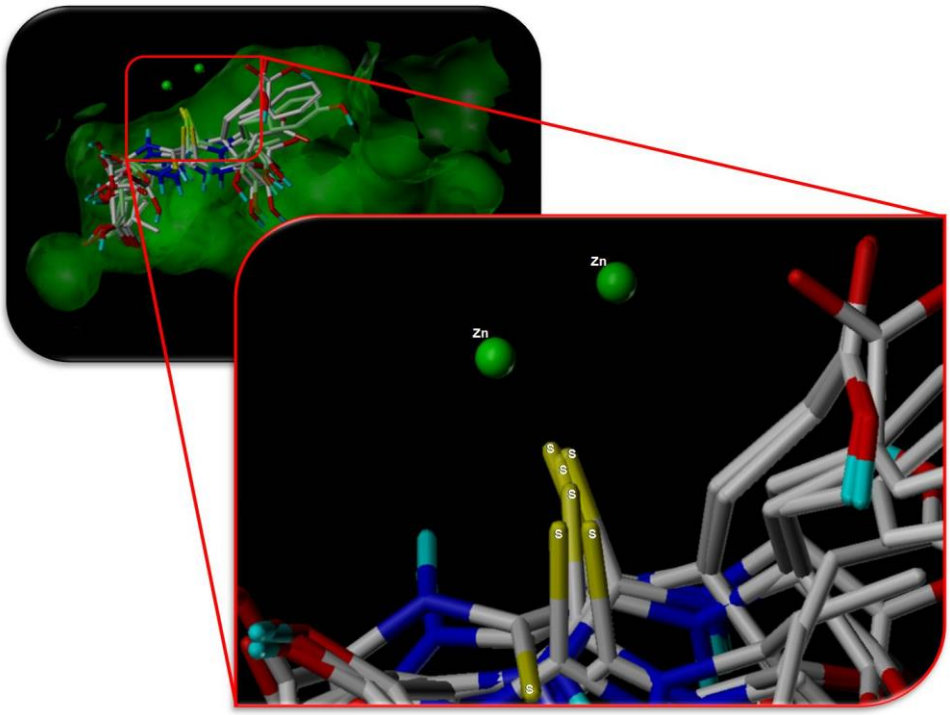

Figure 4.3 Superimposed dock poses of thiourea based derivatives (**1a-j**) at PSMA active cavity with sulphur (yellow colour) atom of the inhibitors oriented toward bimetallic zinc atoms (green spheres) of PSMA enzyme

urea-based inhibitor, JB7. In the molecular docking study, inhibitors are evaluated based on the number of H-bonding and lipophilic interactions with the protein and are ranked with a score. Table 4.1 provides the total score for all the designed thiourea inhibitors. From the total score, it was found out that the glutamic acid based thiourea, **1a**, has been ranked first amongst all the other derivatives **1b**–**j**. Therefore, **1a** was selected to compare the H-bonding interactions with a standard inhibitor, JB7, at the PSMA active cavity. Table 4.2 compares the H-bonding interactions of **1a** and JB7 with the active site amino acid residues of PSMA protein. Figure 4 shows the superimposed orientation of **1a** with co-crystallised JB7. Figure 5a and 5b represent the H-bond interactions of **1a** and JB7 with PSMA active site amino acid residues, respectively.

Table 4.1 Molecular docking score of thiourea based inhibitors

S. No.	Ligand	Total Score
1	**1a**	**10.627**
2	**1b**	10.222
3	**1c**	10.303
4	**1d**	8.4067
5	**1e**	8.682
6	**1f**	8.8746
7	**1g**	9.076
8	**1h**	8.7164
9	**1i**	8.849
10	**1j**	8.0798

Table 4.2 Comparison of amino acid residues of PSMA protein forming hydrogen bonding interactions with JB7 and glutamic acid based thiourea derivative, **1a**

Amino Acid Residues of PSMA	H-Bonding Interactions with JB7	H-Bonding Interactions with 1a
Lys699	Y	Y
Asn257	Y	Y
Arg536	Y	N
Arg534	Y	Y
Asn519	Y	Y
Gly518	Y	Y
Arg210	Y	Y

Glu425	N	Y
Tyr552	Y	N
Tyr700	Y	Y
Ser517	N	Y

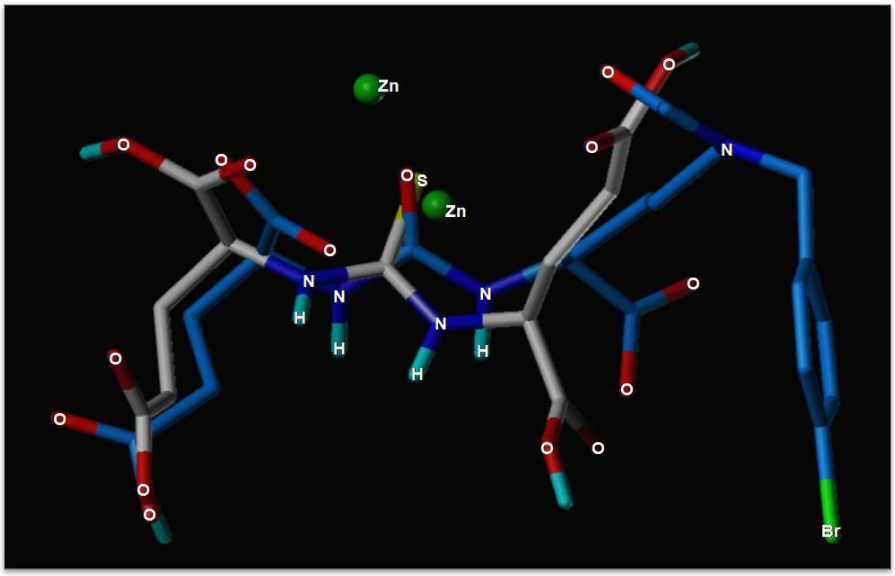

Figure 4.4 Superimposed structure of JB7 (blue) and glutamic acid based thiourea derivative **1a** (gray)

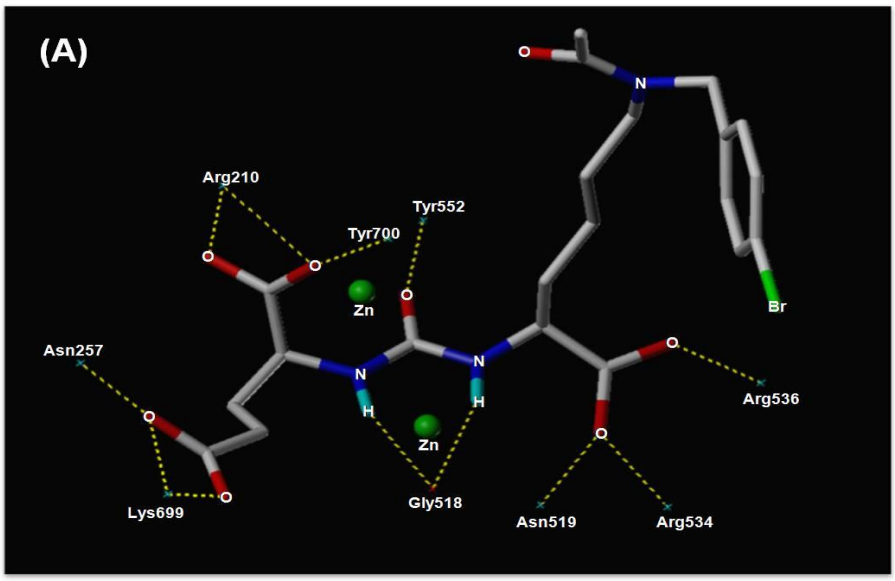

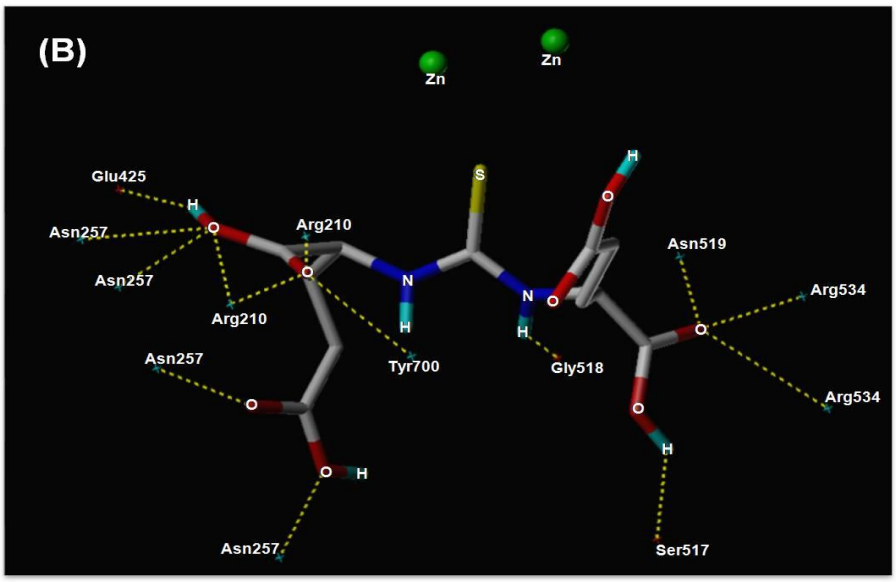

Figure 4.5 (A) Hydrogen bonding interactions of co-crystallized ligand (JB7) and (B) glutamic acid based thiourea derivative, **1a**, at the active site of PSMA

4.2.2 Synthesis

Based on the QSAR model and docking studies, a library of ten *tert*-butylcarboxy protected thiourea derivatives has been synthesized with various hydrophobic and lipophilic substituents. Initially, we have attempted to synthesis the tris(*tert*-butylcarboxy)carboxylic acid precursor **6a** as outlined in scheme 4.1. Briefly, bis(*tert*-butyl)-L-glutamic acid hydrochloride **2** was treated with thiophosgene via nucleophilic substitution reaction at low temperature in the presence of diisopropylethylamine as base to form isothiocyanate intermediate **3** which was *in situ* reacted with γ-benzyl-α-*tert*-butyl-L-glutamic acid hydrochloride **4** to give the corresponding tris(*tert*-butylcarboxy)benzylester thiourea **5a** in high yield (80%) as yellowish liquid (Scheme 4.1).

Scheme 4.1 Synthesis of tris(*tert*-butylcarboxy)benzylester of thiourea derivative **5a**

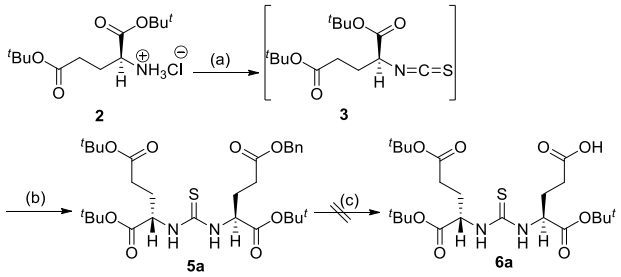

Reagents and conditions: (a) $CSCl_2$, DIPEA/THF, −78°C, 2 h; (b) L-Glu(OBn)-O^{t}Bu (**4**)**,** DIPEA/THF, −78 °C to rt, 12 h, 80%; (c) H_2 (1-atm)/Pd-C, CH_2Cl_2, 24 h

Computational analysis demonstrates[21] glutamic acid based thiourea derivative bind strongly in the binding pocket of PSMA without the involvement of one of its γ-carboxylic acid (Figure 4.1). The free γ-carboxylic acid can be used as a handle to attach the thiourea targeting ligand to an imaging agent or chelating moiety via a peptidic spacer in the solid phase peptide synthesis. Our attempts to deprotect **5a** to tris(*tert*-butylcarboxy)carboxylic acid precursor **6a** was unsuccessful (Table 4.3)

Table 4.3 Various reaction conditions for debenzylation of **5a** to **6a**

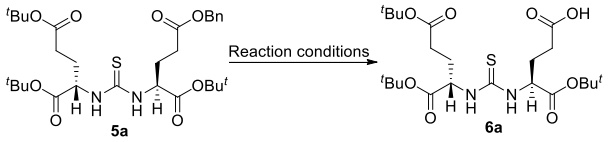

Entry	Reaction condition	Solvent	Result
1	H_2(1-atm)/Pd-C (30 mol%), 24 h	CH_2Cl_2	No reaction
2	H_2(1-atm)/Pd-C (30 mol%), 24 h	MeOH	No reaction
3	H_2(1-atm)/Pd-C (1.0 equiv.), 24 h	MeOH	No reaction
4	$HCOONH_4$/Pd-C (1.0 equiv.), 24 h	MeOH	No reaction

5	H_2(1-atm)/Pd-C (3.0 equiv.), 24 h	MeOH	No reaction
6	H_2/Pd$(OH)_2$/C (3.0 equiv.), 3 d	MeOH	Little conversion
7	$Ba(OH)_2.H_2O$ (1.0 equiv.), 3 h, rt	EtOH:H_2O	Decomposition
8	LiOH, 0 ^oC – rt / 20 h	THF:H_2O	No product
9	LiDBB/THF/-78 ^oC–0 ^oC/2 h	THF	Multiple spots

using various palladium catalyzed reactions in the presence of a hydrogen source (Entries 1–6, Table 4.3). Selective hydrolysis of benzylester in **5a** using either LiOH or $Ba(OH)_2$ resulted only in the decomposition of **5a** (Entries 7–8, Table 4.3). Finally, our effort using lithium 4,4′-di-*tert*-butylbiphenylide (LiDBB, Freeman's reagent) mediated free radical elimination of benzylester at lower temperature was also unsuccessful (Entry 9, Table 4.3). The failure of palladium-catalyzed debenzylation (Entries 1–6, Table 4.3) is attributed due to the poisoning of the metal catalyst by the sulfur atom present in **5a**. Therefore, we opined to introduce methyl carboxyester group at γ-position using γ-methyl-α-*tert*-butyl-L-glutamate **8** as a component during the preparation of thiourea ligand (Scheme 4.2). Thus, we have prepared **8** by the reaction of γ-methyl-L-glutamic acid **7** with *tert*-butylacetate in the presence of perchloric acid as shown in scheme 4.2. The isothiocyanate intermediate **3** generated from **2** was *in situ* reacted with **7** to give the corresponding tris(*tert*-butylcarboxy)methylester thiourea **9** in 80% yield (Scheme 4.2). The γ-methylester in **9** was selectively hydrolyzed using trimethyltin hydroxide[23] in 1,2-dichloroethane at 80 $^{\circ}C$ to generate the required ligand precursor tris(*tert*-butylcarboxy)carboxylic acid **6a** in moderate yield.

Synthesis of thiourea derivatives **5a** or **9** involves direct usage of thiophosgene which is toxic, pungent, moisture sensitive and difficult to handle. In addition, inert condition and maintenance of sub-zero temperature are essential to perform the required transformations.

Scheme 4.2 Synthesis of tris(*tert*-butylcarboxy)methylester thiourea derivative **9** and its hydrolysis to **6a**

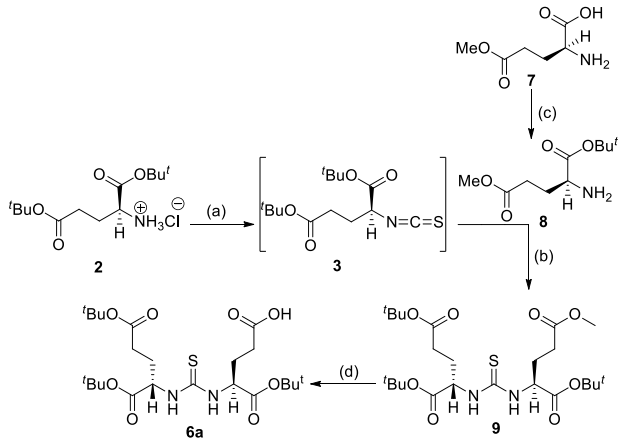

Reagents and conditions: (a) $CSCl_2$, DIPEA/THF, −78 °C, 2 h; (b) L-Glu(OMe)-O^{t}Bu **(8)**, DIPEA/THF, −78 °C to rt, 12 h, 80%; (c) ^{t}BuOAc, 70% $HClO_4$, 24 h, rt; (d) Me_3SnOH, 1,2-dichloroethane, 80 °C, 8 h, 52%.

The severe drawbacks of thiophosgene can be circumvented by converting thiophosgene to a more stable and moisture insensitive derivative, bis(benzotriazolyl)methanethione **12**, by the reaction of thiophosgene with two moles of benzotriazole (Scheme 4.3) following a literature procedure.[20] Bis(benzotriazolyl)methanethione **12** is a yellow crystalline solid, easy to handle, not sensitive to moisture and displacement of benzotriazole groups can be achieved by a nucleophilic attack at room temperature to smoothly transfer the thiocarbonyl group during thiourea preparation.

Scheme 4.3 Synthesis of stable, moisture insensitive, bis(benzotriazolyl)methanethione **12** as a thiocarbonyl transfer reagent

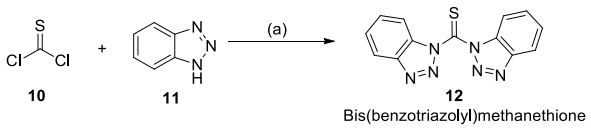

Reagents and conditions: (a) DCM, 0 °C–rt, 3 h

With these lucrative features of **12**, a novel one-pot synthetic strategy has been developed to synthesize tris(*tert*-butylcarboxyester)thiourea derivatives **9**, **16a**–**j** (Scheme 4.5). The reaction conditions are benign, and the amino group of *tert*-butylcarboxy amino esters **13** reacts with **12** to give the respective monobenzotriazolylcarbothioamide derivatives **14** within 2 h at room temperature.

Scheme 4.4 Preparation of *tert*-butylcarboxyaminoesters **15b**, **15d**–**i**

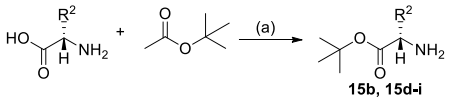

R^2 = -CH_2Ph
= -CH_3
= -$CH(CH_3)_2$
= -$CH(CH_3)$-CH_2-CH_3
= -CH_2-$CH(CH_3)_2$
= -CH_2OH
= -CH_2COOH

15b, R^2 = -CH_2Ph
15d, R^2 = -CH_3
15e, R^2 = -$CH(CH_3)_2$
15f, R^2 = -$CH(CH_3)$-CH_2-CH_3
15g, R^2 = -CH_2-$CH(CH_3)_2$
15h, R^2 = -CH_2OBu^t
15i, R^2 = -CH_2COOBu^t

Reagents and conditions: (a) (i) 70% $HClO_4$, rt, 12–24 h; (ii) $NaHCO_3$, pH>7.

Scheme 4.5 Synthesis of tris(*tert*-butylcarboxy) protected thiourea inhibitors **9**, **16a**–**j**

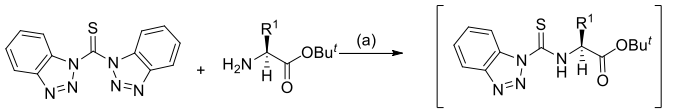

9, R^1 = -$CH_2CH_2COOBu^t$, R^2 = -CH_2CH_2COOMe, 80%
16a, R^1 = -$CH_2CH_2COOBu^t$, R^2 = -$CH_2CH_2COOBu^t$, 75%
16b, R^1 = -$CH_2CH_2COOBu^t$, R^2 = -$CH_2C_6H_5$, 78%
16c, R^1 = -$CH_2CH_2COOBu^t$, R^2 = *p*-OH-$C_6H_4CH_2$-, 75%
16d, R^1 = -$CH_2CH_2COOBu^t$, R^2 = -CH_3, 78%
16e, R^1 = -$CH_2CH_2COOBu^t$, R^2 = -$CH(CH_3)_2$, 80%
16f, R^1 = -$CH_2CH_2COOBu^t$, R^2 = -$CH(CH_3)CH_2CH_3$, 79%
16g, R^1 = -$CH_2CH_2COOBu^t$, R^2 = -$CH_2CH(CH_3)_2$, 75%
16h, R^1 = -$CH_2CH_2COOBu^t$, R^2 = -CH_2OBu^t, 85%
16i, R^1 = -$CH_2CH_2COOBu^t$, R^2 = -CH_2COOBu^t, 87%
16j, R^1 = -CH_2OBu^t, R^2 = -CH_2COOBu^t, 70%

Reagents and conditions: (a) CH_2Cl_2, 2 h, rt; (b) DIPEA, CH_2Cl_2, 12 h.

Without further isolation of the intermediate **14**, the next *tert*-butylcarboxy amino esters **15a**–**j**, preparation of which is described in scheme 4.4, was

added to the reaction mixture along with one equivalent of a base to increase the nucleophilicity of amine functionality in **15a**–**j** for the displacement of benzotriazole leaving group in **14**. Using this newly developed protocol, we have successfully synthesized a library of tris(*tert*-butylcarboxy) protected thiourea inhibitors **9**, **16a**–**j** in high yields and the compounds were thoroughly characterized using various spectroscopic techniques (Scheme 4.5). Since structure activity relationships (SAR) study show that glutamic acid based thiourea inhibitor **1a** have the highest binding affinity, tris(*tert*-butylcarboxy)carboxylic acid precursor **6a** was selected for further conjugation to the chelating moiety via a peptide spacer during solid phase peptide synthesis of PSMA targeted bioconjugate **18**.

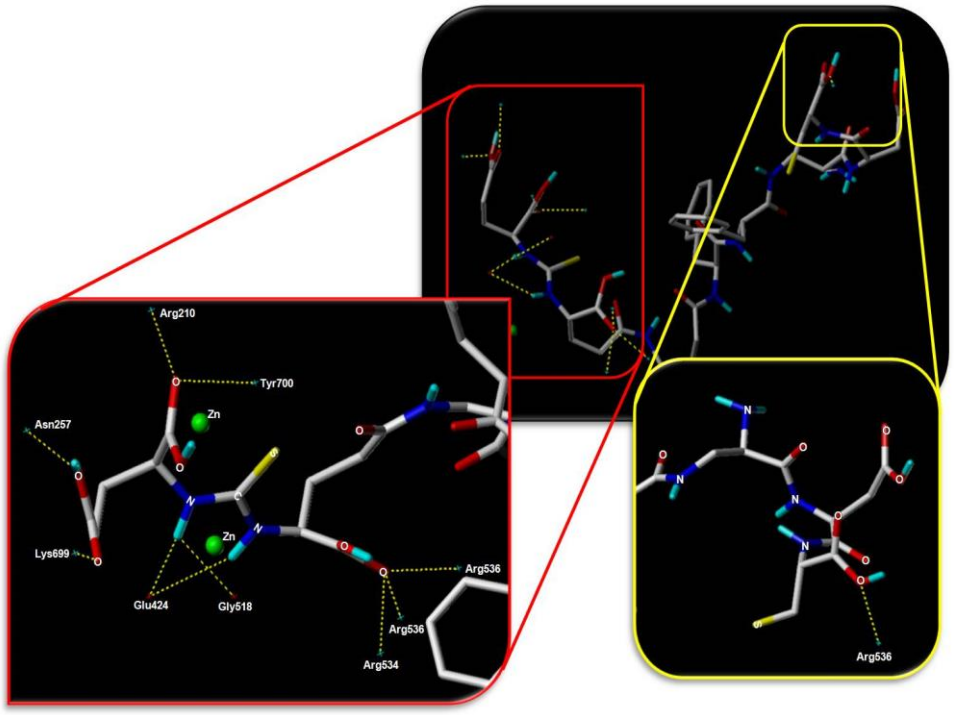

Figure 4.6 Hydrogen bonding interactions of PSMA targeted bioconjugate **18** at the active site of PSMA

The chelating moiety is necessary to complex ^{99m}Tc radioisotope for drug delivery technique and to identity PSMA^{+} cancers at an early stage.

Moreover, it is crucial to analyze the influence of peptidic spacer of **18** on PSMA binding affinity. A detailed molecular docking study has been performed to investigate the conformational fit of **18** through 20 Å tunnel of the PSMA protein.[8] The docking study of **18** shows that after conjugation with chelating moiety via a hydrophobic peptidic spacer, the thiourea targeting ligand interacts at the binding pocket of the PSMA protein similar to that of co-crystallised ligand, JB7 (Figure 5.6).

4.2.3 Design and synthesis of ^{99m}Tc-thiourea (19) based radiopharmaceutical

^{99m}Tc is a metastable nuclear isotope of technetium-99 and to chelate ^{99m}Tc with high affinity and stability a chelating core design has been adapted using a peptide sequence[26] of Dap-Asp-Cys. The peptide spacer to link thiourea targeting ligand and the chelating core has been constituted to prevent loss of binding affinity of small molecule inhibitor at the PSMA active cavity. Starting from commercially available cysteine capped chlorotrityl resin, H-L-Cys(Trt)-2-ClTrt (**17**), we begin the synthesis of bioconjugate **18** as shown in Scheme 4.6. Using standard Fmoc solid phase peptide synthesis methodology, amino acids such as Fmoc-Asp(O^{t}Bu)-OH, Boc-Dap(Fmoc)-OH, two Fmoc-Phe-OH residues, 8-aminocaprylic acid and tris(*tert*-butylcarboxy)carboxylic acid precursor **6a** were coupled in sequence to cysteine amino acid attached to chlorotrityl resin **17**. Protecting groups such as Boc, *t*-butyl, and Trt present in diaminopropionic acid, aspartic acid and cysteine thiol aminoacids, respectively, were cleaved using a cocktail of trifluoroacetic acid, triisopropyl silane, ethanedithiol in water to provide PSMA targeted bioconjugate **18** in moderate yield and purity (Scheme 4.6). The bioconjugate **18** was purified using preparative RP-HPLC and characterized by analytical RP-HPLC and HRMS. Due to the short half-life of ^{99m}Tc, a formulation kit was required which would enable rapid and

efficient labeling of thiourea conjugate immediately, before cell binding assay.

Scheme 4.6 Synthesis of ^{99m}Tc-thiourea **19**

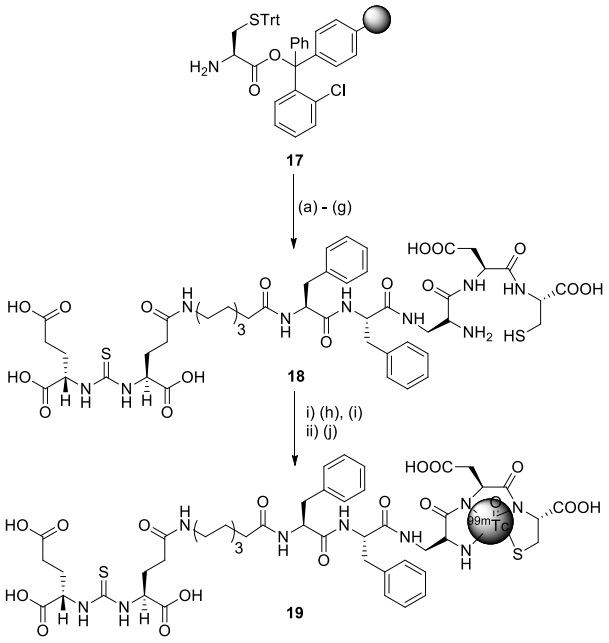

Reagents and conditions: (a) Fmoc-Asp(O^{t}Bu)-OH, PyBOP, DIPEA, DMF, rt, 6 h; (b) (i) 20% Piperidine/DMF, rt, 30 min; (ii) Fmoc-diaminopropionic acid, PyBOP, DIPEA, DMF, rt, 6 h; (c) (i) 20% Piperidine/DMF, rt, 30 min; (ii) Fmoc-Phe-OH, PyBOP, DIPEA, DMF, rt, 6 h; (d) (i) 20% Piperidine/DMF, rt, 30 min; (ii) Fmoc-Phe-OH, PyBOP, DIPEA, DMF, rt, 6 h; (e) (i) 20% Piperidine/DMF, rt, 30 min; (ii) Fmoc-8-aminooctanoic acid, PyBOP, DIPEA, DMF, rt, 6 h; (f) (i) 20% Piperidine/DMF, rt, 30 min; (ii) **6a**, PyBOP, DIPEA, DMF, rt, 6 h; (g) TFA:EDT:TIPS:H_2O (92.5:2.5:2.5:2.5), (1 × 5 mL, 30 min; 2 × 5 mL, 15 min each); (h) $SnCl_2$, sodium glucoheptonate/H_2O; (i) aq. $NaHCO_3$/pH=6.8; (j) sodium pertechnetate/saline, 100 °C, 18 min.

The formulation kit was prepared using a lyophilized mixture of **18**, stannous chloride to reduce ^{99m}Tc-pertechnetate, and sodium α-D-glucoheptonate to stabilize the Sn (II) and ^{99m}Tc (IV) intermediates. After

addition of $Na^{99m}TcO_4$, complexation of the radiotracer was achieved by heating the solution for 18 min to boiling and then cooling to room temperature. The radiopharmaceutical **19** was obtained in high yield (>98%) and high specific radioactivity (purity >98%).

During the cleavage of desired peptide bioconjugate **18** from chlorotrityl resin, we have observed the formation of an undesirable conjugate **20** which was purified through preparative RP-HPLC and characterized by mass spectrometry. The structure of the undesirable conjugate **20** was assigned to be either **20a** or **20b** as depicted in figure 7 where α or α'-carboxylic acid functionality of the thiourea ligand undergoes intramolecular cyclization with the thiocarbonyl sulfur atom to form a thiazolone derivative. A cold formulation kit was prepared using a lyophilized mixture of conjugate **20**, stannous chloride and sodium α-D-glucoheptonate for performing cell binding assay after complexation with $Na^{99m}TcO_4$.

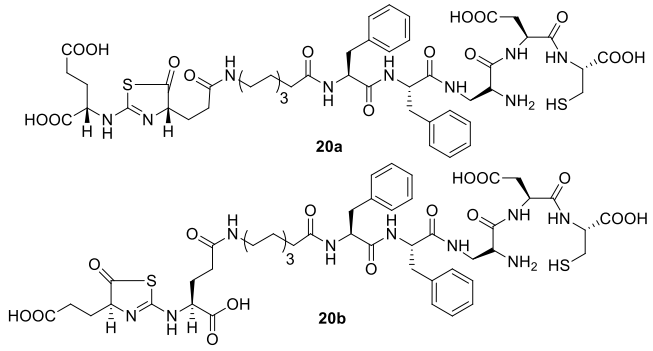

Figure 4.7 Probable structure of undesirable bioconjugate **20** during the cleavage of **18** from the 2-chlorotrityl resin.

4.2.4 Binding affinity studies of radiotracer ^{99m}Tc-thiourea radiotracer (19) and ^{99m}Tc-thiazolone tracer (21) in PSMA$^+$ LNCaP and 22RV1 cells

Binding affinity study of the two radiotracers, ^{99m}Tc-thiourea (**19**) (Figure 4.8), and ^{99m}Tc-thiazolone (**21**) derived from **20a** or **20b** (Figures 4.9 and

4.10) help evaluate and analyze the interactions of the radiotracers with PSMA protein expressed on LNCaP and 22RV1 cell lines. The dissociation constant (K_D) values calculated experimentally for ^{99m}Tc-thiourea radiotracer in LNCaP (K_D = 114 nM) as well as 22RV1 (K_D = 162 nM) cell lines are shown in Figure 4.8.

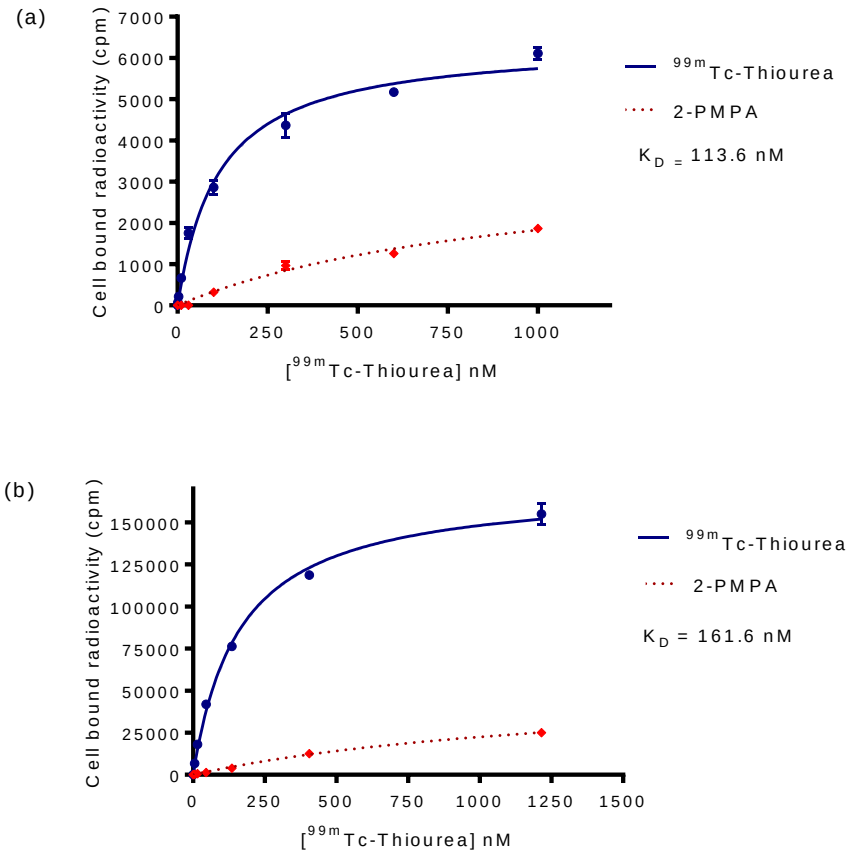

Figure 4.8 Binding affinity study of ^{99m}Tc-thiourea radiotracer (**19**) in (a) $PSMA^+$ LNCaP cells and (b) $PSMA^+$ 22RV1 cells (blue) along with competition study (red) using 100-fold excess of 2-PMPA (n = 3, error bars for triplicates)

The competition studies performed using 100-fold excess of a known inhibitor (2-PMPA) of NAALADase show that internalization of the radiotracer is via PSMA receptor-mediated endocytosis and not through non-specific uptake (Figure 4.8). Cell binding analysis with ^{99m}Tc-

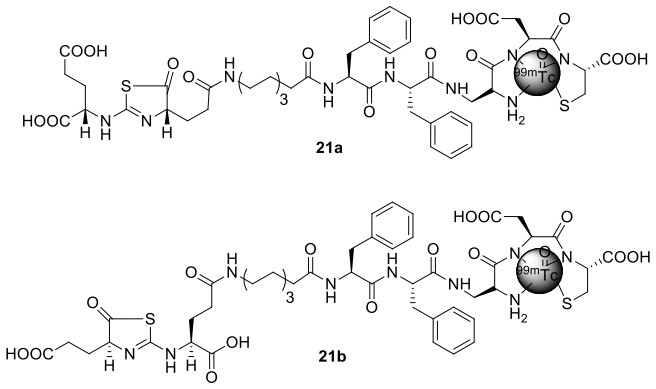

Figure 4.9 Probable structure of ^{99m}Tc-thiazolone radiotracer, **21**

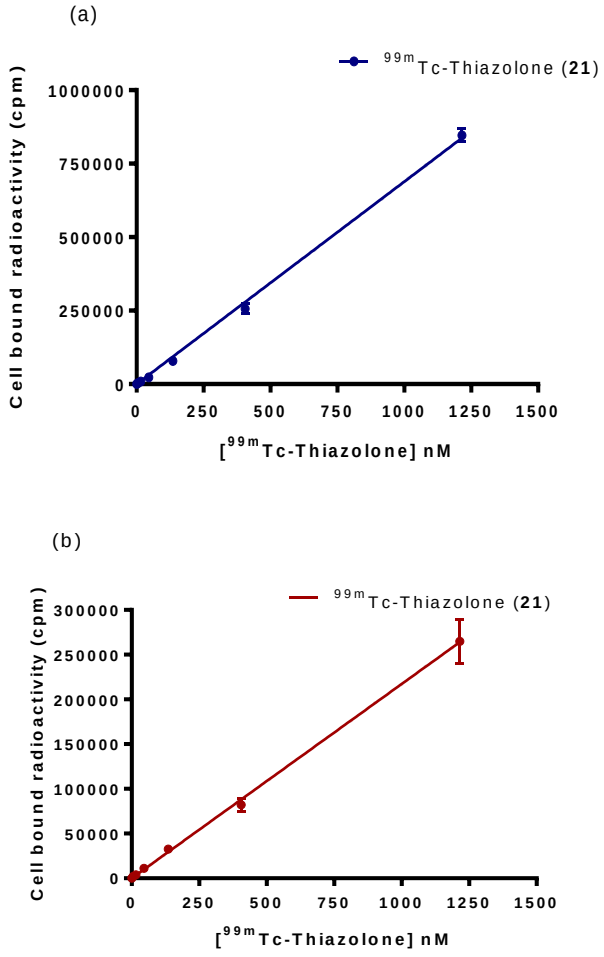

Figure 4.10 Binding affinity study of ^{99m}Tc-thiazolone radiotracer **21** in (a) PSMA$^+$ LNCaP cells (blue) and (b) PSMA$^+$ 22RV1 cells (red) (n = 3, error bars for triplicates).

thiazolone (**21**) in $PSMA^+$ cell lines such as LNCaP and 22RV1 doesn't show any hyperbola curve but a linear graph with increasing concentrations of the radiotracer (Figure 4.10).

4.3 Discussion

4.3.1 *In silico* study

The PSMA protein biomarker is an attractive target for developing a sensitive imaging probe for the detection of PCa. Urea-based heterodimer inhibitors have expanded the arsenal with high affinity, specific small molecule ligands for targeting PSMA. A library of thiourea inhibitors or ligands is designed in this report to explore further the possibility of designing new high-affinity small molecules for PSMA. The hypothesis was first verified by performing exhaustive computational analysis. Based on previously published QSAR model (CoMFA) from our research group, predicted activity (K_i) of the ten thiourea derivatives (**1a**–**j**) were calculated. From the predicted K_i values, the effect of different substituents on the inhibitory activity of the ligand is rationalized. The serine-aspartic acid based thiourea derivative (**1j**) is found to be almost inactive with a K_i value of greater than 400 nM. This is due to the shortening of carbon chain length in the pentanedioic acid moiety resulting in loss of H-bonding interactions. The absence of hydrophobic interactions in the S1 pocket rendered alanine (**1d**), valine (**1e**) and aspartic acid (**1i**) thiourea derivatives inferior in comparison to phenylalanine (**1b**) and tyrosine (**1c**) based thiourea derivatives.

Presence of branched alkyl group in the side chain of isoleucine (**1f**) and leucine (**1g**) thiourea derivatives and a hydroxyl group in serine thiourea analogue (**1h**) allow them to form few hydrophobic interactions in the S1 binding pocket of PSMA. By virtue of these interactions, the derivatives, **1f–h**, are found to have predicted inhibitory activity in the range of 168–183 nM concentration. The aromatic substituent in the side chain of

phenylalanine (**1b**) and tyrosine (**1c**) thiourea derivatives enable these analogues to form pi-pi (π-π) stacking interactions in the hydrophobic sub-pocket and hence these derivatives are superior to the alkyl substituted analogue. Despite this, the glutamic acid based thiourea (**1a**) is predicted to have the best inhibitory activity. This could be explained as per our previously published QSAR study which suggests that the presence of the γ' and γ-carboxylic moieties favour better interactions with the PSMA cavity. This is evident from the fact that the total numbers of hydrogen bonding interactions present in JB7 and **1a** with the PSMA protein are similar (Table 4.2).

Next, molecular docking study was performed, by considering PSMA protein (PDB 4NGM) as a receptor and the designed thiourea derivatives (**1a**–**j**) as a ligand, to validate the activity predicted by QSAR model. Amongst all the thiourea derivatives, docking score of glutamic acid based thiourea ligand **1a** is found to be the highest followed by **1c** and **1b** (Table 4.1). The least molecular docking total score was calculated for **1j**, **1d,** and **1e** derivatives. The docking results are also in consistency with the predicted K_i values from the QSAR model. Figure 4.3 depicts the docking pose of newly designed thiourea derivatives (**1a**–**j**) at the PSMA active cavity. It is very interesting to note that the sulfur atoms of thiocarbonyl moiety of **1a**–**j** are oriented towards the zinc metal atoms of PSMA protein. As zinc plays a very important role in PSMA catalytic activity, binding of any ligand at the vicinity of zinc leads to inhibition of protein activity. This result validates our hypothesis which suggests that the PSMA inhibitory activity of a molecule would be similar after insertion of thiocarbonyl moiety in the ligand architecture. Further, H-bonding interactions of **1a** were analyzed and compared with co-crystallised JB7 to understand the PSMA binding pattern of thiourea derivatives. The superimposed pose of **1a** with co-crystallised JB7 shown in figure 4.4 indicates perfect alignment of **1a**. The number of amino acid interactions

for JB7 (co-crystallized ligand) and **1a**, provided in table 4.2 and figure 4.5, post-docking show JB7 interacts with nine amino acid residues of PSMA through H-bond interactions whereas **1a** interacts with only seven amino acid residues. However, **1a** is found to interact with two new amino acid residues of PSMA active cavity (Glu425 and Ser517) which are absent in JB7 ligand thereby equalizing the total number of H-bonding interactions found in JB7.

These H-bonding interactions confirm that sulphur atom in the thiourea moiety is well tolerated in the PSMA binding pocket. Further, it can infer that the sulphur atom can interact better with the zinc atoms of PSMA through coordinate bonds because of its larger size and more polarizability compared to an oxygen atom. Therefore, in our study, thiourea based ligands have emerged as another class of potent PSMA inhibitors and to experimentally validate our theoretical concepts, thiourea derivatives have been synthesized and evaluated for targeted drug delivery techniques to detect PCa selectively.

4.3.2 Chemical synthesis of tris(*tert*-butylcarboxy) protected thiourea precursors **9**, **16a**–**j**

Conventional protocol for the synthesis of thiourea derivatives **16a**–**j** begins with the reaction of thiophosgene and the corresponding α-aminoesters. This methodology suffers from several drawbacks like toxicity, strong odour, moisture sensitivity of thiophosgene in addition to the requirement of inert and controlled conditions to perform the desired transformations. The synthetic strategy developed in this report employs bis(benzotriazolyl)methanethione, a thiocarbonyl transfer agent[20] synthesized from thiophosgene and benzotriazole. Bis(benzotriazolyl)methanethione is crystalline, stable, resistant to moisture and easy to handle reagent without the requirement of any controlled reaction conditions. Moreover, sequential replacement of

benzotriazole groups can be easily achieved by nucleophilic substitution with α-aminoesters at room temperature to prepare unsymmetrical thiourea inhibitors in excellent yield. Using this reagent, we have developed a novel, one-pot synthetic strategy to synthesize a library of unsymmetrical tris(*tert*-butylcarboxy) protected thiourea derivatives **9**, **16a**–**j** (Scheme 4.5) that are precursors of the required thiourea inhibitors **1a**–**j** for targeting PSMA. Because structure-activity relationships (SAR) study predicted highest inhibitory activity for the glutamic acid based thiourea inhibitor, **1a**, we have selected **6a**, a precursor of **1a**, for further conjugation to a chelating core via a peptidic linker to deliver radioisotopes such as ^{99m}Tc for targeted delivery applications.

Using H-Cys(Trt)-(2-ClTrt) resin **17**, by standard Fmoc-solid phase peptide synthesis methodology, biconjugate **18** was synthesized with a spacer containing hydrophobic phenylalanine amino acid residues and 8-aminocaprylic acid to separate the spacer from PSMA targeting thiourea moiety. The chelating core attached to the further end of the spacer is composed of Dap, Asp, Cys amino acids to efficiently chelate ^{99m}Tc radioisotope. Analysis of the peptidic spacer of **18** on PSMA binding affinity by a detailed molecular docking study shows that for the perfect conformational fit of **18** through 20 Å tunnel of the PSMA protein, two phenyl alanine, and a long chain amino acid residue are indispensable. The docking study of **18** shows that after conjugation with chelation moiety, the thiourea targeting ligand interacts at the binding pocket of the PSMA protein without appreciable loss of binding affinity (Figure 4.6). During the cleavage of ligand attached peptide from trityl resin, the formation of a minor (**18**) and major (**20**) peptide conjugates with a molecular mass of 1076.45 $gmol^{-1}$ and 1058.44 $gmol^{-1}$, respectively, is observed. The major product (**20**) is formed due to favourable acid-catalyzed intra-molecular cyclization of thiocarbonyl sulfur atom with either α or α'-carboxylic acid of the thiourea ligand (Figure 4.7). The side

product bioconjugate (**20**) is proved to be useful, later, during the binding analysis to show the importance of the presence of three carboxylic acid groups in the inhibitor for effective binding with PSMA.

4.3.3 Analysis of binding affinity of ^{99m}Tc-thiourea radiotracer (19) and ^{99m}Tc-thiazolone tracer (21) in PSMA^{+} PCa cell lines

The binding affinity analysis of the two radiolabelled tracers ^{99m}Tc-Thiourea (**19**) and ^{99m}Tc-thiazolone (**21**) show the necessary interactions of thiourea ligand with PSMA protein expressed on LNCaP and 22RV1 cells. The experimental dissociation constants (K_D) for ^{99m}Tc-thiourea radiotracer (**19**) in LNCaP (K_D = 114 nM) as well as 22RV1 (K_D = 162 nM) cell shows that ^{99m}Tc-thiourea tracer exhibit excellent binding affinity in the nanomolar range to PSMA (Figure 4.8).

According to computational analysis, engagement of both hydrophilic and hydrophobic pockets at the PSMA cavity requires three free carboxylic acid groups (α, α' and γ) in the thiourea moiety and lack of any one of them will severely hamper the binding affinity of the ^{99m}Tc-thiazolone radiotracer (Figure 4.9). The *in vitro* binding affinity experiments of ^{99m}Tc-thiazolone radiotracer on PSMA^{+} cell lines such as LNCaP (Figure 4.10a) and 22RV1 (Figure 4.10b) experimentally demonstrate the requirement of all the three carboxylic acid groups for effective binding with PSMA protein. The analysis of the binding affinity graph shows that as the concentration of the ^{99m}Tc-thiazolone radiotracer (**21**) increases, the PSMA receptors are never or not fully occupied resulting in a linear variation of the graph rather than a non-linear hyperbola curve at higher concentrations of the radiotracer. This result unequivocally proves the importance of α, α' and γ-carboxylic acids of the targeting moiety for active binding with the PSMA protein.

Therefore, in this study, we have developed a novel small molecule radio-imaging agent for targeting PCa. Based on the hypothesis that sulfur atom

can avidly form coordinate bonds with Zn atoms present at the active site of PSMA, a PSMA targeting thiourea based structural template of ligands was designed. Molecular docking studies have revealed that glutamic acid based thiourea moiety show similar hydrogen bonding interactions when compared with a co-crystallized ligand. This study opened a new class of PSMA inhibitors with potential applications as a diagnostic tool for prostate cancer.

4.4 Conclusion

In conclusion, a small library of protected glutamate thiourea heterodimers as a precursor of a new class of potent small molecule inhibitors for PSMA has been designed and synthesized. Inhibition constant (K_i) values of all designed inhibitors have been determined by an established QSAR model. Molecular docking studies show that amongst all the designed derivatives, glutamic acid based thiourea moiety shows similar interactions when compared with a co-crystallized ligand, JB7, at the active site of PSMA. Binding affinity and specificity studies were carried out on $PSMA^+$ cell lines with a radiolabeled bioconjugate, ^{99m}Tc-thiourea, to show targeted drug-delivery applications in the detection of PCa. Our study shows that thiourea derivatives can be a new class of small molecule inhibitor which show sub nano-molar binding affinity to PSMA. The thiourea-derived novel radio-imaging agent can be used to identify the early stages of prostate cancer. The promising activity during *in vitro* study of this radio labelled thiourea moiety paves the way for future *in vivo* and clinical developments.

4.5 Experimental section

4.5.1 *In silico* study

The *in silico* studies were performed to analyze the PSMA inhibitory activity of thiourea based ligands. Based on a previously developed QSAR

model from our group,[21] the PSMA inhibitory activity (K_i) was predicted for the newly designed ligands with hydrophobic, hydrophilic substituents and reported as mentioned in figure 4.2. CoMFA module of SYBYL X 2.1.1 was employed for the prediction of PSMA inhibitory activity of the new thiourea inhibitors. The binding mode of the ligands over the PSMA protein was analysed by molecular docking study. Following the same protocol for docking study as published earlier, the protein was prepared. After protein preparation, protomol was generated at the site of co-crystallised ligand and docking was performed. The binding interactions between PSMA protein and the ligand were analyzed by MOLCAD program of SYBYL. This generates an appropriate color coding for the hydrogen bonding, lipophilic field, hydrogen bond donor and acceptor field interactions.

4.5.2 General information:

H-Cys(Trt)-2-ClTrt resin, Fmoc-amino acids, coupling agents, reagents and solvents used in solid phase peptide synthesis (SPPS) as well as in chemical synthesis were purchased from Iris Biotech GmbH, Sigma Aldrich and NovaBiochem, Merck and Spectrochem. Peptide synthesis was performed manually by using peptide vessels (Chemglass) and standard peptide coupling procedures. Bis(benzotriazolyl)methanethione was prepared as reported in the literature.[20] Various dry solvents were prepared by using appropriate drying agents and standard procedures. Moisture sensitive reactions were carried out under nitrogen atmosphere, and the reaction progress was monitored through TLC using Merck 60 F_{254} pre-coated silica gel plates, and the products were visualized under UV light. The products were purified by column chromatography using distilled hexane and ethyl acetate as eluents on 100–200 or 230–400 mesh silica-gel as the stationary phase.

Peptide synthesis was performed manually by using peptide vessels (Chemglass) and standard peptide coupling procedures. ^{1}H and ^{13}C NMR

spectra were recorded using Bruker AV 400 MHz NMR spectrometer with TMS as an internal standard. ^{1}H NMR signals were reported in ppm with reference to residual $CHCl_3$ (7.25 ppm) and multiplicity was reported as s = singlet, d = doublet, t = triplet, q = quartet, m = multiplet or unresolved, and brs = broad singlet, with coupling constants in Hz. $CDCl_3$ was used as the solvent for recording NMR spectra. Mass spectra were recorded on Bruker micro TOF-Q II instrument using positive or negative mode electrospray ionization methods. The peptide bioconjugates were purified using a preparative reverse phase (RP)-HPLC (Waters, xTerra C_{18} 10 μm; 19 × 250 mm) and analyzed by analytical RP-HPLC (Waters, X-Bridge C_{18} 5 μm; 3.0 × 50 mm).

4.5.3 Chemical synthesis

4.5.3.1 Bis(benzotriazolyl)methanethione 12

Yellow coloured micro needle shaped crystals (yield = 90%); R_f = 0.65 (EtOAc : hexane = 1:9); IR (CH_2Cl_2): 3144, 2990 (=C–H), 2958, 2908 (C–H), 1682 (N–H), 1514 (C=C), 1446 (C–H), 1064 (C=S), 740, 651 (=C–H) cm^{-1}; ^{1}H NMR (400 MHz, $CDCl_3$): δ = 8.26 (d, J = 8.28 Hz, 2H), 8.20 (d, J = 8.28 Hz, 2H), 7.72 (t, J = 7.76 Hz, 2H), 7.58 (t, J = 7.8 Hz, 2H); ^{13}C NMR (100 MHz, $CDCl_3$): δ = 169.7, 146.9, 133.1, 130.6, 126.9, 121.1, 113.9; HRMS (ESI) m/z calcd for $C_{13}H_8N_6S$ $[M+K]^+$: 319.0163, found 319.0183.

4.5.3.2 Synthesis of (*S*)-5-benzyl-1-*tert*-butyl-2-(3-((*S*)-1,5-di-*tert*-butoxy-1,5-dioxopentan-2-yl)thioureido)pentanedioate (5a)

Thiophosgene (0.067 mL, 0.869 mmol) was dissolved in dry THF (2 mL) and the solution was stirred at −78 °C in a 25 mL two-neck round-bottom flask under an inert atmosphere. Bis(*tert*-butyl)-L-glutamate.HCl (0.257 g, 0.869 mmol) dissolved in dry THF (3 mL) was added to the thiophosgene solution at −78 °C and diisopropylethylamine (0.45 mL, 2.607 mmol) was

added dropwise to the reaction mixture. The reaction mixture was stirred for 2 h at the same temperature and a solution of L-glutamic-γ-benzyl-α-*tert*-butyl. HCl (0.286 g, 0.869 mmol) in THF (3 mL) and diisopropylethylamine (0.45 mL, 2.607 mmol) was added to the reaction mixture at −78 °C and stirred for another 1 h at the same temperature. The progress of the reaction was monitored through TLC using ethyl ac etate and hexane mixture (1:2) as eluent. The reaction mixture was further stirred overnight at room temperature. After the completion of the reaction, THF was evaporated under reduced pressure, and the residue was dissolved in saturated NH_4Cl solution (10 mL), extracted with ethyl acetate (3 × 10 mL), washed with water (2 × 15 mL) followed by brine solution (15 mL). The organic layer was dried over anhydrous Na_2SO_4, filtered and the solvent was evaporated under reduced pressure to afford the crude product which was purified by column chromatography using 100-200 mesh silica gel using 25% ethyl acetate and hexane as eluent. The product **5a** was obtained as colorless viscous liquid. Colorless gummy liquid (yield = 80%); R_f = 0.4 (EtOAc : hexane = 1:2); IR (CH_2Cl_2): 3366 (N–H), 3123, 2979 (=C–H), 2932 (C–H), 1732 (C=O), 1642 (N–H), 1557(C=C), 1456 (C–H), 1155 (C–O), 1030 (C=S), 750, 699 (=C–H) cm^{-1}; ^1H NMR (400 MHz, $CDCl_3$): δ = 7.60–7.27 (m, 5H), 6.63 (brs, 2H), 5.10 (s, 2H), 5.05–4.50 (m, 2H), 2.60–2.43 (m, 2H), 2.42–2.29 (m, 2H), 2.28–2.17 (m, 1H), 2.16–1.97 (m, 3H), 1.45 (s, 18H), 1.42 (s, 9H); ^{13}C NMR (100 MHz, $CDCl_3$): δ = 182.2, 172.9, 172.6, 170.9, 135.7, 128.5, 128.3, 128.2, 82.7, 81.1, 80.9, 66.6, 56.7, 31.2, 30.2, 28.1, 27.9, 27.7, 27.6; HRMS (ESI) m/z calcd for $C_{30}H_{46}N_2O_8S$ $[M+Na]^+$: 617.2867, found 617.2862.

4.5.3.3 General procedure for the synthesis of *tert*-butylcarboxy amino esters 15b, 15d–i

70% Perchloric acid (0.09 mL, 1.5 mmol) was added dropwise to a solution of *L*-amino acids (1.0 mmol) in *tert*-butyl acetate (6.70 mL, 50 mmol) at 0 °C in a 50 mL round-bottom flask with constant stirring (Scheme 4.4). The reaction mixture[22] was further stirred at room temperature for 12–24 h. The reaction progress was monitored through TLC using ethyl acetate as eluent. After the completion of the reaction, 0.5 N HCl (30 mL) was added to the reaction mixture and stirred for 30 minutes. The aqueous layer was separated through a separating funnel, and the resultant aqueous solution was adjusted to pH>7 by slow addition of solid $NaHCO_3$, extracted with ether (3 × 15 mL) and washed with brine solution (20 mL). The combined ether layer was dried over anhy. Na_2SO_4, filtered and concentrated to obtain the desired *tert*-butylcarboxy amino esters **15b, 15d–i** (Scheme 4.4). The *tert*-butylcarboxy amino esters **15b, 15d–i w**ere used as such for the preparation of thiourea derivatives.

4.5.3.4 (*S*)-Di-*tert*-butyl-2-(3-((S)-1-(*tert*-butoxy)-5-methoxy-1,5-dioxopentan-2-yl)thioureido) pentanedioate (9)

Thiophosgene (0.067 mL, 0.869 mmol) was dissolved in dry THF (2 mL), and the solution was stirred at −78 °C in a 20 mL two-neck round-bottom flask under an inert atmosphere. Bis(*tert*-butyl)-L-glutamate.HCl (0.257 g, 0.869 mmol) dissolved in dry THF (3 mL) was added to the thiophosgene solution at −78 °C and diisopropylethylamine (0.45 mL, 2.607 mmol) was added dropwise to the reaction mixture. The reaction mixture was stirred for 2 h at the same temperature and a solution of γ-methyl-α-*tert*-butyl-L-glutamate (0.188 g, 0.869 mmol) in THF (3 mL) and diisopropylethylamine (0.45 mL, 2.607 mmol) was added to the reaction mixture at –78 °C and stirred for another 1 h at the same temperature. The progress of the reaction was monitored through TLC using ethyl acetate

and hexane mixture (1:2) as eluent. The reaction mixture was further stirred overnight at room temperature. After the completion of the reaction, THF was evaporated under reduced pressure, and the residue was dissolved in saturated NH_4Cl solution (10 mL), extracted with ethyl acetate (3 × 10 mL), washed with water (2 × 15 mL) followed by brine solution (15 mL). The organic layer was dried over anhydrous Na_2SO_4, filtered and the solvent was evaporated under reduced pressure to afford the crude product which was purified by column chromatography using 100-200 mesh silica gel using 25% ethyl acetate and hexane as eluent. The product **9** was obtained as a yellowish viscous liquid. Yellowish viscous liquid (Yield = 80%), R_f = 0.43 (EtOAc : hexane = 1:4); IR (CH_2Cl_2): 3366 (N–H), 3123, 2979 (=C–H), 2932 (C–H), 1732 (C=O), 1642 (N–H), 1557(C=C), 1456 (C–H), 1155 (C–O), 1030 (C=S), 750, 699 (=C–H) cm^{-1}. ^1H NMR (400MHz, $CDCl_3$): δ = 6.71 (brs, 1H), 6.62 (brs, 1H), 5.25–4.30 (m, 2H), 3.67 (s, 3H), 2.54–2.43 (m, 2H), 2.42–2.32 (m, 2H), 2.25–1.99 (m, 4H), 1.46 (s, 9H), 1.45 (s, 9H), 1.43 (s, 9H); ^{13}C NMR (100MHz, $CDCl_3$): δ = 182.3, 173.5, 172.6, 170.9, 82.6, 81.0, 80.9, 56.7, 51.8, 31.3, 29.9, 28.0, 27.9, 27.7, 27.6; HRMS (ESI) m/z calcd for $C_{24}H_{42}N_2O_8S$ $[M+Na]^+$: 541.2554, found 541.2556.

4.5.3.5 General procedure for the preparation of thiourea derivatives 9, 16a–j

Bis(benzotriazolyl)methanethione **12** (1 mmol, 0.280 mg) was dissolved in CH_2Cl_2 (4 mL) in a 50 mL round bottom flask and then appropriate *tert*-butylcarboxy amino esters, **13** (1.0 mmol) was added to the reaction mixture at room temperature. The reaction mixture was stirred at the same temperature for 2 h, the reaction progress was monitored through TLC. After the complete consumption of the bis(benzotriazolyl)methanethione and without the isolation of the intermediate, the next *tert*-butylcarboxy amino ester **15a**–**j** (1.0 mmol) in CH_2Cl_2 (2 mL) and DIPEA (0.17 mL, 1.0 mmol) were added dropwise to the reaction mixture at room temperature.

The reaction mixture was stirred for 12 h and concentrated under reduced pressure. The residue was dissolved in ethyl acetate (30 mL), the organic layer was washed with 5% Na_2CO_3 solution (3 × 15 mL), followed by distilled water (3 × 15 mL). The organic layer was dried over anhydrous Na_2SO_4, filtered and the solvent was evaporated under reduced pressure. The crude thiourea derivatives **16a**–**j** were purified by column chromatography using 100–200 mesh silica gel and ethyl acetate-hexane mixture as eluent.

The thiourea derivatives **16a**–**j** were fully characterized by different spectroscopic techniques (^{1}H, ^{13}C, HRMS, and IR).

4.5.3.5.1 (2*S*,2'*S*)-Tetra-*tert*-butyl-2,2'-(thiocarbonylbis(azanediyl)) dipentanedioate (16a)

White solid (Yield = 75%); R_f = 0.28 (EtOAc : hexane = 1:3); IR (CH_2Cl_2): 3344 (N–H), 2967 (=C–H), 2935, 2922 (C–H), 1738 (C=O), 1540 (C=C), 1457 (C–H), 1148 (C–O), 1030 (C=S), 750 (=C–H) cm^{-1}; ^{1}H NMR (400 MHz, $CDCl_3$): δ = 6.67 (brs, 2H), 5.14–4.60 (m, 2H), 2.44–2.23 (m, 4H), 2.22–2.08 (m, 2H), 2.06–1.95 (m, 2H) 1.46 (s, 18H), 1.42 (s, 18H); ^{13}C NMR (100 MHz, $CDCl_3$): δ = 182.6, 172.6, 172.5, 82.5, 80.9, 56.9, 31.3, 28.1, 28.0, 27.7; HRMS (ESI) m/z calcd for $C_{27}H_{48}N_2O_8S$ $[M+Na]^+$: 583.3024, found 583.3241.

4.5.3.5.2 (*S*)-Di-*tert*-butyl-2-(3-((*S*)-1-(*tert*-butoxy)-1-oxo-3-phenylpropan-2-yl)thioureido)pentanedioate (16b)

White solid (Yield = 78%); R_f = 0.34 (EtOAc : hexane = 1:3); IR (CH_2Cl_2): 3366 (N–H), 3123, 2979 (=C–H), 2932 (C–H), 1732 (C=O), 1642 (N–H), 1557 (C=C), 1456 (C–H), 1155 (C–O), 1030 (C=S), 750, 699 (=C–H) cm^{-1}; ^{1}H NMR (400 MHz, $CDCl_3$): δ = 7.40–7.20 (m, 5H), 6.64–6.31 (m, 2H), 5.44–5.06 (m, 1H), 5.04–4.69 (m, 1H), 3.26 (d, J = 4.8 Hz, 2H), 2.45–2.25 (m, 2H), 2.25–2.06 (m, 1H), 2.05–1.90 (m, 1H), 1.53

(s, 9H), 1.49 (s, 9H), 1.44 (s, 9H); ^{13}C NMR (100MHz, $CDCl_3$): δ = 181.8, 172.4, 171.2, 170.8, 136.3, 129.6, 128.3, 126.9, 82.6, 82.5, 80.8, 58.4, 56.5, 38.1, 31.3, 28.1, 28.0, 27.9, 27.5; HRMS (ESI) m/z calcd for $C_{27}H_{42}N_2O_6S$ $[M+Na]^+$: 545.2656, found 545.2720.

4.5.3.5.3 (*S*)-Di-*tert*-butyl-2-(3-((*S*)-1-(*tert*-butoxy)-3-(4-hydroxyphenyl)-1-oxopropan-2-yl)thioureido)pentanedioate (16c)

Yellowish solid (Yield = 75%); R_f = 0.32 (EtOAc : hexane = 1:2); IR (CH_2Cl_2): 3366 (N–H), 3123, 2979 (=C–H), 2932 (C–H), 1732 (C=O), 1642 (N–H), 1557(C=C), 1456 (C–H), 1155 (C–O), 1030 (C=S), 750, 699 (=C–H) cm^{-1}; ^{1}H NMR (400 MHz, $CDCl_3$): δ = 6.99 (d, *J* = 7.12 Hz, 2H), 6.70 (d, *J* = 7.12 Hz, 2H), 6.60–6.20 (m, 2H), 5.79 (brs, 1H), 5.35–4.60 (m, 2H), 3.24–3.14 (m, 1H), 3.12–2.96 (m, 1H), 2.41–2.18 (m, 2H), 2.12–1.97 (m, 1H), 1.90–1.77 (m, 1H), 1.46 (s, 9H), 1.42 (s, 18H); ^{13}C NMR (100MHz, $CDCl_3$): δ = 181.2, 172.6, 172.5, 171.7, 155.4, 130.6, 127.5, 115.5, 82.3, 82.1, 80.7, 54.7, 52.9, 37.7, 31.6, 28.3, 28.04, 28.0; HRMS (ESI) m/z calcd for $C_{27}H_{42}N_2O_7S$ $[M+Na]^+$: 561.2605, found 561.2604.

4.5.3.5.4 (*S*)-Di-*tert*-butyl-2-(3-((*S*)-1-(*tert*-butoxy)-1-oxopropan-2-yl)thioureido)pentanedioate (16d)

Yellowish liquid (Yield = 85%); R_f = 0.27 (EtOAc : hexane = 1:3); IR (CH_2Cl_2): 3342 (N–H), 3122, 2980 (=C–H), 2933 (C–H), 1732 (C=O), 1537(C=C), 1454 (C–H), 1156 (C–O), 1054 (C=S), 756, 670 (=C–H) cm^{-1}; ^{1}H NMR (400 MHz, $CDCl_3$): δ = 6.54 (d, *J* = 7.04, 2H), 4.96–4.67 (m, 2H), 2.41–2.27 (m, 2H), 2.14–1.96 (m, 2H), 1.46 (s, 9H), 1.46 (s, 9H), 1.44 (s, 3H), 1.43 (s, 9H); ^{13}C NMR (100MHz, $CDCl_3$): δ = 181.7, 172.9, 172.7,172.3, 82.7, 82.1, 80.9, 56.6, 53.4, 31.2, 28.1, 28.9, 27.9, 27.7, 18.5; HRMS (ESI) m/z calcd for $C_{21}H_{38}N_2O_6S$ $[M+Na]^+$: 469.2343, found 469.2530.

4.5.3.5.5 (*S*)-Di-*tert*-butyl-2-(3-((*S*)-1-(*tert*-butoxy)-3-methyl-1-oxobutan-2-yl)thioureido)pentanedioate (16e)

Yellowish liquid (Yield = 82%); R_f = 0.44 (EtOAc : hexane = 1:3); IR (CH_2Cl_2): 3366 (N–H), 3123, 2979 (=C–H), 2932 (C–H), 1732 (C=O), 1642 (N–H), 1557(C=C), 1456 (C–H), 1155 (C–O), 1030 (C=S), 750, 699 (=C–H) cm^{-1}; ^1H NMR (400 MHz, $CDCl_3$): δ = 6.70–6.35 (m, 2H), 5.06–4.48 (m, 2H), 2.44–2.20 (m, 3H), 2.17–1.98 (m, 2H), 1.46 (s, 18H), 1.43 (s, 9H), 1.01–0.94 (m, 6H); ^{13}C NMR (100MHz, $CDCl_3$): δ = 182.7, 172.8, 172.5 (2C*), 82.2, 80.9, 80.8, 62.6, 56.8, 31.6, 31.4, 28.1 (2C*), 28.0 , 27.7, 18.6; HRMS (ESI) m/z calcd for $C_{23}H_{42}N_2O_6S$ [M+Na]+ : 497.2656, found 497.2645.

*Higher intensity peak

4.5.3.5.6 (2*S*)-Di-*tert*-butyl-2-(3-((2*S*)-1-(*tert*-butoxy)-3-methyl-1-oxopentan-2-yl)thioureido)pentanedioate (16f)

Colourless liquid (Yield = 79%); R_f = 0.47 (EtOAc : hexane = 1:3); IR (CH_2Cl_2): 3356 (N–H), 2976 (=C–H), 2930, 2878 (C–H), 1733 (C=O), 1537(C=C), 1457 (C–H), 1156 (C–O), 1032 (C=S), 750 (=C–H) cm^{-1}; ^1H NMR (400 MHz, $CDCl_3$): δ = 6.70–6.45 (d, J = 2H), 5.25–4.30 (brs, 2H), 2.40–2.24 (m, 2H), 2.15–1.96 (m, 3H), 1.87–1.70 (m, 1H), 1.62–1.51 (m, 1H), 1.46 (s, 18H), 1.42 (s, 9H), 0.98–0.88 (m, 6H); ^{13}C NMR (100MHz, $CDCl_3$): δ = 182.1, 172.7, 172.5 (2C*), 82.6, 82.3, 80.9, 61.6, 56.7, 38.2, 31.2, 28.1 (2C*), 27.9, 27.7, 26.1, 15.0, 11.8; HRMS (ESI) m/z calcd for $C_{24}H_{44}N_2O_6S$ $[M+Na]^+$: 511.2812, found 511.2837.

*Higher intensity peak

4.5.3.5.7 (*S*)-Di-*tert*-butyl-2-(3-((*S*)-1-(*tert*-butoxy)-4-methyl-1-oxopentan-2-yl)thioureido)pentanedioate (16g)

Colourless liquid (Yield = 75%); R_f = 0.47 (EtOAc : hexane = 1:3); IR (CH_2Cl_2): 3356 (N–H), 2979 (=C–H), 2932 (C–H), 1730 (C=O), 1535 (C=C), 1456 (C–H), 1155 (C–O), 1030 (C=S), 750, 699 (=C–H) cm^{-1}. ^1H NMR (400 MHz, $CDCl_3$): δ = 6.90–6.30 (m, 2H), 5.04–4.47 (m, 2H), 2.45–2.25 (m, 2H), 2.15–1.95 (m, 2H), 1.75–1.60 (m, 3H), 1.45 (s, 18H), 1.42 (s, 9H), 0.96–0.92 (m, 6H); ^{13}C NMR (100MHz, $CDCl_3$): δ = 182.1, 172.6, 172.3, 171.1, 82.7, 82.1, 80.9, 56.6, 41.4, 31.1, 29.7, 28.1, 28.0, 27.9, 27.8, 24.9, 22.6, 22.5; HRMS (ESI) m/z calcd for $C_{24}H_{44}N_2O_6S$ $[M+Na]^+$: 511.2812, found 511.2818.

4.5.3.5.8 (*S*)-Di-*tert*-butyl-2-(3-((*S*)-1-(*tert*-butoxy)-3-hydroxy-1-oxopropan-2-yl)thioureido)pentanedioate (16h)

Colourless liquid (Yield = 87%), R_f = 0.35 (EtOAc : hexane = 1:3); IR (CH_2Cl_2): 3360 (N–H), 2979 (=C–H), 2933 (C–H), 1744 (C=O), 1539 (C=C), 1457 (C–H), 1148 (C–O), 1052 (C=S), 750, 652 (=C–H) cm^{-1}. ^1H NMR (400 MHz, $CDCl_3$): δ = 6.54 (brs, 2H), 5.20–4.63 (m, 2H), 3.85–3.50 (m, 2H), 2.45–2.35 (m, 1H), 2.34–2.24 (m, 1H), 2.21–2.13 (m, 1H), 2.06–1.94 (m, 1H), 1.46 (s, 18H), 1.43 (s, 9H), 1.15 (s, 9H); ^{13}C NMR (100MHz, $CDCl_3$): δ = 181.5, 172.3 (2C*), 172.2, 82.5, 80.7, 80.6 (2C*), 62.8, 58.4, 56.9, 31.4, 28.1, 28.0 (2C*), 27.9, 27.4; HRMS (ESI) m/z calcd for $C_{25}H_{46}N_2O_7S$ $[M+Na]^+$: 541.2918, found 541.3086.

*Higher intensity peak

4.5.3.5.9 (*S*)-Di-*tert*-butyl-2-(3-((*S*)-1,4-di-*tert*-butoxy-1,4-dioxobutan-2-yl)thioureido)pentanedioate (16i)

Colourless liquid (Yield = 85%); R_f = 0.52 (EtOAc : hexane = 1:3); IR (CH_2Cl_2): 3357 (N–H), 3105, 2979 (=C–H), 2933 (C–H), 1730 (C=O),

1531 (C=C), 1456 (C–H), 1151 (C–O), 1032 (C=S), 753, 699 (=C–H) cm^{-1}. ^1H NMR (400 MHz, $CDCl_3$): δ = 6.75 (d, J = 6.24 Hz, 1H), 6.72–6.55 (m, 1H), 5.25–5.05 (m, 1H), 5.02–4.74 (m, 1H), 2.95–2.84 (m, 2H), 2.40–2.23 (m, 2H), 2.21–2.10 (m, 1H), 2.09–1.90 (m, 1H), 1.46 (s, 9H), 1.44 (s, 9H), 1.42 (s, 18H); ^{13}C NMR (100MHz, $CDCl_3$): δ = 182.4, 172.4, 172.3, 170.8, 170.2, 82.5, 82.4, 81.5, 80.7, 56.9, 54.1, 37.7, 31.3, 28.07, 28.06, 28.0, 27.9, 27.7; HRMS (ESI) m/z calcd for $C_{26}H_{46}N_2O_8S$ $[M+Na]^+$: 569.2867, found 569.2988.

4.5.3.5.10 (*S*)-Di-*tert*-butyl-2-(3-((*S*)-1-(*tert*-butoxy)-3-hydroxy-1-oxopropan-2-yl)thioureido)succinate (16j)

Yellowish gummy liquid (Yield = 70%); R_f = 0.3 (EtOAc : hexane = 1:3); IR (CH_2Cl_2): 3361 (N–H), 3118, 2977 (=C–H), 2930 (C–H), 1736 (C=O), 1642 (N–H), 1538 (C=C), 1458 (C–H), 1157 (C–O), 1052 (C=S), 750 (=C–H) cm^{-1}. ^1H NMR (400 MHz, $CDCl_3$): δ = 6.71 (brs, 1H), 6.51 (brs, 1H), 5.40–4.75 (m, 2H), 3.87–3.63 (m, 2H), 3.00–2.81 (m, 2H), 1.45 (s, 18H), 1.43 (s, 9H), 1.14 (s, 9H); ^{13}C NMR (100MHz, $CDCl_3$): δ = 182.2, 170.8, 170.6, 170.0, 82.4, 82.3, 81.5, 81.4, 62.5, 58.3, 54.1, 37.7, 28.09, 28.06, 28.0, 27.9; HRMS (ESI) m/z calcd for $C_{24}H_{44}N_2O_7S$ $[M+Na]^+$: 527.2761, found 527.2856.

4.5.3.6 Procedure for the preparation of tris(*tert*-butylcarboxy)carboxylic acid precursor 6a by methylester hydrolysis in 9 using trimethyltinhydroxide

9 (100 mg, 0.193 mmol) was dissolved in 1,2-dichloroethane (5 mL) in a 25 mL round-bottom flask and after addition of solid trimethyltin hydroxide (105 mg, 0.579 mmol), the mixture was heated at 80 °C using a reflux condenser. The reaction mixture was stirred at the same temperature for 8 h.[23] After the completion of the reaction, the mixture was concentrated under reduced pressure, and the residue was dissolved in

ethyl acetate (20 mL). The organic layer was washed with aqueous 0.01 N $KHSO_4$ (2 × 10 mL) followed by brine (2 × 10 mL). The organic layer was dried over anhydrous sodium sulphate, filtered and concentrated under reduced pressure to afford the crude product **6a** which was purified through column chromatography using 100–200 mesh silica gel and 75% ethyl acetate-hexane mixture as eluent.

4.5.3.6.1 (*S*)-5-(*Tert*-butoxy)-4-(3-((*S*)-1,5-di-*tert*-butoxy-1,5-dioxopentan-2-yl)thioureido)-5-oxopentanoic acid (6a)

Yellowish gummy liquid (51 mg, 52%); R_f = 0.3 (EtOAc); IR (CH_2Cl_2): 3414 (O–H), 3357 (N–H), 3124, 2980 (=C–H), 2936 (C–H), 1731 (C=O), 1638 (N–H), 1545 (C=C), 1458 (C–H), 1158 (C–O), 1041 (C=S), 750, 657 (=C–H) cm^{-1}. ^1H NMR (400 MHz, $CDCl_3$): δ = 5.87 (d, J = 8.52 Hz, 1H), 5.45 (d, J = 7.24 Hz, 1H), 4.42 (ddd, J = 6.24, 5.9, 4.76 Hz, 1H) 4.36–4.27 (m, 1H), 2.42–2.22 (m, 4H), 2.18–2.03 (m, 2H), 1.95-1.79 (m, 2H), 1.46 (s, 9H), 1.44 (s, 9H), 1.42 (s, 9H); ^{13}C NMR (100 MHz, $CDCl_3$): δ = 182.4, 176.2, 173.1, 172.5, 171.9, 82.6, 82.1, 80.7, 53.4, 53.0, 31.6, 30.4, 28.4, 28.1, 28.0, 27.9, 27.8; HRMS (ESI) m/z calcd for $C_{23}H_{40}N_2O_8S$ $[M-H]^-$: 503.2423, found 503.2422.

4.5.3.5 Solid phase peptide synthesis

4.5.3.5.1 Resin swelling

All resins used in the solid phase peptide synthesis were swelled initially with DCM (5 mL) for 30 minutes by bubbling nitrogen gas. After draining the DCM, the resin beads were swelled again thrice with DMF (3 × 5 mL) for 15 minutes each.

4.5.3.5.2 Kaiser test

Few resin beads were taken in a test-tube and two drops of each of ninhydrin, phenol and 0.1% potassium cyanide solution were added to the

test-tube and heated for 2 minutes at 110 °C in a sand bath. The presence of a free amine group was confirmed by the appearance of dark blue-colored resin beads in the test tube. The Kaiser test was conducted to ascertain the completion of the coupling reaction with each amino acid.

4.5.3.5.3 General procedure for NHFmoc deprotection

The NHFmoc-amino group in the growing peptide chain was deprotected in each step using a freshly prepared solution of 20% piperidine in DMF (10 mL). Initially, 4 mL of the 20% piperidine solution in DMF was added to the resin beads and mixed for 10 minutes by bubbling nitrogen gas. The solution was drained from the resin beads, and the procedure was repeated twice with the remaining 20% piperidine solution (2 × 3 mL) for 10 minutes each to ensure complete deprotection of NHFmoc protecting group.

4.5.3.5.4 Resin cleavage

A mixture of 9.25 mL trifluoroacetic acid (TFA), 0.25 mL triisopropylsilane (TIPS), 0.25 mL ethane dithiol (EDT) and 0.25 mL Millipore water (H_2O) was prepared in a 10 mL centrifuge tube and thoroughly mixed by vortex. 5 mL of this cocktail solution was added to the dried resin beads containing peptide conjugate, and nitrogen gas was bubbled through the resin beads and cocktail mixture for 30 minutes. The cleaved peptide solution was drained from the resin beads into a single-neck round-bottomed flask (25 mL). The cleavage procedure was repeated twice (2 × 2.5 mL) with the resin beads using the remaining cocktail solution for 15 minutes each as mentioned before. The cleaved peptide solution from the peptide vessel was pooled together into a single-neck round-bottomed flask (25 mL) and then transferred to a 15 mL centrifuge tube using a Pasteur pipette. The mother liquor from cleavage was concentrated under reduced pressure using rotavapor to evaporate trifluoroacetic acid, and the concentrated viscous liquid was treated with

ice cold diethyl ether (2-3 mL) to precipitate the desired ligand targeted peptide conjugate. The upper ether layer was discarded, and the precipitated conjugate was washed thrice with ice-cold ether (3 × 3 mL). The precipitated conjugate was dried by a stream of nitrogen gas through the centrifuge tube fitted with a septum and an outlet needle for 45 minutes.

4.5.3.5.5 General procedure for solid phase peptide synthesis of PSMA-targeted thiourea-chelating linker conjugate, thiourea-NH-$(CH_2)_7$CO-Phe-Phe-Dap-Asp-Cys (18)

H-Cys-2-ClTrt resin (0.050 g, 0.045 mmol) was swelled initially with 5 mL of DCM by bubbling nitrogen gas for 30 minutes. After draining the DCM, the resin was swelled with 5 mL DMF thrice for 15 minutes each. *N*-Fmoc-Asp(O^{t}Bu)-OH (0.046 g, 0.113 mmol), PyBOP (0.059 g, 0.113 mmol) and DIPEA (0.08 mL, 0.45 mmol) in DMF (0.5 mL) were added to the resin beads in the peptide vessel, and the coupling reaction was continued for 6 h. The resin was washed with DMF (3 × 3 mL) followed by isopropanol (3 × 3 mL), and the beads were dried by a stream of nitrogen gas. The completion of the reaction was confirmed by performing the Kaiser test with few dried resin beads. A solution of 20% piperidine in DMF (10 mL) was prepared, added to the resin beads in aliquots (1 × 4 mL; 2 × 3 mL), mixed for 10 minutes each, and drained to ensure complete deprotection of Fmoc protecting group of the coupled amino acid as mentioned in the general procedure. The resin beads were washed again with DMF (3 × 3 mL) followed by isopropanol (3 × 3 mL) and dried by a stream of nitrogen gas. The formation of free amine was confirmed by performing the Kaiser test with few resin beads. Consecutively, Boc-Dap(Fmoc)-OH (0.048 g, 0.113 mmol), Fmoc-Phe-OH (0.044 g, 0.113 mmol), Fmoc-Phe-OH (0.044 g, 0.113 mmol) and Fmoc-8-aminocaprylic acid (0.043 g, 0.113 mmol) were coupled to the growing peptide chain as described earlier. After the deprotection of NHFmoc group from the

Fmoc-8-aminocaprylic acid, tris(*tert*-butylcarboxy) protected thiourea **9** (0.034 g, 0.068 mmol), PyBOP (0.059 g, 0.113 mmol) and DIPEA (0.08 mL, 0.45 mmol) in DMF (0.5 ml) was added to the resin beads and swelled for 6 h. The resin beads were washed again with DMF (3 × 3 mL) followed by isopropanol (3 × 3 mL) and dried by a stream of nitrogen gas. The completion of the coupling reaction was confirmed by the Kaiser test. Finally, a mixture of 9.25 mL trifluoroacetic acid (TFA), 0.25 mL ethanedithiol (EDT), 0.25 mL triisopropylsilane (TIPS), and 0.25 mL H_2O was prepared, and 5 mL of this cocktail solution was added to the resin beads, and nitrogen gas was bubbled through the beads for 30 minutes. The same procedure was repeated twice (2 × 2.5 mL) using the remaining cocktail solution for 15 minutes each. After the peptide cleavage from the resin, the mother liquor from cleavage was transferred to a 15 mL centrifuge tube fitted with a rubber septum and a needle, and concentrated under reduced pressure using rotary evaporator for 45 minutes. Ice-cold ether (5 mL) was added to the viscous solution to precipitate bioconjugates **18** and **20** as white solid. The bioconjugates **18** and **20** were purified using preparative RP-HPLC [λ = 254 nm; solvent gradient: 1% to 50% B in 25 min, 80% B wash 30 min run; A = 20 mM NH_4OAc in water, pH = 5; B = acetonitrile (ACN)]. ACN was removed under reduced pressure, and the pure fractions were freeze-dried to yield **18** or **20** as white solid. Analytical RP-HPLC: t_R = 4.78 min for **18** or t_R = 5.24 min for **20** [A = 20 mM NH_4OAc in water, pH = 5.0, B = acetonitrile (ACN), solvent gradient: 1% to 50% B in 10 min]. ESI-MS for **18** (*m*/*z*): $(M + H)^+$ calcd for $C_{47}H_{65}N_9O_{16}S_2$, 1076.4; found, 1076.4. UV/vis: λ_{max} = 280 nm; ESI-MS for **20** (*m*/*z*): $(M + H)^+$ calcd for $C_{47}H_{63}N_9O_{15}S_2$, 1058.2; found, 1058.4. UV/vis: λ_{max} = 280 nm.

4.5.3.6 General procedure for preparation of non-radioactive kit and procedure for labeling with ^{99m}Tc-radioisotope

A solution of stannous chloride dihydrate (0.80 mg, 0.003 mmol) in 0.02 M HCl (0.80 mL) was added to a solution of sodium α-D-glucoheptonate dihydrate (800 mg, 2.815 mmol) in argon purged water (5.0 mL). The bioconjugate **18 or 20** (0.001 mmol) was then added to the reaction mixture while purging with argon. After adjusting the pH of the solution to 6.8 ± 0.2 using 0.1 N NaOH, argon purged water was added to achieve a total volume of 10.0 mL. The solution mixture was dispensed into 5.0 mL vials (1.0 mL/ vial) under an argon atmosphere and lyophilized for 36 h. The vials were sealed under an argon atmosphere to yield the nonradioactive formulation kits, which were stored at −20 °C until use. A solution of sodium pertechnetate ^{99m}Tc (1.0 mL, 15 mCi) was added to a vial containing **18** or **20**, heated in a boiling water bath for 18 min, and then cooled to room temperature before use. The radiochemical purity of **19** or **21** was analyzed using RP-HPLC before further usage.

4.5.4 *In vitro* evaluation

4.5.4.1 Culture of cell lines

LNCaP cells used in the following studies were purchased from National Centre for Cell Science (NCCS), Pune. The 22RV1 suspension cell line was a kind gift from Prof. Philip S. Low, Purdue University, West Lafayette, USA. The cells were grown in a 5% carbon dioxide: 95% air-humidified atmosphere at 37 ˚C in a monolayer in RPMI 1640 medium supplemented with 10% heat-inactivated fetal bovine serum, 1% penicillin-streptomycin antibiotics and 100 mM sodium pyruvate. 22RV1 cell line culture medium was also supplemented with 100 mM MEM non-essential amino acids.

4.5.4.2 *In vitro* binding affinity, specificity, and uptake studies of ^{99m}Tc-thiourea radiotracer (19) in PSMA^{+} cell lines

LNCaP or 22RV1 cells were seeded in 24-well (100,000 cells/ well) Corning plates and allowed to form monolayers over a period of 48 h. The spent medium in each well was replaced with fresh medium (0.5 mL) containing increasing concentrations of ^{99m}Tc-thiourea radiotracer (**19**) in the presence or absence of 100-fold excess PMPA. After incubating for 1 h at 37 °C, the cells were washed with fresh incomplete medium (3 × 1.0 mL) and tris buffer (1 × 1.0 mL) to remove traces of unbound radiopharmaceutical agent. After dissolving the cells in 0.25 M $NaOH_{(aq)}$ (0.5 mL), the solution (0.45 mL) was transferred to individual γ-counter tubes and radioactivity was counted using a γ-counter. The data was compiled, plotted and non-linear regression analysis was performed assuming one-site specific binding equilibrium using GraphPad Prism 6.02 software. The dissociation constant (K_D) was calculated from the graph of cell-bound radioactivity versus concentration of radiopharmaceutical agent.

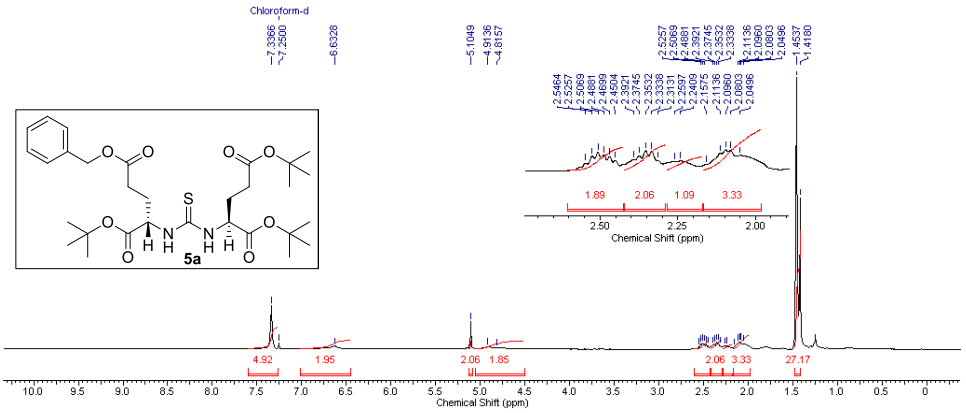

Figure 4.11 ^{1}H NMR spectrum (400 MHz, $CDCl_3$) of **5a**

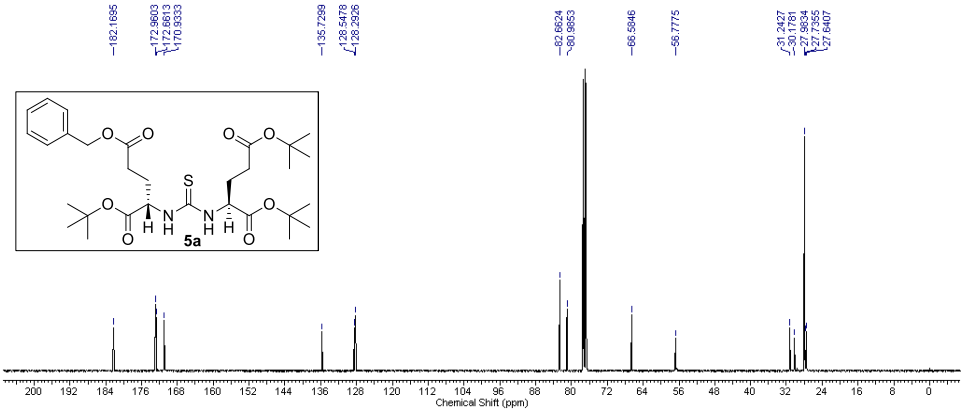

Figure 4.12 ^{13}C NMR spectrum (100 MHz, $CDCl_3$) of **5a**

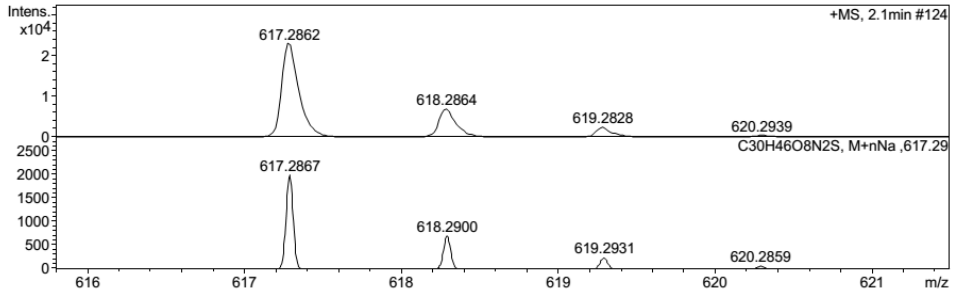

Figure 4.13 HRMS of **5a**

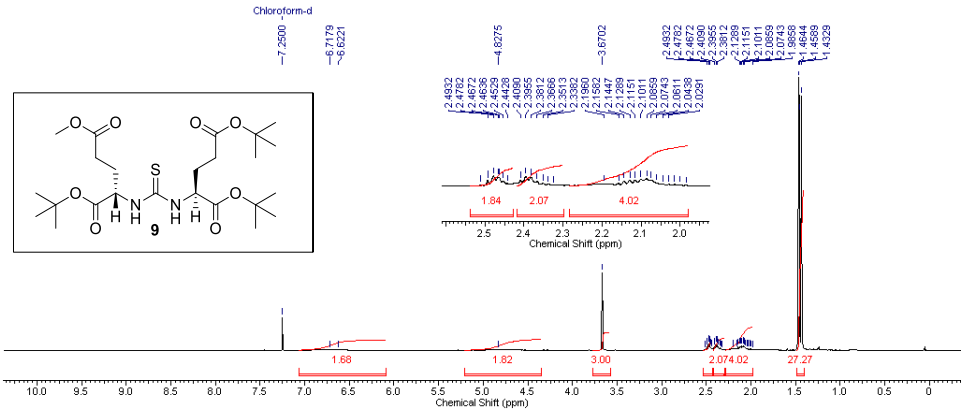

Figure 4.14 ^{1}H NMR spectrum (400 MHz, $CDCl_3$) of **9**

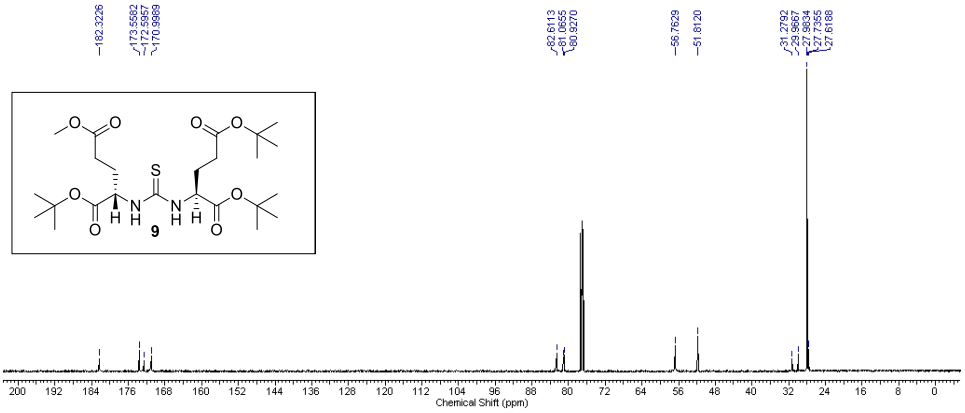

Figure 4.15 ^{13}C NMR spectrum (100 MHz, $CDCl_3$) of **9**

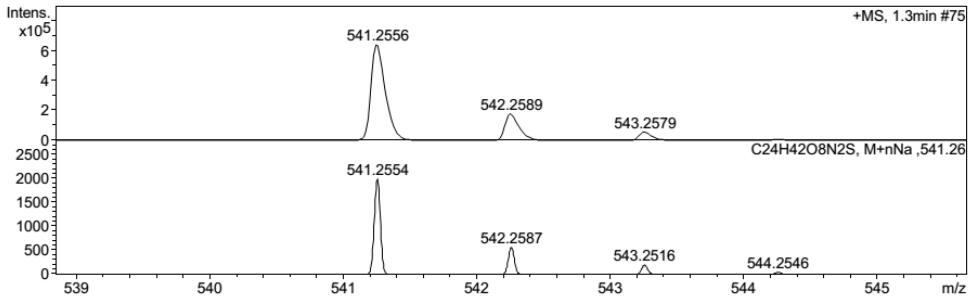

Figure 4.16 HRMS of **9**

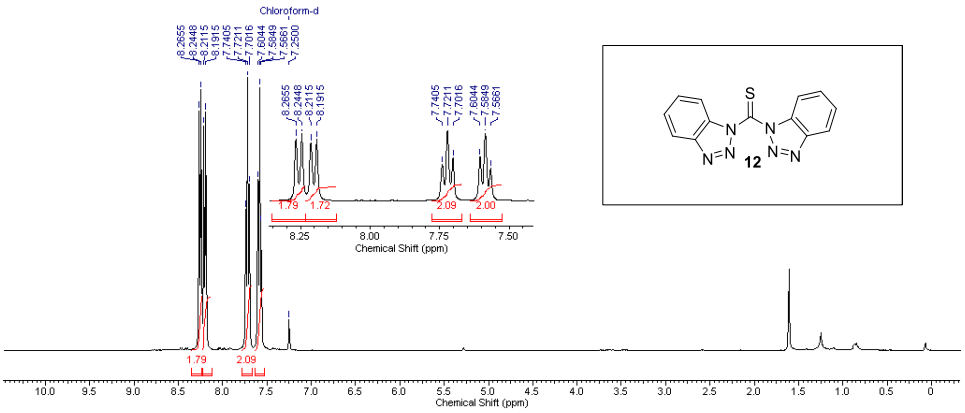

Figure 4.17 ^{1}H NMR spectrum (400 MHz, $CDCl_3$) of **12**

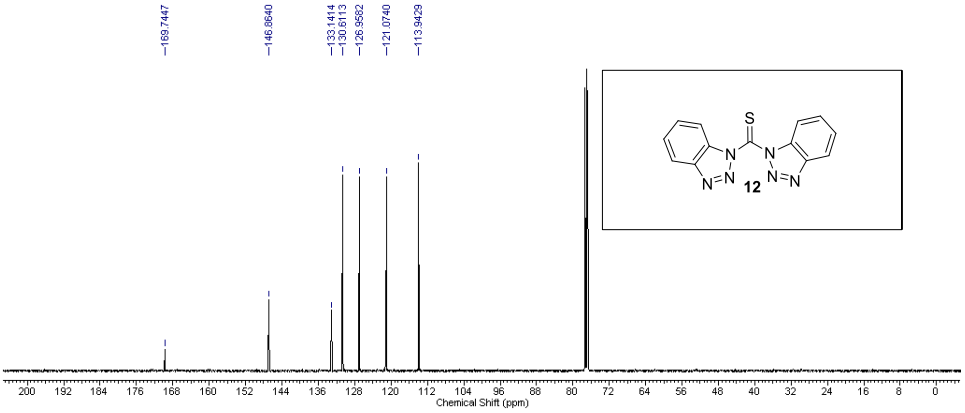

Figure 4.18 ^{13}C NMR spectrum (100 MHz, $CDCl_3$) of **12**

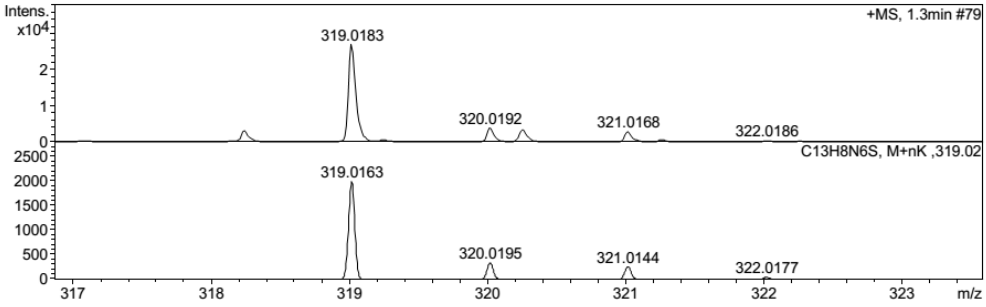

Figure 4.19 HRMS of **12**

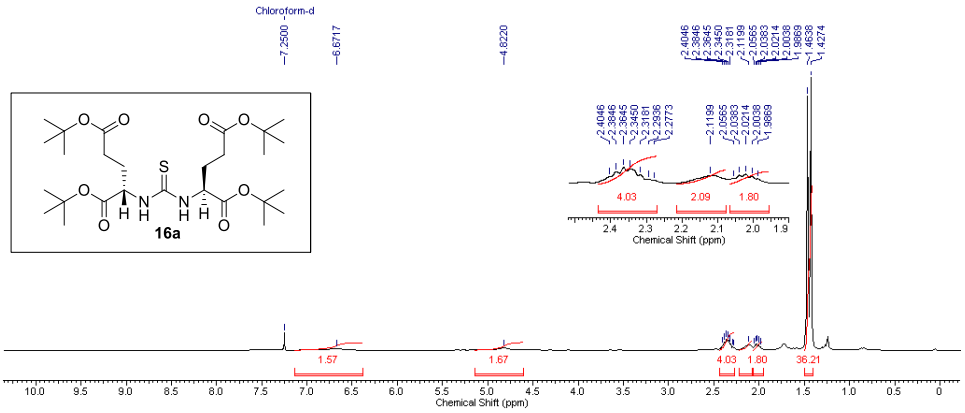

Figure 4.20 ^{1}H NMR spectrum (400 MHz, $CDCl_3$) of **16a**

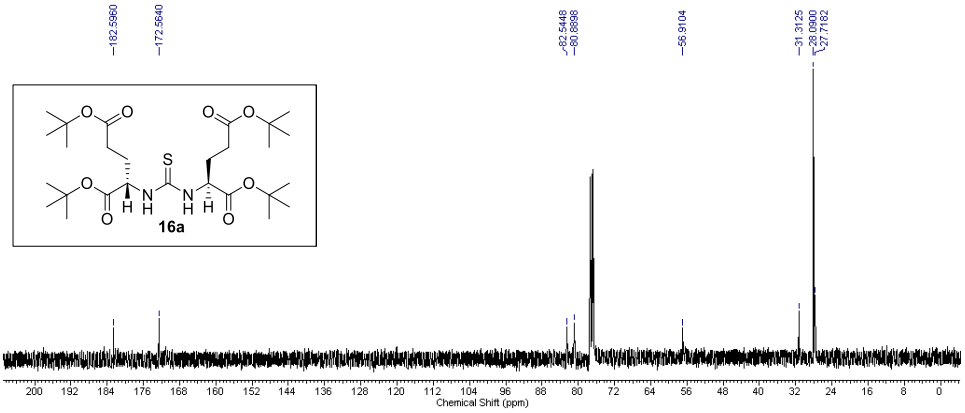

Figure 4.21 ^{13}C NMR spectrum (100 MHz, $CDCl_3$) of **16a**

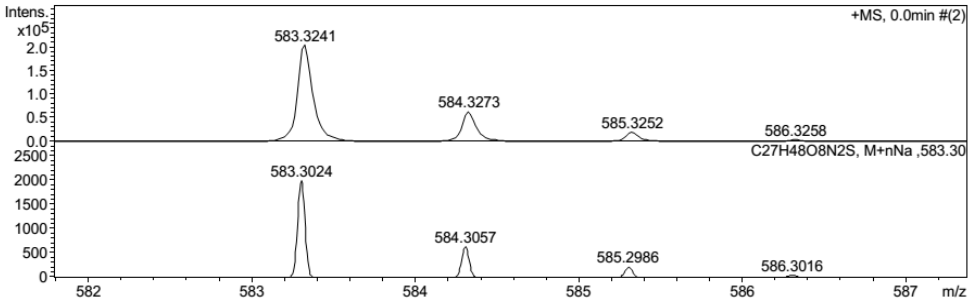

Figure 4.22 HRMS of **16a**

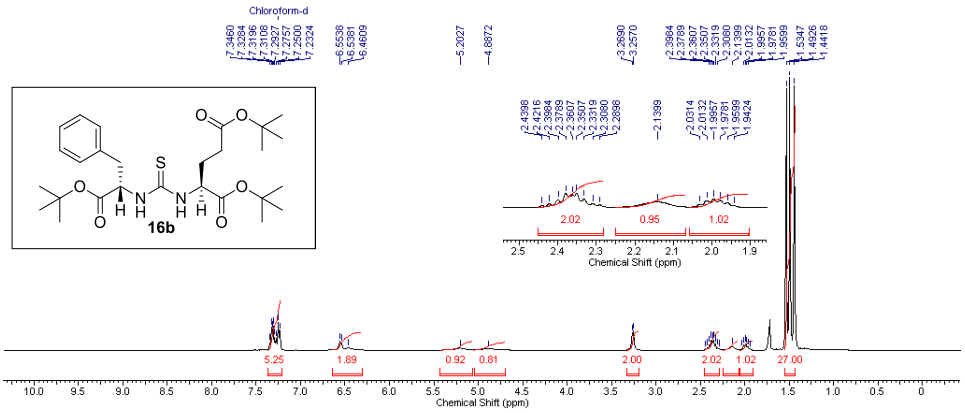

Figure 4.23 ^{1}H NMR spectrum (400 MHz, $CDCl_3$) of **16b**

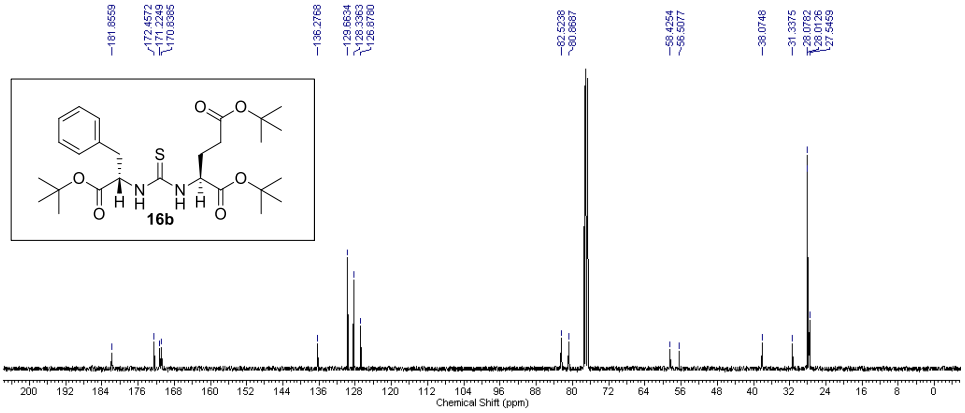

Figure 4.24 ^{13}C NMR spectrum (100 MHz, $CDCl_3$) of **16b**

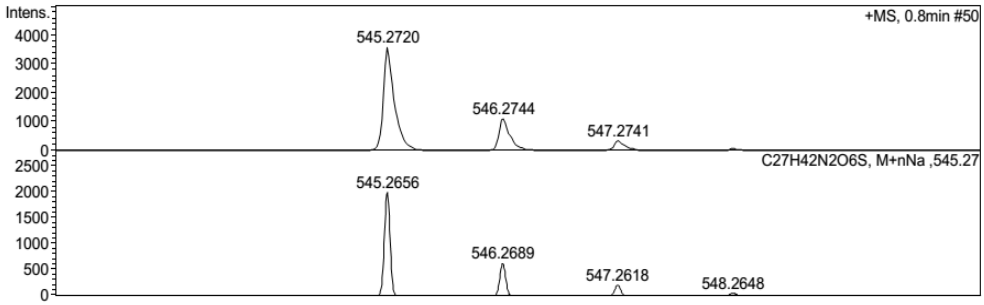

Figure 4.25 HRMS of **16b**

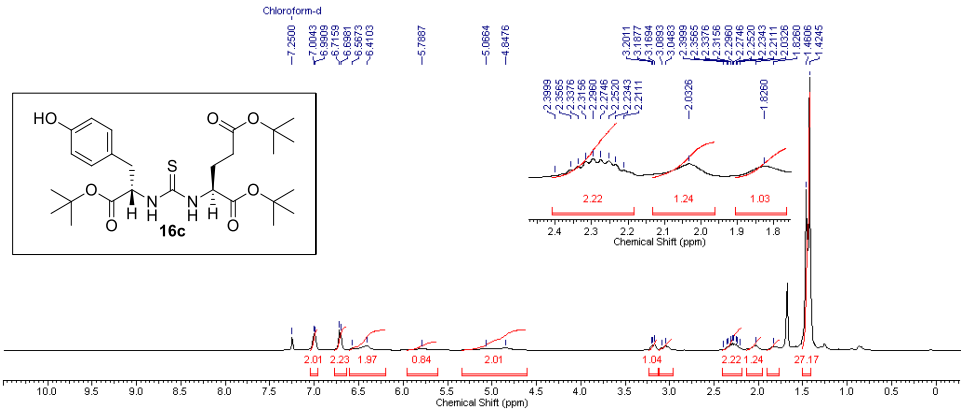

Figure 4.26 ^{1}H NMR spectrum (400 MHz, $CDCl_3$) of **16c**

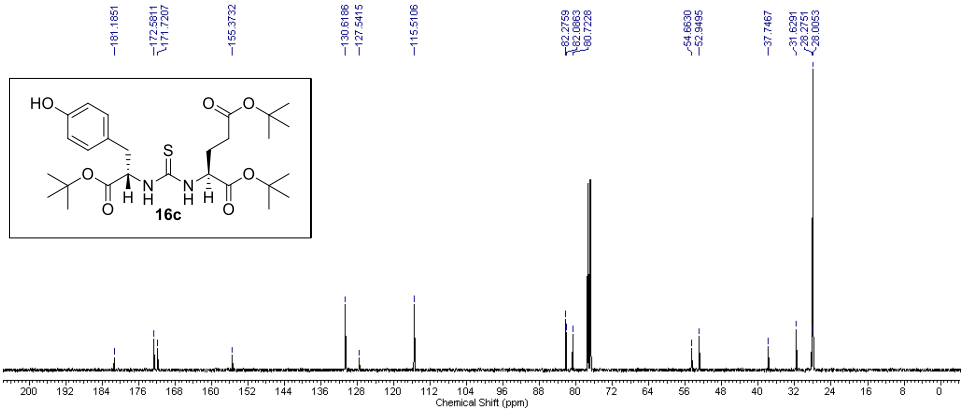

Figure 4.27 ^{13}C NMR spectrum (100 MHz, $CDCl_3$) of **16c**

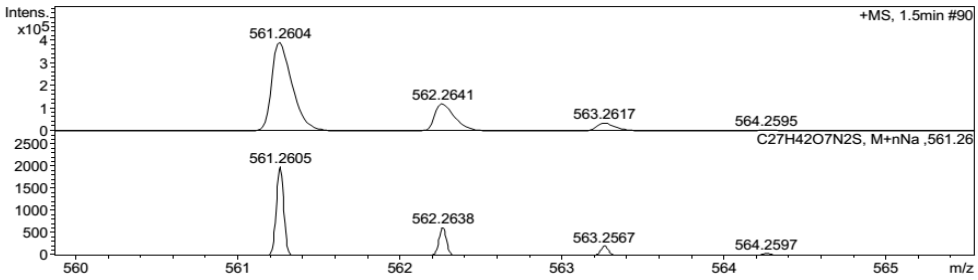

Figure 4.28 HRMS of **16c**

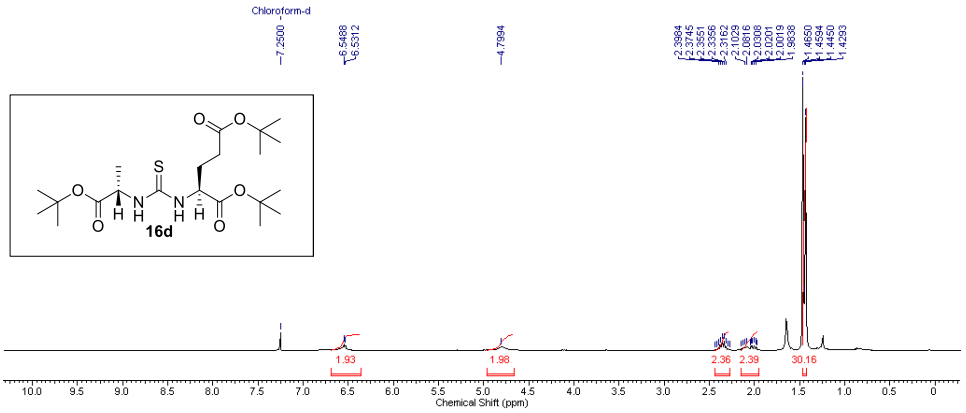

Figure 4.29 ^{1}H NMR spectrum (400 MHz, $CDCl_3$) of **16d**

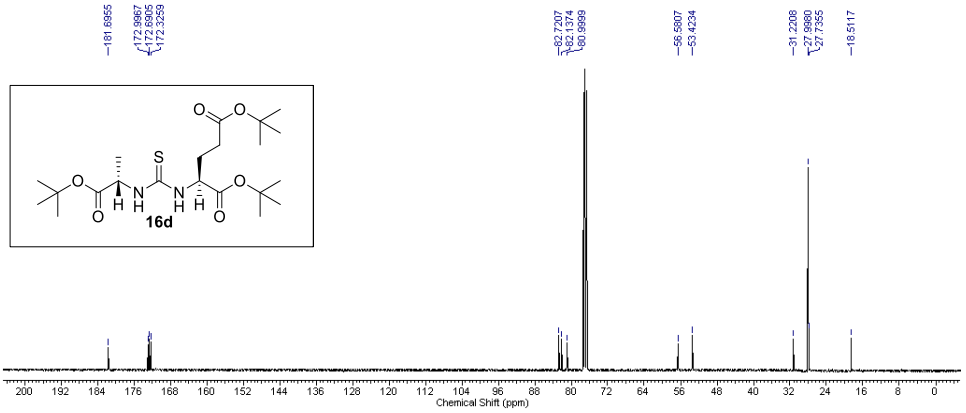

Figure 4.30 ^{13}C NMR spectrum (100 MHz, $CDCl_3$) of **16d**

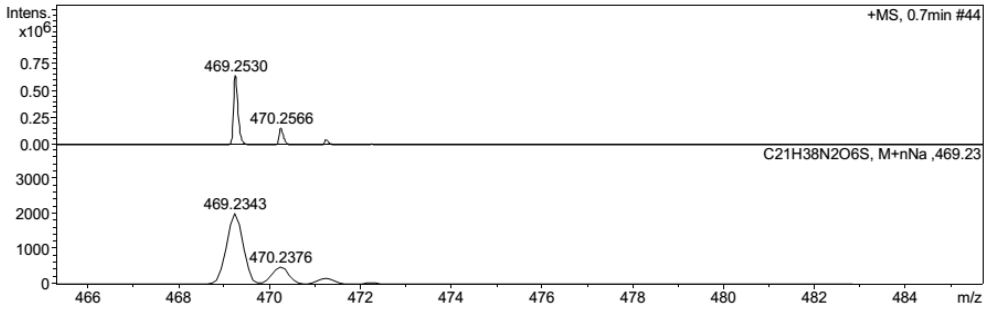

Figure 4.31 HRMS of **16d**

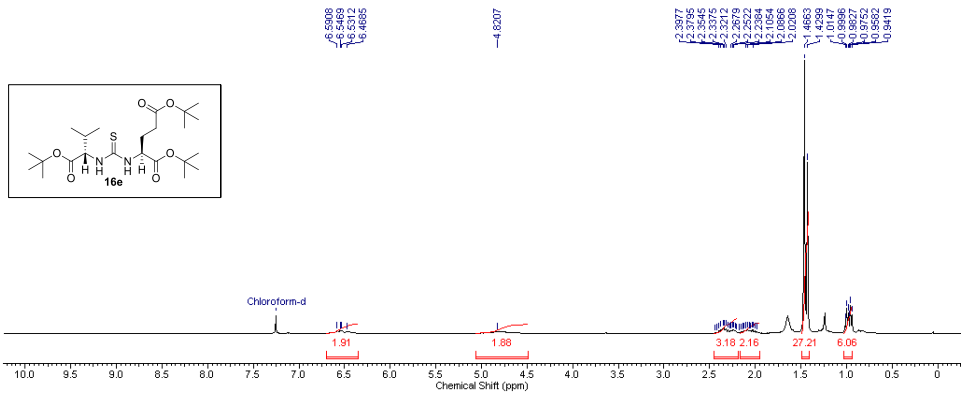

Figure 4.32 ^{1}H NMR spectrum (400 MHz, $CDCl_3$) of **16e**

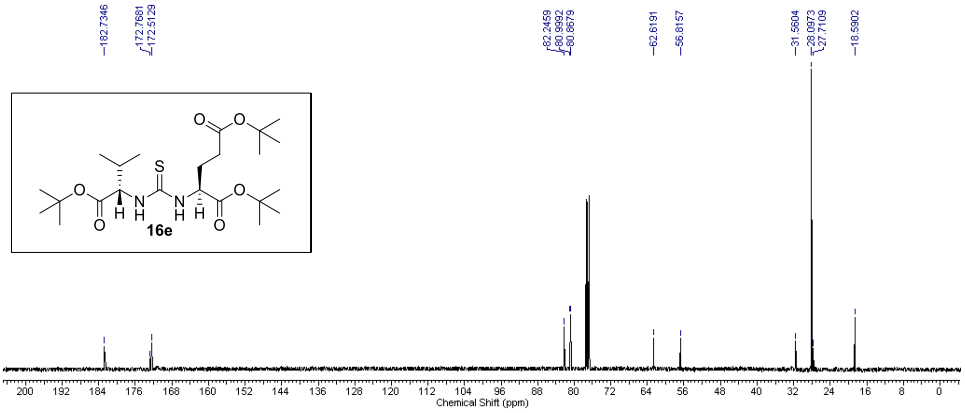

Figure 4.33 ^{13}C NMR spectrum (100 MHz, $CDCl_3$) of **16e**

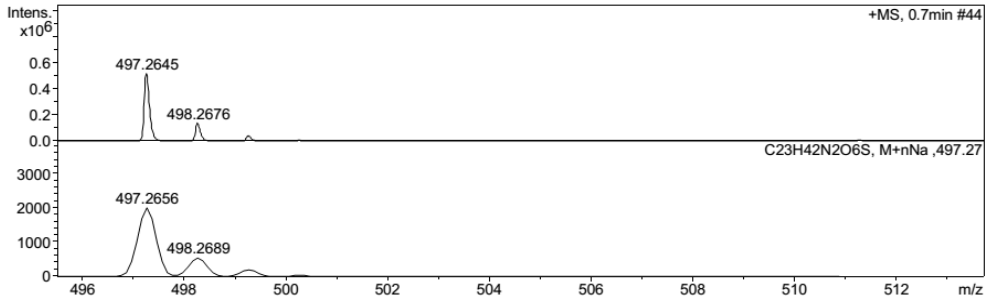

Figure 4.34 HRMS of **16e**

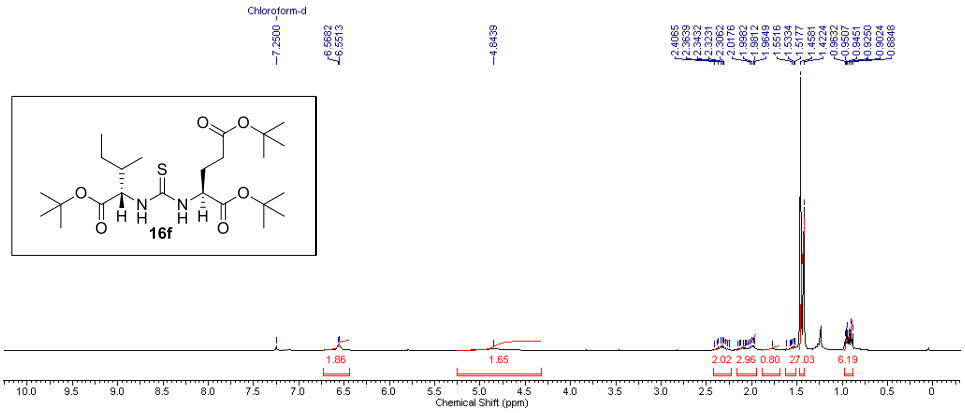

Figure 4.35 ^{1}H NMR spectrum (400 MHz, $CDCl_3$) of **16f**

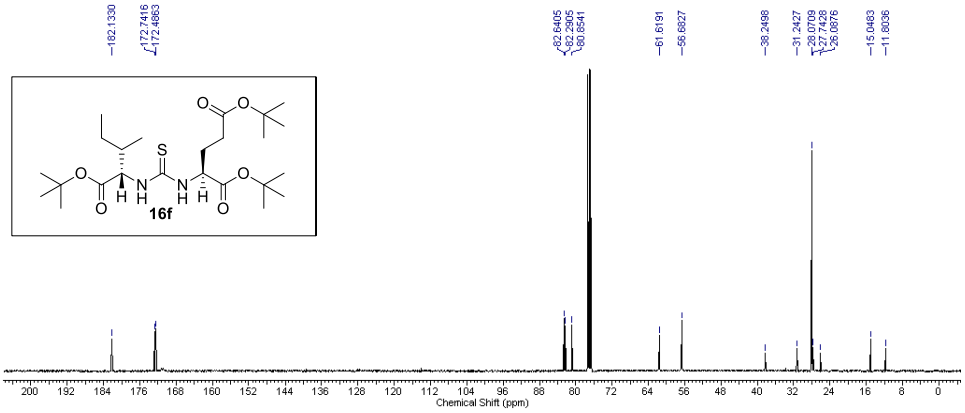

Figure 4.36 ^{13}C NMR spectrum (100 MHz, $CDCl_3$) of **16f**

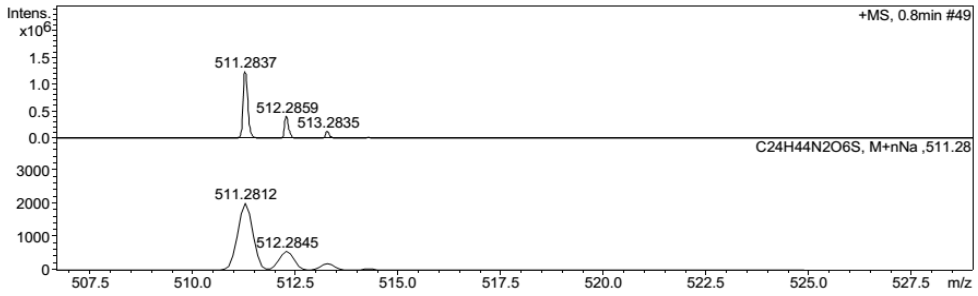

Figure 4.37 HRMS of **16f**

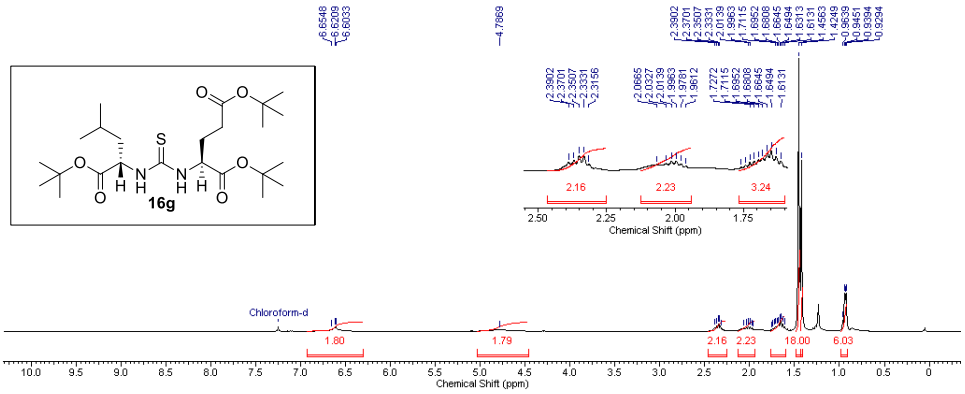

Figure 4.38 ^{1}H NMR spectrum (400 MHz, $CDCl_3$) of **16g**

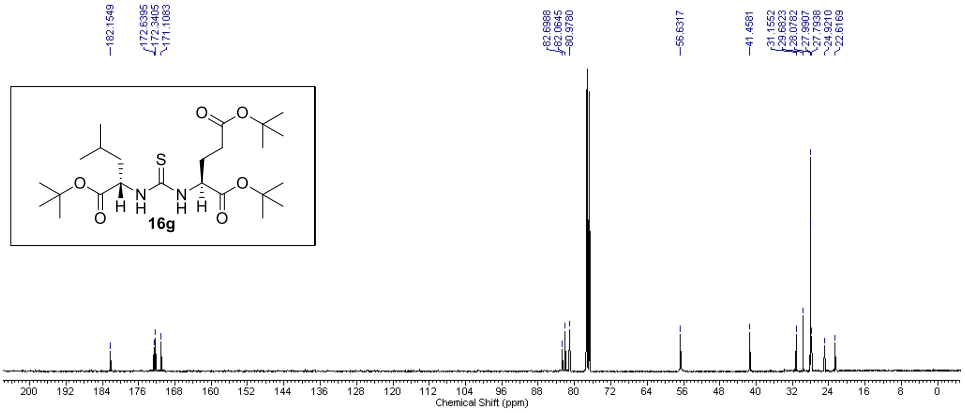

Figure 4.39 ^{13}C NMR spectrum (100 MHz, $CDCl_3$) of **16g**

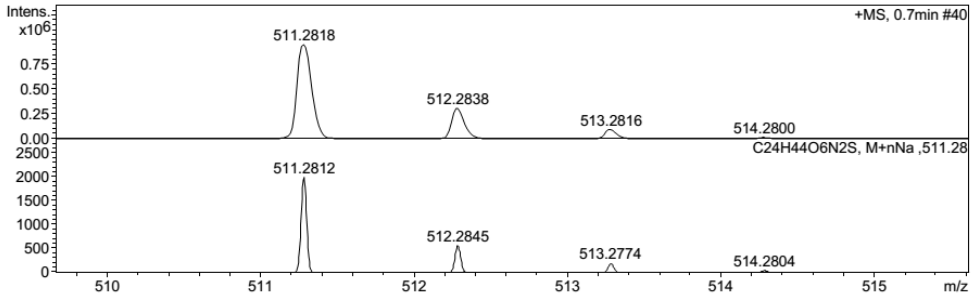

Figure 4.40 HRMS of **16g**

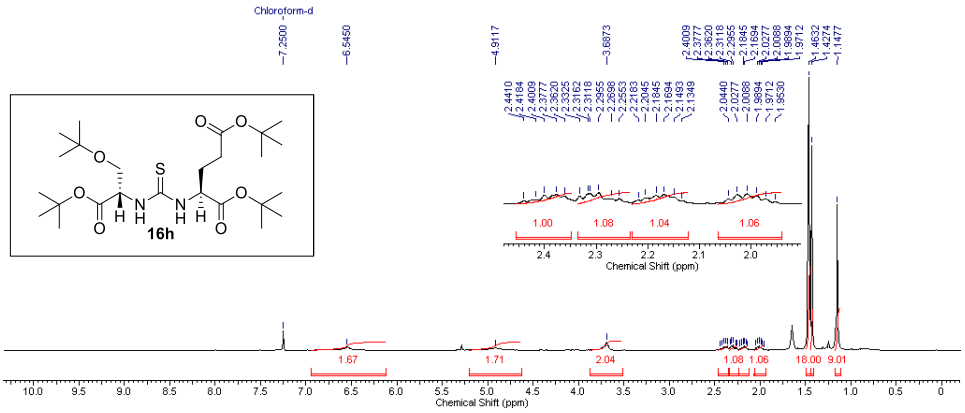

Figure 4.41 ^{1}H NMR spectrum (400 MHz, $CDCl_3$) of **16h**

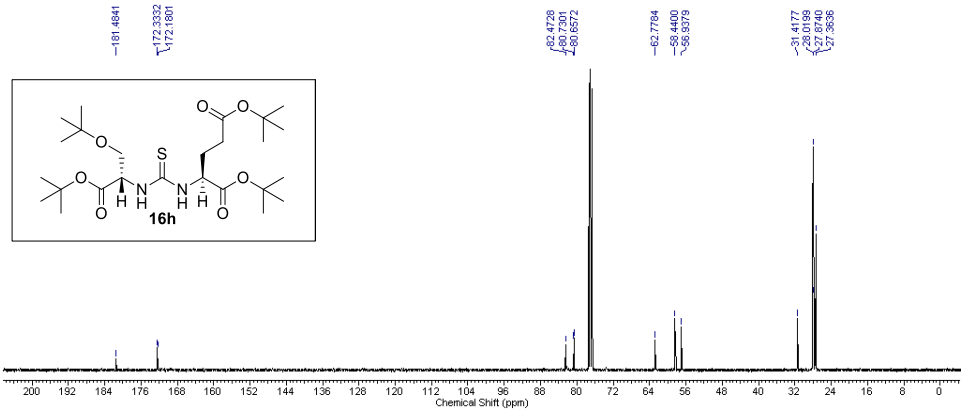

Figure 4.42 ^{13}C NMR spectrum (100 MHz, $CDCl_3$) of **16h**

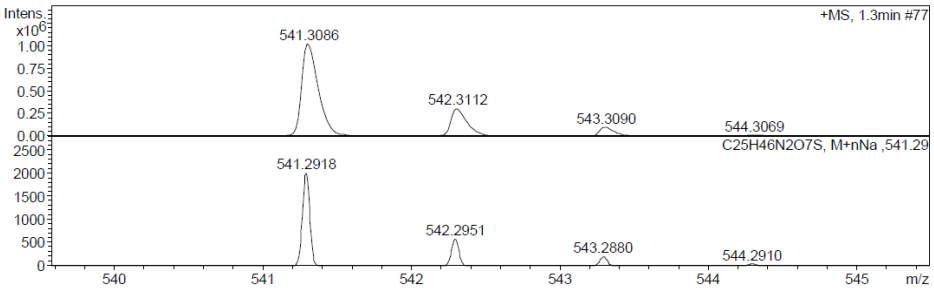

Figure 4.43 HRMS of **16h**

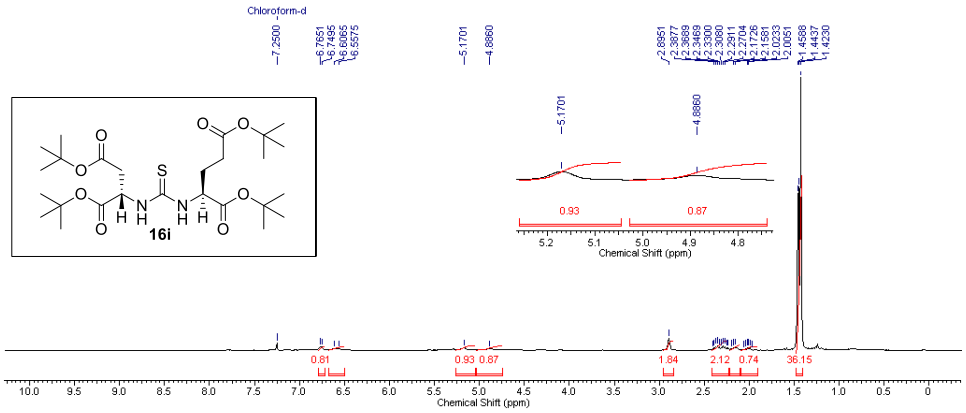

Figure 4.44 ^{1}H NMR spectrum (400 MHz, $CDCl_3$) of **16i**

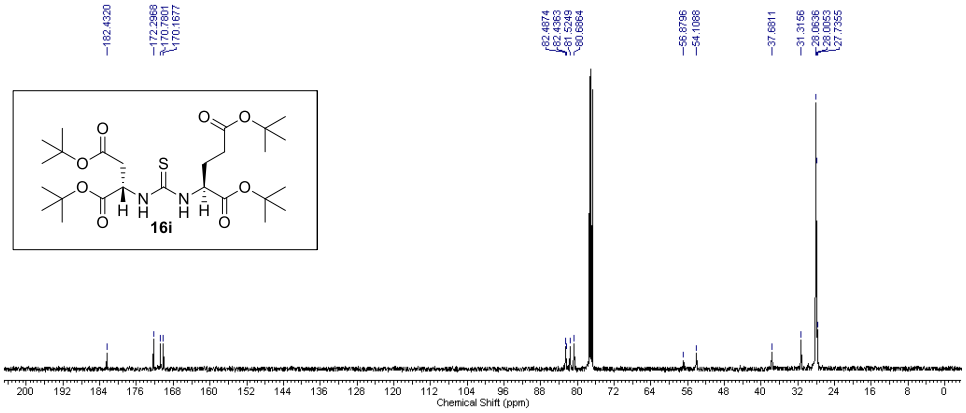

Figure 4.45 ^{13}C NMR spectrum (100 MHz, $CDCl_3$) of **16i**

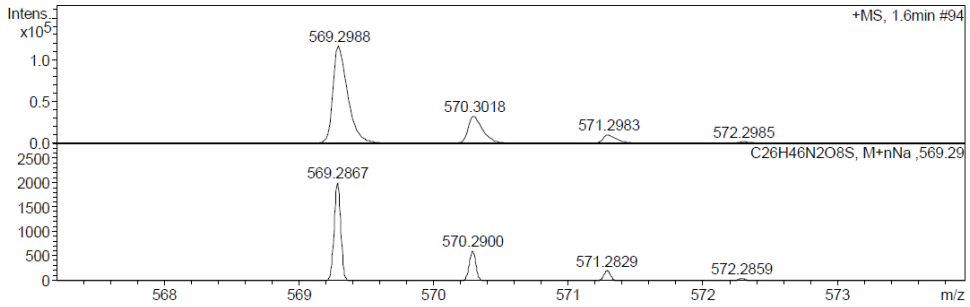

Figure 4.46 HRMS of **16i**

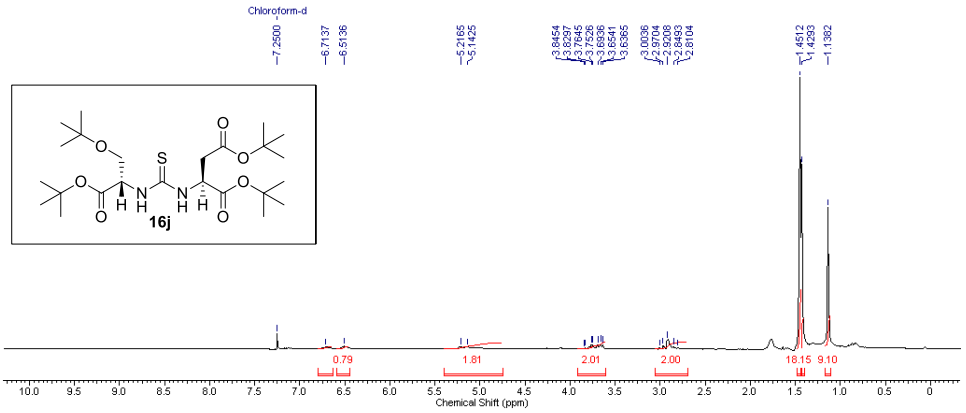

Figure 4.47 ^{1}H NMR spectrum (400 MHz, $CDCl_3$) of **16j**

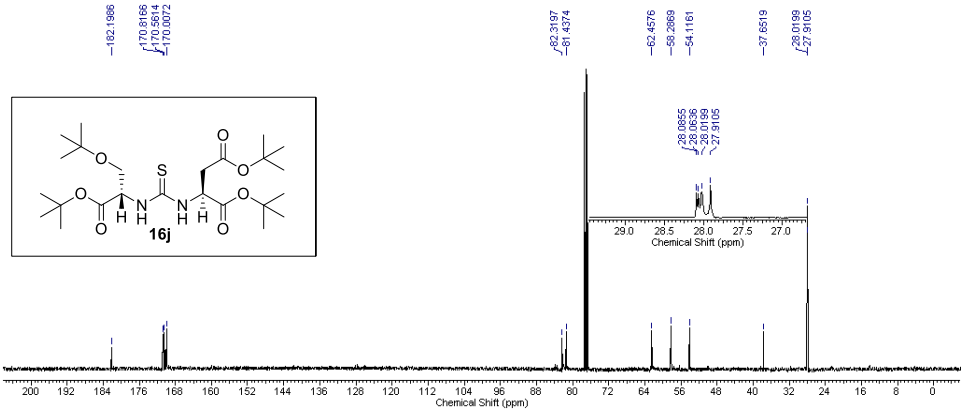

Figure 4.48 ^{13}C NMR spectrum (100 MHz, $CDCl_3$) of **16j**

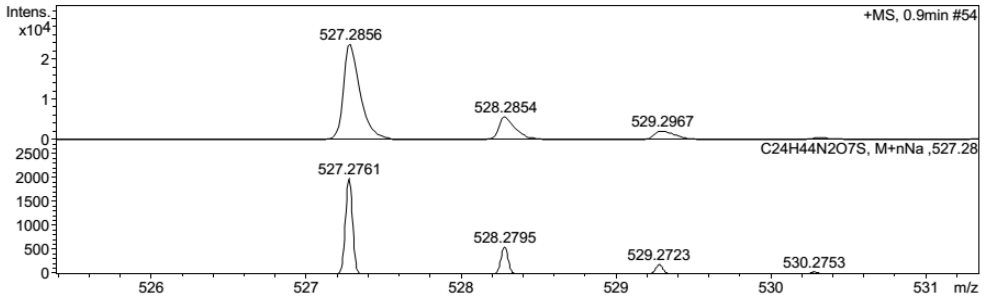

Figure 4.49 HRMS of **16j**

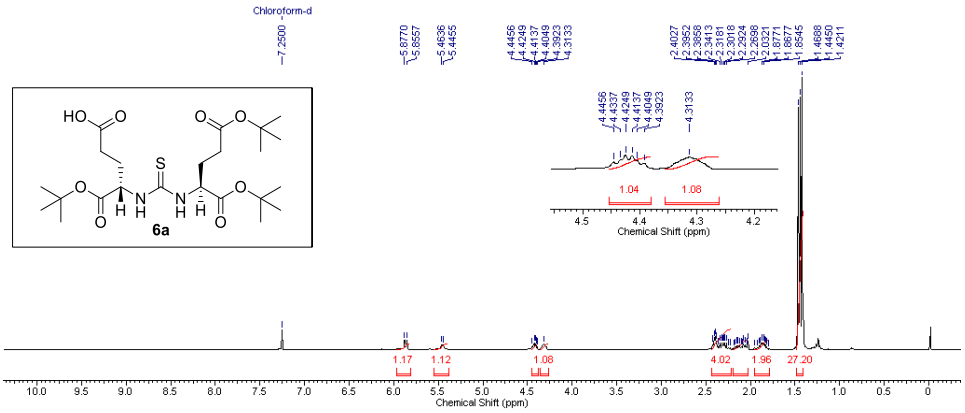

Figure 4.50 ^{1}H NMR spectrum (400 MHz, $CDCl_3$) of **6a**

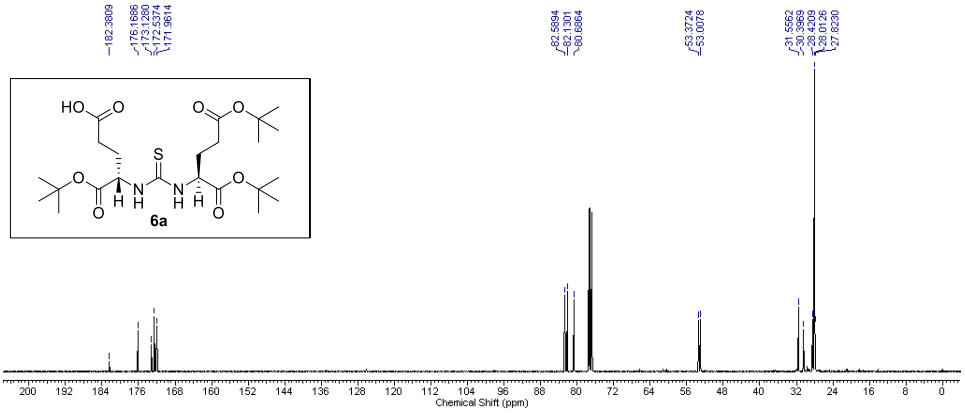

Figure 4.51 ^{13}C NMR spectrum (100 MHz, $CDCl_3$) of **6a**

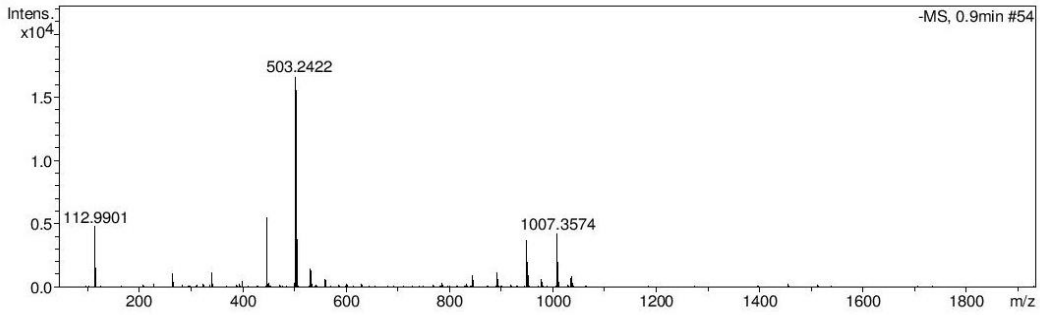

Figure 4.52 HRMS of **6a**

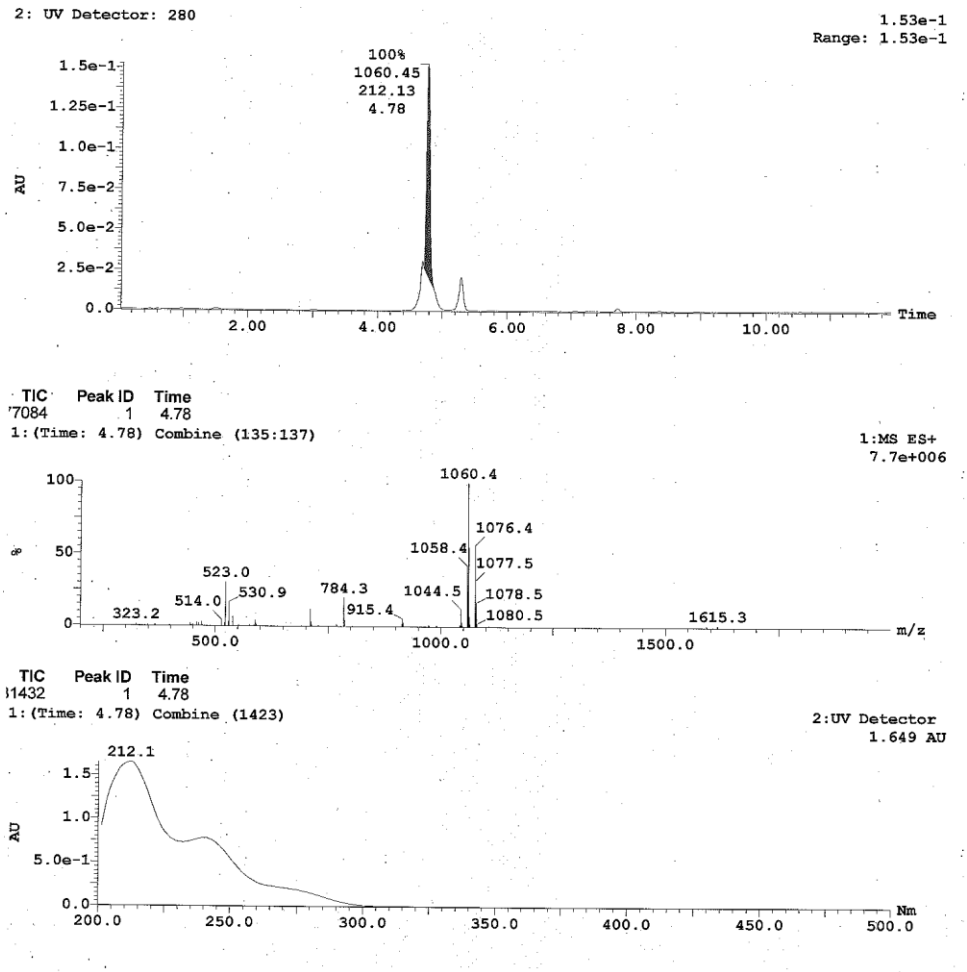

Figure 4.53 LC-MS of PSMA targeted thiourea-chelating linker conjugate **18**

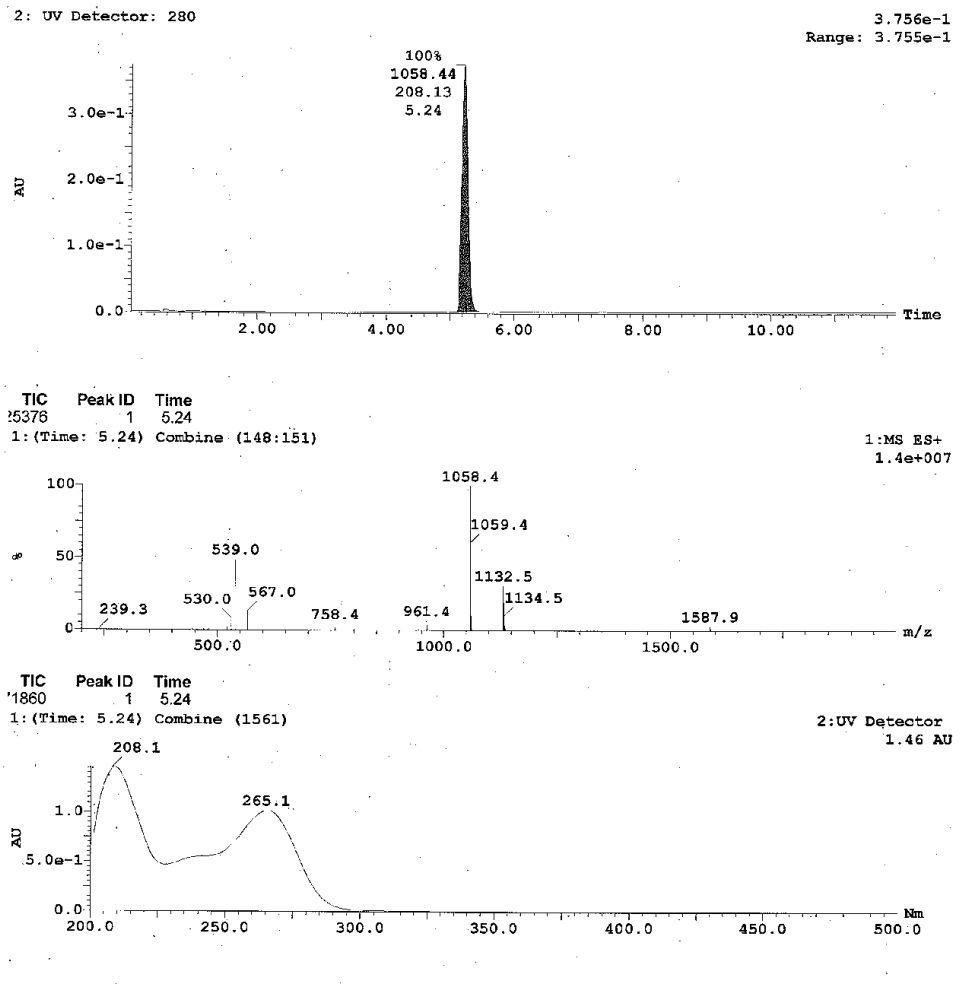

Figure 4.54 LC-MS of thiazolone chelating linker conjugate **20a** or **20b**

4.6 References

1. Siegel R. L., Miller K. D., Jemal A. (2019), Cancer Statistics, 2019, CA Cancer J. Clin., 69, 7–34 (DOI: 10.3322/caac.21551).
2. Holves A. M., Heesakkers R. A. M., Adang E. M. (2008), The diagnostic accuracy of CT and MRI in the pelvis of lymph nodes in patients with prostate cancer: a meta-analysis, Clin. Radiol., 63, 387–395 (DOI: 10.1016/j.crad.2007.05.022).
3. Jia J. B., Houshyar R., Verma S., Uchio E., Lall C. (2016), Prostate cancer on computed tomography: A direct comparison with multi-parametric magnetic resonance imaging and tissue pathology, Eur. J. Radiol., 85, 261−267 (DOI: 10.1016/j.ejrad.2015.10.013).
4. Harvey C. J., Pilcher J., Richenberg J., Patel U., Frauscher F. (2012), Applications of transrectal ultrasound in prostate cancer, Br. J. Radiol., 85, S3−S17 (DOI: 10.1259/bjr/56357549).
5. Barinka C., Rojas C., Slusher B., Pomper M. (2012), Glutamate carboxypeptidase II in diagnosis and treatment of neurologic disorders and prostate cancer, Curr. Med. Chem., 19, 856−870 (DOI: 10.2174/092986712799034888).
6. Cutler C. S., Hennkens H. M., Sisay N., Hucklier-Markai S., Jurisson S. S. (2013), Radiometal for combined imaging and therapy, Chem. Rev., 113, 858–883 (DOI: 10.1021/cr3003104).
7. Kularatne S. A., Wang K., Santhapuram H. K. R., Low P. S. (2009), Prostate-specific membrane antigen targeted imaging and therapy of prostate cancer using a PSMA inhibitor as a homing ligand, Mol. Pharm., 6, 780–789 (DOI: 10.1021/mp900069d).
8. Kularatne S. A., Zhou Z., Yang J., Post C. B., Low P. S. (2009), Design, synthesis, and preclinical evaluation of prostate-specific membrane antigen targeted ^{99m}Tc-radioimaging agents, Mol. Pharm., 6, 790–800 (DOI: 10.1021/mp9000712).

9. Banerjee S. R., Chen Z., Pullambhatla M., Lisok A., Chen J., Mease R. C., Pomper M. G. (2016), Preclinical comparative study of ^{68}Ga-labeled DOTA, NOTA, and HBED-CC chelated radiotracers for targeting PSMA. Bioconjugate Chem., 27, 1447–1455 (DOI: 10.1021/acs.bioconjchem.5b00679).
10. Yang X., Mease R. C., Pullambhatla M., Lisok A., Chen Y., Foss C. A., Wang Y., Shallal H., Edelman H., Hoye A. T., Attardo G., Nimmagadda S., Pomper M. G. (2016), [^{18}F]-Fluorobenzoyllysinepentanedioic acid carbamates: New scaffolds for positron emission tomography (PET) imaging of prostate-specific membrane antigen (PSMA), J. Med. Chem., 59, 206–218 (DOI: 10.1021/acs.jmedchem.5b01268).
11. Banerjee S. R., Pullambhatla M., Foss C. A., Nimmagadda S., Ferdani R., Anderson C. J., Mease R. C., Pomper M. G. (2014), ^{64}Cu-labeled inhibitors of prostate-specific membrane antigen for PET imaging of prostate cancer, Bioconjugate Chem., 57, 2657–2669 (DOI: 10.1021/jm401921j).
12. Banerjee S. R., Pullambhatla M., Foss C. A., Falk A., Byun Y., Nimmagadda S., Mease R. C., Pomper M. G. (2013), Effect of chelators on the pharmacokinetics of ^{99m}Tc-labeled imaging agents for the prostate-specific membrane antigen (PSMA), J. Med. Chem., 56, 6108–6121 (DOI: 10.1021/jm400823w).
13. Chen Y., Pullambhatla M., Banerjee S. R., Byun Y., Stathis M., Rojas C., Slusher B. S., Mease R. C. Pomper M. G. (2012), Synthesis and biological evaluation of low molecular weight fluorescent imaging agents for the prostate-specific membrane antigen, Bioconjugate. Chem., 23, 2377–2385 (DOI: 10.1021/bc3003919).
14. Banerjee S. R., Pullambhatla M., Byun Y., Nimmagadda S., Green G., Fox J. J., Horti A., Mease R. C., Pomper M. G. (2010), 68Ga-labeled inhibitors of prostate-specific membrane antigen (PSMA)

for imaging prostate cancer, J. Med. Chem., 53, 5333–5341 (DOI: 10.1021/jm100623e).

15. Choy C. J., Ling X., Geruntho J. J., Beyer S. K., Latoche J. D., Langton-Webster B., Anderson C. J., Berkman C. E. (2017), PSMA Inhibitors: The effect of an albumin binder on biodistribution and therapeutic efficacy in prostate tumor-bearing mice, Theranostics, **7**, 1928–1939 (DOI: 10.7150/thno.18719).

16. Dannoon S., Ganguly T., Cahaya H., Geruntho J. J., Galliher M. S., Beyer S. K., Choy C. J., Hopkins M. R., Regan M., Blecha J. E., Skultetyova L., Drake C. R., Jivan S., Barinka C., Jones E. F., Berkman C. E., VanBrocklin H. F. (2016), Structure-activity relationship of ^{18}F-labeled phosphoramidate peptidomimetic prostate-specific membrane antigen (PSMA)-targeted inhibitor analogues for PET imaging of prostate cancer, J. Med. Chem., 59, 5684–5694 (DOI: 10.1021/acs.jmedchem.5b01850).

17. Graham K., Lesche R., Gromov A. V., Böhnke N., Schäfer M., Hassfeld J., Dinkelborg L. Kettschau G. (2012), Radiofluorinated derivatives of 2-(phosphonomethyl)pentanedioic acid as inhibitors of prostate specific membrane antigen (PSMA) for the imaging of prostate cancer, J. Med. Chem., 55, 9510–9520 (DOI: 10.1021/jm300710j).

18. Lapi S. E., Wahnishe H., Pham D., Wu L. Y., Nedrow-Byers J. R., Liu T., Vejdani K., VanBrocklin H. F., Berkman C. E., Jones E. F. (2009), Assessment of an 18F-labeled phosphoramidate peptidomimetic as a new prostate-specific membrane antigen-targeted imaging agent for prostate cancer, J. Nucl. Med., 50, 2042–2048 (DOI: 10.2967/jnumed.109.066589).

19. Misra P., Humblet V., Pannier N., Maison W., Frangioni J. V. (2007), Production of multimeric prostate-specific membrane antigen small molecule radiotracers using a solid-phase ^{99m}Tc

preloading strategy, J. Nucl. Med., 48, 1379−1389 (DOI: 10.2967/jnumed.107.040303).

20. Katritzky, A. R.; Tao, H.; Kirichenko, K. (2007), Microwave mediated syntheses of β-enamino thioic acid derivatives, ARKIVOC.**,** 5, 142−151.

21. Pandit A., Sengupta S., Krishnan M. A., Reddy R. B., Sharma R, Venkatesh C. (2018), First report on 3D-QSAR and molecular dynamics based docking studies of GCPII inhibitors for targeted drug delivery applications, J. Mol. Struct., 1159, 179-192 (DOI: 10.1016/j.molstruc.2018.01.059).

22. Mock J. N., Taliaferro J. P., Lu X., Patel S. K., Cummings B. S., Long T. E. (2012), Haloenol pyranones and morpholinones as antineoplastic agents of prostate cancer, Bioorg. Med. Chem. Lett., 22, 4854–4858 (10.1016/j.bmcl.2012.05.038).

23. Nicolaou, K. C.; Estrada, A. A.; Zak, M.; Lee, S. H.; Safina, B. S. (2005), A mild and selective method for the hydrolysis of esters with trimethyltin hydroxide, Angew. Chem. Int. Ed., 44, 1378–1382.

24. Harada N., Kimura H., Ono M., Saji H. (2013), Preparation of asymmetric urea derivatives that target prostate specific membrane antigen for SPECT imaging, J. Med. Chem., 56, 7890−7901 (DOI: 10.1021/jm400895s).

25. Mesters J. R., Barinka C., Li W., Tsukamoto T., Majer P., Slusher B. S., Konvalinka J., Hilgenfeld R. (2006), Structure of glutamate carboxypeptidase II, a drug target in neuronal damage and prostate cancer, EMBO J., 25, 1375–1384 (DOI: 10.1038/sj.emboj.7600969).

26. Leamon, C. P.; Parker, M. A.; Vlahoc, I. R. (2002), Synthesis and biological evaluation of EC20: a new folate-derived 99mTc-based radiopharmacetical, Bioconjugate Chem., 13, 1200–1210 (DOI:10.1021/bc0200430).

Chapter 5

Tyrosine-based Asymmetric Urea Ligand for Prostate Carcinoma: Tuning Biological Efficacy through *in silico* Studies

5.1 Introduction

Prostate cancer (PCa) is the second most diagnosed malignancy after lung cancer in western countries.[1] Cancer statistics on PCa depicts 174,650 newly diagnosed cases and 31,620 estimated deaths in the calendar year of 2019.[2] The available diagnostic techniques for detection of PCa are a digital rectal examination, blood prostate specific antigen (PSA) measurement, and ultrasound-guided prostate biopsy.[3] Despite the successful adaption of these diagnostic modalities for detecting PCa, the methods have several disadvantages,[4–6] leaving most early malignancies and sites of metastasis in advanced disease undetected, for which complementary or alternative diagnostic methods are needed. Targeting biomarkers over-expressed during pathological diseased state such as cancer is one of the reliable methods to diagnose as well as to treat the disease.[7] Therefore, identification of specific biomarkers is strongly recommended so that the patients receive appropriate treatment at an early stage before the advancement of the disease.

Prostate specific membrane antigen (PSMA) is an integral membrane protein (binuclear zinc peptidase) present in the prostate epithelial cells and upregulated to several folds in high-grade, metastatic and androgen-insensitive prostate carcinomas.[8,9] It is pertinent to understand the architecture of PSMA binding site, and its interaction with the natural ligand, NAAG, for the design and development of a new small molecule inhibitors of PSMA. The active site of PSMA consists[10] of two binding pockets (S1 and S1') and the interactions of NAAG with this cavity shows that the glutamate functionality of NAAG interacts with the S1' pocket

while the rest of the inhibitor interacts with the S1 pocket. Glutamic acid-based urea inhibitors,[11,12] glutamic lysine-based urea heterodimers[13–18] and phosphoramidates[19–22] are well documented small molecule inhibitors which are proved to be highly specific towards PSMA. These molecules have shown excellent activity *in vitro* and *in vivo* studies and generally considered as potential clinical candidates for the treatment and diagnosis of early malignancy of prostate gland.

In recent times, radionuclear imaging has been extensively practiced for cancer diagnosis. In this technique, radionuclides are incorporated or chelated to targeting ligands through a chelating moiety via a peptidic spacer. However, the scope of radionuclear imaging agents is limited due to the requirement of sophisticated instruments and facilities. On the contrary, optical imaging modality has an upper-hand due to lack of radionuclide components, acquisition of high-resolution images of diseased tissues, higher sensitivity, ability to penetrate deep tissues, inexpensiveness and easy accessibility.[23]

During our current *in silico* studies on the interactions of urea ligands in the PSMA cavity, we have opined that incorporating a modified tyrosine unit in the targeting ligand may improve the binding affinity drastically. The binding mode and modifications of Tyr-urea-Glu ligand were found to be unexplored except a reported radiosynthesis of [^{18}F]Et-Tyr-urea-Glu ligand devoid of any binding affinity and biological evaluation studies in PCa cells.[24] The phenolic –OH group of the tyrosine moiety provides an opportunity to design novel urea ligands with improved interactions in the S1 pocket and better binding affinity. The presence of a phenyl ring improves hydrophobic interactions in the protein cavity, simultaneously, phenolic –OH can be modified into a bio-conjugate handle to attach peptidic spacer and a fluorescence tag. The enhanced chemical interactions of CYUE ligand with neighbouring amino acid residues in the active site of the PSMA increases the affinity and specificity of the ligand

due to the presence of an additional hydrogen bond acceptor (carbonyl moiety of the carboxylic group) and hydrogen bond donor functionality (–OH group of carboxylic acid moiety). The designed ligand was initially validated for improved binding interactions in the PSMA cavity via computational docking study and later synthesized to verify the hypothesis by biological evaluation in $PSMA^+$ and $PSMA^-$ cell lines.

Although many reports have discussed interesting ligands for PSMA, only a few studies have focused on the structural modification of PSMA ligands by skillful analysis of the protein cavity. We know that bioactive functional fragments or skeletons play a crucial role in the biological activity, and careful modifications of chemical structures of these bio-active entities can amend the biological efficacy. In this report, the designed PSMA ligand CYUE was chemically synthesized and its fluorescent version was systematically evaluated *in vitro* in $PSMA^+$ and $PSMA^-$ cells for efficient detection of prostate cancer in nanomolar concentration using optical imaging method.

5.2 Results and discussion

5.2.1 *In silico* study

5.2.1.1 QSAR Analysis

Recently, we have reported structure-activity relationship (SAR) studies of urea-based molecules as potent GCPII inhibitors.[25] Using this SAR model, we have modified the glutamic acid-urea-tyrosine (YUE, **1**) inhibitor by introducing methylene carboxylic acid moiety through the phenolic hydroxy group. Through this critical alteration, we have introduced an electron withdrawing group in the form of carbonyl oxygen, a hydrogen bond donor in the form of –OH moiety of carboxylic acid (Figure 5.1), well recommended from our SAR study. The newly designed inhibitor, CYUE, **3**, was analyzed through QSAR and the inhibitory constant was

predicted (Table 5.1). The predicted K_i value of CYUE ligand, **3** was found to be better than its parent ligand, YUE, **1**.

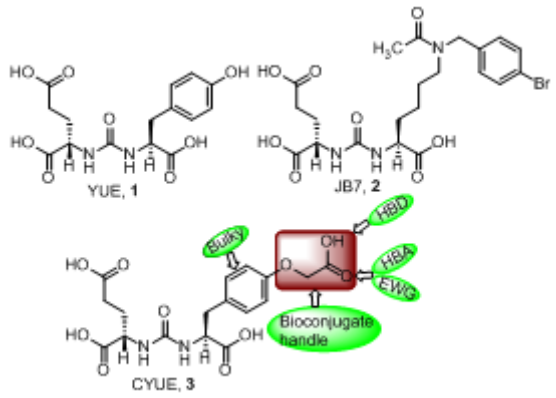

Figure 5.1 Structure of GCPII inhibitors: Tyrosine glutamic acid-based urea ligand YUE, **1**; GCPII co-crystallized ligand JB7, **2** (PDB 4NGM); Carboxymethyl protected tyrosine glutamic acid-based urea ligand CYUE, **3**

Table 5.1 Prediction of GCPII inhibitory activity of CYUE (**3**) and YUE (**1**) ligands.

Ligands	**Predicted GCPII inhibitory activity by QSAR model**	
	pK_i	**K_i (nM)**
CYUE (**3**)	**7.2580**	55.21
YUE (**1**)	6.9566	110.51

5.2.1.2 Molecular docking analysis

It is well documented that in GCPII cavity, several amino acids present in S1 and S1′ pockets are crucial for better protein-ligand interactions. Moreover, the orientation of the amino acids and bimetallic zinc centers of GCPII determine the overall binding affinity of the ligand. Arg 210, Asn 257, Lys 699, Tyr 552, Tyr 700, Glu 424, and Glu 425 residues constitute

the S1′ binding site in the protein and interact with the glutamic acid functionality of the urea ligand. The β15/ β16 hairpin bend with Lys 699 and Tyr 700 amino acid residues acts as a "glutarate sensor"[10] which has been carefully preserved in designing new ligands for PSMA. Any modifications in this part of the ligand may be detrimental resulting in loss of binding efficacy to PSMA. However, the S1 site of PSMA consisting of Gly 518, Asn 519, Arg 534, Arg 536 amino acid residues has considerable scope for modification of ligand architecture.

Keeping this in mind, a detailed docking study was performed on the designed urea ligand, CYUE. JB7, a urea-based inhibitor, co-crystallized with GCPII (PDB: 4NGM) was selected from the protein data bank as a reference for performing the computational study. To validate the docking protocol, JB7 was re-docked in the active site of GCPII, and RMSD value was calculated to be 1.09 Å with respect to its co-crystallised orientation. The RMSD value was found to be less than the crystal resolution of 4NGM protein structure (1.84 Å) which suggests that the docking protocol is reliable. The similarity score of pre and post-docking poses of JB7, which is a crucial indicator for the validation of the protocol, was found to be 0.917 (Figures 5.2 and 5.3).

After the validation, the same docking protocol was implemented for YUE and newly designed CYUE ligands to predict the probable interactions with the amino acid residues that might be responsible for GCPII inhibitory activity. According to the post-docking orientation of the three ligands (CYUE, YUE, JB7), glutamic acid moieties were superimposed on each other at the S1′ site of GCPII protein (Figure 5.4). The α–carboxylic acid group of tyrosine amino acid in YUE (**1**) was positioned differently as compared to α–carboxylic acid of lysine in JB7.

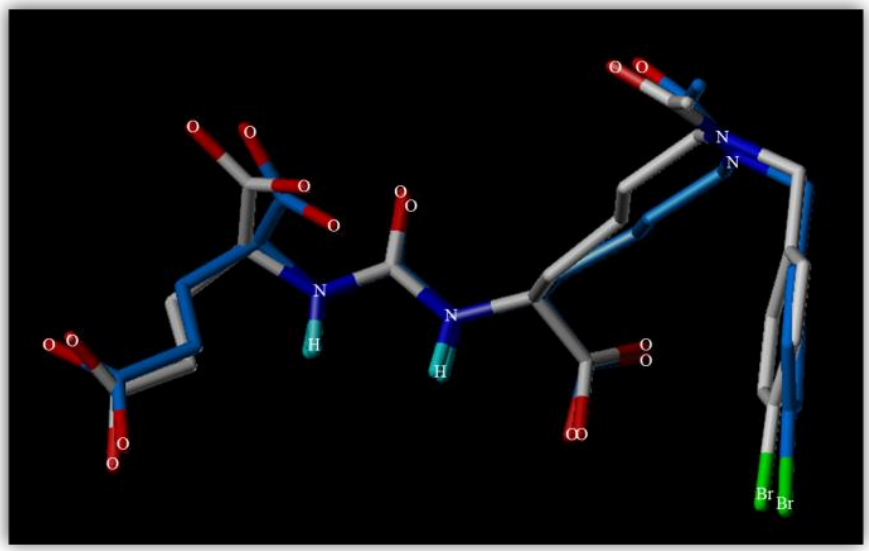

Figure 5.2 Superimposed orientation of GCPII co-crystallised (PDB 4NGM) with ligand JB7; native (blue) and docked orientations (white)

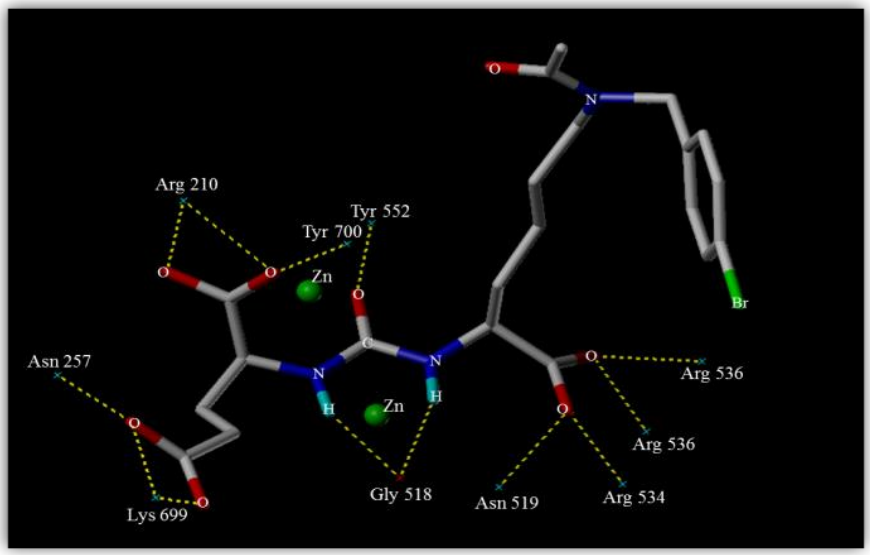

Figure 5.3 Post-docking hydrogen bonding interactions of JB7 in the cavity of GCPII protein (PDB 4NGM)

On the contrary, in CYUE (**3**), the orientation of α–carboxylic acid of modified tyrosine was perfectly aligned to the α–carboxylic acid of lysine in JB7.

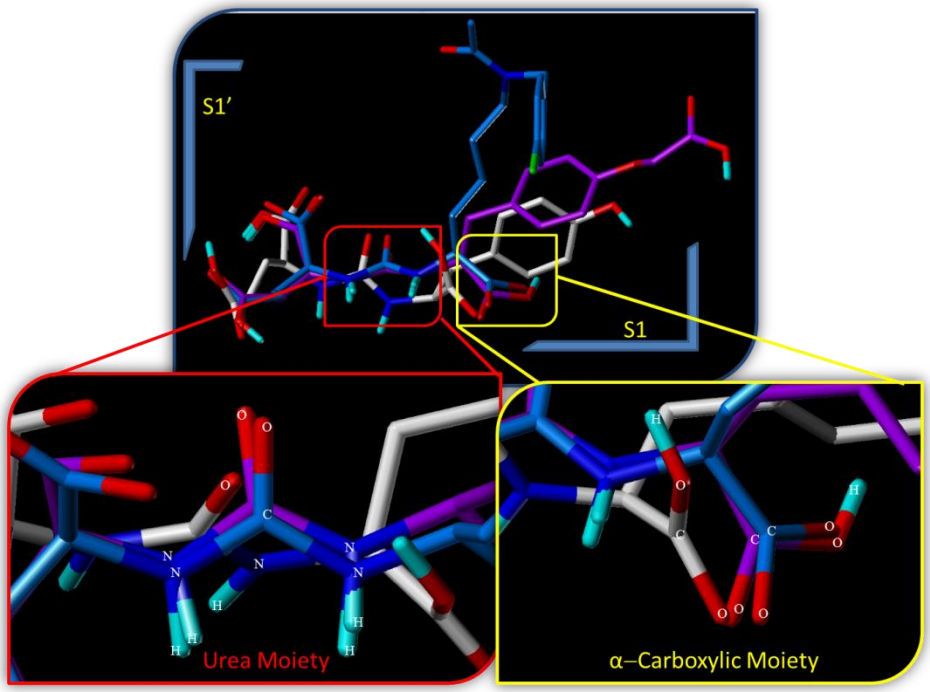

Figure 5.4 Super-imposed docked poses of JB7 (**2**, blue), CYUE (**3**, purple) and YUE (**1**, white) ligands, at the active site of GCPII protein. S1′ and S1 are the sites present in the active cavity of GCPII protein. The urea moiety of the ligands **1–3** is mentioned within the red box and the α–carboxylic group in the yellow box

Furthermore, urea moiety of YUE (**1**) was in a different alignment as compared to JB7 (Figure 4). As a result, carbonyl oxygen of urea moiety moved away from the catalytic Zn atoms of GCPII. For YUE (**1**), the distances between oxygen and zinc-1 or zinc-2 atoms were calculated to be 3.52Å and 5.33Å, respectively, which are much higher than the corresponding distances in the native orientation of JB7. After the strategic modification in YUE (**1**), the carbonyl oxygen of urea in CYUE (**3**) shifted towards the zinc atoms and the resultant distance between oxygen and zinc-1 or zinc-2 atoms reduced to 1.97 Å and 3.82 Å, respectively. This has led to a sharp reduction in the overall potential energy of the protein-ligand complex, leading to an improvement in the

binding affinity of CYUE (**3**) ligand. Additionally, the docking score of **3** was found to be 13.54 which were higher than for **1** (Table 5.2).

Table 5.2 Docking scores of ligands JB7, CYUE and YUE

Ligands	Total Score	Similarity Score
JB7 (**2**)	16.46	0.917
CYUE (**3**)	13.54	0.545
YUE (**1**)	12.31	0.482

In the hydrogen bonding interaction analysis, at S1′ site, CYUE (**3**) interacts with six amino acid residues (Arg 210, Asn 257, Lys 699, Tyr 552, Tyr 700 and Glu 425) present in the protein cavity (Figure 5.5) whereas YUE (**1**) interacts with only five of the amino acid residues at the GCPII S1′ site (Figure 5.6). Due to the strategic incorporation of carboxylic acid methylene spacer, CYUE (**3**) ligand has generated two new hydrogen bonding interactions with Asn 257 and Tyr 700 residues at S1′ site. At S1 site, due to the introduction of structural modification, a drastic change in the interaction of CYUE (**3**) is noticed. The CYUE (**3**) ligand generates five new hydrogen bonding interactions with the three new amino acid residues (Gly 518, Arg 536 and Asn 544). In summary, CYUE (**3**) interacts with twelve amino acid residues resulting in the formation of fifteen H-bonds, whereas YUE (**1**) interacts with only eight amino acid residues through thirteen H-bonds (Table 5.3). The enhanced interactions of CYUE (**3**) with a greater number of amino acids at GCPII active site has reflected in better docking score of **3** and improved binding affinity. The docking orientation and H-bonding interactions of CYUE (**3**) and YUE (**1**) with GCPII are depicted in figures 5.5 and 5.6, respectively.

Table 5.3 Comparative analysis of H-bonding interactions of JB7 (**2**), CYUE (**3**) and YUE (**1**) ligands at the GCPII active site (H-bond lengths are mentioned in Å).

Site	Amino Acid Residues	JB7-Natural Interactions	JB7 Post Docking Interactions	CYUE (3)	YUE (1)
S1' site of GCPII receptor	**Arg 210**	2.80	2.13, 2.41	2.69, 2.27	2.33, 1.95
	Asn 257	2.89	2.04	1.82	
	Lys 699	2.70	1.84, 2.62	1.79	1.97, 2.11
	Tyr 552	2.63	1.67	2.35	1.98
	Tyr 700	2.53	1.87	2.33	
	Glu 424	3.01			2.32, 2.01 1.94
	Glu 425			2.41	2.19, 2.47
S1 site of GCPII receptor	**Gly 518**	3.04, 3.05	2.13, 2.05	2.23, 2.37	
	Asn 519	2.98	2.51	1.86	1.90
	Arg 534	2.84	2.03	1.99	2.11
	Arg 536	2.99, 3.00	2.11, 2.40	2.04. 2.02	
	Glu 457			2.42	1.81
	Asn 544			1.91	
Distance between urea carbonyl oxygen and Zn-1 atom		2.57	2.66	1.97	3.52
Distance between urea carbonyl oxygen and Zn-2 atom		4.55	4.61	3.82	5.33

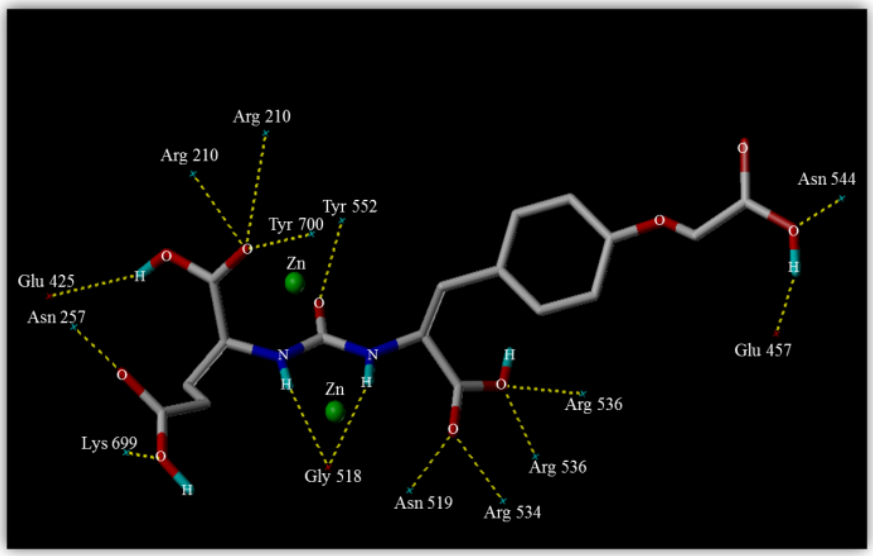

Figure 5.5 Docking orientation and hydrogen bonding interactions of CYUE (**3**) ligand at the site of GCPII protein (PDB 4NGM)

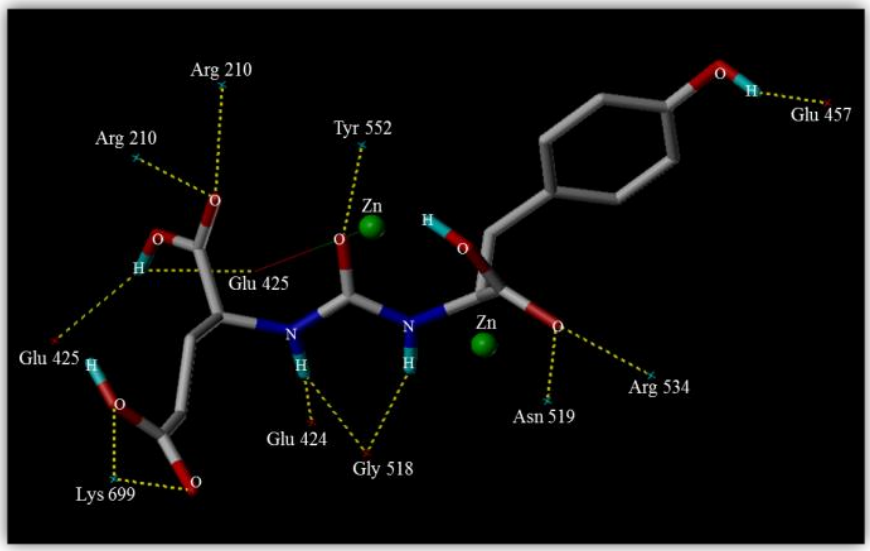

Figure 5.6 Docking orientation and hydrogen bonding interactions of YUE (**1**) at the site of GCPII protein (PDB 4NGM)

After a thorough analysis of docking and hydrogen bonding interactions of CYUE (**3**), we plan to conjugate CYUE (**3**) ligand to a fluorescent agent, rhodamine B, through a peptidic spacer for the development of a

diagnostic tool, **16**, for imaging $PSMA^{+}$ cancers. Before synthesizing the complete bio-construct, **16**, we were also curious to analyze the binding mode of **16** in the PSMA active site. The docking studies as depicted in figure 5.7 clearly indicates that the H-bonding interactions of **16** are like that of the non-conjugated CYUE (**3**) ligand in addition to the presence of few extra H-bonding interactions with Arg 463 and Lys 514 residues of the protein. The superimposition of fluorescent conjugate **16** with JB7 native pose clarifies that the conjugated CYUE (**3**) ligand is well aligned with the co-crystallised ligand (JB7) while the bulky rhodamine B moiety remains suspended outside the protein cavity and does not hamper the binding of **16** at the active site of GCPII (Figure 5.8).

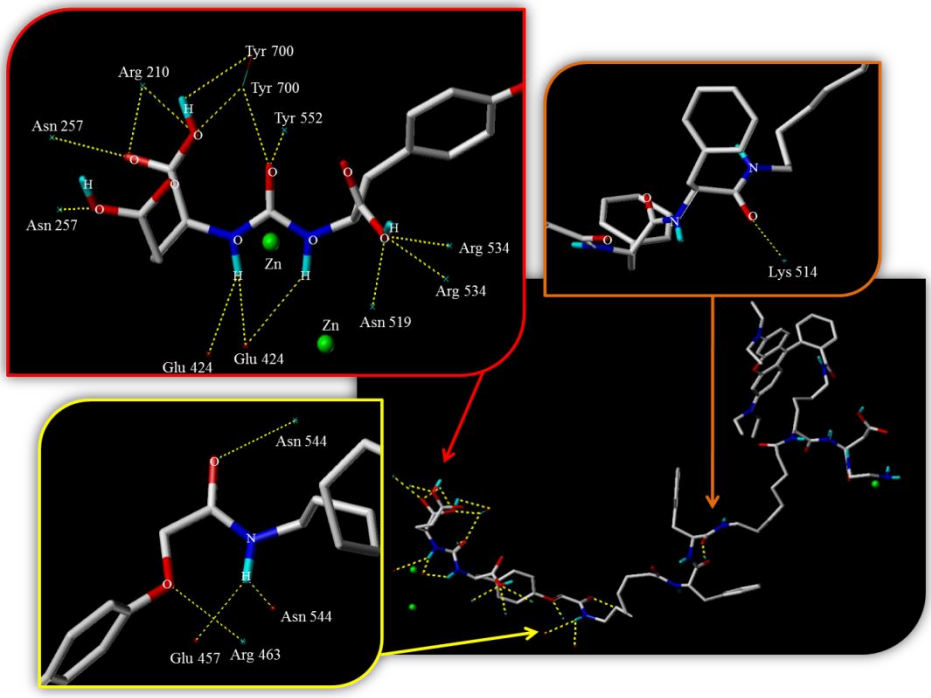

Figure 5.7 Docking orientation and hydrogen bonding interactions of CYUE-Rhodamine B conjugate (**16**) at the site of GCPII protein (PDB 4NGM)

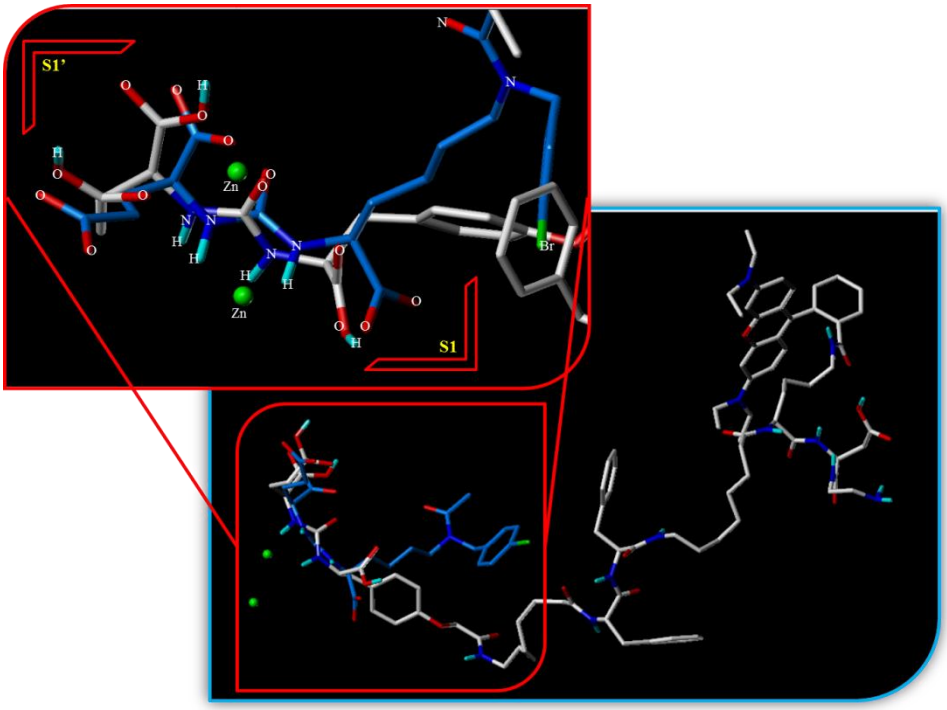

Figure 5.8 Superimposed docked orientations of CYUE-Rhodamine conjugate (**16**, white) and JB7 (**2**, blue)

5.2.2 Chemical synthesis

The synthetic route to prepare the targeting ligand, CYUE (**3**) and fluorescent conjugate (**16**) are depicted in the Schemes 5.1 and 5.2. As outlined in Scheme 5.1, bis(*tert*-butyl)-*L*-glutamate **4** was treated with triphosgene in the presence of triethylamine to form an isocyanate intermediate **5**. *In situ* reaction of **5** with *L*-tyrosine *tert*-butyl ester **6** resulted in the formation of the tris(*tert*-butyl)carboxylic acid protected urea precursor **7**. To our delight, free phenolic hydroxyl present in *L*-tyrosine *tert*-butyl ester **6** doesn't compete with the reaction of **5** to form a carbamate. However, the amino group of **6** reacted exclusively with **5** to give **7** in an excellent yield of 90%. Further, the phenolic hydroxy group of **7** was alkylated with α-bromomethylacetate **8**, in the presence of Cs_2CO_3 in DMF at room temperature to provide **9** in moderate yield. The crucial step for regenerating the carboxylic acid group from **9**, required for

solid phase peptide synthesis of bio-construct **16**, was carried out by the hydrolysis of the methylester **9** using trimethyltin hydroxide as a saponification agent. The methylester **9** was successfully hydrolyzed in a good yield of 76% to provide the required, tris(*tert*-butyl)carboxylic acid protected PSMA ligand precursor **10** (Scheme 1).

Scheme 5.1 Synthesis of PSMA ligand precursor **10**

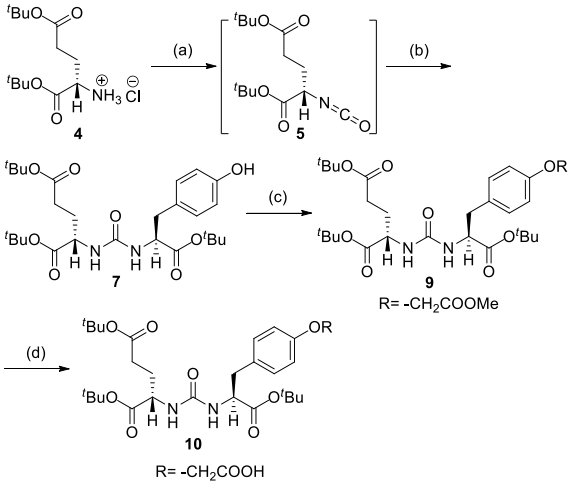

Reagents and conditions: (a) Triphosgene, triethylamine, dichloromethane (CH_2Cl_2), –50 °C to rt, 1.5 h; (b) *L*-Tyrosine *tert*-butyl ester (**6**), triethylamine, dichloromethane (CH_2Cl_2), rt, overnight; (c) α-Bromomethylacetate (**8**), Cs_2CO_3, *N*,*N*-dimethyl formamide (DMF), rt, 4 h; (d) Me_3SnOH, 1,2-dichloroethane (DCE), 80 °C, 4 h

An elaborate solid phase peptide synthesis for the construction of required PSMA targeted fluorescent conjugate **16** is described in Scheme 5.2. Solid phase peptide synthesis of **16** was performed using commercially available 1,2-diaminoethanetrityl resin **11**. The primary amino group present in **11** was coupled with Fmoc-Asp(O^{t}Bu)-OH using PyBOP as a coupling agent to provide the dipeptide **12**. The NHFmoc amino group in the growing dipeptide chain **12** was deprotected using a solution of 20% piperidine in DMF. The Fmoc free amino group generated from **12** was coupled with Fmoc-Lys(Tfa)-OH using standard coupling reagent to provide the

growing tripeptide chain **13.** It is important to mention that the α-amino group of lysine protected as NHFmoc was labile to 20% piperidine in DMF and readily available for construction of next amide bond in the growing tripeptide chain whereas the ε-amino group of lysine protected as trifluoroacetyl group was stable under NHFmoc cleavage condition and it readily undergoes deprotection in 2M aqueous piperidine. The selection of α- and ε-amine protecting groups in the lysine amino acid, which are labile under different basic conditions, was crucial to our strategy of attaching a fluorescent agent to ε-amino group of lysine in the final step of the preparation of conjugate **16**. The NHFmoc amino group in the growing tripeptide chain **13** was deprotected using a solution of 20% piperidine in DMF. The Fmoc free amino group in **13** was now sequentially coupled with Fmoc-8-aminocaprylic acid, two molecules of Fmoc-Phe-OH and another molecule of Fmoc-8-aminocaprylic acid using standard amide coupling reagents to provide the growing heptapeptide chain **14**. Addition of two molecules of 8-aminocaprylic acid to the peptide chain provides a 16-carbon atoms alkyl thread and ensures that the cargo of fluorescent agent is safely distanced away from the hydrophobic pocket along 20Å deep tunnel present in the PSMA protein. In the peptidic spacer, the attachment of two phenylalanine moieties was essential and added to provide necessary hydrophobic interactions with the binding pocket present in the 20Å tunnel of the PSMA protein.[12] The amino group present in the NHFmoc protected heptapeptide chain **14** now awaits final attachment of tris(*tert*-butyl)carboxylic acid protected PSMA ligand precursor **10**. This was successfully achieved to provide the required trifluoroacetyl amino protected lysine polypeptide chain **15** and confirmed by observation of the negative Kaiser test. Having constructed the masked polypeptide chain **15**, the final step was deprotection of trifluoroacetyl protected ε-amino group of lysine using aqueous piperidine conditions to expose the free ε-amino group that can be tagged with a fluorescent agent, rhodamine B. The ε-amino trifluoroacetyl protecting group in **15** was

Scheme 5.2 Synthesis of PSMA targeting rhodamine B conjugate **16**

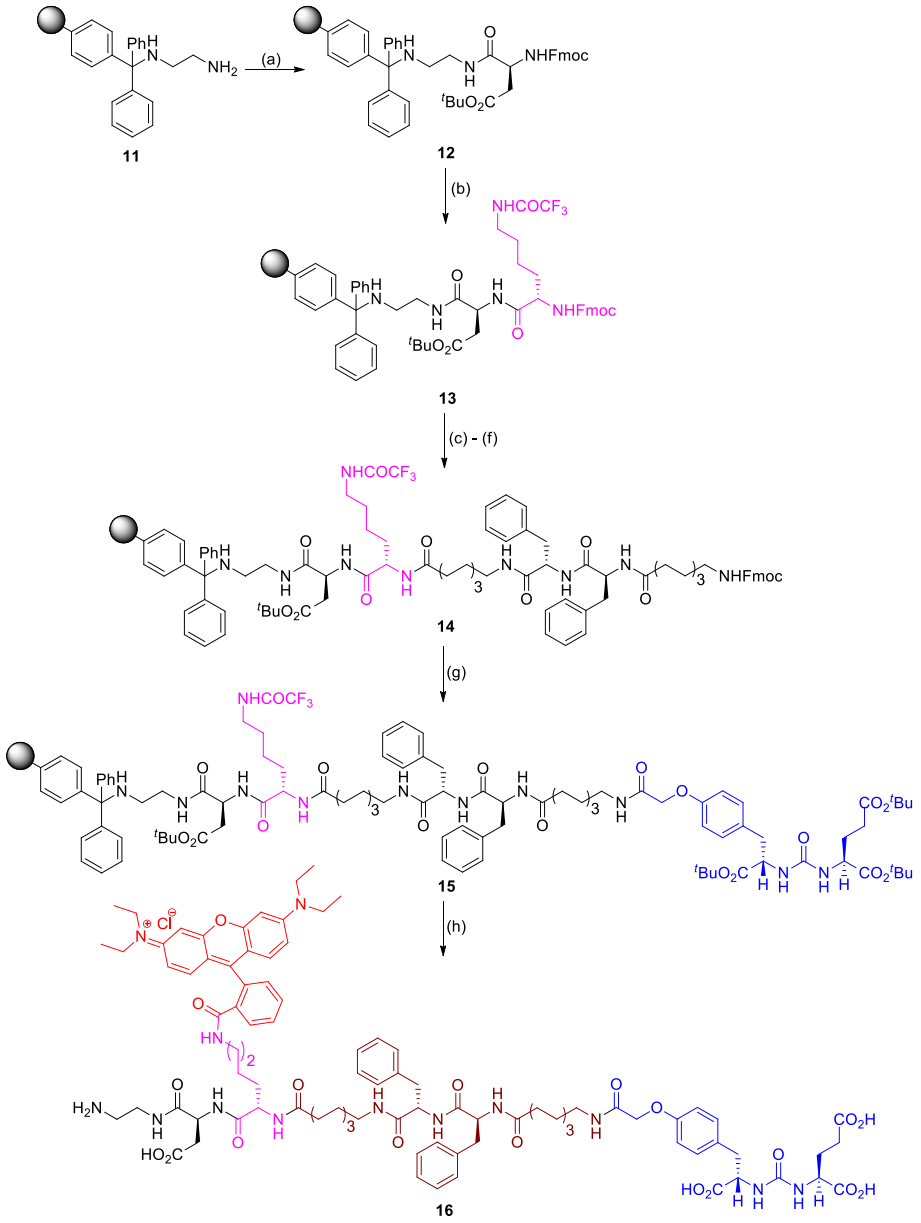

Reagents and conditions: (a) Fmoc-Asp(O^{t}Bu)-OH, PyBOP, DIPEA, DMF, 6 h; (b) (i) 20% Piperidine in DMF, rt, 30 min; (ii) Fmoc-Lys(Tfa)-OH, PyBOP, DIPEA, DMF, 6 h; (c) (i) 20% Piperidine in DMF, rt, 30 min; (ii) Fmoc-8-aminocaprylic acid, PyBOP, DIPEA, DMF, 6 h; (d) (i) 20% Piperidine in DMF, rt, 30 min; (ii) Fmoc-Phe-OH, PyBOP, DIPEA, DMF, 6 h; (e) (i) 20% Piperidine in DMF, rt, 30 min; (ii) Fmoc-Phe-OH,

PyBOP, DIPEA, DMF, 6 h; (f) (i) 20% Piperidine in DMF, rt, 30 min; (ii) Fmoc-8-aminocaprylic acid, PyBOP, DIPEA, DMF, 6 h; (g) (i) 20% Piperidine in DMF, rt, 30 min; (ii) CYUE($O^tBu)_3$-OH, PyBOP, DIPEA, DMF, 6 h; (h) (i) 2M Piperidine in water, rt, 6–12 h; (ii) Rhodamine B, PyBOP, DIPEA, DMF, 6 h; (iii) TFA:TIS:H_2O (95:2.5:2.5) (1 × 5 mL, 30 min; 2 × 2.5 mL, 15 min); (iv) Evaporate TFA; (v) Precipitate in ice-cold diethylether

deprotected successfully using 2M aqueous piperidine[26] and the fluorescent agent, rhodamine B was coupled using PyBOP as a coupling agent to give *t*-butylcarboxylic acid protected precursor of the final conjugate **16**. The PSMA targeting rhodamine B conjugate **16** was released from the 1,2-diaminoethanetrityl resin, and simultaneously all the *tert*-butylcarboxylic acids are deprotected with the help of a cleaving cocktail TFA:TIS:H_2O (95:2.5:2.5). Excess trifluoroacetic acid was evaporated under reduced pressure using rotary evaporator, and the turbid pink viscous liquid is precipitated by the addition of ice-cold ether. The pink colored precipitate was washed thrice with ice-cold ether, centrifuged and dried under an inert atmosphere to provide the final PSMA targeting rhodamine B conjugate **16** that was purified using reverse phase HPLC.

5.2.3 *In vitro* studies

The selective uptake of the newly synthesized bio-construct **16** was evaluated by confocal laser scanning microscopy (CLSM) in LNCaP cells (PSMA +ve) and PC-3 cells (PSMA –ve). LNCaP and PC-3 cells were incubated with four different concentrations of the fluorescent conjugate viz., 10, 25, 50 and 100 nM (Figure 5.22). The fluorescence intensity in the cytoplasm of the LNCaP cells increases with the increase in the concentrations of **16**. The microscopic studies also reveal the distribution of the bio-construct **16** throughout the cytoplasm of $PSMA^+$ LNCaP cells. The lack of fluorescence signal in the PC-3 cells proves that the ligand

conjugate **16** is protein specific. *In vitro* specificity of bioconjugate **16** was further examined by prior incubation of LNCaP cells with a 100-fold excess of a standard inhibitor, 2-PMPA. PSMA receptors blocked LNCaP cells display minimal uptake confirming the uptake of the bioconjugate **16** via receptor-mediated endocytosis and not through non-specific pathways (Figure 5.9). Thus, we have successfully demonstrated that the fluorescent conjugate **16** traffic to the cytoplasm of the prostate cancer cells via PSMA mediated receptor endocytosis mechanism. The bio-construct **16** is target specific, proving it to be an excellent potential candidate for delivery of payloads to cancer cells.

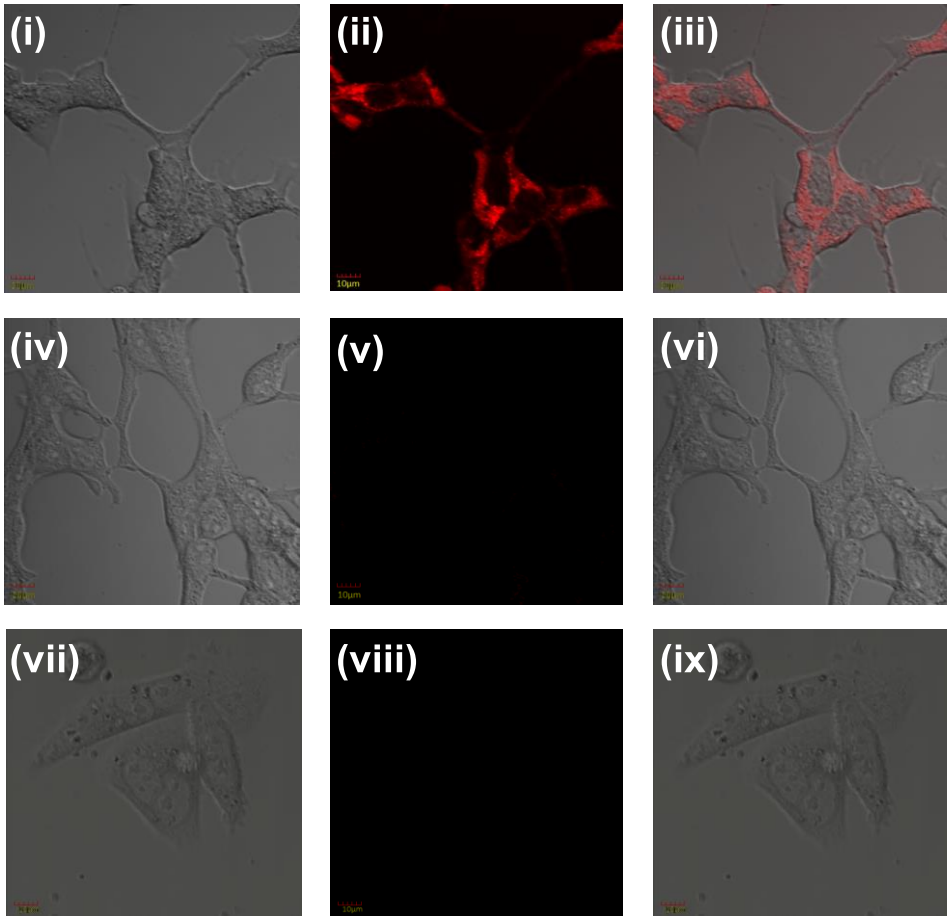

Figure 5.9 (i) and (iv) DIC images of LNCaP cells ($PSMA^+$), (ii) Binding and internalization of CYUE rhodamine B conjugate **16** in LNCaP cells ($PSMA^+$) at 100 nM concentration, (iii) Overlay of (i) and (ii) to show that

the uptake of **16** is in the cytoplasm of LNCaP cells, (v) Binding and internalization of **16** in the presence of 100-fold excess of 2-PMPA to block the PSMA receptors, (vi) Overlay of (iv) and (v) showing negligible uptake of CYUE rhodamine B conjugate, (vii) DIC image of PC-3 cells ($PSMA^-$), (viii) Specificity of CYUE rhodamine B conjugate in PC-3 cells ($PSMA^-$), (ix) Overlay of (vii) and (viii)

The binding affinity of CYUE fluorescent conjugate **16** on $PSMA^+$ cells was estimated by analyzing uptake studies in LNCaP cells using Fluorescence Activated Cell Sorting (FACS) technique. The conjugate's ability to bind to PSMA is evaluated by measuring the mean fluorescence intensity per cell for different concentrations of the conjugate. A hyperbolic curve of different concentrations of the fluorescent inhibitor against the mean fluorescence intensity of **16** by $PSMA^+$ LNCaP cells yielded a dissociation constant K_D value of 88 nM (Figure 5.10).

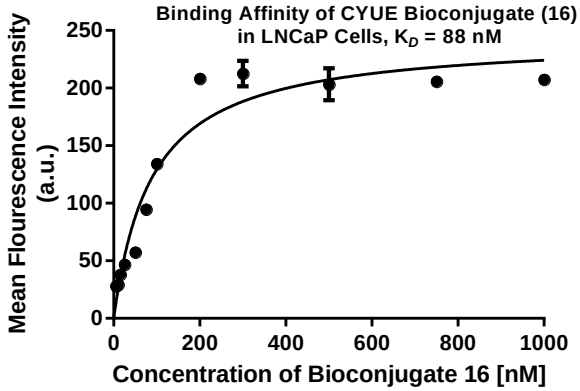

Figure 5.10 Binding of CYUE-Rhodamine conjugate **16** in $PSMA^+$ LNCaP cells for a range of concentrations plotted against the mean fluorescence intensity to yield a dissociation constant K_D of 88 nM

The curve shows a slow exponential increase in the uptake of the fluorescent conjugate **16** targeted to the PSMA receptor followed by saturation of the curve for concentrations higher than 200 nM due to full occupancy of PSMA receptors present in the LNCaP cells with the

conjugate **16**. The low dissociation constant value (< 100 nM) gives undisputable evidence of the high affinity of the ligand-peptide spacer to the PSMA protein and its perfect fit inside the protein tunnel.

5.3 Conclusion

In summary, we have developed a novel tyrosine-based asymmetric urea ligand (CYUE) for targeting $PSMA^+$ cancers based on a comprehensive SAR studies established from our research findings. Through docking studies, a reasonable explanation was provided for the improved binding affinity of the new PSMA ligand. Further, CYUE ligand was chemically synthesized and transformed into a fluorescent labeled oligopeptide bio-construct to target $PSMA^+$ cancers. Successful *in vitro* application by targeted delivery and binding affinity measurement studies have set the platform for future *in vivo* studies and clinical use of the bio-construct as an imaging agent for detection of deeply seated tumour tissues during intraoperative surgery.

5.4 Experimental section

5.4.1 Molecular docking study

The crystal structure of the target protein Glutamate carboxypeptidase II (PDB: 4NGM) was retrieved from the protein data bank. In 4NGM, GCPII was co-crystallised with a urea-based ligand JB7, which is structurally very close to the designed CYUE (**3**) ligand. Docking studies were performed by the Surflex Dock method using Sybyl X 2.1.1 software.

All the water molecules were removed from 4NGM, and the missing hydrogen atoms were added. Force field AMBER7FF99 was applied to minimize the energy of the protein. A protomol was generated at the active site of protein and CYUE (**3**), YUE (**1**) and JB7 (**2**) ligands were docked into the PSMA cavity to check their respective interactions with the protein by using the same protocol. Later, to obtain an insight into the

binding interactions of CYUE-Rhodamine B conjugate **16** with PSMA protein, bigger protomol was generated, and the docking study was performed by keeping all the other *in silico* parameters constant.

RMSD values were calculated for co-crystallised JB7 and re-docked JB7 by importing docking outputs files in Discovery studio 4.0. RMSD values lesser than 2Å are generally considered as an indicator of docking protocol validity.

The Surflex docking module of software Sybyl uses a similarity score (ranging from -1 to +1) to compare the orientation of newly designed ligand with the reference ligand, and +1 is considered as ideal match according to the orientation of ligand in the protein cavity.

5.4.2 Synthesis

1,2-Diaminoethanetrityl resin, Fmoc-amino acids, coupling reagents and solvents used in the solid phase peptide synthesis (SPPS) as well as in the chemical synthesis were purchased from Iris Biotech GmbH, Sigma Aldrich, Merck, and Spectrochem. Various dry solvents were prepared by using appropriate drying agents and standard procedures. Moisture and oxygen sensitive reactions were carried out under a nitrogen atmosphere. Thin layer chromatography (TLC) was performed on silica gel glass TLC plates (60 F_{254}) and visualized under UV light to monitor the progress of the reaction. All compounds were purified by column chromatography using 100–200 or 230–400 mesh silica-gel as the stationary phase. Distilled hexane and ethyl acetate were used as eluents in the column chromatography.

Peptide synthesis was performed manually by using peptide vessels (Chemglass) and standard peptide coupling procedures. ^{1}H and ^{13}C NMR spectra were recorded using Bruker AV 400 MHz NMR spectrometer with TMS as an internal standard. ^{1}H NMR signals were reported in ppm with

reference to residual $CHCl_3$ (7.25 ppm), and multiplicity was reported as s = singlet, d = doublet, t = triplet, q = quartet, m = multiplet or unresolved, and brs = broad singlet, with coupling constants in Hz. $CDCl_3$ was used as the solvent for recording NMR spectra. Mass spectra were recorded on Bruker micro TOF-Q II instrument using positive or negative mode electrospray ionization methods.

The purity of CYUE-Rhodamine B peptide conjugate **16** was analyzed using Dionex HPLC-Ultimate 3000 Analytical HPLC instrument. The peptide conjugate **16** was purified using RP-PFP column (XSelect CSH Prep Fluorophenyl 5 µm OBD, 19 mm × 150 mm) in Buchi Reveleris High Performance Preparative Chromatography instrument.

5.4.2.1 Synthesis of PSMA ligand precursor 10

5.4.2.1.1 Synthesis of (*S*)-di-*tert*-butyl 2-(3-((*S*)-1-(*tert*-butoxy)-3-(4-hydroxyphenyl)-1-oxopropan-2-yl)ureido)pentane dioate (7)

Triphosgene (0.100 g, 0.33 mmol) was dissolved in dry dichloromethane (5 mL) and the solution was stirred at –50 °C under an inert atmosphere in a double-neck round-bottom flask (50 mL). Bis(*tert*-butyl)-*L*-glutamate hydrochloride salt **4** (0.296 g, 1.00 mmol) dissolved dry DCM (2 mL) was added to the triphosgene solution at –50 °C and triethylamine (0.460 mL, 3.3 mmol) was added dropwise to the reaction mixture. The reaction mixture was stirred for 1.5 h at –50 °C and stirred for another 1.5 h at room temperature for the generation of isocyanate intermediate **5**. Thereafter, a solution of *L*-tyrosine-*tert*-butyl ester **6** (0.237 g, 1.0 mmol) and triethylamine (0.1 mL, 0.66 mmol) in dry DCM (2 mL) was added to the reaction mixture and the progress of reaction was monitored through TLC using ethyl acetate and hexane (1:2) mixture as eluent. The reaction mixture was further stirred for overnight at room temperature. After the completion of the reaction, the reaction mixture was concentrated under reduced pressure, diluted with ethyl acetate (25 mL), washed with water (2

× 10 mL) and brine (2 × 10 mL). The organic layer was dried over anhydrous Na_2SO_4, filtered and the solvent was evaporated under reduced pressure to afford the crude reaction mixture which was purified by column chromatography over 100–200 mesh silica gel using 25–30% ethyl acetate and hexane as eluent. The purified compound **7** was obtained as a colourless viscous liquid which gradually solidified to white solid; Yield 90% (0.469 g); R_f = 0.4 (EtOAc: hexane = 1:2); IR (CH_2Cl_2) 3366 (O–H), 3123 (N–H), 2979 (=C–H), 2932 (C–H), 1732 (C=O), 1642 (N–H), 1557 (C=C), 1455 (C–H), 1155 (C–O), 751, 698 (=C–H) cm^{-1}; ^1H NMR ($CDCl_3$, 400 MHz) δ 6.97 (d, J = 7.80 Hz, 2H), 6.69 (d, J = 7.80 Hz, 2H), 6.44 (brs, 1H) 5.18 (d, J = 7.52 Hz, 1H), 5.06 (d, J = 7.52 Hz, 1H), 4.62–4.47 (m, 1H), 4.38–4.25 (m, 1H), 2.98–2.91 (m, 2H), 2.35–2.15 (m, 2H), 2.10–1.94 (m, 1H) 1.83–1.69 (m, 1H), 1.44 (s, 9H), 1.41 (s, 18H); ^{13}C NMR ($CDCl_3$, 100 MHz) δ 172.6, 172.5, 171.7, 156.9, 155.4, 130.6, 127.5, 115.5, 82.3, 82.1, 80.7, 54.7, 52.9, 37.7, 31.6, 28.3, 28.05, 28.0; HRMS (ESI) m/z calcd for $C_{27}H_{42}N_2O_8$ $[M+Na]^+$ 545.2833, found 545.2734.

5.4.2.1.2 Synthesis of (*S*)-di-*tert*-butyl-2-(3-((*S*)-1-(*tert*-butoxy)-3-(4-(2-methoxy-2-oxoethoxy)phenyl)-1-oxopropan-2-yl)ureido)pentanedioate (9)

Compound **7** (0.400 g, 0.77 mmol) and Cs_2CO_3 (0.375 g, 1.15 mmol) were suspended in freshly distilled dry DMF (5 mL) in a round-bottom flask (50 mL) and the resulting mixture was stirred for 30 minutes at room temperature. α-Bromomethylacetate **8** (0.17 mL, 1.53 mmol) was added to the reaction mixture and the reaction progress was monitored by TLC using ethyl acetate and hexane as eluent. The reaction was continued for 4 h until all the starting material was consumed and quenched immediately to avoid side product formation by adding brine solution (15 mL) followed by ethyl acetate (25 mL). The organic layer was extracted with ethyl acetate (2 × 25 mL) and dried over anhydrous Na_2SO_4. The solvent was

filtered, concentrated under reduced pressure using rotary evaporator. The crude reaction mixture was purified through column chromatography using 100–200 mesh silica gel using 25% ethyl acetate-hexane mixture as eluent. The pure compound **9** was obtained as colourless viscous liquid which solidified on standing; Yield 89% (0.409 g); R_f = 0.42 (EtOAc: hexane = 1:2); IR (CH_2Cl_2) 3341 (N–H), 2979 (=C–H), 2932 (C–H), 1732 (C=O), 1657 (N–H), 1517 (C=C), 1455 (C–H), 1155 (C–O), 748, 698 (=C–H) cm^{-1}. ^1H NMR ($CDCl_3$, 400 MHz) δ 7.08 (d, *J* = 8.28 Hz, 2H), 6.81 (d, *J* = 8.28 Hz, 2H), 4.95 (d, *J* = 7.80 Hz, 1H), 4.87 (d, *J* = 7.80 Hz, 1H), 4.59 (s, 2H), 4.58–4.52 (m, 1H), 4.76 (ddd, *J* = 6.26, 5.50, 5.00 Hz, 1H), 3.79 (s, 3H), 3.02 (dd, *J* = 14.04, 5.24 Hz, 1H), 2.96 (dd, *J* = 14.04, 6.28 Hz, 1H), 2.40–2.15 (m, 2H), 2.12–1.98 (m, 1H), 1.89–1.76 (m, 1H), 1.46 (s, 9H); 1.41 (s, 9H), 1.38 (s, 9H); ^{13}C NMR ($CDCl_3$, 100 MHz) δ 171.4, 171.0, 170.3, 168.4, 155.7, 155.40, 129.8, 128.7, 113.5, 81.04, 81.01, 79.5, 64.4, 53.5, 52.0, 51.2, 36.8, 30.6, 27.3, 27.0, 26.99, 26.96; HRMS (ESI) m/z calcd for $C_{30}H_{46}N_2O_{10}$ $[M+Na]^+$ 617.3045, found 617.2944.

5.4.2.1.3 Synthesis of 2-(4-((*S*)-3-(*tert*-butoxy)-2-(3-((*S*)-1,5-di-*tert*-butoxy-1,5-dioxopentan-2-yl)ureido)-3-oxopropyl) phenoxy)acetic acid (10)

A mixture of **9** (0.235 g, 0.40 mmol), Me_3SnOH (0.215 g, 1.19 mmol) and dry 1,2-dicloroethane (5 mL) were taken in a single neck round-bottom flask (25 mL). A reflux condenser was fitted with the round bottom flask and the reaction mixture was heated at 80 °C in an oil bath for 4 h. The reaction progress was monitored by TLC. After 4 h, the reaction mixture was concentrated under reduced pressure, diluted with ethyl acetate (25 mL) and washed with 0.1N $KHSO_4$ solution (15 mL). The organic layer was extracted with ethyl acetate (2 × 25 mL), dried over anhydrous Na_2SO_4, filtered and then concentrated under reduced pressure. The crude reaction mixture was purified through column chromatography using 100–

200 mesh silica gel using 75% ethyl acetate and hexane as eluent. The pure product of **10** was obtained as colourless viscous liquid; Yield 76% (0.172 g); R_f = 0.23 (EtOAc); IR (CH_2Cl_2) 3414 (O–H), 3357, 3124 (N–H), 2980 (=C–H), 2936 (C–H), 1731, 1707 (C=O), 1638 (N–H), 1545 (C=C), 1458 (C–H), 1158 (C–O), 750, 657 (=C–H) cm^{-1}. ^1H NMR ($CDCl_3$, 400 MHz) δ 7.04 (d, J = 7.52 Hz, 2H), 6.78 (d, J = 7.52 Hz, 2H), 5.55 (brs, 1H), 5.36 (brs, 1H), 4.70–4.20 (m, 4H), 2.97 (s, 2H), 2.35–2.15 (m, 2H), 2.10–1.95 (m, 1H), 1.87–1.72 (m, 1H), 1.45 (s, 9H), 1.41 (s, 18H); ^{13}C NMR ($CDCl_3$, 100 MHz) δ 172.7, 172.6, 172.5, 171.7, 157.1, 156.6, 130.8, 129.4, 114.5, 82.3, 82.1, 80.6, 65.4, 54.6, 52.9, 37.6, 31.6, 28.3, 28.1, 27.9*; HRMS (ESI) m/z calcd for $C_{29}H_{44}N_2O_{10}$ $[M+Na]^+$ 603.2888, found 603.2792.

*higher intensity carbon

5.4.2.2 Synthesis of fluorescent labeled CYUE bio-conjugate 16

5.4.2.2.1 Resin swelling

All the resins used in solid phase peptide synthesis were swelled initially with CH_2Cl_2 (5 mL) for 30 minutes by bubbling nitrogen, and after draining CH_2Cl_2, the resin was swelled thrice with DMF (3 × 5 mL) for 15 minutes each.

5.4.2.2.2 General procedure for the Kaiser test

Few resin beads were taken in a test-tube and 2 drops of each of ninhydrin, phenol and 0.1% potassium cyanide solution were added to the test-tube and heated for 2 minutes at 110 °C in a sand bath. The presence of a free amine group was confirmed by the appearance of dark blue colored resin beads in the test tube. The test was conducted after performing coupling of each amino acids following the aforementioned procedure.

5.4.2.2.3 General procedure for NHFmoc deprotection

The NHFmoc-amino group in the growing peptide chain was deprotected in each step using a freshly prepared solution of 20% piperidine in DMF (10 mL). Initially, 4 mL of the 20% piperidine solution in DMF was added to the resin beads and mixed for 10 minutes by bubbling nitrogen gas. The solution was drained from the resin beads, and the procedure was repeated twice with the remaining 20% piperidine solution (2 × 3 mL) for 10 minutes each to ensure complete deprotection of NHFmoc protecting group.

5.4.2.2.4 Typical solid phase peptide synthesis (SPPS) procedure

1,2-Diaminoethanetrityl resin (0.050 g, 0.06 mmol) was swelled initially with 5 mL of DCM by bubbling nitrogen gas for 30 minutes. After draining the DCM, the resin was swelled with 5 mL DMF thrice for 15 minutes each. *N*-Fmoc-Asp(O^{t}Bu)-OH (0.061 g, 0.15 mmol), PyBOP (0.078 g, 0.15 mmol) and DIPEA (0.10 mL, 0.60 mmol) in 0.5 mL DMF was added to peptide vessel containing resin beads and the coupling reaction was continued for 6 h. The resin beads were washed with DMF (3 × 3 mL) followed by isopropanol (3 × 3 mL), and the beads were dried by a stream of nitrogen gas. The completion of the reaction was confirmed by performing the Kaiser test with few dried resin beads. A solution of 20% piperidine in DMF (10 mL) was prepared, added to the resin beads in aliquots (1 × 4 mL; 2 × 3 mL), mixed for 10 minutes each, and drained to ensure complete deprotection of Fmoc protecting group of the coupled amino acid as mentioned in the general procedure. The resin beads were washed again with DMF (3 × 3 mL) followed by isopropanol (3 × 3 mL) and dried by a stream of nitrogen gas. The formation of free amine was confirmed by performing the Kaiser test with few resin beads. A series of amino acids such as Fmoc-Lys(Tfa)-OH (0.070 g, 0.15 mmol), Fmoc-8-aminocaprylic acid (0.057 g, 0.15 mmol), Fmoc-Phe-OH (0.058 g, 0.15

mmol), Fmoc-Phe-OH (0.058 g, 0.15 mmol) and Fmoc-8-aminocaprylic acid (0.057 g, 0.15 mmol) were coupled to the growing peptide chain in a similar way as mentioned before. After the deprotection of Fmoc group from the last amino acid, Fmoc-8-aminocaprylic acid, tris-*tert*-butylcarboxylic protected CYUE precursor **10** (0.052 g, 0.09 mmol), PyBOP (0.078 g, 0.15 mmol) and DIPEA (0.10 mL, 0.6 mmol) in 0.5 ml DMF was added to the vessel and reacted for 6 h. The resin beads were washed again with DMF (3 × 3 mL) followed by isopropanol (3 × 3 mL) and dried by a stream of nitrogen gas. The completion of the reaction was confirmed by the Kaiser test with few dried resin beads. Finally, the trifluoroacetyl group of lysine was cleaved by 6–12 h treatment with 2M aqueous piperidine at room temperature and the complete deprotection of Tfa was confirmed by the Kaiser test. Rhodamine B dye (0.043 g, 0.09 mmol), PyBOP (0.078 g, 0.15 mmol) and DIPEA (0.01 mL, 0.6 mmol) in 0.5 ml DMF was added to the peptide vessel and swelled for 6 h at room temperature. The completion of the rhodamine B coupling reaction was confirmed by the Kaiser test.

5.4.2.2.5 General procedure for peptide cleavage from resin beads

A mixture of 9.50 mL trifluoroacetic acid (TFA), 0.25 mL triisopropylsilane (TIPS) and 0.25 mL Millipore water (H_2O) was prepared in a 10 mL centrifuge tube and thoroughly mixed by vortex. 5 mL of this cocktail solution was added to the dried resin beads containing peptide conjugate, and nitrogen gas was bubbled through the resin beads and cocktail mixture for 30 minutes. The cleaved peptide solution was drained from the resin beads into a single-neck round-bottomed flask (25 mL). The cleavage procedure was repeated twice (2 × 2.5 mL) with the resin beads using the remaining cocktail solution for 15 minutes each as mentioned before. The cleaved peptide solution from the peptide vessel was pooled together into a single-neck round-bottomed flask (25 mL) and then transferred to a 15 mL centrifuge tube using a Pasteur pipette. The

mother liquor from cleavage was concentrated under reduced pressure using rotavapor to evaporate trifluoroacetic acid, and the concentrated viscous liquid was treated with ice cold diethyl ether (2-3 mL) to precipitate the desired ligand-targeted peptide conjugate. The upper ether layer was discarded, and the precipitated conjugate was washed thrice with ice-cold ether (3 × 3 mL). The precipitated conjugate was dried by a stream of nitrogen gas through the centrifuge tube fitted with a septum and an outlet needle for 45 minutes.

5.4.2.2.6 Analytical HPLC method

The purity of bio-conjugate **16** was analyzed using a Dionex HPLC-Ultimate 3000 system. Typically a solution of bio-conjugate **16** (20 µL, 1.0 mg/1.0 mL) in a mixture of CH_3CN:H_2O (1: 1) was injected via autosampler and eluted using Dionex Acclaim ® 120 C_{18}, 5 µm, 4.6 mm × 250 mm analytical column at a flow rate of 1 mL/min (mobile phase, A = 0.1% trifluoro acetic acid/H_2O and B = acetonitrile). An isocratic flow of 40% B (v/v) was used during the run for 0 to 4 min, and gradually gradient of B was increased to 100% B (v/v) over a period of 40-min. The chromatogram of **16** was recorded on the Ultimate 3000 RS variable wavelength detector at 225–280 nm with t_R = 19.5 min.

5.4.2.2.7 Preparative HPLC method

The purification of bioconjugate **16** was performed using Buchi Reveleris Prep HPLC System. Crude bioconjugate **16** (20 mg) was dissolved in 1:1 ratio of CH_3CN:H_2O (1 mL) and injected into the sample injector for elution using RP-PFP (Reverse Phase PentafluoroPhenyl) preparative column (XSelect CSH Prep Fluorophenyl 5 µm OBD, 19 mm × 150 mm). A flow rate of 10 mL/min (mobile phase, A = 0.1% trifluoro acetic acid/H_2O and B = acetonitrile) is maintained throughout the run and the mobile phase gradient was increased from 1% B (v/v) to 50% B (v/v) over a period of 40 min. The mobile phase gradient was further increased to

80% B (v/v) in the next 15 min, and the chromatogram was recorded at λ = 280 or 555 nm. Pure fractions of **16** were collected using automatic fraction collector, acetonitrile was evaporated under reduced pressure, and after lyophilization pure bioconjugate **16** was obtained. HRMS (+ESI) calcd for $[M\text{-}Cl]^+$ $(C_{91}H_{120}N_{13}O_{19})^+$ 1698.8818 found 1698.8807.

5.4.3 *In vitro* studies

5.4.3.1 Culture of cell lines

LNCaP and PC-3 cell lines were purchased from the National Centre for Cell Science (NCCS), Pune, India. The cell lines were grown as a monolayer until confluent in sterile filtered RPMI 1640 medium supplemented with 10% heat-inactivated fetal bovine serum (HIFBS), 1% Penicillin-Streptomycin antibiotic and 100 mM of sodium pyruvate in 5% CO_2:95% air humidified atmosphere, at 37 ºC.

5.4.3.2 Confocal laser scanning microscopy (CLSM) studies

LNCaP (50,000 cells/well in 0.5 mL medium) and PC-3 (25,000 cells/well in 0.5 mL medium) cells were trypsinized and seeded into Nunc Lab Tek II Chambered Coverglass System for 72 h and 48 h respectively. The spent medium was replaced with increasing concentrations (10, 25, 50, 100 nM) of **16** prepared in medium (0.5 mL) and incubated at 37 °C for 1 h. For a competition experiment, LNCaP cells were incubated at 37 °C with 100–fold excess concentration of 2-PMPA before incubation with compound **16.** After rinsing with fresh medium (3 × 1.0 mL) to remove unbound conjugates, confocal images were acquired using a laser scanning confocal microscopy (FV 1000, Olympus) by excitation at 559 nm (yellow diode laser) and emission at 618 nm.

5.4.3.3 Binding affinity study in LNCaP cells

LNCaP cells were seeded in T-75 flasks and were grown for 72 hours. After 95% confluency, cells were trypsinized and centrifuged to form a cell pellet. Flow cytometry buffer was prepared by mixing 1X DPBS (50 mL), 25 mM HEPES buffer (1 mL) and EDTA (84 mg) and sterile filtered before use. 75,000 LNCaP cells in 100 uL of the medium were suspended in each of the Eppendorf tubes. The fluorescent conjugate **16** (400 uL medium) was added to the cell suspension (100 uL) to a final concentration of 5 to 1000 nM and incubated for 1 h at 4 °C. The treated cell suspension in each tube was centrifuged and washed with ice cold FACS buffer (3 × 1 mL), and the LNCaP cell pellet was suspended in ice-cold FACS buffer (1 mL) for flow cytometry analysis. The mean fluorescence intensity was measured for each sample concentration (10,000 events) using flow cytometer (LSR Fortessa, BD Biosciences). A plot of mean fluorescence intensity (a.u.) versus concentration of the test article afforded a dissociation constant (K_D) value of 88 nM for the bioconjugate **16** in LNCaP cells. The method of non-linear regression analysis was employed assuming one-site specific binding during the calculation of K_D using GraphPad Prism 6.02 software.

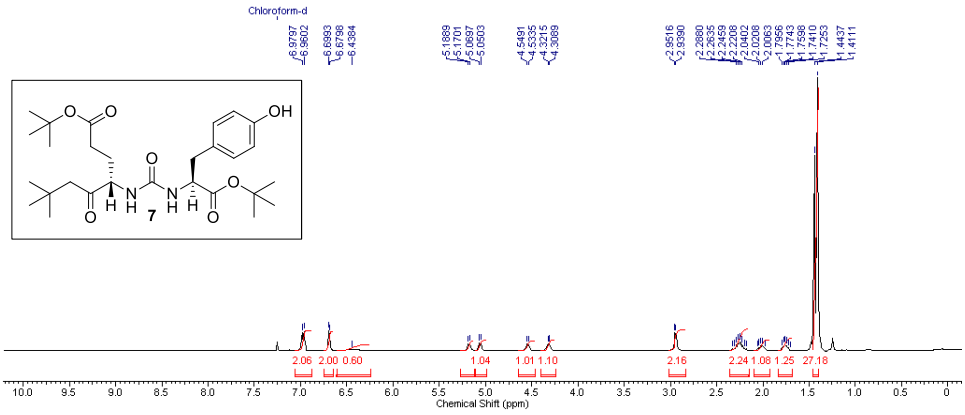

Figure 5.11 ^{1}H NMR spectrum (400 MHz, $CDCl_3$) of **7**

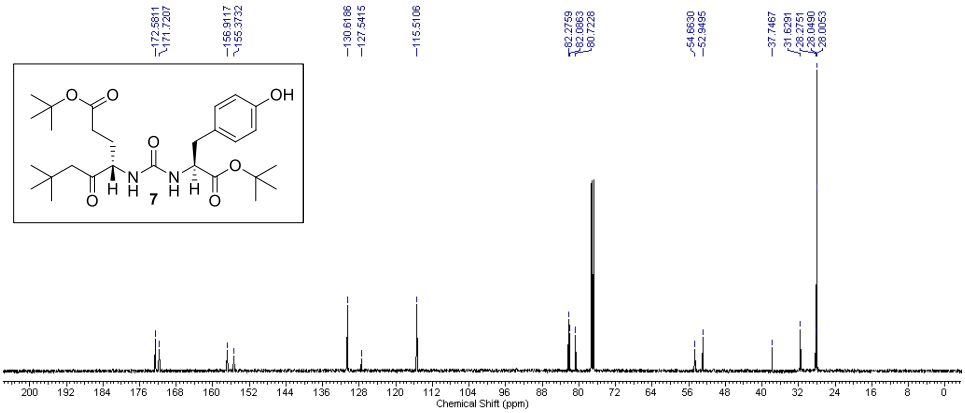

Figure 5.12 ^{13}C NMR spectrum (100 MHz, $CDCl_3$) of **7**

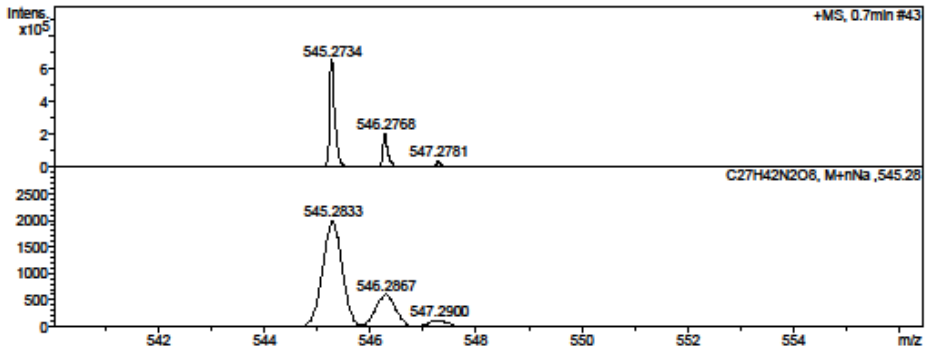

Figure 5.13 HRMS of **7**

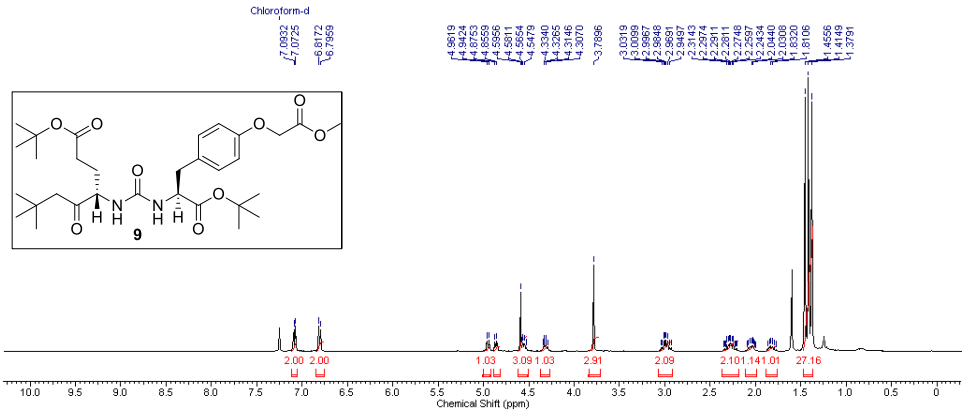

Figure 5.14 ^{1}H NMR spectrum (400 MHz, $CDCl_3$) **9**

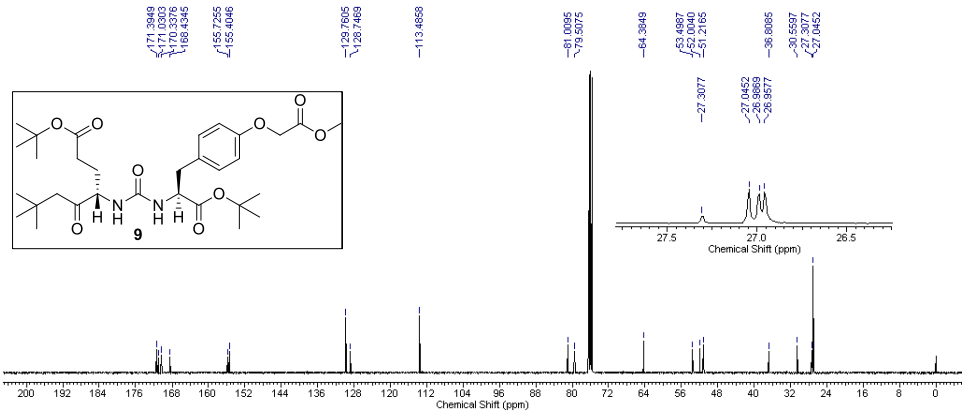

Figure 5.15 ^{13}C NMR spectrum (100 MHz, $CDCl_3$) of **9**

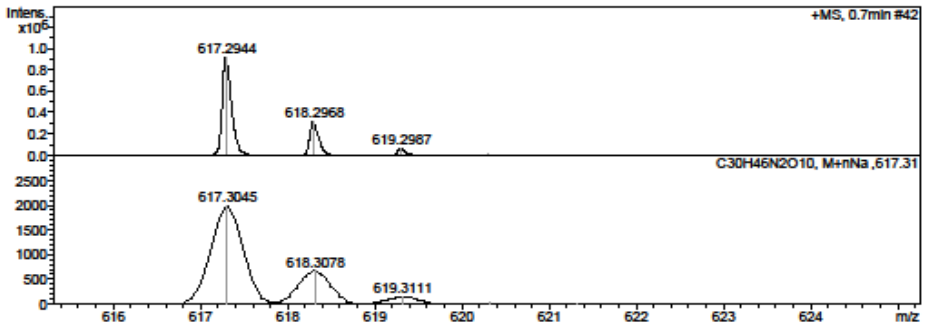

Figure 5.16 HRMS of **9**

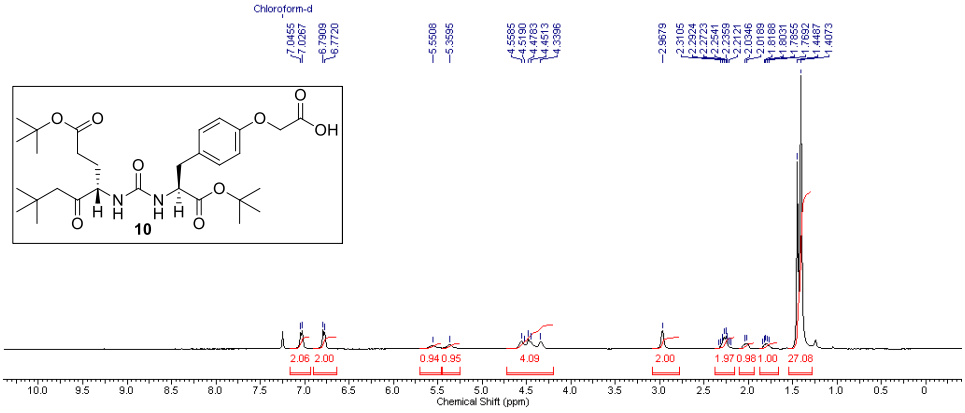

Figure 5.17 ^{1}H NMR spectrum (400 MHz, $CDCl_3$) of **10**

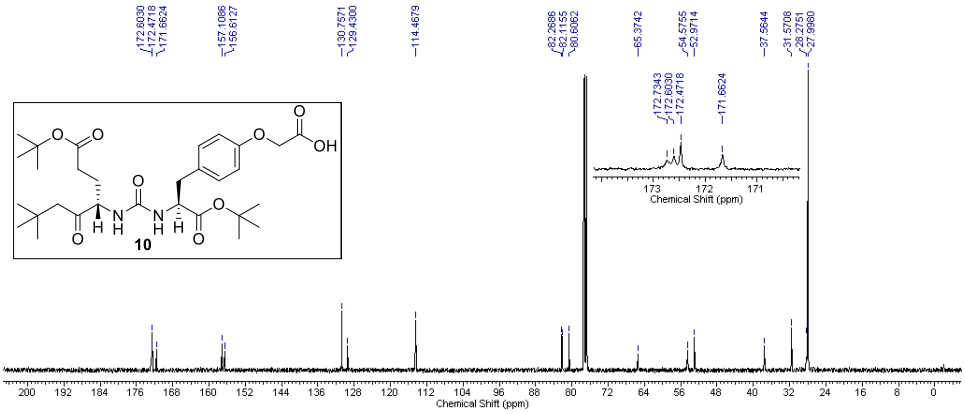

Figure 5.18 ^{13}C NMR spectrum (100 MHz, $CDCl_3$) of **10**

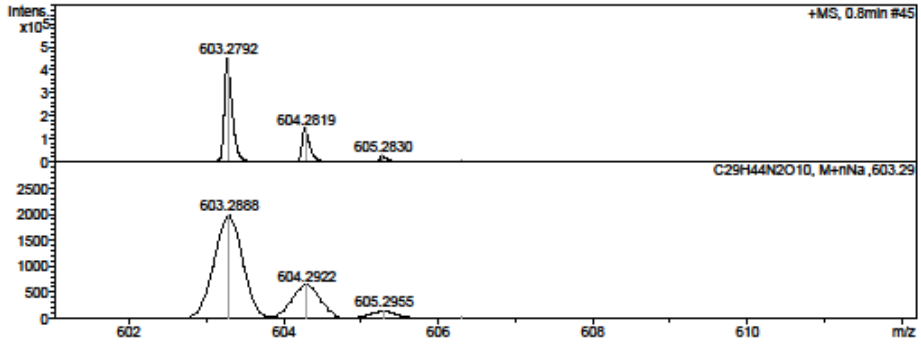

Figure 5.19 HRMS of **10**

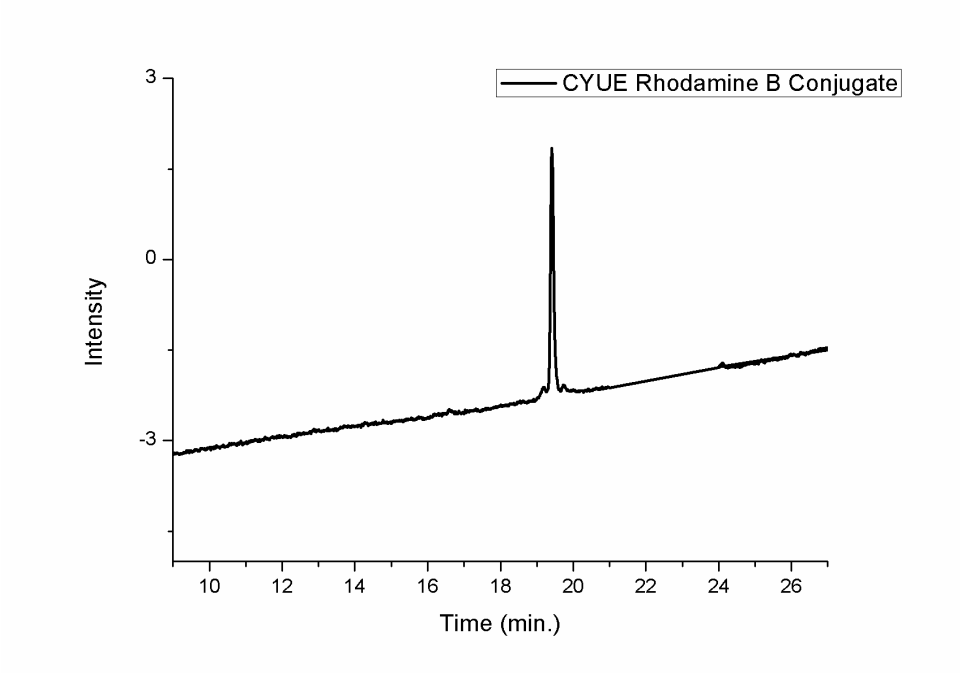

Figure 5.20 Analytical LC of pure CYUE_Rhodamine B conjugate **16** (λ at 256 nm)

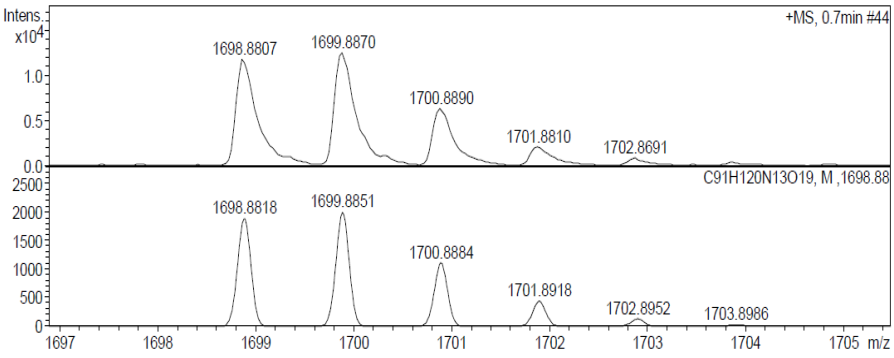

Figure 5.21 HRMS of CYUE_Rhodamine B conjugate **16**

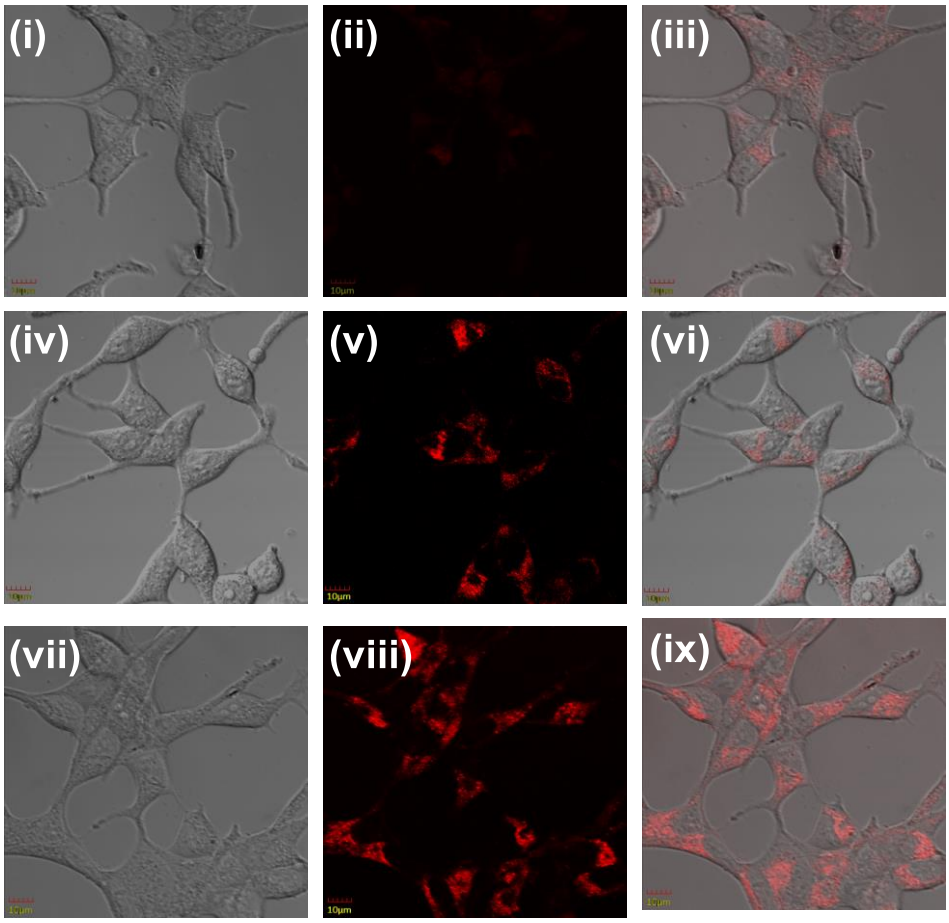

Figure 5.22 (i), (iv), (vii) DIC image of LNCaP cells at 10 nM, 25 nM, 50 nM, respectively; (ii), (v), (viii) Binding and internalization of CYUE-Rhodamine B conjugate **16** to $PSMA^{+}$ LNCaP cells at concentration of 10 nM, 25 nM, 50 nM, respectively; (iii), (vi), (ix) Overlay of images [(i),(ii)], [(iv),(v)], and [(vii),(viii)] to show that the uptake of CYUE-Rhodamine B conjugate is in the cytoplasm of LNCaP cells

5.5 References

1. Wong M. C. S., Goggins W. B., Wang H. H. X., Fung F. D. H., Leung C., Wong S. Y. S., Ng C. F., Sung J. J. Y. (2016), Global incidence and mortality for prostate Cancer: Analysis of temporal patterns and trends in 36 countries, Eur. Urol., 70, 862–874 (DOI: 10.1016/j.eururo.2016.05.043).

2. Siegel R. L., Miller K. D., Jemal A. (2019), Cancer Statistics, 2019, CA Cancer J. Clin., 69, 7–34 (DOI: 10.3322/caac.21551)

3. Zeller J. L. (2007), Grading of Prostate Cancer, JAMA., 298, 1596 (DOI:10.1001/jama.298.13.1596).

4. Chodak G. W., Keller P., Schoenberg H. W. (1989), Assessment of screening for prostate cancer using the digital rectal examination, J. Urol., 141, 1136–1138 (DOI: 10.1016/s0022-5347(17)41192-x).

5. Essink-Bot M., de Koning H. J., Nijs H. G. J., Kirkels W. J., van der Mass P. J., Schroder F. H. (1998), Short-term effects of population-based screening for prostate cancer on health-related quality of life, J. Natl. Cancer Inst., 90, 925–931 (DOI: 10.1093/jnci/90.12.925).

6. Linn M. M., Ball R. A. Maradiegue A. (2007), Prostate specific antigen screening: Friend or foe? Urol. Nurs., 27, 481–489.

7. Bernsen M. R., Kooiman K., Segbers M., van Leeuwen F. W. B., de Jong M. (2015), Biomarkers in preclinical cancer imaging, Eur. J. Nucl. Med. Mol. Imaging, 42, 579–596 (DOI: 10.1007/s00259-014-2980-7).

8. Gong M. C., Chang S. S., Sadelain M., Bander N. H., Heston W. D. (1999), Prostate-specific membrane antigen (PSMA)-specific monoclonal antibodies in the treatment of prostate and other

cancers, Cancer Metastasis Rev., 18, 483–490 (DOI: org/10.1023/A:1006308826967).

9. Ghosh A., Heston W. D. (2004), Tumor Target Prostate Specific Membrane Antigen (PSMA) and its Regulation in Prostate Cancer, J. Cell. Biochem., 91, 528–539 (DOI: 10.1002/jcb.10661).

10. Mesters J. R.., Barinka C., Li W., Tsukamoto T., Majer P., Slusher B. S., Konvalinka J., Hilgenfeld R. (2006), Structure of glutamate carboxypeptidase II, a drug target in neuronal damage and prostate cancer, EMBO J., 25, 1375–1384 (DOI: 10.1038/sj.emboj.7600969) .

11. Kularatne S. A., Wang K., Santhapuram H. K. R., Low P. S. (2009), Prostate-specific membrane antigen targeted imaging and therapy of prostate cancer using a PSMA inhibitor as a homing ligand. Mol. Pharm., 6, 780–789 (DOI: 10.1021/mp900069d).

12. Kularatne S. A., Zhou Z., Yang J., Post C. B., Low P. S. (2009), Design, synthesis, and preclinical evaluation of prostate-specific membrane antigen targeted ^{99m}Tc-radioimaging agents, Mol. Pharm., 6, 790–800 (DOI: 10.1021/mp9000712)

13. Banerjee S. R., Chen Z., Pullambhatla M., Lisok A., Chen J., Mease R. C., Pomper M. G. (2016), Preclinical comparative study of ^{68}Ga-labeled DOTA, NOTA, and HBED-CC chelated radiotracers for targeting PSMA, Bioconjugate Chem., 27, 1447–1455 (DOI: 10.1021/acs.bioconjchem.5b00679).

14. Yang X., Mease R. C., Pullambhatla M., Lisok A., Chen Y., Foss C. A., Wang Y., Shallal H., Edelman H., Hoye A. T., Attardo G., Nimmagadda S., Pomper M. G. (2016), Fluorobenzoyllysinepentanedioic acid carbamates: New scaffolds for positron emission tomography (PET) imaging of prostate-

specific membrane antigen (PSMA), J. Med. Chem., 59, 206–218 (DOI: 10.1021/acs.jmedchem.5b01268).

15. Banerjee S. R., Pullambhatla M., Foss C. A., Nimmagadda S., Ferdani R., Anderson C. J., Mease R. C., Pomper M. G. (2014), ^{64}Cu-labeled inhibitors of prostate-specific membrane antigen for PET imaging of prostate cancer, Bioconjugate Chem., 57, 2657–2669 (DOI: 10.1021/jm401921j).

16. Banerjee S. R., Pullambhatla M., Foss C. A., Falk A., Byun Y., Nimmagadda S., Mease R. C., Pomper M. G. (2013), Effect of chelators on the pharmacokinetics of ^{99m}Tc-labeled imaging agents for the prostate-specific membrane antigen (PSMA), J. Med. Chem., 56, 6108–6121 (DOI: 10.1021/jm400823w).

17. Chen Y., Pullambhatla M., Banerjee S. R., Byun Y., Stathis M., Rojas C., Slusher B. S., Mease R. C. Pomper M. G. (2012), Synthesis and biological evaluation of low molecular weight fluorescent imaging agents for the prostate-specific membrane antigen, Bioconjugate Chem., 23, 2377–2385 (DOI: 10.1021/bc3003919).

18. Banerjee S. R., Pullambhatla M., Byun Y., Nimmagadda S., Green G., Fox J. J., Horti A., Mease R. C., Pomper M. G. (2010), 68Ga-labeled inhibitors of prostate-specific membrane antigen (PSMA) for imaging prostate cancer, J. Med. Chem., 53, 5333–5341 (DOI: 10.1021/jm100623e).

19. Choy C. J., Ling X., Geruntho J. J., Beyer S. K., Latoche J. D., Langton-Webster B., Anderson C. J., Berkman C. E. (2017), PSMA Inhibitors: The effect of an albumin binder on biodistribution and therapeutic efficacy in prostate tumor-bearing mice, Theranostics, **7**, 1928–1939 (DOI: 10.7150/thno.18719).

20. Dannoon S., Ganguly T., Cahaya H., Geruntho J. J., Galliher M. S., Beyer S. K., Choy C. J., Hopkins M. R., Regan M., Blecha J. E., Skultetyova L., Drake C. R., Jivan S., Barinka C., Jones E. F., Berkman C. E., VanBrocklin H. F. (2016), Structure-activity relationship of ^{18}F-labeled phosphoramidate peptidomimetic prostate-specific membrane antigen (PSMA)-targeted inhibitor analogues for PET imaging of prostate cancer, J. Med. Chem., 59, 5684–5694 (DOI: 10.1021/acs.jmedchem.5b01850).

21. Graham K., Lesche R., Gromov A. V., Böhnke N., Schäfer M., Hassfeld J., Dinkelborg L. Kettschau G. (2012), Radiofluorinated derivatives of 2-(phosphonomethyl)pentanedioic acid as inhibitors of prostate specific membrane antigen (PSMA) for the imaging of prostate cancer, J. Med. Chem., 55, 9510–9520 (DOI: 10.1021/jm300710j).

22. Lapi S. E., Wahnishe H., Pham D., Wu L. Y., Nedrow-Byers J. R., Liu T., Vejdani K., VanBrocklin H. F., Berkman C. E., Jones E. F. (2009), Assessment of an 18F-labeled phosphoramidate peptidomimetic as a new prostate-specific membrane antigen-targeted imaging agent for prostate cancer, J. Nucl. Med., 50, 2042–2048 (DOI: 10.2967/jnumed.109.066589).

23. Boppart S. A., Richards-Kortum R. (2014), Point-of-care and point-of-procedure optical imaging technologies for primary care and global health, Sci. Transl. Med., 6, 1–12 (DOI: 10.1126/scitranslmed.3009725).

24. Al-Momani E., Malik N., Machulla H.-J., Reske S. N., Solbach C. (2013), Radiosynthesis of [^{18}F]FEt-Tyr-urea-Glu ([^{18}F]FEtTUG) as a new PSMA ligand, J. Radioanal. Nucl. Chem., 295, 2289–2294 (DOI: 10.1007/s10967-012-2293-x).

25. Pandit A., Sengupta S., Krishnan M. A., Reddy R. B., Sharma R, Venkatesh C. (2018), First report on 3D-QSAR and molecular dynamics based docking studies of GCPII inhibitors for targeted drug delivery applications, J. Mol. Struct., 1159, 179-192 (DOI: 10.1016/j.molstruc.2018.01.059).

26. Sengupta S., Krishnan M. A., Dudhe P., Reddy R. B., Giri B., Chattopadhyay S., Chelvam V. (2018), Novel solid-phase strategy for the synthesis of ligand-targeted fluorescent-labelled chelating peptide conjugates as a theranostic tool for cancer, Beilstein J. Org. Chem., 14, 2665–2679 (DOI: 10.3762/bjoc.14.244)

Chapter 6

Novel Solid Phase Strategy for Synthesis of Ligand Targeted Fluorescent Labelled Chelating Peptide Conjugates as a Theranostic Tool for Cancer

6.1 Introduction

The Understanding of cell processes is indispensable to devise new strategies for diagnosis and treatment of cancer and inflammatory diseases through targeted drug delivery techniques.[1] The complex molecular processes in a cell are discerned by tagging fluorescent probes or radioactive tracers to a targeting ligand that will undergo internalization after binding to cell surface proteins overexpressed in diseased conditions. The internalized tracers along with targeting ligand act as a tracking molecule to understand the destination of delivered cargos or biologics. For bio-imaging of cancer and inflammatory diseases through specific biomarkers,[2] several methods including single positron emission computed tomography (SPECT), positron emission tomography (PET) and magnetic resonance imaging (MRI), etc., are exploited, and each modality has its own strengths and weaknesses.[3] However, imaging studies using fluorescent probes[4] or radioactive isotopes[5,6] offers real-time, non-invasive, high-resolution images, during the examination of a pathological diseased state.

Prostate specific membrane antigen (PSMA)[7–9] and folate receptor[10–13] are well characterized and most attractive cancer biomarkers present in primary and metastatic stages of prostate and ovarian cancers respectively. PSMA belongs to a family of type II membrane-bound glycoprotein over-expressed on the cell surface of prostate, brain, bladder and breast cancers. Whereas folate receptors are attached to the cell membrane by a glycophosphatidylinositol anchor and over-expressed on several cancers as well as activated macrophages during inflammation. Moreover, folate

receptors were also discovered to be overexpressed on activated macrophages[14] but not on resting macrophages.[15] Many inflammatory diseases such as rheumatoid arthritis, inflammatory osteoarthritis, ischemia-reperfusion injury, atherosclerosis, psoriasis, vasculitis, lupus, diabetes, glomerulonephritis, sarcoidosis, Crohn's and Sjogren's disease are caused by activated macrophages.[16] Recently, EC17, (λ_{ex} = 465–490 nm and λ_{em} = 520–530 nm) a conjugate of folic acid and fluorescein isothiocyanate has been used for intraoperative surgery of ovarian cancer,[17] lung adenocarcinoma,[18–20] and breast cancer.[21]Therefore, targeting these biomarkers brings forth new insight to know the cause and treatment for such ailments. These biomarkers belong to a family of cell surface trans-membrane proteins[22] over-expressed mainly in diseased tissues and exploited in delivering chemical tools for early diagnosis of malignancy[23] and inflammatory diseases. They are also utilized for targeted drug delivery[24–25] of therapeutics to avoid any off-site toxicity to normal and healthy cells. Unfortunately, strategies to construct diagnostic and therapeutic chemical tools consisting of a polypeptidic spacer, a homing ligand for biomarkers, a fluorescent tag and a chelating moiety for tethering cargo in a continuous process using solid phase peptide synthesis is poorly developed. Traditional solid phase peptide synthesis methods for preparation of bioconstructs employ orthogonally protected functional moieties present in commercial resins such as Universal Nova tag or hyperacid labile resins such as Rink acid,[26] 4-hydroxymethylphenoxybutyryl (HMPB), chlorotrityl,[27] SASRIN[28] and Sieber amide.[29] even though such resins are very useful, they suffer from several disadvantages. For example, i) they are cost ineffective ii) possess low resin loading iii) incompatible in medium to strongly acidic[30] or basic conditions employed for deprotection of coupled amino acids and iv) undergo premature cleavage of polypeptide chain from solid support resulting in moderate yield during deprotection of acid sensitive side chain protecting moieties to introduce fluorescent tag.

In addition to the above drawbacks, conventional methods for the synthesis of targeted fluorescent tagged bioconjugates[31] are a mixed approach of both solid and solution phase synthesis[32]. These involve several intermediary purification steps to separate side products and unreacted fluorescent components. Moreover, there are reports wherein receptor targeted multimodal tools have been synthesized solely by employing solution phase chemistry.[33–35] These multistep synthetic protocol results in the escalation of the cost of intra-operative imaging tools that would otherwise be produced by our methodology with a single purification step. Even though Universal Nova tag resin[36] (Figure 6.1a) has resolved this problem to some extent, it suffers from a problem of employing acidic condition to deprotect side chain 4-methoxytrityl (Mmt) amino protecting group before attachment of fluorescent tag with the peptidic spacer. This results in premature cleavage of peptide chain and loss of chemical yield during the bioconjugate synthesis. Further, attaching a radiotracer chelating core containing acid-sensitive functional groups and the amino acid cysteine is also cumbersome and challenging. Recently, Low *et al.* reported the synthesis of various targeted conjugate molecules in which fluorescent tag[37] has been attached in a solution phase reaction. Also, they have reported the synthesis of ligand conjugated peptides containing radiotracer segment[38] without fluorescent tag using wang resin that is cleaved in strongly acidic conditions.

Contrary to the aforementioned drawbacks, present manuscript elicits a novel synthetic strategy for building new bioconstructs with several components in a continuous process methodology without isolation of any of the intermediates involved during the synthesis. The various components that are assembled include cell surface protein recognition ligand, peptide spacer for enhanced solubility and binding affinity, a

fluorescent tag for tissue staining and a chelating core containing cysteine amino acid to tether therapeutic cargos.

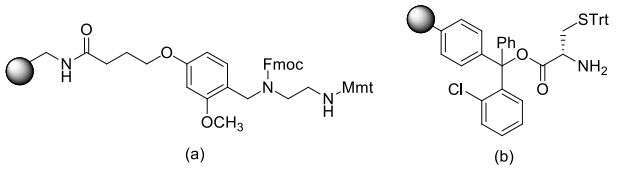

Figure 6.1 (a) Structure of Universal Nova Tag Resin, (b) Structure of H-*L*-Cys(Trt)-2-ClTrt resin

This goal is smoothly achieved in high chemical yield and purity by strategically introducing differentially protected amino functionalities of a dibasic amino acid such as lysine whose α- and ε-amino groups are protected as base labile Fmoc and trifluoroacetyl (Tfa) protecting groups respectively. The whole concept is successfully illustrated in the case of commonly available and less expensive cysteine labeled 2-chlorotrityl resin (Figure 6.1b). The methodology is general and can be significantly useful for acid-sensitive resins that contain acid labile orthogonal amino acids with 4-methoxytrityl (Mmt), 4-methyltrityl (Mtt) protecting groups.

6.2 Results and Discussion

6.2.1 Designing of bio-constructs

PSMA has very high affinity[39] for a small molecule homing ligand called DUPA or 2-[3-(1,3-dicarboxypropyl)ureido]pentanedioic acid with inhibition constant K_i of 8 nM. Folate protein binds to folic acid and their derivatives[40] such as pteroate ligand[41] with a high degree of specificity (K_d = ~10 nM) to deliver attached cargos to the interior of cells. These targeting ligands, DUPA, and pteroate, have been exploited in the design and synthesis of our new ligand-targeted tracer conjugates **13** and **17** (Figure 6.2) to target $PSMA^+$ and FR^+ diseased conditions.

Analysis of the crystal structure[42] of PSMA reveals that small molecule ligands such as DUPA could reach the PSMA active site through a gradually narrowing amino acids tunnel of 20 Å length.

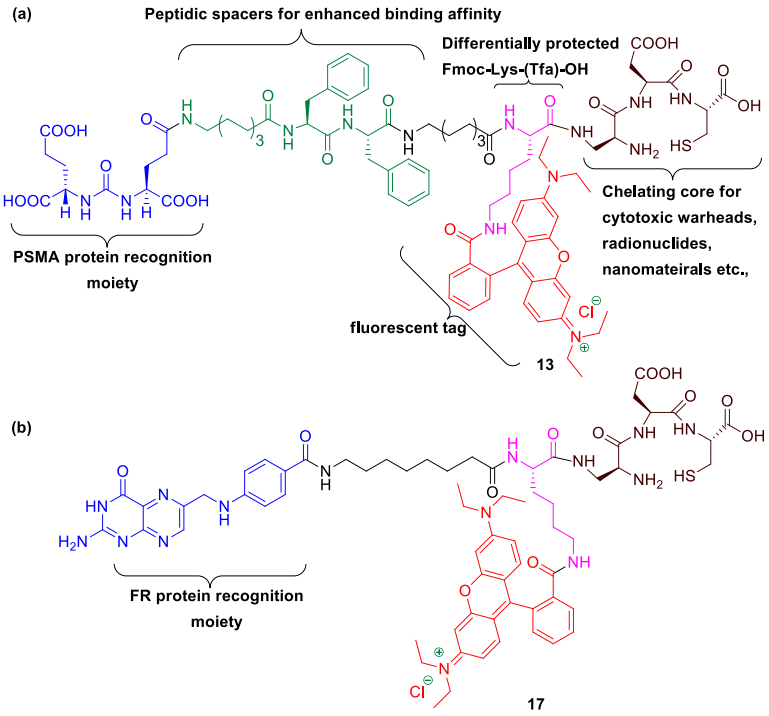

Figure 6.2 (a) PSMA targeting DUPA rhodamine B chelating conjugate **13**, (b) Folate receptor targeting pteroate rhodamine B chelating conjugate **17**

Moreover, the inner surface of the PSMA tunnel possesses two hydrophobic pockets suitable for hydrophobic interactions with the amino acids present in the peptide spacer. Therefore, it is pertinent to design a PSMA targeted conjugate that can pass through the tunnel smoothly and reach the active site as well as fit in hydrophobic pockets via hydrophobic interactions. Additionally, carbonyl oxygen of urea moiety of DUPA directly coordinates with two zinc atoms present in the active site of PSMA. The α and α′-carboxylic acids of DUPA ligand interacts with Arg210 and Arg534 amino acid residues whereas a salt bridge is formed between Lys699 residue and γ-carboxylic acid of DUPA. The γ′-

carboxylic acid of DUPA ligand doesn't play a significant role in the interaction with PSMA active site and hence exploited as a handle for the construction of peptidic spacer of bioconjugate **13**.

While designing the required peptide spacer[38] of **13** (Figure 6.2) for the tunnel, an eight-carbon amino acid such as 8-aminocaprylic acid has been covalently attached to γ′-carboxylic acid of the DUPA ligand. This ensures the adequate distance between targeting ligand and peptidic spacer so that the specific binding to the protein is not compromised. The additional distance and hydrophobic pockets present in the 20 Å channel is crossed over by introduction of two phenylalanine (Phe) amino acids in the spacer. The polypeptide chain is also attached to another molecule of 8-aminocaprylic acid to ensure that the molecular position of a fluorescent tag and chelating core would lie outside the surface of the protein tunnel. Moreover, differentially protected α- and ε-amino groups of lysine (Lys) amino acid, Fmoc-Lys-(Tfa)-OH, is also introduced in the peptide chain. The main purpose of this exercise is to connect the chelating core through carboxylic acid of lysine and attachment of fluorescent probe via ε-amino group present in the lysine amino acid. Increased hydrophobicity due to the introduction of long chain amino acids, aromatic amino acids in the targeted ligand peptide conjugate **13** would decrease the solubility. This is compensated by the introduction of dibasic amino acid like diaminopropionic acid (Dap), an acidic amino acid like aspartic acid (Asp) and polar cysteine amino acid (Cys) that makes up the chelating core.

In the case of FR targeted fluorescent conjugate **17**, the targeting ligand, folic acid, is modified by removal of *L*-glutamic acid residue to give pteroic acid moiety (Figure 6.2). The binding affinity of the modified folate is relatively weaker than folic acid.[41] The targeting ligand, pteroic acid, is covalently coupled to 8-aminocaprylic acid to separate the active binding site of folate protein from the interference of fluorescent cargo attached to lysine amino acid and chelating core as described for **13**. Thus

our newly designed bioconstructs **13** and **17** have the following four components, (i) cell surface protein recognition ligand, (ii) peptidic spacer which enhances binding affinity of targeting ligand as well as minimizes the repulsive interaction between bulky dye molecule and targeted protein active site, (iii) a fluorescent tag to track the cellular destination of bioconjugates and visualization aid for tissue staining, (iv) Chelating core as a multipurpose handle for loading drug cargos, radionuclides, or nanomaterials.

6.2.2 Initial Attempts to synthesize bio-constructs

Starting from commercially available cysteine capped chlorotrityl resin, H-*L*-Cys(Trt)-2-ClTrt **5,** we begin the synthesis of bioconjugate **13** (Scheme 6.2). Using standard Fmoc solid phase peptide synthesis methodology, amino acids such as Fmoc-Asp(O^{t}Bu)-OH, Boc-Dap(Fmoc)-OH were coupled in sequence to cysteine amino acid attached to chlorotrityl resin via dipeptide intermediate **6** to give the tripeptide intermediate **7.** The tripeptide **7** was then attached to strategic lysine amino acid, Fmoc-Lys-(Pg)-OH, whose ε-amino group is protected as either Mtt (4-methyltrityl) or Mmt(4-methoxytrityl) protecting groups (Pg) to give tetrapeptides **8a** and **8b.** The tetrapeptides **8a** and **8b** were tethered sequentially to 8-aminocaprylic acid, two phenylalanine residues, another 8-aminocaprylic acid and finally to DUPA precursor **4** (Scheme 6.1), to provide polypeptide chains **9a** and **9b** (Scheme 6.2). The tris(tert-butoxy) protected DUPA precursor **4** required for the preparation of conjugate **13** was prepared as per reported procedure[38] (scheme 6.1). The ε-amino protecting group present in the polypeptide chains **9a** (Pg = Mtt) and **9b** (Pg = Mmt) are generally cleaved under acidic conditions. Therefore, it becomes pertinent to analyze the stability of chlorotrityl resin and ε-amino protecting groups in the polypeptide chains **9a** and **9b** to achieve our multiple objectives in a continuous synthetic process without the isolation of any of the intermediates.

Scheme 6.1 Synthesis of PSMA tri(*tert*-butoxy) protected DUPA ligand **4**

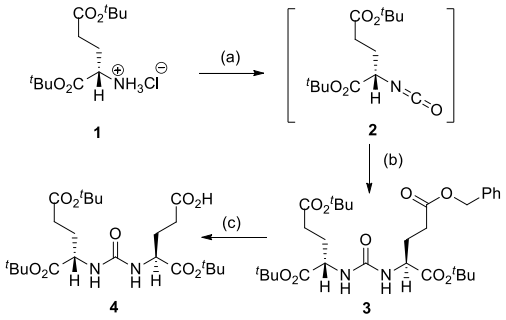

Reagents and conditions: (a) Triphosgene, triethylamine, dichloromethane (DCM), –50 °C to rt; (b) *L*-glutamic acid γ-benzyl-α-*tert*-butyl ester hydrochloride, triethylamine, DCM, rt, overnight; (c) H_2, Pd/C, CH_2Cl_2, 24 h, rt.

The peptide chain cleavage conditions for chlorotrityl resin are well established and the ε-amino trityl protecting groups of Fmoc-Lys-(Mtt or Mmt)-OH of the side chain are usually acid labile with an order of stability: Trt (chlorotrityl) > Mtt (4-methyltrityl) > Mmt (4-methoxytrityl). In our initial attempt, we opined that the Mtt (4-methyltrityl) protected ε-amino group of Fmoc-Lys-(Mtt)-OH amino acid should undergo selective cleavage in mild acidic conditions without cleavage of polypeptide chain **9a** from the resin. Selective deprotection of Mtt protecting group was achieved when **9a** was treated with either 1% TFA in dichloromethane or a mixture of acetic acid/trifluoroethanol/DCM in 1:2:7 ratio for 1 h at room temperature.[43] Unfortunately, the polypeptide chain **9a** cleaved off too from the resin beads (Scheme 6.2). Therefore, it became difficult to identify and marginally separate the acidic conditions required for selective cleavage of Mtt protecting group in the side chain of **9a** from chlorotrityl resin.

Scheme 6.2 Attempted synthesis of PSMA targeted DUPA rhodamine B chelating conjugate **13** using Fmoc-Lys(Mtt/mmt)-OH

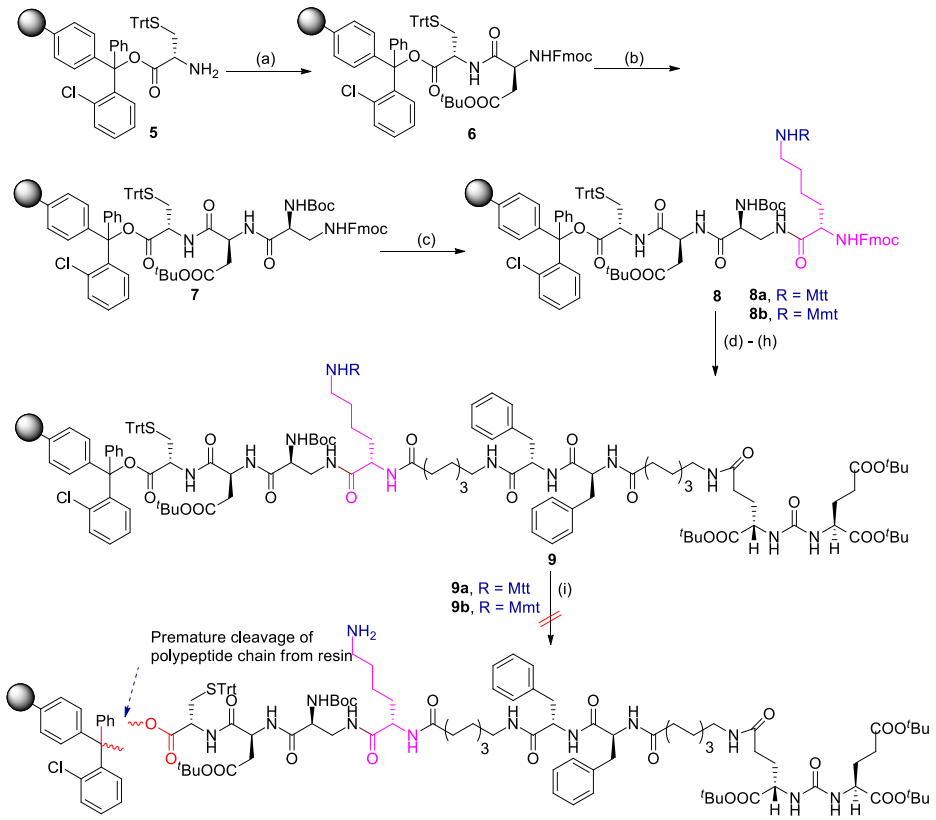

Reagents and conditions: (a) Fmoc-Asp(O^{t}Bu)-OH, PyBOP, DIPEA, DMF, 6 h; (b) (i) 20% Piperidine in DMF, rt, 30 min; (ii) Boc-Dap(Fmoc)-OH, PyBOP, DIPEA, DMF, 6 h; (c) (i) 20% Piperidine in DMF, rt, 30 min; (ii) Fmoc-Lys(Mmt/Mtt)-OH, PyBOP, DIPEA, DMF, 6 h; (d) (i) 20% Piperidine in DMF, rt, 30 min; (ii) Fmoc-8-aminocaprylic acid, PyBOP, DIPEA, DMF, 6 h; (e) (i) 20% Piperidine in DMF, rt, 30 min; (ii) Fmoc-Phe-OH, PyBOP, DIPEA, DMF, 6 h; (f) (i) 20% Piperidine in DMF, rt, 30 min; (ii) Fmoc-Phe-OH, PyBOP, DIPEA, DMF, 6 h; (g) (i) 20% Piperidine in DMF, rt, 30 min; (ii) Fmoc-8-aminocaprylic acid, PyBOP, DIPEA, DMF, 6 h; (h) (i) 20% Piperidine in DMF, rt, 30 min; (ii) DUPA(O^{t}Bu)$_3$-OH , PyBOP, DIPEA, DMF, 6 h; (i) acetic acid/ trifluoroethanol/ DCM (1:2:7), rt, 1 h or 1(M) HOBt in DCM/TFE (1:1), 1 h.

Because of this reason we questioned the introduction of better electron releasing groups such as 4-methoxytrityl (Mmt) instead of Mtt group in the strategic amino acid, as in the case of Fmoc-Lys-(Mmt)-OH. This would increase the margin of difference and lower the acid strength required for exclusive cleavage of Mmt protecting group in the side chain of **9b** from chlorotrityl resin. With this view, **9b** containing Fmoc-Lys-(Mmt)-OH is subjected to cleavage under milder acidic conditions using 1M HOBt (hydroxybenzotriazole) in trifluoroethanol/dichloromethane (1:1). However, this condition did not provide the required solution and failed to differentiate the acidic strength needed for exclusive cleavage of Mmt protecting group in the side chain of **9b** from chlorotrityl resin resulting in the detachment of polypeptide chain **9b** (Scheme 6.2). Therefore, we turned our attention to replace the acid labile trityl protecting groups with a base labile protecting group such as trifluoroacetyl (Tfa) as in the case of Fmoc-Lys-(Tfa)-OH amino acid.

6.2.3 Synthetic strategy

With the hope that the introduction of the base labile protecting group in lysine could provide the required solution, we begin the synthesis of polypeptide chain **10** with Fmoc-Lys-(Tfa)-OH derivative (Scheme 6.3). This idea for the synthesis of polypeptide chain **10** has been adapted from an earlier work reported by Moroder *et al.* in which trifluoroacetyl (Tfa) moiety was deprotected during a peptide synthesis[44] using 1M aqueous piperidine at ice cold temperature. The polypeptide chain **10** was thus subjected to 1M aqueous piperidine at 0 °C to deprotect the ε-amino trifluoroacetyl moiety. The literature reported condition, however, failed to deprotect Tfa group from polypeptide chain **10**. We have tested few reaction conditions, and after optimization, we have successfully deprotected ε-amino Tfa protecting group from side chain using 2M aqueous piperidine at room temperature for 6–12 h (the completion of the reaction being monitored through Kaiser's test) to give polypeptide chain

11 with free ε-amino group. It is also interesting to note that the reaction is smooth, clean without resulting in rupture of polypeptide chain **10** from chlorotrityl resin. The protecting groups of other amino acids present in **11** remain intact during this process. After the successful cleavage of Tfa protecting group to give **11**, the free ε-amino group was covalently bonded to fluorescent tag such as rhodamine B using standard peptide coupling chemistry to afford rhodamine B conjugated polypeptide chain **12**. Amino acid protecting groups such as Boc, *t*-butyl and Trt of diaminopropionic acid, aspartic acid, and cysteine thiol moieties, respectively, in **12** were cleaved traceless using a cocktail of trifluoroacetic acid, triisopropyl silane, ethanedithiol in water. The final PSMA targeted rhodamine B peptide conjugate **13** was thus obtained from chlorotrityl resin as shown in scheme 6.3 in high yield and purity. By using this new procedure, we have successfully demonstrated for the first time a selective cleavage of base sensitive ε-amino protecting group (Tfa) in the side chain of the growing polypeptide chain.

The methodology could be extended to incorporate any basic natural or unnatural amino acids in a peptide chain in which α-amino group is protected as Fmoc and side chain amino group, in any position (β, γ, δ) along with carbon side chain, is protected as trifluoroacetyl moiety. The methodology is thus successfully utilized to install fluorescent tags that are sensitive to strong inorganic bases. Moreover, the methodology applies to resins that are sensitive to mild and strong acidic conditions and peptide chains that contain side chain protecting groups such as Trt(chlorotrityl), Mtt (4-methyltrityl), Mmt (4-methoxytrityl) for the synthesis of targeted fluorescent bioconjugates.

Scheme 6.3 Synthesis of PSMA targeted DUPA rhodamine B chelating conjugate **13**

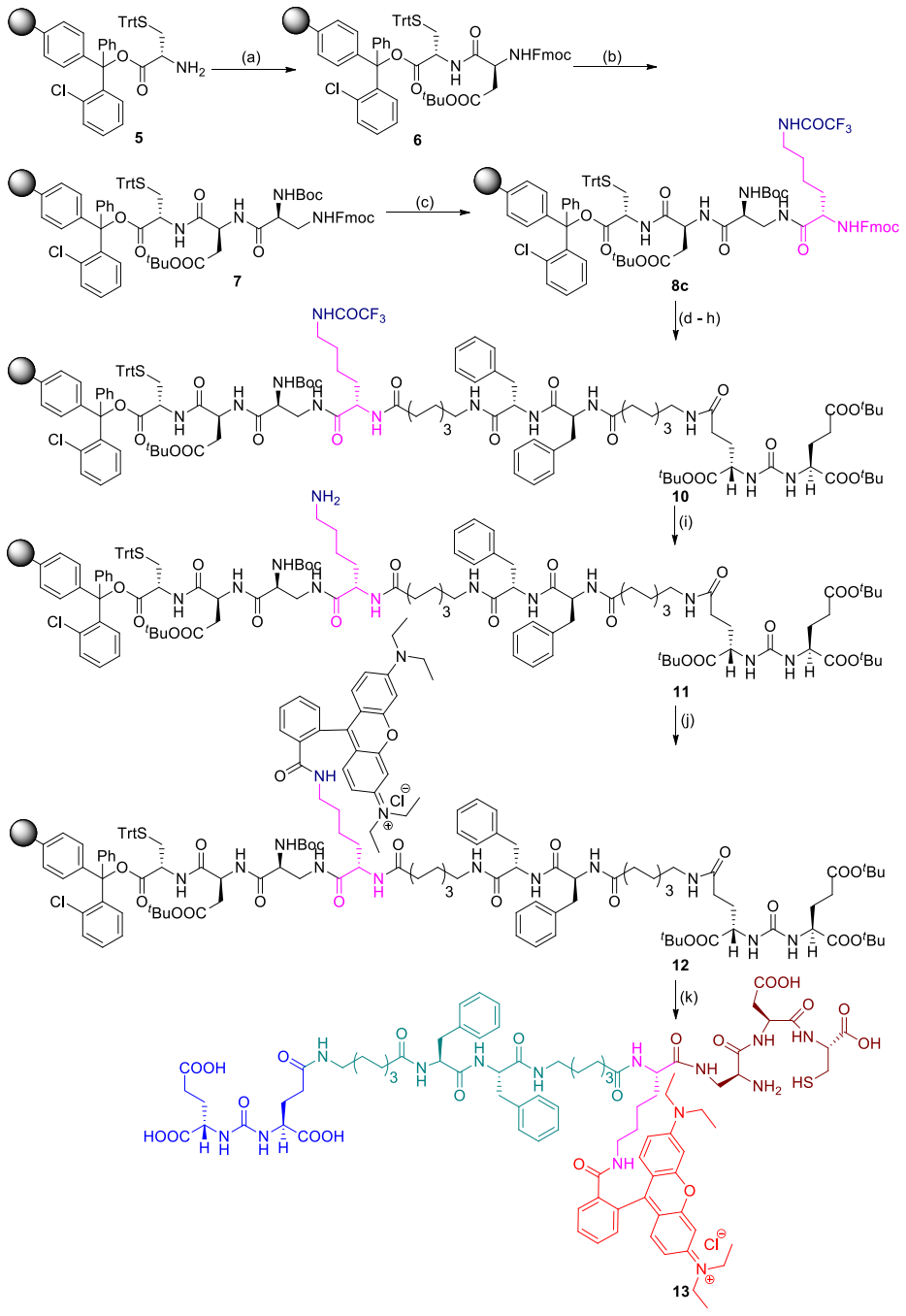

Reagents and conditions: (a) Fmoc-Asp(O^{t}Bu)-OH, PyBOP, DIPEA, DMF, 6 h; (b) (i) 20% Piperidine in DMF, rt, 30 min; (ii) Boc-Dap(Fmoc)-OH, PyBOP, DIPEA, DMF, 6 h; (c) (i) 20% Piperidine in DMF, rt, 30

min; (ii) Fmoc-Lys(Tfa)-OH, PyBOP, DIPEA, DMF, 6 h; (d) (i) 20% Piperidine in DMF, rt, 30 min; (ii) Fmoc-8-aminocaprylic acid, PyBOP, DIPEA, DMF, 6 h; (e) (i) 20% Piperidine in DMF, rt, 30 min; (ii) Fmoc-Phe-OH, PyBOP, DIPEA, DMF, 6 h; (f) (i) 20% Piperidine in DMF, rt, 30 min; (ii) Fmoc-Phe-OH, PyBOP, DIPEA, DMF, 6 h; (g) (i) 20% Piperidine in DMF, rt, 30 min; (ii) Fmoc-8-aminocaprylic acid, PyBOP, DIPEA, DMF, 6 h; (h) (i) 20% Piperidine in DMF, rt, 30 min; (ii) DUPA(O^tBu)$_3$-OH, PyBOP, DIPEA, DMF, 6 h; (i) 2M Piperidine in water, rt, 6–12 h; (j) Rhodamine B, PyBOP, DIPEA, DMF, 6 h; (k) (i) TFA/TIS/EDT/H_2O (92.5:2.5:2.5:2.5) (1 × 5 mL, 30 min; 2 × 5 mL, 5 min); (ii) Evaporate TFA; (iii) Precipitate in ice cold diethylether

The methodology was further extended to synthesis FR targeted fluorescent chelating conjugate **17** as shown in scheme 6.4. Using standard Fmoc SPPS methodology, Fmoc amino acids such as Fmoc-Asp(O^tBu)-OH, Boc-Dap(Fmoc)-OH were coupled in sequence to STrt protected cysteine amino acid attached to the chlorotrityl resin to give dipeptide **6** and tripeptide **7** intermediates**.** The tripeptide **7** was then attached to Fmoc-Lys-(Tfa)-OH to give tetrapeptide **8c.** The tetrapeptide **8c** was coupled to Fmoc-8-aminocaprylic acid followed by the introduction of folate protein targeting ligand in the form of N^{10}-(trifluoroacetyl) pteroic acid to give polypeptide **14**. It's noteworthy to mention that the ligand-targeted chelating polypeptide **14** contains two different trifluoroacetyl moieties which protect 2° amine of the pteroate core as well as 1° amine of ε-amino lysine residue. The N^{10}-(trifluoroacetyl) or 2° amine protecting a group of pteroic acid is selectively cleaved using 1% $NH_2NH_2.H_2O$ in DMF without affecting the trifluoroacetyl protecting group of a lysine residue.

Scheme 6.4 Synthesis of folate receptor targeted pteroate rhodamine B chelating conjugate **17**

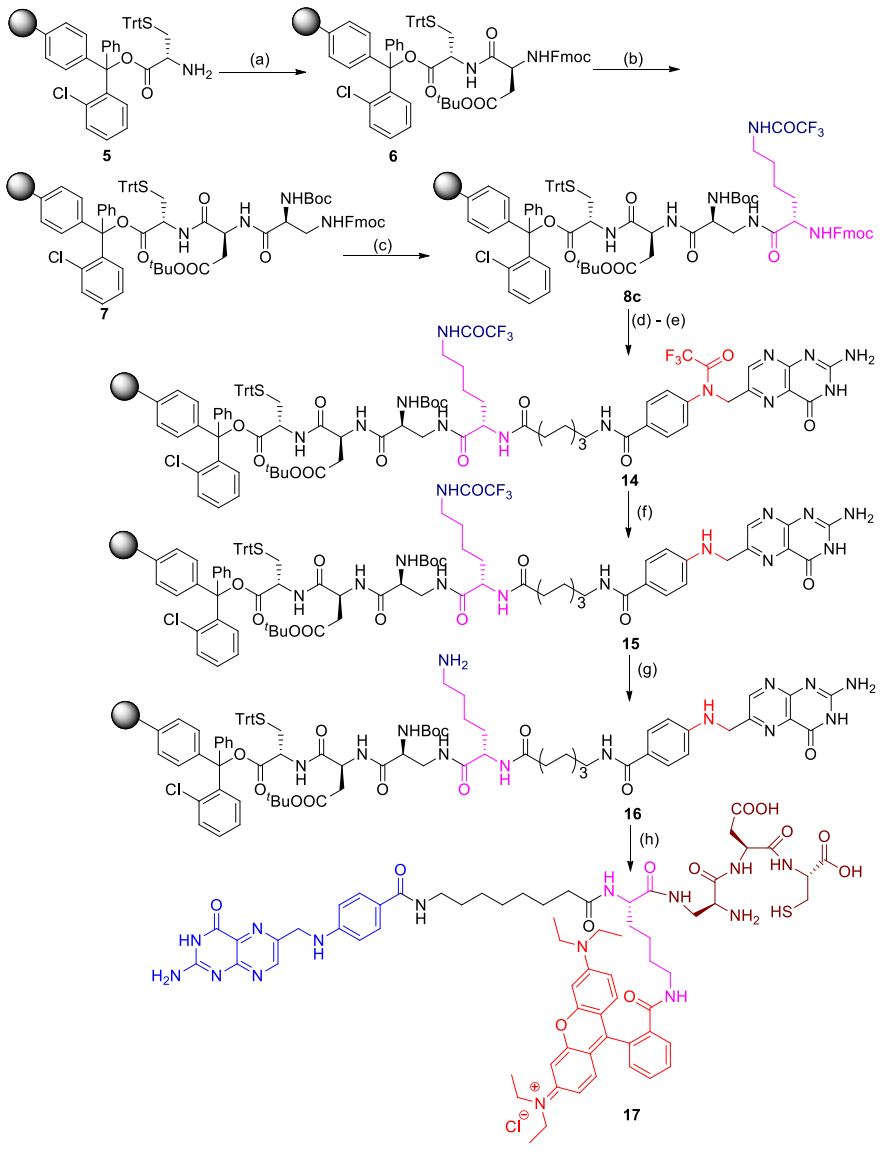

Reagents and conditions: (a) Fmoc-Asp(O^{t}Bu)-OH, PyBOP, DIPEA, DMF, 6 h; (b) (i) 20% Piperidine in DMF, rt, 30 min; (ii) Boc-Dap(Fmoc)-OH, PyBOP, DIPEA, DMF, 6 h; (c) (i) 20% Piperidine in DMF, rt, 30 min; (ii) Fmoc-Lys(Tfa)-OH, PyBOP, DIPEA, DMF, 6 h; (d) (i) 20% Piperidine in DMF, rt, 30 min; (ii) Fmoc-8-aminocaprylic acid, PyBOP, DIPEA, DMF, 6 h; (e) (i) 20% Piperidine in DMF, rt, 30 min; (ii) N^{10}-(trifluoroacetyl)Pteroic acid, PyBop, HOBt. xH_2O, DIPEA, DMSO, DMF,

6 h (f) 1% $NH_2NH_2.H_2O$, DMF (3 × 2 mL) 10 min each; (g) 2M Piperidine in water, rt, 6–12 h; (h) (i) Rhodamine B, PyBOP, DIPEA, DMF, 6 h; (iii) TFA/TIS/EDT/H_2O (9.25:0.25:0.25:0.25) (1 × 5 mL, 30 min; 2 × 5 mL, 5 min); (iv) Evaporate TFA; (v) Precipitate in ice cold diethylether

This is unequivocally confirmed by performing the Kaiser test on polypeptide chain **15** which doesn't turn dark blue after the cleavage of N^{10}-(trifluoroacetyl) group from pteroate entity (Scheme 6.4). The 2° amine of pteroate core generated in **15** after the cleavage of N^{10}-(trifluoroacetyl) group doesn't give positive Kaiser test (see experimental section).

Using 2M aqueous piperidine, we successfully cleaved Tfa protecting group from the side chain of **15** to give a polypeptide chain **16** that is still intact with the resin. The successful cleavage of Tfa group from lysine side chain is confirmed by performing the Kaiser test on resin beads containing polypeptide chain **16** which turned dark blue. The free ε-amino group thus liberated was covalently attached to fluorescent tag such as tetraethylrhodamine B by standard peptide bond formation chemistry. Protecting groups such as Boc, *t*-butyl, and Trt present in diaminopropionic acid, aspartic acids, and cysteine thiol aminoacids, respectively, were cleaved using a cocktail of trifluoroacetic acid, triisopropyl silane, ethanedithiol in water to give folate receptor-targeted chelating rhodamine B conjugate **17** in high yield and purity (Scheme 6.4).

Because bioconjugates **13** and **17** have cysteine amino acid in the peptide chain, which is an essential requirement for construction of chelating core, other protected ε-amino lysine derivatives[45,46] such as N-Fmoc-Lys(Alloc)-OH have not been employed in our synthetic strategy. Usually allyl protecting group in N-Fmoc-Lys(Alloc)-OH is deprotected using $Pd(PPh_3)_4$ catalyst. However, sulfur atom present in cysteine moiety of

chelating core is known to poison palladium catalyst resulting in complete failure of the deprotection of ε-amino allyl protecting moiety. Moreover, palladium is a heavy metal and traceless removal of it from the resulting bioconjugates **13** and **17** are near to impossible. Since the prepared bioconjugates **13** and **17** are to be utilized for imaging of human cancer cell lines, presence of any heavy metals in the synthetic strategy would cause unwanted toxicity and inaccuracy in the biological study. The –SH group present in the bioconjugate handle or chelating core of compound **13** and **17** can be utilized for the attachment of drugs,[47] nanomaterial and radionuclide for therapeutic purposes. This added advantage makes the bioconjugates as a potential theranostic tool for cancer.

6.2.4 *In vitro* evaluation

The newly synthesized bioconjugates **13** and **17**, that can selectively target $PSMA^+$ and FR^+ cancers, were further evaluated by performing *in vitro* studies using laser scanning confocal microscopy on $PSMA^+$ LNCaP cells, FR^+ epithelial CHO-β cells and $PSMA^-$, FR^- PC-3 cells (Figure 6.3). The negative cell line was used to prove the protein specificity of newly synthesized ligand targeted bioconjugates **13** and **17**. In figure 6.3 the confocal microscopic images depicts the delivery of conjugates to cells via receptor mediated endocytosis negating any possibility of non-specific uptake. The specificity of bioconjugates is indispensable to prevent collateral damage and toxicity to healthy cells when the chelating core is tethered to deliver radionuclides or cytotoxic drugs. The confocal microscopic images in figure 6.3, panel (ii) shows the uptake of chelating DUPA rhodamine-B conjugate in LNCaP cells at 100 nM concentration, panel (vi) shows the uptake of chelating pteroate rhodamine-B conjugate in CHO-β cells at 150 nM concentration. The specificity of the ligand conjugates was further established by studying the uptake of bioconjugates **13** and **17** in malignant cells which express neither PSMA nor folate receptors [panels (iv) and (viii)]. Absence of any rhodamine-B

bioconjugates **13** and **17** uptake in the cytoplasm of negative cell line, PC-3 cells, show that the bioconjugates are very specific which is an important criterion in targeted drug delivery systems for avoiding off-site toxicity.

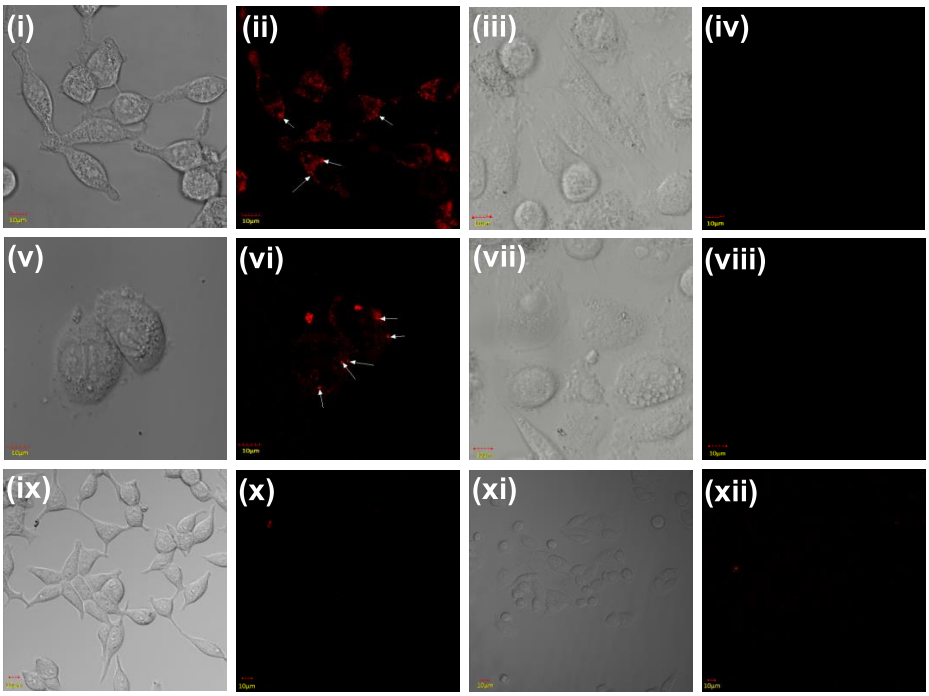

Figure 6.3 (i) and (ix) DIC image of LNCaP cells ($PSMA^{+}$) (ii) Binding and internalization of DUPA-Rhodamine B conjugate **13** to LNCaP cells by confocal microscopy at 100 nM concentration [endosomes are marked with white arrows] (iii) and (vii) DIC image of PC-3 cells ($PSMA^{-}$ and FR^{-}) (iv) Specificity of DUPA-Rhodamine-B conjugate **13** in $PSMA^{-}$ cell line such as PC-3 cells. (v) and (xi) DIC image of cells CHO-β cells (FR^{+}) (vi) Binding and internalization of pteroate-Rhodamine B conjugate **17** in CHO-β cells by confocal microscopy at 150 nM concentration [endosomes are marked with white arrows] (viii) Specificity of pteroate-Rhodamine B conjugate **17** in FR^{-} cell line such as PC-3 cells (DIC = Differential interference contrast) (x) Binding and internalization of DUPA-Rhodamine B conjugate **13** to LNCaP cells in the presence of 100-fold excess 2-PMPA (xii) Binding and internalization of pteroate-

Rhodamine B conjugate **17** to CHO-β cells in the presence of 100-fold excess folic acid

In vitro specificity of bioconjugates **13** and **17** were further examined by prior incubation of LNCaP cells and CHO-β cells with 100-fold excess of 2-PMPA and folic acid to block PSMA and folate receptors respectively. Receptor blocked LNCaP and CHO-β cells display minimal uptake of bioconjugates **13** and **17** [panels (x) and (xii)], confirming the specificity of the synthesized bioconjugates. Thus, we have developed a novel strategy to synthesize targeted fluorescent tagged bioconjugates by introducing differentially protected α and ε-amino groups of lysine amino acid derivative, Fmoc-Lys-(Tfa)-OH. Thus, our primary goal of introducing all the four components in **13** and **17** viz., targeting ligand, peptidic spacer, fluorescent tag as well as chelating core in a continuous synthesis process in cost effective manner, was achieved in high yield, purity and free of any heavy metal usually employed in other synthesis that is detrimental for biological studies.

6.3 Conclusion

In conclusion, we have developed a new synthetic strategy for assembling targeting ligand, peptidic spacer, a fluorescent tag and chelating core in a continuous process without isolation of intermediates during the bioconjugate synthesis. The synthesis is carried out from a relatively non-expensive and commercially available H-Cys(trt)-(2-Cltrt) resin. The mode of linking the fluorophore to the growing peptide chain using lysine derivative such as Fmoc-Lys(Tfa)-OH containing differentially protected amino groups that are labile only in basic conditions was found to be crucial in synthesizing the conjugates. With this synthetic protocol we have synthesized chelating DUPA rhodamine B and pteroate rhodamine B conjugates for targeting malignant cells as well as inflammatory cells expressing PSMA and folate receptors. The in *vitro* uptake study has been

performed using laser scanning confocal microscopy and the bioconjugates are found to be delivered specifically to cells expressing corresponding cell surface proteins. The small molecule targeted imaging probes prepared in this study are designed for diagnosis and deep tissue imaging of cancers and inflammatory diseases. Near infrared fluorophores containing a free or activated carboxylic group (e.g. IRDye 800CW NHS ester) can also be conjugated with the peptidic spacer using this methodology through amide coupling reaction. Moreover, the bioconjugates can be employed as potential theranostic tools by attaching macromolecules, cytotoxic warheads, radioactive tracers, nanomaterials etc., via the chelating core.

6.4 Experimental section

6.4.1 Materials and methods

H-Cys-2-ClTrt resin, Fmoc amino acids and amide coupling agents, reagents and solvents used in solid phase peptide synthesis (SPPS) as well as in chemical synthesis were purchased from Iris Biotech GmbH, Sigma Aldrich, Merck and Spectrochem. Dry solvents were prepared by using drying agents and following usual methods. Peptide syntheses were carried out in sintered glass peptide vessels (Chemglass) by standard peptide coupling procedures. ^{1}H and ^{13}C NMR data were recorded using Bruker AV 400MHz NMR spectrometer with TMS (tetramethyl silane) as internal reference. Mass spectra were recorded on Brukermicro TOF-Q II by positive mode and negative mode electrospray ionization methods. Reactions were monitored by TLC using MERCK 60 F_{254} pre-coated silica gel plates and the products were visualized under UV light. The purity of ligand targeted rhodamine B peptide conjugates was confirmed by Dionex HPLC-Ultimate 3000 instrument and peptide conjugates were purified through Buchi reveleris prep instrument using RP-PFP column (XSelect CSH Prep Fluorophenyl 5 µm OBD).

6.4.2 Synthesis of targeting ligand

6.4.2.1 Procedure for synthesis (*S*)-5-benzyl 1-*tert*-butyl 2-(3-((*S*)-1,5-di-*tert*-butoxy-1,5-dioxopentan-2-yl)ureido)pentanedioate (3)

Triphosgene (0.050 g, 0.169 mmol) was dissolved in 3 mL dry DCM, and the solution was stirred at −50 °C under an inert atmosphere in a two-neck 50 mL round bottom flask (Scheme 6.1). Bis(*tert*-butyl)-L-glutamate.HCl **1** (0.150 g, 0.507 mmol) dissolved in 2 mL of dry DCM was added to triphosgene solution at −50 °C, and triethylamine (0.5657 mL, 4.056 mmol) was added dropwise to the reaction mixture. The reaction mixture was stirred for 1.5 h at –50 °C and stirred for another 1.5 h at room temperature for the generation of isocyanate intermediate **2**. After that, a solution of L-glutamic-γ-benzyl-α-*tert*-butyl.HCl (0.159 g, 0.507 mmol) and triethylamine (0.14 mL, 1.014 mmol) in DCM was added to the reaction mixture, and the progress of the reaction was monitored through TLC using ethyl acetate and hexane (1:3) mixture as eluent. The reaction mixture was further stirred for overnight at room temperature. After the completion of the reaction, the reaction mixture was concentrated under reduced pressure, diluted with ethyl acetate, washed with water and brine. The organic layer was dried over anhydrous Na_2SO_4, filtered and the solvent was evaporated under reduced pressure to afford crude reaction mixture which was purified by column chromatography over 100-200 mesh silica gel using 25% ethyl acetate and hexane as eluent. The purified benzyl tris(*tert*-butoxy) protected DUPA precursor **3**. Yellowish gummy liquid (yield = 85%, 249 mg), R_f = 0.29 (EtOAc : hexane = 1:3); ^{1}H NMR (400 MHz, $CDCl_3$): δ 7.33 (m, 5H), 5.10–5.04 (m, 4H), 4.38–4.28 (m, 2H), 2.51–2.37 (m, 2H), 2.32–2.23 (m, 2H), 2.20–2.12 (m, 1H), 2.09–2.00 (m, 1H), 1.96–1.81 (m, 2H), 1.44 (s, 9H), 1.43 (s, 9H), 1.41 (s, 9H). ^{13}C NMR (100 MHz, $CDCl_3$): δ 172.9, 172.5, 172.0, 171.9, 156.8, 135.8, 128.5, 128.2, 82.1, 82.0, 80.5, 66.4, 53.1, 53.0, 31.5, 30.3, 28.4, 28.3, 28.1,

28.0. HRMS (ESI) m/z $[M+Na]^+$ calcd. for $C_{30}H_{46}N_2O_9$, 601.3096, found, 601.3092.

6.4.2.2 Procedure for debenzylation of benzyl tris(*tert*-butoxy) protected DUPA precursor (3) to give (*S*)-5-(*tert*-butoxy)-4-(3-((*S*)-1,5-di-*tert*-butoxy-1,5-dioxopentan-2-yl)ureido)-5-oxopentanoic acid (4)

To a solution of benzyl tris(*tert*-butoxy) protected DUPA precursor **3** (0.250 g, 0.434 mmol) in dichloromethane (10 mL), 10 mol% Pd/C (40 mg) was added. The reaction mixture was hydrogenated under an atmosphere of H_2 gas (1atm.) for 24 h at room temperature. After the completion of the reaction, Pd/C was filtered through celite bed and washed with DCM (3 × 5 mL). The solvent was evaporated under reduced pressure, and the crude product was purified through column chromatography (hexane: ethyl acetate = 50:50) to afford tris(*tert*-butoxy) protected DUPA precursor **4** which was further used for peptide coupling reaction in the solid phase peptide synthesis. Colourless viscous liquid solidified on standing (yield = 80%, 169 mg), R_f = 0.48 (EtOAc : hexane = 1:1); ^{1}H NMR (400 MHz, $CDCl_3$): δ 5.01 (d, *J* = 7.76 Hz, 2H), 4.32 (ddd, *J* = 5.0, 5.26, 7.76 Hz, 2H), 2.37–2.21 (m, 4H), 2.10–2.01 (m, 2H), 1.89–1.80 (m, 2H), 1.45 (s, 9H), 1.42 (s, 18H). ^{13}C NMR (100 MHz, $CDCl_3$): δ 176.1, 173.1, 172.5, 171.9, 157.8, 82.5, 82.1, 80.6, 53.3, 53.0, 31.5, 30.3, 28.4, 28.1, 28.0, 27.9, 27.8. HRMS (ESI) m/z $[M+Na]^+$ calcd. for $C_{23}H_{40}N_2O_9$, 511.2626, found, 511.2640.

6.4.3 General procedure for solid phase synthesis

6.4.3.1 Resin swelling

All the resins used in solid phase peptide synthesis were swelled initially with 5 mL of DCM for 30 minutes by bubbling nitrogen and after draining DCM, the resin is swelled once again with 5 mL DMF thrice for 15 minutes each.

6.4.3.2 General procedure for the Kaiser test

Few resin beads were taken in a test-tube and two drops of each of ninhydrin, phenol and 0.1% potassium cyanide solution were added to the test-tube and heated for 2 minutes at 110 °C in a sand bath. The presence of a free amine group was confirmed by the appearance of dark blue colored resin beads in the test tube. The test was performed after performing coupling of each amino acid by the aforementioned procedure.

6.4.3.3 General procedure for NHFmoc deprotection

The NHFmoc-amino group in the growing peptide chain was deprotected in each step using a freshly prepared solution of 20% piperidine in DMF (10 mL). Initially, 4 mL of the 20% piperidine solution in DMF was added to the resin beads and mixed for 10 minutes by bubbling nitrogen gas. The solution was drained from the resin beads, and the procedure was repeated twice with the remaining 20% piperidine solution (2 × 3 mL) for 10 minutes each to ensure complete deprotection of NHFmoc protecting group.

6.4.3.4 General procedure for peptide cleavage from resin beads

A mixture of 9.25 mL trifluoroacetic acid (TFA), 0.25 mL triisopropylsilane (TIPS), 0.25 mL Ethanedithiol (EDT) and 0.25 mL Millipore water (H_2O) was prepared in a 10 mL centrifuge tube and thoroughly mixed by vortex. 5 mL of this cocktail solution was added to the dried resin beads containing peptide conjugate, and nitrogen gas was bubbled through the resin beads and cocktail mixture for 30 minutes. The cleaved peptide solution was drained from the resin beads into a single-neck round-bottomed flask (25 mL). The cleavage procedure was repeated twice (2 × 2.5 mL) with the resin beads using the remaining cocktail solution for 15 minutes each as mentioned before. The cleaved peptide solution from the peptide vessel was pooled together into a single-neck

round-bottomed flask (25 mL) and then transferred to a 15 mL centrifuge tube using a Pasteur pipette. The mother liquor from cleavage was concentrated under reduced pressure using rotavapor to evaporate trifluoroacetic acid, and the concentrated viscous liquid was treated with ice-cold diethyl ether (2-3 mL) to precipitate the desired ligand-targeted peptide conjugate. The upper ether layer was discarded, and the precipitated conjugate was washed thrice with ice-cold ether (3 × 3 mL). The precipitated conjugate was dried by a stream of nitrogen gas through the centrifuge tube fitted with a septum and an outlet needle for 45 minutes.

6.4.3.5 Synthesis of PSMA targeted DUPA Rhodamine B conjugate 13, DUPA-NH-$(CH_2)_7$CO-Phe-Phe-NH-$(CH_2)_7$CO-Lys(RhodamineB)-Dap-Asp-Cys

H-Cys-2-ClTrt resin (0.050 g, 0.031 mmol) was swelled initially with 5 mL of DCM by bubbling nitrogen gas for 30 minutes. After draining the DCM, the resin was swelled with 5 mL DMF thrice for 15 minutes each. *N*-Fmoc-Asp(O^{t}Bu)-OH (0.032 g, 0.078 mmol), PyBOP (0.040 g, 0.078 mmol) and DIPEA (0.135 mL, 0.78 mmol) in 0.5 mL DMF was added to peptide vessel containing resin beads and the coupling reaction was continued for 6 h. The resin beads were washed with DMF (3 × 3 mL) followed by isopropanol (3 × 3 mL), and the beads were dried by a stream of nitrogen gas. The completion of the reaction was confirmed by performing the Kaiser test with few dried resin beads. A solution of 20% piperidine in DMF (10 mL) was prepared, added to the resin beads in aliquots (1 × 4 mL; 2 × 3 mL), mixed for 10 minutes each, and drained to ensure complete deprotection of Fmoc protecting group of the coupled amino acid as mentioned in the general procedure. The resin beads were washed again with DMF (3 × 3 mL) followed by isopropanol (3 × 3 mL) and dried by a stream of nitrogen gas. The formation of free amine was confirmed by performing the Kaiser test with few resin beads. After the

swelling of resin in DMF, Boc-DAP(Fmoc)-OH (0.033 g, 0.078 mmol), PyBOP (0.040 g, 0.078 mmol) and DIPEA (0.135 mL, 0.78 mmol) in 0.5 mL DMF was added to the resin beads, and the same steps were followed as described above. A series of amino acids including of Fmoc-Lys(Tfa)-OH (0.036 g, 0.078 mmol), Fmoc-8-aminocaprylic acid (0.030g, 0.078 mmol), Fmoc-Phe-OH (0.030 g, 0.078 mmol), Phe-OH (0.030 g, 0.078 mmol) followed by Fmoc-8-aminocaprylic acid (0.030g, 0.078 mmol) were coupled to the growing peptide chain as described earlier. After deprotection of Fmoc group tri(*tert*-butyl) protected DUPA (0.023g, 0.047 mmol), PyBOP (0.040 g, 0.078 mmol) and DIPEA (0.135 mL, 0.78 mmol) in 0.5 ml DMF was added to the resin beads and swelled for 6 h. The resin beads were washed again with DMF (3 × 3 mL) followed by isopropanol (3 × 3 mL) and dried by a stream of nitrogen gas. The completion of the reaction was confirmed by the Kaiser test with few dried resin beads. At last trifluoroacetyl protected amino group of lysine was cleaved by 6–12 h treatment with 2M aqueous piperidine at room temperature and the complete deprotection of Tfa group was confirmed by the Kaiser test following a similar procedure as described in the earlier step. Rhodamine B (0.023g, 0.047), PyBOP (0.040 g, 0.078 mmol) and DIPEA (0.135 mL, 0.78 mmol) in 0.5 ml DMF was added to the peptide vessel and swelled for 6 h at room temperature. The completion of the rhodamine B coupling reaction was confirmed by the Kaiser test. Finally, the resin was cleaved using a cocktail solution as described earlier in the experimental section. The crude fluorescent peptide conjugate was concentrated under reduced pressure to evaporate TFA, and ice-cold ether was added to precipitate the DUPA Rhodamine B conjugate **13** as bright red solid. The crude product **13** was purified through Buchi reveleris prep instrument using RP-PFP preparative column (XSelect CSH Prep Fluorophenyl 5 µm OBD) (5 µm, 19 mm × 150 mm) at λ = 280 or 555 nm (detailed procedure was mentioned in preparative HPLC chromatography method). Acetonitrile was removed under reduced pressure, and pure fractions were freeze-dried

to yield DUPA Rhodamine B conjugate **13** as red solid. The yield of **9** was 76% (41 mg), and the purity of the conjugate **13** is further confirmed by reverse phase analytical high-pressure liquid chromatography (RP-HPLC) t_R = 9.8 min. The molecular mass is determined by LC-MS. HRMS (+ESI) calcd for $[M\text{-}Cl]^+$ $(C_{89}H_{121}N_{14}O_{21}S)^+$: 1753.8546 found 1753.8557.

6.4.3.6 General procedure for solid phase peptide synthesis of pteroate Rhodamine B conjugate 17, pteroate-NH-$(CH_2)_7$CO-Lys(Rhodamine B)-DAP-Asp-Cys

H-Cys(Trt)-2-ClTrt resin (0.050 g, 0.031 mmol) was swelled first using DCM (5 mL) followed by DMF (5 mL) according to the aforementioned procedure. Fmoc-Asp(O^{t}Bu)-OH (0.032g, 0.078 mmol), PyBOP (0.040 g, 0.078 mmol) and DIPEA (0.135 mL, 0.78 mmol) in 0.3 mL DMF was added to peptide vessel with resin beads and bubbled using nitrogen gas for 6 h. The resin beads were washed with DMF (3 × 3 mL) followed by isopropanol (3 × 3 mL), and the beads were dried by a stream of nitrogen gas. The completion of the reaction was confirmed by performing the Kaiser test with few dried resin beads. A solution of 20% piperidine in DMF (10 mL) was prepared, added to the resin beads in aliquots (1 × 4 mL; 2 × 3 mL), mixed for 10 minutes each, and drained to ensure complete deprotection of Fmoc protecting group of the coupled amino acid as mentioned in the general procedure. The resin beads were washed again with DMF (3 × 3 mL) followed by isopropanol (3 × 3 mL) and dried by a stream of nitrogen gas. The formation of free amine was confirmed by performing the Kaiser test with few resin beads. After swelling the resin again in DMF, Boc-Dap(Fmoc)-OH (0.033 g, 0.078 mmol), PyBOP (0.040 g, 0.078 mmol) and DIPEA (0.135 mL, 0.78 mmol) in 0.5 mL DMF was added to the resin and same steps were followed as described above. Amino acids Fmoc-Lys(Tfa)-OH (0.036 g, 0.078 mmol), Fmoc-8-aminocaprylic acid (0.030g, 0.078 mmol) were coupled sequentially to the peptide chain following a similar procedure. Finally after the cleavage of

NHFmoc group from the peptide chain using 20% piperidine in DMF (1 × 4 mL; 2 × 3 mL), N^{10}-(trifluoroacetyl)pteroic acid (0.046 g, 0.019 mmol), PyBOP (0.040 g, 0.078 mmol) and DIPEA (0.135 mL, 0.78 mmol) in 0.3 mL DMSO was added to the resin beads in peptide vessel and bubbled for 6 h. The peptide vessel was wrapped with aluminum foil to protect from light. The completion of the reaction was ensured by the Kaiser test after washing the resin beads with DMF (3 × 5 mL) and isopropanol (3 × 5 mL). An aliquot of 1% hydrazine in DMF (3 × 2 mL) was added to the resin beads to deprotect N^{10}-(trifluoroacetyl) protecting group by bubbling through resin beads for 10 min each. The resin beads were washed with DMF (3 × 3 mL) followed by isopropanol (3 × 3 mL). The 2° amine group generated in the pteroate core doesn't give positive Kaiser test. The lysine trifluoroacetyl protected amino group was now deprotected by 6–12 h treatment with 2M aqueous piperidine at room temperature and the completion of deprotection was confirmed by the Kaiser test. Rhodamine B (0.023g, 0.047 mmol), PyBOP (0.040 g, 0.078 mmol) and DIPEA (0.135 mL, 0.78 mmol) in 0.5 ml DMF was added to the resin beads in peptide vessel, and the coupling was continued for 6 h at room temperature. The completion of the reaction was confirmed by the Kaiser test. The resin beads were dried for 30-minutes under a nitrogen atmosphere. The pteroate Rhodamine B conjugate **17** obtained as a red precipitate after cleavage from the resin beads. The crude product **78** was purified through Buchi reveleris prep instrument using RP-PFP (pentafluorophenyl) preparative column (5 μm, 19 mm × 150 mm) at λ = 280 or 555 nm (detailed procedure was mentioned in preparative HPLC chromatography method). Acetonitrile was removed under reduced pressure, and pure fractions were freeze-dried to yield pteroate rhodamine B conjugate **17** as red solid. The yield of the product **17** was 70% (33 mg), and the purity of the conjugate **17** is further confirmed by reverse phase analytical high-pressure liquid chromatography, (RP-HPLC) t_R = 3.09

min. The molecular mass is determined by LC-MS and HRMS (+ESI) calcd for $[M\text{-}Cl]^+$ $(C_{66}H_{84}N_{15}O_{12}S)^+$: 1310.6139 found 1310.6352.

6.4.4 Analytical HPLC method

The purity of bioconjugates **13** and **17** were analyzed using a Dionex HPLC-Ultimate 3000 system. Typically a solution of either **13** or **17** (20 µL, 1.0 mg/1.0 mL) dissolved in a mixture of CH_3CN:H_2O (1: 1) was injected via autosampler and eluted using Dionex Acclaim ® 120 C_{18}, 5 µm, 4.6 mm × 250 mm analytical column at a flow rate of 1 mL/min (mobile phase, A = 0.1% trifluoro acetic acid/H_2O and B = acetonitrile). An isocratic flow of 40% B (v/v) was used during the run for 0 to 4-min, and gradually a linear gradient of B up to 100% B (v/v) was applied over a period of 40-min. The chromatogram was recorded using the Ultimate 3000 RS Variable Wavelength detector at 225–280 nm.

6.4.5 Preparative HPLC method

The purification of bioconjugates **13** and **17** was performed using Buchi Reveleris Prep HPLC System. Crude bioconjugates **13** or **17** was dissolved in a mixture of CH_3CN:H_2O (1: 1) (1 mL) and injected into the sample injector for elution using RP-PFP (Reverse Phase PentafluoroPhenyl) preparative column (XSelect CSH Prep Fluorophenyl 5 µm OBD, 19 mm × 150 mm). A flow rate of 10 mL/min (mobile phase, A = 0.1% trifluoro acetic acid/H_2O and B = acetonitrile) is maintained throughout the run and the mobile phase gradient was changed from 1% B (v/v) to 50% B (v/v) over a period of 40-min. The mobile phase gradient was further changed to 80% B (v/v) in the next 15-min, and the chromatogram was recorded at λ = 280 or 555 nm. Pure fractions of **13** or **17** were collected using automatic fraction collector, acetonitrile was evaporated under reduced pressure and freeze-dried to obtain pure conjugates **13** or **17**.

6.4.6 Culture of human cancer and epithelial cell lines

LNCaP and CHO-β cells were obtained as a gift from Prof. Philip S. Low, Purdue University, West Lafayette, USA whereas PC-3 cell line was purchased from NCCS, Pune, India. LNCaP cells were grown as a monolayer using 1640 RPMI medium containing 10% heat-inactivated fetal bovine serum and 1% penicillin-streptomycin and CHO-β cells in folate-deficient RPMI 1640 containing 10% heat-inactivated foetal bovine serum and supplemented with 1% penicillin-streptomycin. Both the cell lines were grown in a 5% CO_2:95% air-humidified atmosphere at 37 °C**.**

6.4.7 Procedure for uptake study of peptide conjugates 13 and 17 using laser scanning confocal microscope in human cancer cell lines LNCaP, PC-3 and epithelial cell line CHO-β

LNCaP cells (15,000 cells/well in 1 mL), CHO-β (10,000 cells/well in 1mL) and PC-3 (10,000 cells/well) were seeded into German borosilicate confocal dishes and allowed cells to form monolayers over 24 h. Spent medium was replaced with fresh medium containing DUPA-Rhodamine B, **13** (100 nM) and pteroate-Rhodamine B, **17** (150 nM) in LNCaP and CHO- β cells respectively and the cells were incubated with the compound for 1 h at 37 °C. For competition experiment, 100-fold excess concentration of binding ligand, 2-PMPA for LNCap cells and folic acid for CHO-β cells were incubated for 1 h at 37 °C before incubation with bioconjugate **13** (100 nM) and **17** (150 nM) respectively. After rinsing with fresh medium (3 × 1.0 mL) to remove unbound conjugates, confocal images were acquired using a laser scanning confocal microscopy (FV 1000, Olympus) by excitation at 559 nm (yellow diode laser) and emission at 618 nm.

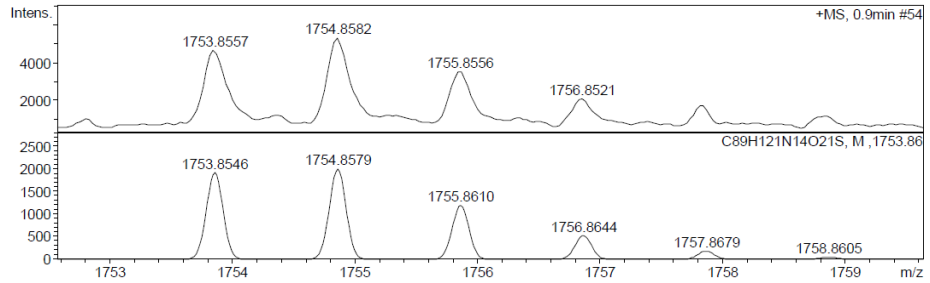

Figure 6.4 HRMS of PSMA targeted DUPA rhodamine B chelating conjugate **13**

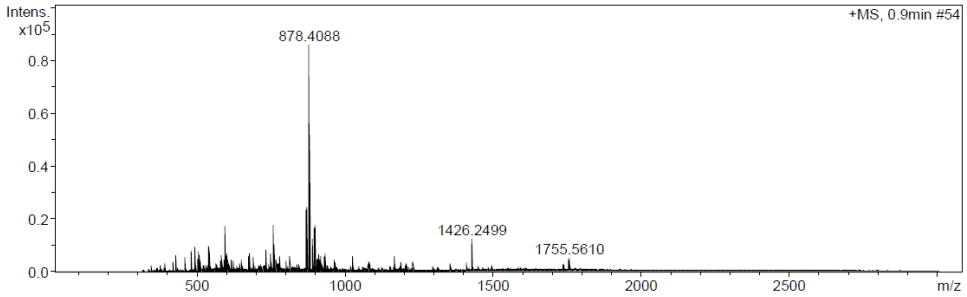

Figure 6.5 ESI-MS of PSMA targeted DUPA rhodamine B chelating conjugate **13**

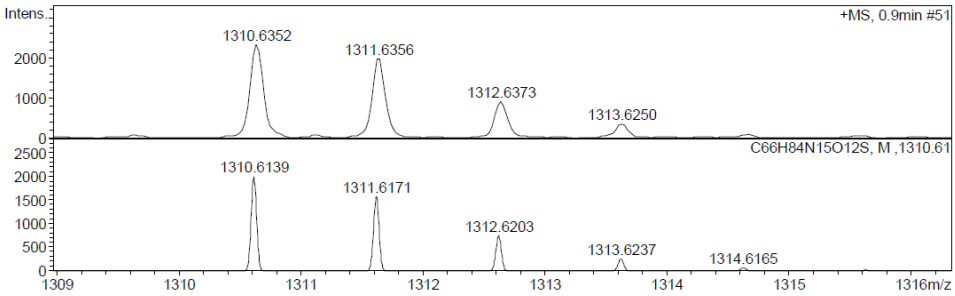

Figure 6.6 HRMS of pteroate rhodamine B chelating conjugate **17**

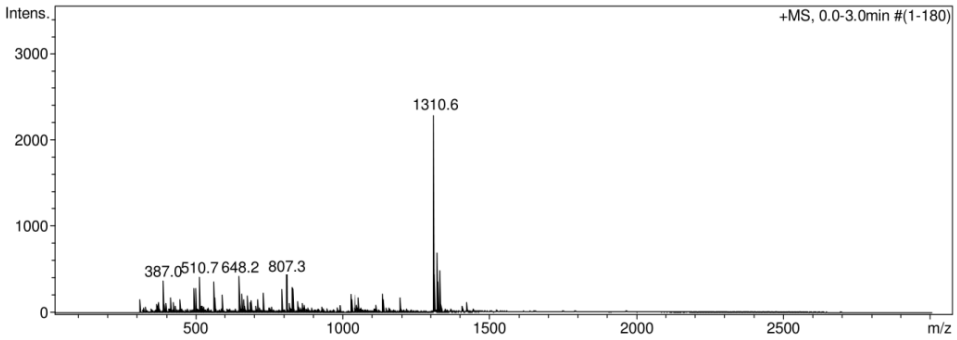

Figure 6.7 ESI-MS of pteroate rhodamine B chelating conjugate **17**

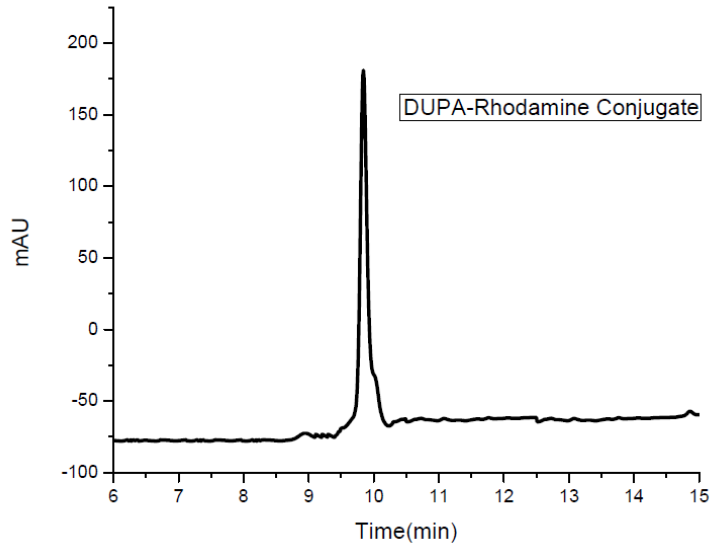

Figure 6.8 Analytical LC of pure DUPA rhodamine B chelating conjugate **13** (Abs. at 254 nm)

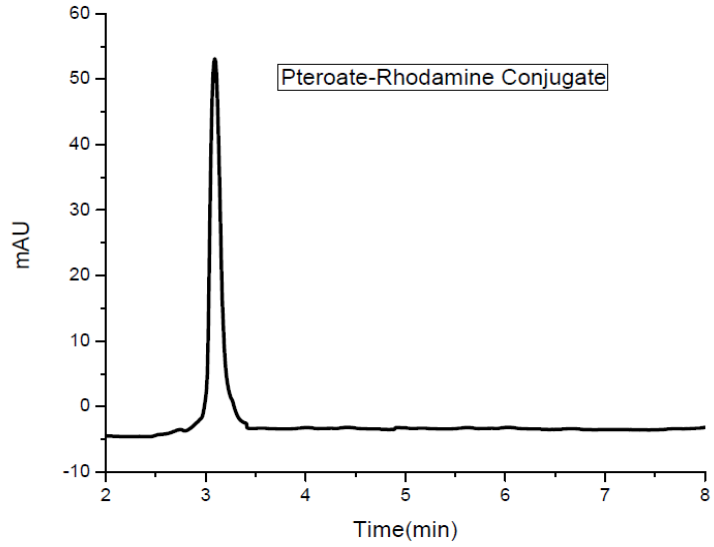

Figure 6.9 Analytical LC of pure pteroate rhodamine B chelating conjugate **17** (Abs. at 254 nm)

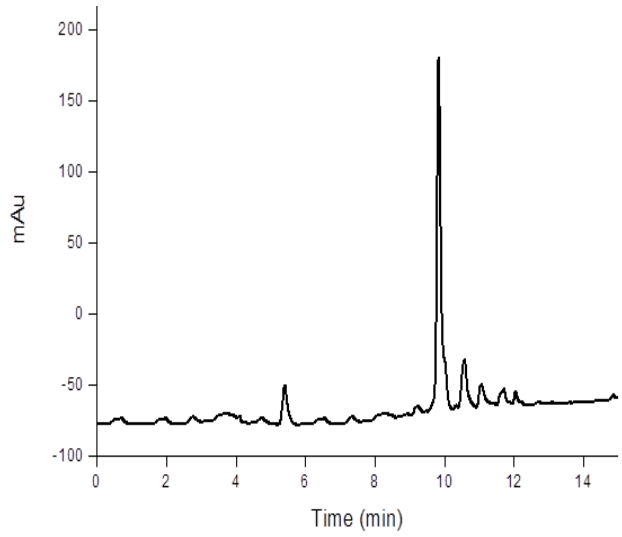

Figure 6.10 Analytical LC of crude DUPA rhodamine B chelating conjugate **13** (Abs.at 225 nm)

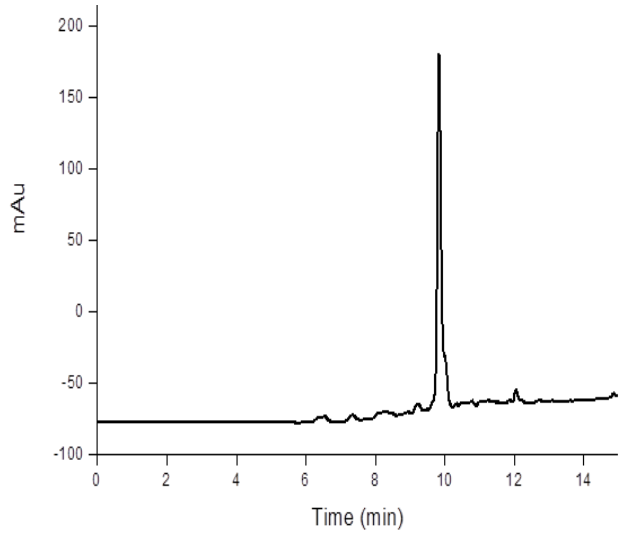

Figure 6.11 Analytical LC pure DUPA rhodamine B chelating conjugate **13** (Abs. at 225 nm)

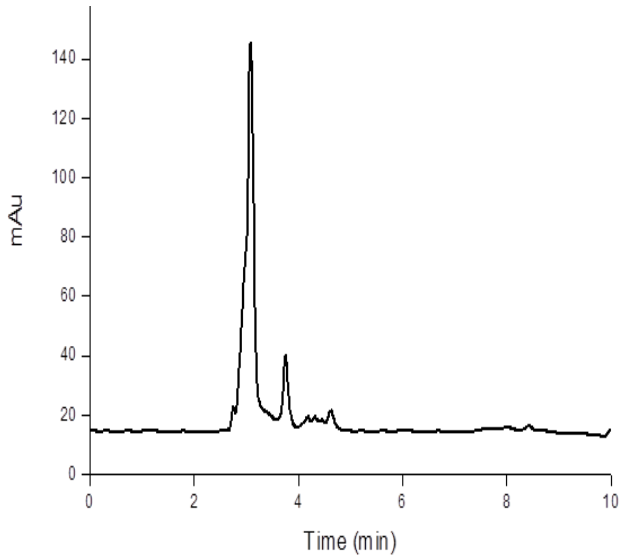

Figure 6.12 Analytical LC of crude pteroate rhodamine B chelating conjugate **17 (**Abs.at 225 nm)

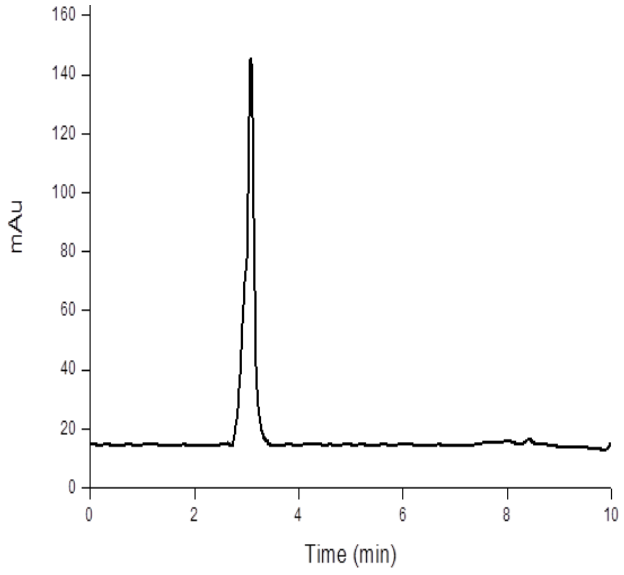

Figure 6.13 Analytical LC data of pure pteroate rhodamine B chelating conjugate **17 (**Abs. at 225 nm)

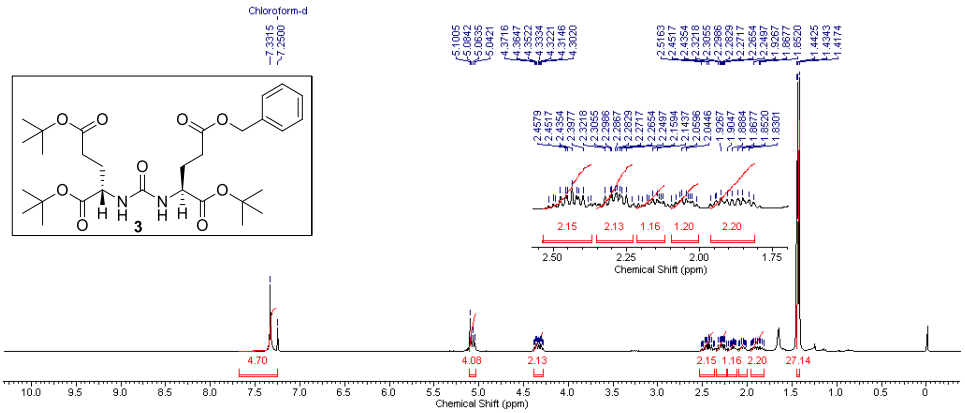

Figure 6.14 ^{1}H NMR spectrum (400 MHz, $CDCl_3$) of **3**

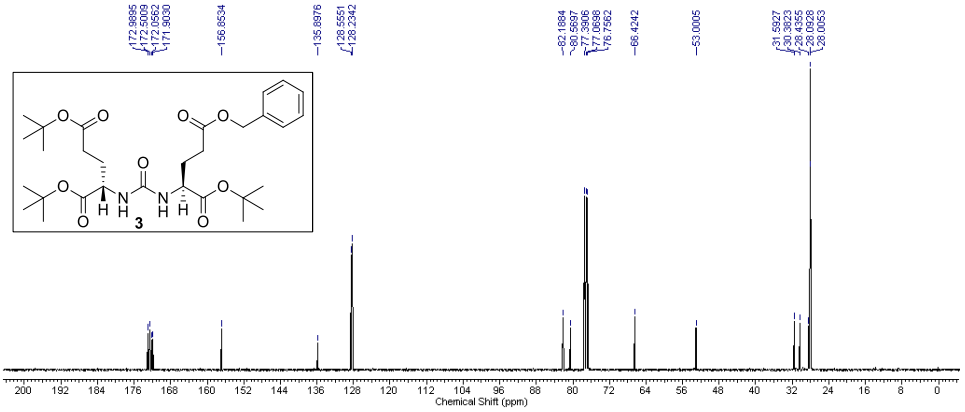

Figure 6.15 ^{13}C NMR spectrum (100 MHz, $CDCl_3$) of **3**

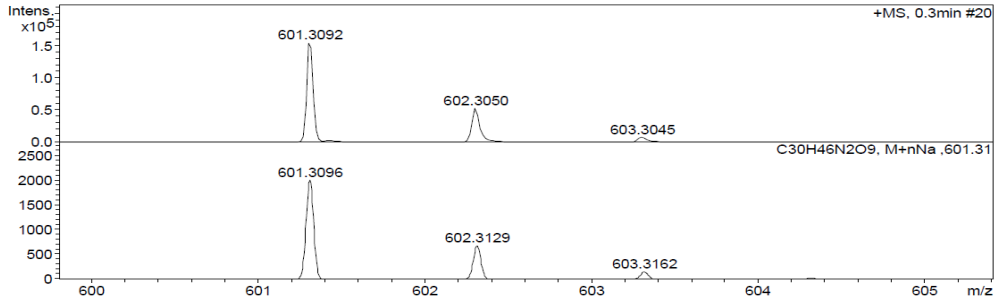

Figure 6.16 HRMS of **3**

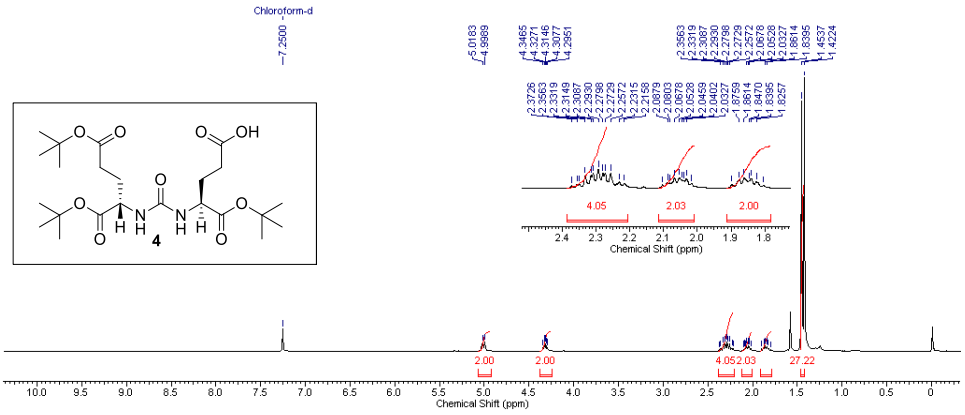

Figure 6.17 ^{1}H NMR spectrum (400 MHz, $CDCl_3$) of **4**

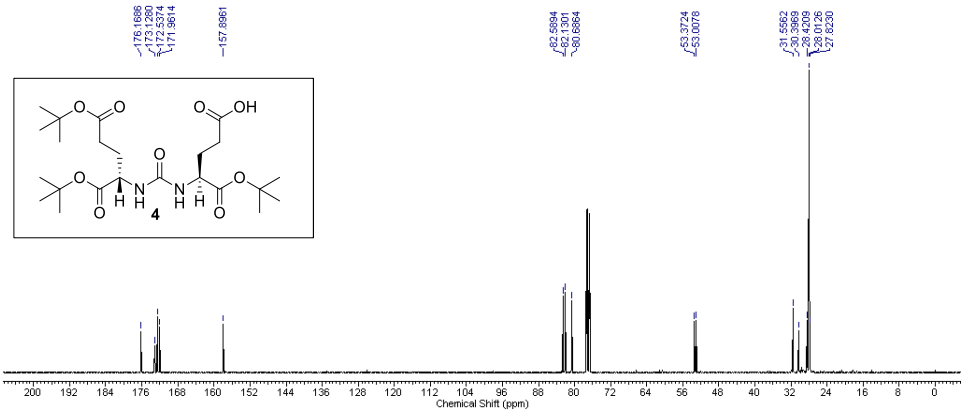

Figure 6.18 ^{13}C NMR spectrum (100 MHz, $CDCl_3$) of **4**

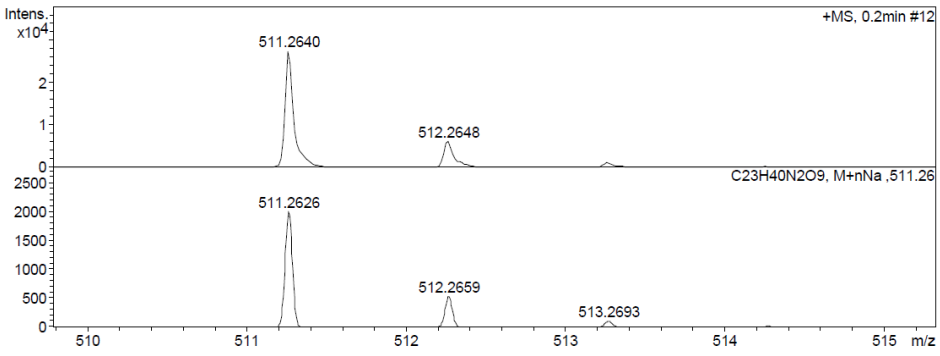

Figure 6.19 HRMS of **4**

6.5 References

1. Srinivasarao M., Low P. S. (2017), Ligand-targeted drug delivery, Chem. Rev.**,** 117, 12133–12164 (DOI: 10.1021/acs.chemrev.7b00013).

2. Bernsen M. R., Kooiman K., Segbers M., van Leeuwen F. W. B., de Jong M. (2015), Biomarkers in preclinical cancer imaging, Eur. J. Nucl. Med. Mol. Imaging, 42, 579–596 (DOI: 10.1007/s00259-014-2980-7).

3. Yankeelov T. E., Abramson R. G., Quarles C. C. (2014), Quantitative multimodality imaging in cancer research and therapy, Nat. Rev. Clin. Oncol., 11, 670–680 (DOI: 10.1038/nrclinonc.2014.134).

4. Gao M., Yu F., Lv C., Choo J., Chen L. (2017), Fluorescent chemical probes for accurate tumor diagnosis and targeting therapy, Chem. Soc. Rev. 46, 2237–2271 (DOI: 10.1039/C6CS00908E).

5. Cutler C. S., Hennkens H. M., Sisay N., Hucklier-Markai S., Jurisson S. S. (2013) Radiometal for combined imaging and therapy, Chem. Rev., 113, 858–883 (DOI: 10.1021/cr3003104).

6. Mather S. (2009), Molecular imaging with bioconjugates in mouse models of cancer, Bioconjugate Chem., 20, 631–643 (DOI: 10.1021/bc800401x).

7. Chang S. S. (2004), Overview of prostate-specific membrane antigen, Rev. Urol., 6, S13-18.

8. Barrio M., Fendler W. P., Czernin J., Herrmann K. (2016), Prostate specific membrane antigen (PSMA) ligands for diagnosis and therapy of prostate cancer, Expert Rev. Mol. Diagn., 16, 1177–1188 (DOI: 10.1080/14737159.2016.1243057).

9. Ristau B. T., O'Keefe D. S., Bacich D. J. (2014), The prostate-specific membrane antigen: Lessons and current clinical implications from 20

years of research, Urol. Oncol., 32, 272–279 (DOI: 10.1016/j.urolonc.2013.09.003).

10. Kalli K. R., Oberg A. L., Keeney G. L., Christianson T. J. H., Low P. S., Knutson K. L., Hartmann L. C. (2008), Folate receptor alpha as a tumor target in epithelial ovarian cancer, Gynecol. Oncol., 108, 619–626 (DOI: 10.1016/j.ygyno.2007.11.020).

11. Lutz R. J. (2015), Targeting the folate receptor for the treatment of ovarian cancer, Transl. Cancer Res., 4, 118–126 (DOI: 10.3978/j.issn.2218-676X.2015.01.04).

12. Sega E. I., Low P. S. (2008), Tumor detection using folate receptor-targeted imaging agents, Cancer Metastasis Rev., 27, 655–664 (DOI: 10.1007/s10555-008-9155-6).

13. Low P. S., Kularatne S. A. (2009), Folate-targeted therapeutic and imaging agents for cancer, Curr. Opin. Chem. Biol., 13, 256–262 (DOI: 10.1016/j.cbpa.2009.03.022).

14. Lu Y., Stinnette T. W., Westrick E., Klein P. J., Gehrke M. A., Cross V. A., Vlahov I. R., Low P.S., Leamon C.P. (2011), Treatment of experimental adjuvant arthritis with a novel folate receptor-targeted folic acid-aminopterin conjugate, Arthritis Res. Ther., 13, R56 (DOI: 10.1186/ar3304).

15. Jager N. A., Teteloshvili N., Zeebregts C. J., Westra J., Bijl M. (2012), Macrophage folate receptor-β (FR-β) expression in auto-immune inflammatory rheumatic diseases: A forthcoming marker for cardiovascular risk?, Autoimmun. Rev., 11, 621–626 (DOI: 10.1016/j.autrev.2011.11.002).

16. Low P. S., Henne W. A., Doorneweerd D. D. (2008), Discovery and development of folic-acid-based receptor targeting for imaging and

therapy of cancer and inflammatory diseases, Acc. Chem. Res., 41, 120–129 (DOI: 10.1021/ar7000815).

17. van Dam G. M., Themelis G., Crane L. M. A., Harlaar N. J., Pleijhuis R. G., Kelder W., Sarantopoulos A., de Jong J. S., Arts H. J. G., van der Zee A. G. J., Bart J., Low P. S**.,** Ntziachristos V. (2011), Intraoperative tumor-specific fluorescence imaging in ovarian cancer by folate receptor-α targeting: First in-human results, Nat. Med., 17, 1315–1320 (DOI: 10.1038/nm.247).

18. Keating J. J., Okusanya O.T., De Jesus E., Judy R., Jiang J., Deshpande C., Nie S., Low P. S., Singhal S. (2016), Intraoperative molecular imaging of lung adenocarcinoma can identify residual tumor cells at the surgical margins, Mol. Imaging. Biol., 18, 209–218 (DOI: 10.1007/s11307-015-0878-9).

19. Kennedy G. T., Okusanya O.T., Keating J. J., Heitjan D. F., Deshpande C., Litzky L. A., Albelda S. N., Drebin J. A., Nie S., Low P. S., Singhal S. (2015), The optical biopsy: a novel technique for rapid intraoperative diagnosis of primary pulmonary adenocarcinomas, Ann. Surg., 262, 602–609 (DOI: 10.1097/SLA.0000000000001452).

20. Okusanya O. T., DeJesus E. M., Jiang J. X., Judy R. P., Venegas O. G., Deshpande C. G., Heitjan D. F., Nie S., Low P. S., Singhal S. (2015), Intraoperative molecular imaging can identify lung adenocarcinomas during pulmonary resection, J. Thorac. Cardiovasc. Surg., 150, 28–35 (DOI: 10.1016/j.jtcvs.2015.05.014).

21. Tummers Q. R. J. G., Hoogstins C. E. S., Gaarenstroom K. N., de Kroon C. D., van Poelgeest M. I. E., Vuyk J., Bosse T., Smit V. T. H. B. M., van de Velde C. J. H., Cohen A. F., Low P. S., Burggraaf J., Vahrmeijer A. L, Intraoperative imaging of folate receptor alpha positive

ovarian and breast cancer using the tumor specific agent EC17, Oncotarget, 7, 32144–32155(DOI: 10.18632/oncotarget.8282).

22. Kelemen L. E. (2006), The role of folate receptor in cancer development, progression and treatment: Cause, consequence or innocent bystander?, Int. J. Cancer**,** 119, 243–250 (DOI: 10.1002/ijc.21712).

23. Bouchelouche K., Choyke P. L., Capala J. (2010), Prostate specific membrane antigen–A target for imaging and therapy with radionuclides, Discov. Med., 9, 55–61.

24. Jin W., Qin B., Chen Z., Liu H., Barve A., Cheng K. (2016), Discovery of PSMA-specific peptide ligands for targeted drug delivery, Int. J. Pharm., 513, 138–147 (DOI: 10.1016/j.ijpharm.2016.08.048).

25. Zhao X., Li H., Lee R. J. (2008), Targeted drug delivery via folate receptors, Expert Opin. Drug Deliv., 5, 309–319 (DOI: 10.1517/17425247.5.3.309).

26. Rink H. (1987), Solid-phase synthesis of protected peptide fragments using a trialkoxy-diphenyl-methylester resin, Tetrahedron Lett., 28, 3787–3790 (DOI: 10.1016/S0040-4039(00)96384-6).

27. Bollhagen R., Schmiedberger M., Barlos K., Grell E. (1994), A new reagent for the cleavage of fully protected peptides synthesised on 2-chlorotrityl chloride resin, J. Chem. Soc., Chem. Commun., 2559–2560 (DOI: 10.1039/c39940002559).

28. Mergler M., Nyfeler R., Tanner R., Gosteli J., Grogg P. (1988), Peptide synthesis by a combination of solid-phase and solution methods II synthesis of fully protected peptide fragments on 2-methoxy-4-alkoxy-benzyl alcohol resin, Tetrahedron Lett., 29, 4009–4012 (DOI: 10.1016/S0040-4039(00)80406-2).

29. Sieber P. (1987), A new acid-labile anchor group for the solid-phase synthesis of C-terminal peptide amides by the fmoc method, Tetrahedron Lett., 28, 2107–2110 (DOI: 10.1016/S0040-4039(00)96055-6).

30. Aletras A., Barlos K., Gatos D., Koutsogianni S., Mamos P. (1995), Preparation of the very acid sensitive Fmoc-Lys(Mtt)-OH: Application in the synthesis of side-chain to side-chain cyclic peptides and oligolysine cores suitable for the solid phase assembly of MAPs and TASPs, Int. J. Peptide Protein Res., 45, 488–496 (DOI: 10.1111/j.1399-3011.1995.tb01065.x).

31. Zhao N., Williams T. M., Zhou Z., Fronczek F. R., Sibrian-Vazquez M., Jois S. D., Vicente M. G. H. (2017), Synthesis of BODIPY-peptide conjugates for fluorescence labeling of EGFR overexpressing cells, Bioconjugate. Chem., 28, 1566–1579 (DOI: 10.1021/acs.bioconjchem.7b00211).

32. Kuil J., Buckle T., Yuan H., van den Berg N. S., Oishi S., Fujii N., Josephson L., van Leeuwen F. W. B. (2011), Synthesis and evaluation of a bimodal CXCR4 antagonistic peptide, Bioconjugate. Chem., 22, 859–864 (DOI: 10.1021/bc2000947).

33. Napp J., Stammes M. A., Claussen J., Prevoo H. A. J. M., Sier C. F. M., Hoeben F. J. M., Robillard M. S., Vahrmeijer A. L., Devling T., Chan A. B., Geus-Oei L. D., Frauke A. (2018), Fluorescence- and multispectral optoacoustic imaging for an optimized detection of deeply located tumors in an orthotopic mouse model of pancreatic carcinoma. Int. J. Cancer, 142, 2118–2129 (DOI:10.1002/ijc.31236).

34. Viehweger K., Barbaro L., García K. P., Joshi T., Geipel G., Steinbach J., Stephan H., Spiccia L., Graham B. (2014), EGF receptor-targeting peptide conjugate incorporating a near-IR fluorescent dye and a novel 1,4,7-triazacyclononane-based ^{64}Cu(II) chelator assembled via click

chemistry, Bioconjugate Chem., 25, 1011–1022 (DOI: 10.1021/bc5001388).

35. Xing T., Yang X., Wang F., Laia B., Yan L. (2012), Synthesis of polypeptide conjugated with near infrared fluorescence probe and doxorubicin for pH-responsive and image-guided drug delivery, J. Mater. Chem., 22, 22290–22300 (DOI: 10.1039/c2jm35627a).

36. Kularatne S. A., Wang K., Santhapuram H. K. R., Low P. S. (2009), Prostate-specific membrane antigen targeted imaging and therapy of prostate cancer using a PSMA inhibitor as a homing ligand, Mol. Pharm., 6, 780–789 (DOI: 10.1021/mp900069d).

37. Kelderhouse L. E., Chelvam V., Wayua C., Mahalingam S., Poh S., Kularatne S. A., Low P. S. (2013), Development of tumor-targeted near infrared probes for fluorescence guided surgery, Bioconjugate. Chem., 24, 1075–1080 (DOI: 10.1021/bc400131a).

38. Kularatne S. A., Zhou Z., Yang J., Post C. B., Low P. S. (2009), Design, synthesis, and preclinical evaluation of prostate-specific membrane antigen targeted ^{99m}Tc-radioimaging agents, Mol. Pharm. 6, 790–800 (DOI: 10.1021/mp9000712).

39. Kozikowski A. P., Zhang J., Nan F., Petukhov P. A., Grajkowska E., Wroblewski J.T., Yamamoto T., Bzdega T., Wroblewska B., Neale J. H. (2004), Synthesis of urea-based inhibitors as active site probes of glutamate carboxypeptidase II: Efficacy as analgesic agents, J. Med. Chem., 47, 1729–1738 (DOI: 10.1021/jm0306226)

40. Ross T. L., Honer M., Muller C., Groehn V., Schibli R., Ametamey S. M. (2010), A new ^{18}F-labeled folic acid derivative with improved properties for the PET imaging of folate receptor–positive tumors, J. Nucl. Med., 51, 1756–1762 (DOI: 10.2967/jnumed.110.079756).

41. Leamon C. P., You F., Santhapuram H. K., Fan M., Vlahov I. R. (2009), Properties Influencing the relative binding affinity of pteroate derivatives and drug conjugates thereof to the folate receptor, Pharm. Res., 26, 1315–1323 (DOI: 10.1007/s11095-009-9840-3)

42. Mesters J. R., Barinka C., Li W., Tsukamoto T., Majer P., Slusher B. S., Konvalinka J., Hilgenfeld R. (2006), Structure of glutamate carboxypeptidase II, a drug target in neuronal damage and prostate cancer, EMBO J., 25, 1375–1384 (DOI: 10.1038/sj.emboj.7600969).

43. Li D., Elbert D. L. (2002), The kinetics of the removal of the *N*-methyltrityl (Mtt) group during the synthesis of branched peptides, J. Peptide Res., 60, 300–303 (DOI: 10.1034/j.1399-3011.2002.21018.x).

44. Moroder L., Filippi B., Borin G., Marchiori F. (1975), Studies on cytochrome *c*. X. Synthesis of N^{α}-benzyloxycarbonyl-[Thr^{107}]-dotetracontapeptide (sequence 67-108) of baker's yeast Iso-1-Cytochrome C., Biopolymers, 14, 2061–2074 (DOI: 10.1002/bip.1975.360141007).

45. Pazos E., Vazquez O., Mascarenas J. L., Vazquez M.E. (2009), Peptide-based fluorescent biosensors. Chem. Soc. Rev., 38, 3348–3359 (DOI: 10.1039/b908546g).

46. Benesova M., Schafer M., Bauder-Wust U., Afshar-Oromieh A., Kratochwil C., Mier W., Haberkorn U., Kopka K., Eder M. (2015), Preclinical evaluation of a tailor-made DOTA-conjugated PSMA inhibitor with optimized linker moiety for imaging and endoradiotherapy of prostate cancer, J. Nucl. Med., 56, 914–920 (DOI: 10.2967/jnumed.114.147413).

47. Kularatne S. A., Chelvam V., Santhapuram H. K. R., Wang K., Vaitilingam B., Henne W. A., Low P. S. (2010), Synthesis and biological analysis of prostate-specific membrane antigen-targeted anticancer prodrugs. J. Med. Chem., 53, 7767–7777 (DOI: 10.1021/jm100729b).

Chapter 7

Conclusions and Scope for Future Work

7.1 Conclusion

Current treatment strategies for cancer are based on precision and personalized medicine which involves drug selection based on the patient's requirement and delivery of therapeutics selectively to diseased cells. One attractive strategy for selective delivery of diagnostic and therapeutic cargos for imaging and treatment of cancer is by tethering required cargo with a protein recognition moiety or targeting ligand that has a selective affinity to the biomarkers expressed during diseased condition. This thesis focusses on design, synthesis and biological evaluation of novel, potent homing ligands with high specificity and affinity to pathological cells. For this purpose, we have expanded the scope of structural modifications of targeting ligands by *in silico* modeling. After successful design and chemical synthesis, the new inhibitors or ligands were transformed into novel diagnostic tools and evaluated *in vitro* to demonstrate their potential as promising candidates for early diagnosis of PCa.

Chapter 1 provides general introduction of the disease, cancer, its' global and national status, conventional techniques employed worldwide for diagnosis and treatment, their merits and demerits, and the significance of cancer biomarkers for targeted delivery of diagnostics and therapeutics. The chapter details the prevalence of PCa worldwide and the importance of PSMA as a biomarker for molecular imaging. It concludes with a literature review of PSMA inhibitors and their applications in diagnosis and therapy of PCa.

Chapter 2 describes the design and synthesis of a new class of small molecule inhibitors called aminoacetamides, developed after performing extensive *in silico* studies mimicking structural features of the peptide

neurotransmitter, N-Acetylaspartylglutamic acid (NAAG). After the optimization of small molecules as ligands by molecular docking studies with PSMA protein, a simple retrosynthetic analysis was identified to synthesize a library of *tertiary* butylcarboxy protected aminoacetamide derivatives. Ten carboxy protected aminoacetamide derivatives were synthesized and characterized by various spectroscopic techniques. I*n vitro* inhibition assay (NAALADase assay) was performed for three of the most promising derivatives identified on the basis of best *in silico* docking scores. The enzyme inhibition assay reveals that the newly designed inhibitors have excellent affinity and specificity to PSMA protein expressed on PCa cells.

Chapter 3 describes the application of homing ligands to selectively detect $PSMA^+$ cancers using fluorescent and radionuclear imaging techniques. Two PSMA targeted fluorescent bioconstructs were prepared, and the aminoacetamide targeting moiety was linked to rhodamine B fluorescent agent via two variations of a peptidic spacer. *In vitro* studies were successfully carried out on malignant cell lines over-expressing PSMA biomarker (LNCaP; $PSMA^+$) and on negative cell lines (PC-3; $PSMA^-$) to prove the specificity of the bioconjugates. Moreover, two PSMA targeted radionuclear chelating conjugates, to deliver radioisotope such as 99m-technetium, to detect $PSMA^+$ cancers were developed and warranted for *in vivo* studies using SPECT techniques.

Chapter 4 deals with a new class of glutamate-thiourea based heterodimers that were designed to explore the tolerance of thiocarbonyl moiety in the binding pocket of PSMA. Guided by computational docking studies, a library of carboxy protected thiourea derivatives have been designed and synthesized by a novel one-pot synthetic strategy. The derivative predicted to have the highest affinity to PSMA, as per *in silico* docking studies, was attached to a chelating moiety via a peptidic spacer to deliver 99m-technetium

radioisotope. I*n vitro* binding affinity analysis on $PSMA^+$ cell lines, LNCaP and 22RV1, demonstrated a nanomolar binding affinity to PSMA protein thereby proving that the radiotracer conjugated thiourea ligand have excellent potential as a diagnostic tool to detect early stages of PCa.

Chapter 5 explores the chemical interactions of tyrosine-based asymmetric urea ligand in the binding pocket of prostate specific membrane antigen (PSMA) through *in silico* studies. The S1 pocket of the PSMA protein offers a decent scope for chemical alteration in the urea ligands to improve the binding affinity. Accordingly, tyrosine-based (*S*)-2-(3((S)-1-carboxy-2-(4(carboxymethoxy)phenyl)ethyl)ureido) pentanedioic acid (CYUE) ligand was designed and synthesized. The novel ligand was further developed into a diagnostic probe to detect $PSMA^+$ cancers. *In vitro* studies on malignant cell lines such as LNCaP and PC-3 were performed to show the efficacy and specificity of the newly synthesized bioconstruct.

Chapter 6 details a novel, continuous process for assembling targeting ligand, peptidic spacer, fluorescent tag and a chelating core for delivery of cytotoxic molecules, radiotracers or nanomaterials using solid phase peptide synthesis methodology in high yield and purity. The attachment of the fluorescent tag to the growing peptide chain was achieved by strategic incorporation of differentially protected amino groups of lysine amino acid derivative such as Fmoc-Lys-(Tfa)-OH in the polypeptide chain. The side chain ε-amino group protected as trifluoroacetyl amide was deprotected under the mild aqueous basic condition without affecting other protecting groups present in the growing peptide chain. The methodology is versatile for solid phase resins that are sensitive to mild and strong acidic conditions when acid sensitive side chain amino protecting groups such as Trt(chlorotrityl), Mtt (4-methyltrityl), Mmt (4-methoxytrityl) are employed to synthesize ligand-targeted fluorescent

tagged bioconjugates with a chelating core or simple polypeptides. Using this method, two fluorescent bioconjugates, DUPA rhodamine B conjugate targeting PSMA and pteroate rhodamine B targeting folate receptor-positive cancers were synthesized. *In vitro* studies were successfully carried out on cell lines such as LNCaP ($PSMA^+$), PC-3 ($PSMA^-$, FR^-) and epithelial cell line CHO-β (FR^+) to demonstrate potential applications of bioconstructs as a tool for fluorescent guided intraoperative surgery.

7.2 Scope for future work

This thesis deals with the design and development of small molecule inhibitors for targeted diagnosis and therapy of PCa. The inhibitors were tethered with imaging agents via peptidic spacers and converted to suitable diagnostic tools. The bioconjugates have important applications in deep tissue imaging as well as removal of single tumor cells or micrometastases during initial stages of cancer by fluorescence-guided surgery.

Aminoacetamide PSMA inhibitors have significant potential in the healthcare sector to treat cancer and neurodegenerative diseases. The aminoacetamide fluorescent conjugates and radionuclear conjugates can be used for early diagnosis, intraoperative guided-surgery, MRI contrast imaging and treatment of prostate cancers that are resistant to hormone therapy such as metastatic castration-resistant prostate cancers (mCRPC). Moreover, the inhibitors can also be used to treat neurodegenerative diseases such as amyotrophic lateral sclerosis (ALS). The ligands and their conjugates show immense potential to become commercial products after preclinical evaluation.